Photophysics of Symmetric and Asymmetric Cyanines in Solution and Conjugated to Biomolecules

by

Monika A. Ciuba

A Thesis Presented in Partial Fulfilment
of the Requirements for the Degree
Doctor of Philosophy

Approved April 2017 by the
Graduate Supervisory Committee:

Marcia Levitus, Chair
Yan Liu
Sara Vaiana

ARIZONA STATE UNIVERSITY

May 2017

© 2017 Monika A. Ciuba
All Rights Reserved

ABSTRACT

Fluorescence spectroscopy is a powerful tool for biophysical studies due to its high sensitivity and broad availability. It is possible to detect fluorescence from single molecules allowing researchers to see the behavior of subpopulations whose presence is obscured by "bulk" collection methods. The fluorescent probes used in these experiments are affected by the solution and macromolecular environments they are in. A misunderstanding of a probe's photophysics can lead researchers to assign observed behavior to biomolecules, when in fact the probe is responsible. On the other hand, a probe's photophysical behavior is a signature of the environment surrounding it; it can be exploited to learn about the biomolecule(s) under study. A thorough examination of a probe's photophysics is critical to data interpretation in both cases and is the focus of this work. This dissertation investigates the photophysical behavior of symmetric and asymmetric cyanines in a variety of solution and biomolecular environments. Using fluorescent techniques—such as time-correlated single photon counting (TCSPC) and fluorescence correlation spectroscopy (FCS)—it was found that cyanines are influenced by the local environment. In the first project, the symmetric cyanines are found to be susceptible to paramagnetic species, such as manganese(II), that enhance the intersystem crossing (ISC) rate increasing triplet blinking and accelerating photobleaching. Another project found the increase in fluorescence of Cy3 in the protein induced fluorescence enhancement (PIFE) technique is due to reduced photoisomerization caused by the proximity of protein to Cy3. The third project focused on asymmetric cyanines; their photophysical behavior has not been previously characterized. Dy630 as a free dye behaves like Cy3; it has a short lifetime and can deactivate via photoisomerization.

Preliminary experiments on Dy dyes conjugated to DNA show these dyes do not photoisomerize, and do not show PIFE potential. Further research will explore other conjugation strategies, with the goal of optimizing conditions in which Dy630 can be used as the red-absorbing analogue of Cy3 for PIFE applications. In summary, this dissertation focused on photophysical investigations, the understanding of which forms the backbone of rigorous fluorescent studies and is vital to the development of the fluorescence field.

ACKNOWLEDGEMENTS

I would like to recognize everyone who generously provided their assistance during the course of my Ph.D. studies. Prof. Marcia Levitus provided the topic and direction of these studies, and taught me all I know about photophysics. Former and current group members were invaluable to the success of this work. I want to recognize Dr. Suman Ranjit and Dr. Elana Stennett for their assistance in training me, and Dr. Elana Stennett for help with the project presented in Chapter 3. David Kanno, Gabe Salmon, George Brockett, and Nikita Kumari provided assistance with experimental measurements. I also want to acknowledge the professionals who assisted in my data collection efforts. Dr. Su Lin for her help in teaching me the TCSPC technique and for her assistance with the EOS transient absorption system. Dr. Gerdenis Kodis for his help with the transient absorption system in the Devens Gust lab. Douglas Daniel for his help with numerous side tasks. I want to also recognize my supervisory committee members, Profs. Yan Liu and Sara Vaiana, for their time and attention to my research work. Finally, I wish to recognize Profs. George Wolf and Andrew Chizmeshya for their participation on my comprehensive examination committee, especially Prof. Chizmeshya who served as the committee chair. Furthermore, I want to express my gratitude to both Profs. Wolf and Chizmeshya for their invaluable support over the years, from writing recommendation letters for my graduate school applications, to listening to my research frustrations, to advising me on future career choices, but above all, for always being on my side. Above all, I wish to thank my grandmother—my first chemistry teacher—my mother, and my family, all who told me to keep going each time I wanted to quit.

TABLE OF CONTENTS

Page

LIST OF TABLES……. ix

LIST OF FIGURES…… x

CHAPTER

1 INTRODUCTION TO PHOTOPHYSICS AND FLUORESCENCE MEASUREMENT……..……..…… 1

1.1 Fluorescence as a Tool for Biophysical Studies……. 1

1.2 Photophysics: Terms and Definitions……. 3

1.3 Background Photophysics of Cyanine Dyes……... 7

1.4 Instrumentation for Fluorescence Measurements……. 18

A. Absorption Spectroscopy…….. 18

B. Steady-State Fluorescence Spectroscopy…….. 21

I. Steady-State Fluorescnece Anisotropy……..……... 24

C. Time-Resolved Fluorescence Spectroscopy……. 27

D. Transient Absorption Spectroscopy…….. 35

E. Fluorescence Correlation Spectroscopy…… 41

2 CYANINE PHOTOBLEACHING AND TRIPLET BLINKING IN THE PRESENCE OF MN^{2+}…… 52

2.1 Introduction and Motivation……. 52

2.2 Materials and Methods…..…… 56

A. Materials……... 56

CHAPTER Page

B. Photobleaching Experiments…… 57

C. Lifetime Measurements…… 58

D. Transient Absorption Experiments……... 59

E. Fluorescence Correlations Spectroscopy Experiments……. 60

2.3 Results……... 61

A. Lifetime Measurements…… 61

B. Photobleaching Experiments…… 65

I. Cy3B……. 65

II. Cy5…… 69

III. Cy3…… 75

C. Transient Absorption Experiments……... 78

I. Cy3B……. 78

II. Cy5…… 83

III. Cy3…… 87

D. Fluorescence Correlation Spectroscopy Experiments…….. 88

2.4 Discussion……. 90

A. Determining the Cause of Photobleaching……... 90

B. Direct Measurement of the Triplet State…….. 95

C. Triplet Observation by Fluorescence Correlation Spectroscopy.. 97

I. Optical Saturation Effect in FCS…….. 98

2.5 Conclusion…….. 102

3 CHARACTERIZING THE PHOTOPHYSICS BEHIND PROTEIN INDUCED

CHAPTER Page

FLUORESCENCE ENHANCEMENT…….…… 105

3.1 Introduction and Motivation……... 105

3.2 Materials and Methods…… 109

A. Materials……. 109

B. Time-Resolved Fluorescence and Anisotropy Measurements… 109

C. Transient Absorption Measurements…….. 110

3.3 Results……. 111

A. Emission Spectra……. 111

B. Lifetimes and Anisotropies……. 112

C. Transient Absorption Measurements…….. 114

3.4 Discussion……... 116

A. Explanation for “Dip-and-Rise” Anisotropy Shape…… 116

B. Simulating the Associated Anisotropy of Dy3-DNA/KF……... 119

C. Direct Evidence of Decreased Photoisomerization……. 121

D. Determining the Fraction of DNA at the *exo* Site……... 122

3.5 Conclusion…….. 124

4 PHOTOPHYSICS OF DY DYES IN SOLUTION AND CONJUGATED TO DNA, AND EVALUATION OF THEIR POTETIAL AS PIFE PROBES…… 126

4.1 Introduction and Motivation……... 126

4.2 Materials and Methods…… 132

A. Materials……. 132

B. Absorption and Emission Measurements…… 133

CHAPTER Page

C. Time-Resolved Fluorescence and Anisotropy Measurements… 134

D. Transient Absorption Measurements…… 134

4.3 Results…… 135

A. Absorption, Emission, and Fluorescence Quantum Yield…….. 135

B. Lifetime Measurements…….. 138

C. Lifetimes and Fluorescence Anisotropies with Klenow Fragment

……. 145

I. Cy5-dsDNA…… 145

II. Dy635-dsDNA…… 148

III. Dy632-dsDNA…… 150

IV. Dy630-dsDNA…… 153

D. Transient Absorption Measurements…….. 155

4.4 Discussion……... 157

A. Dy Dyes Compared to Cy3……. 157

B. DNA Construct Evaluation……. 159

4.5 Conclusion…….. 162

CONCLUSIONS…… 164

REFERENCES……... 166

APPENDIX

I PIFE WITH BAMHI AND HRPA AND ASSOCIATED ANISOTROPY ANALYSIS…… 182

II POLYMERASE REACTION ON DNA AND BINDING OF KLENOW

APPENDIX Page

FRAGMENT…….. 198

III TOTAL INTERNAL REFLECTION FLUORESCENCE SPECTROSCOPY. 213

LIST OF TABLES

Table		Page
2.1	Lifetimes of Cy3B and Cy5 in the Presence of Cations……...	64
2.2	Fit Parameters for FCS Decays of Cy3B……..	89
3.1	Lifetimes of Cy3-DNA in the Presence of Klenow Fragment……	113
4.1	Quantum Yield of Free Dy630……...	137
4.2	Lifetimes of Free Dy630 in Organic Solvents……	139
4.3	Lifetimes of Dy630 Conjugated to DNA……	139
4.4	Lifetimes of Dy632 Conjugated to DNA……	141
4.5	Lifetimes of Dy635 Conjugated to DNA……	142
4.6	Lifetimes of Free Cy5 in Organic Solvents……	144
4.7	Lifetimes of Cy5 Conjugated to DNA……	144
4.8	Lifetimes of Cy5-dsDNA with KF…….	147
4.9	Polymerase Reaction Lifetimes of Cy5-dsDNA…….	148
4.10	Lifetimes of Dy635-dsDNA with KF…….	149
4.11	Polymerase Reaction Lifetimes of Dy635-dsDNA……	150
4.12	Lifetimes of Dy632-dsDNA with KF Titration……..	151
4.13	Polymerase Reaction Lifetimes of Dy632-dsDNA…….	152
4.14	Polymerase Reaction Lifetimes of Dy630-dsDNA…….	154
4.15	Lifetimes of Dy630-dsDNA with KF Titration……..	155
4.16	Polymerase Reaction Lifetimes of Cy3-dsDNA…….	158

LIST OF FIGURES

Figure		Page
1.1	Jablonski Diagram……..	3
1.2	Structure of Cy3 and Cy5……...	8
1.3	Absorption and Emission Spectra of Cy3 and Cy5……	9
1.4	Potential Energy Surfaces for Cy3……	10
1.5	Structure of Cy3B…….	14
1.6	Suggested Potential Energy Surfaces for Long Cyanines……	15
1.7	Extinction Coefficient of Pyrene……..	20
1.8	Schematic of a Fluorimeter……...	22
1.9	Example of Steady State Anisotropy……	25
1.10	Time-resolved Anisotropy of Cy5……	33
1.11	Schematic of Transient Absorption Equipment……	37
1.12	Examples of Transient Absorption Data……..	40
1.13	Schematic of Fluorescence Correlation Spectroscopy Equipment……..	42
1.14	Examples of Fluorescence Correlation Spectroscopy Data……..	47
2.1	Structure of TAMRA Dye……	54
2.2	Lifetime of TAMRA in the Presence of Dications……...	56
2.3	Cy3 Lifetime in the Presence of Dications……...	61
2.4	Comparison of Cy3 Lifetimes in the Presence of Dications…….	61
2.5	Cy3B Lifetime in the Presence of Dications…….	62
2.6	Lifetimes of Cy3B and Cy5 with Dications and TEMPOL……..	63

Figure Page

2.7 Cy5 Lifetime in the Presence of Dications……... 65

2.8 Comparison of Cy5 Lifetimes in the Presence of Dications……. 65

2.9 Photobleaching of Cy3B in the Presence of Cations…… 66

2.10 Absorption Spectra of Cy3B Pre- and Post-Photobleaching…… 67

2.11 Photobleaching of Cy3B with COT, Azide, and D_2O…….. 68

2.12 Photobleaching of Cy3B-dsDNA in the Presence of Dications…… 68

2.13 Photobleaching of Cy5 in the Presence of Cations……... 69

2.14 Absorption Spectra of Cy5 Pre- and Post-Photobleaching……... 70

2.15 Photobleaching of Cy5 in Argon…….. 71

2.16 Photobleaching of Cy5 with Iron(II)……. 72

2.17 Photobleaching of Cy5 with Azide and D_2O…… 72

2.18 Photobleaching of Cy5 with COT…… 73

2.19 Photobleaching of iCy5-dsDNA in the Presence of Dications……. 74

2.20 Photobleaching of Cy5 in the Presence of ROXS…… 75

2.21 Photobleaching of Cy3 in the Presence of Dications…… 75

2.22 Absorption Spectra of Cy3 Pre- and Post-Photobleaching……... 76

2.23 Free Cy3 vs. Cy3-dsDNA: Photobleaching in the Presence of Dications 77

2.24 Photobleaching of Cy3 on DNA with Varying Mn^{2+} Concentration…… 77

2.25 Difference Spectrum and Kinetic Traces of Cy3B/Mn^{2+}…….. 79

2.26 Difference Spectrum and Kinetic Traces of Cy3B/Mn^{2+}/COT……. 79

2.27 Cy3B/Mn^{2+}/COT Kinetic Traces Compared with Cy3B/Mn^{2+}……. 80

2.28 Difference Spectrum and Kinetic Traces of Cy3B/Mg^{2+}…….. 81

Figure Page

2.29 Kinetic Traces of Cy3B in the Presence of Cations…….. 81

2.30 Kinetic Traces of Cy3B in the Presence of Zinc(II)……. 82

2.31 Kinetic Traces of Cy3B in the Presence of TEMPOL and Mn^{2+}……. 82

2.32 Difference Spectra of Cy5 in the Presence of Mn^{2+} and Mg^{2+}……. 83

2.33 Difference Spectra of Cy5 in the Presence of Mg^{2+} and Iodide……... 84

2.34 Kinetic Traces of Cy5 in the Presence of Ions and COT…….. 85

2.35 Kinetic Traces of Cy5 in the Presence of Ions and Triplet Quenchers…. 85

2.36 Kinetic Trace of Cy5 in the Presence of TEMPOL…….. 86

2.37 Kinetic Traces of Cy5 in Oxygen Saturated Solution……... 86

2.38 Kinetic Traces of Cy3 in the Presence of Ions and COT…….. 87

2.39 Kinetic Traces of Cy3 at Long Times……... 88

2.40 FCS Decays of Cy3B in the Presence of Cations……. 88

2.41 FCS Decays of Cy3B with Fit Results……. 89

2.42 Structure of TEMPOL…….. 90

2.43 Fluorescence Saturation Rate Model…….. 100

2.44 FCS Point-Spread Function at Saturation……... 101

3.1 Schematic Representation of Polymerase Function of Klenow Fragment……. 107

3.2 Emission Spectrum of Cy3-dsDNA with Klenow Fragment…….. 111

3.3 Lifetimes of Cy3-dsDNA with Klenow Fragment…….. 112

3.4 Anisotropy of Cy3-DNA in the Presence of Klenow Fragment……. 114

3.5 Difference Spectra of Cy3-DNA in the Presence of Klenow Fragment. 115

Figure Page

3.6 DNA Binding to Klenow Fragment…… 117

3.7 Comparison of Simulated and Measured Anisotropy for Cy3-DNA/KF …… 121

4.1 Structure of Dy630 and Dy635……... 127

4.2 Schematic of DNA Samples……... 131

4.3 Absorption Spectra of Free Dy630……. 135

4.4 Absorption Spectra of Dy Dyes on DNA……... 136

4.5 Spectra of Free Dy630 in Organic Solvents……... 136

4.6 Temperature Dependence of Fluorescence Quantum Yield of Free Dy630 …… 138

4.7 Lifetimes of Dy630……. 139

4.8 Lifetimes of Dy630-dsDNA……... 140

4.9 Lifetimes of Dy630-ssDNA…… 140

4.10 Lifetimes of Dy632-dsDNA……... 141

4.11 Lifetimes of Dy632-DNA with Salt…… 142

4.12 Lifetime of Dy635-dsDNA……. 142

4.13 Lifetime of Dy635-ssDNA……. 143

4.14 Lifetimes of Cy5……. 144

4.15 Lifetimes of Cy5-DNA in Salt and Sucrose……... 145

4.16 Lifetimes of All Samples Compared…….. 145

4.17 Cy5-dsDNA with Klenow Fragment…….. 146

4.18 Polymerase Reaction on Cy5-dsDNA…… 147

Figure Page

4.19 Dy635-dsDNA with Klenow Fragment…….. 149

4.20 Polymerase Reaction on Dy635-dsDNA…… 150

4.21 Lifetime of Dy632-dsDNA with Klenow Fragment……... 151

4.22 Polymerase Reaction on Dy632-dsDNA…… 152

4.23 Polymerase Reaction on Dy630-dsDNA…… 154

4.24 Lifetime of Dy630-dsDNA with Klenow Fragment……... 154

4.25 Kinetic Traces and Difference Spectra of Dy630……... 155

4.26 Kinetic Traces and Difference Spectra of Cy5-dsDNA…….. 156

4.27 Lifetimes of Free Cy3 and Cy3-dsDNA……. 157

4.28 Fluorescence Response of Dy630 to dGMP……... 161

CHAPTER ONE

INTRODUCTION TO PHOTOPHYSICS AND FLUORESCENCE MEASUREMENT

1.1 Fluorescence as a Tool for Biophysical Studies

Fluorescent techniques have grown in popularity as a means to study biological macromolecules due to their high sensitivity and broad availability. A number of reviews are available discussing the basics of fluorescence and the equipment used[1], advanced techniques used for live cell imaging[2], and the synthesis and applications of fluorescent quantum dots for biological studies[3]. Fluorescence is used to study nucleic acids[4-6], proteins, using extrinsic as well as intrinsic fluorescence[7-10], and other biological macromolecules such as membranes and ion channels[11, 12]. As photodetectors increased in sensitivity it became possible to detect fluorescence from smaller samples, until it became possible to detect emitted photons from a single molecule[13, 14]. Single molecule detection allows the observation and quantification of subpopulations of molecules which would otherwise be "drowned out" by the large, average signal from bulk experiments. Single molecule experiments allow the observation of dynamic changes to a biomolecule's structure[8, 9, 15-17]. Fluorophores for fluorescence experiments fall into two categories, intrinsic and extrinsic. Intrinsic fluorophores are found in proteins; tryptophan, tyrosine, and phenylalanine are fluorescent amino acid residues[18]. Tryptophan, via its indole group, is primarily responsible for protein UV fluorescence; tyrosine fluorescence is frequently quenched, and emission from phenylalanine is only observed if the protein lacks tryptophan and tyrosine residues, which is rare[19]. Tryptophan fluorescence is subject to its local environment; its spectrum can shift in

response to binding, unfolding, and other dynamics, and its emission can be quenched by iodide, acrylamide, and even protonated histidine residues[19]. The presence of multiple tryptophan residues in a protein results in multi-exponential intensity decays—due to each residue's unique environment—which can be difficult to interpret. For work involving nucleic acids, low quantum yield is a problem; DNA bases have a fluorescence quantum yield on the order of 10^{-4} [20]. To avoid these problems, and the autofluorescence and high background that come with working in the UV most biomolecules are tagged with an extrinsic fluorophore which absorbs in the visible region, is photostable, and has a high extinction coefficient and fluorescence quantum yield. These characteristics can minimize photobleaching, autofluorescence, and Raman scattering[21, 22]. These extrinsic fluorophores can be either fluorescent organic molecules[23, 24], fluorescent proteins[24-27], or quantum dots[3, 28-30]. Among these choices organic fluorophores have the additional advantage of small size—they have molecular weights on the order of 0.5 kDa; this is much smaller than green fluorescent protein (26.9 kDa)[24], or quantum dots, which can have diameters of a few nanometers to tens of nanometers[3]. Conjugation of a probe to the biomolecule under study can potentially alter the behavior of that biomolecule, hence the smaller the probe the better. This dissertation focuses on organic fluorophores, in particular cyanine dyes, and studies their photophysical behavior in a multitude of environments, e.g., as a free molecule in solution, and conjugated to DNA and proteins. Given the widespread use of cyanines in single molecule fluorescent work involving biomolecules an understanding of their photophysical behavior is essential for the proper interpretation of data. The following introductory sections will discuss terms relevant to the photophysical field, provide a brief history of cyanine photophysics, and give an

overview of instruments used for the collection of fluorescent data.

1.2 Photophysics: Terms and Definitions

Photophysics is the study of the processes chromophores undergo upon absorption of light, and are typically illustrated using a Jablonski diagram (Figure 1.1), which shows the ground and excited electronic states of a molecule, and a few of their vibrational states. Photophysical behavior begins with the absorption of light, a process occurring on the femtosecond timescale, too fast for the nuclei to rearrange during the process. The rate of absorption is represented by k_{ex}, where *ex* refers to excitation. After absorption, the molecule is in the first singlet excited state, S_1—or, if higher energy light was

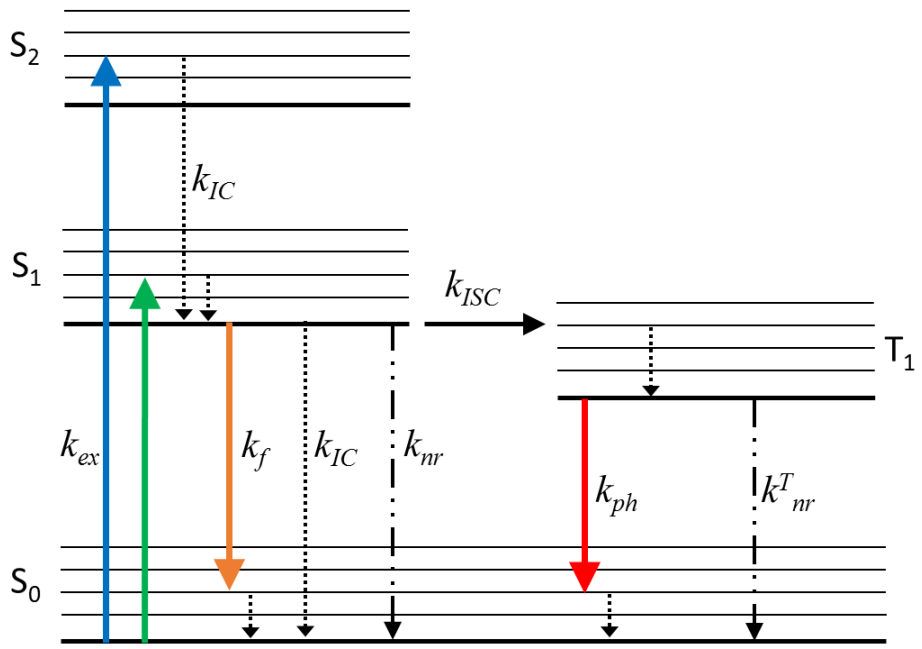


Figure 1.1: Jablonski Diagram. A standard energy level diagram for describing photophysical processes. Rates are described in the text. Colored arrows signify absorption and emission of light, dotted arrows signify deactivation via internal conversion, dot-dot-dash lines signify deactivation via other non-radiative means.

absorbed it will be in the second singlet excited state or S_2, or the molecule may end up in

the third singlet excited state, S_3, etc. More precisely, the molecule will be in an excited vibrational level of the particular excited state and will rapidly, in picoseconds, undergointernal conversion (with rate k_{IC}) relaxing to the ground vibrational level of S_1 (molecules in S_2, S_3, etc., will also return to the ground vibrational level of S_1). Internal conversion is defined as a non-radiative transition between two states of the same spin multiplicity. Fluorescence, with rate k_f, occurs from the ground vibrational level of S_1 to an excited vibrational level of S_0, and in a matter of picoseconds, internal conversion will return the probe to thermal equilibrium, usually the ground vibrational level of S_0; the timescale (of fluorescence) is anywhere from a few to several tens of nanoseconds. It should be noted that the emission of a photon is as fast as absorption of one (femtoseconds); the nanosecond timescale of fluorescence refers to how long the molecule remains in its excited state before emission (called the excited state lifetime, τ).

These behaviors explain the Stokes shift and vibrational structure, two characteristics seen in emission spectra. The Stokes shift is the difference in energy between the maximum of the first absorption band and the maximum of the fluorescence; it arises from the fast internal conversion which returns the molecule to the lowest vibrational level of the lowest excited electronic state. Thus, fluorescence of molecules will be red-shifted compared to the absorbed wavelengths. This also explains why, regardless of excitation wavelength, the emission spectrum will always look the same. The vibrational structure is seen in emission spectra since fluorescence populates multiple vibrational energy levels in the ground electronic state (and the population in those vibrational levels reaches thermal equilibrium rapidly due to internal conversion). This creates a “mirror image” between absorption and emission spectra; vibrational

structure is also seen in absorption spectra due to absorption populating various vibrational states in the excited electronic state, and vibrational energy spacings are similar in the ground and excited states (excitation happens too quickly for the molecular geometry, and hence the potential energy surface, to change significantly).

Excited state fluorophores can also deactivate via a non-radiative, spin conversion process called intersystem crossing (ISC), when converting from a singlet to a triplet state. ISC takes place between two isoenergetic vibrational levels, e.g. from the ground vibrational energy level of S_1 to an isoenergetic vibrational level in T_1; this process occurs with rate k_{ISC}. Spin conversion is called a "forbidden" process, but spin-orbit coupling may be large enough to allow it: the magnitude of the coupling is proportional to the fourth power of the atomic number. As such, ISC is more favorable in the presence of heavy atoms. It can compete with fluorescence as it takes place on comparable timescales of up to hundreds of nanoseconds. As with the singlet states, once in the T_n electronic state internal conversion brings the fluorophore to the ground vibrational level of T_1. Transitions from triplet to singlet states are similarly unlikely, and phosphorescence—the emission of a photon from the lowest triplet state, k_{ph}—is rarely observed. Deactivation from T_1 to S_0 can also occur via non-radiative means, with rate k_{nr}^{T}. The triplet state lifetime, τ_T, typically on the order of microseconds, is the average time a fluorophore remains in the triplet state.

The lifetime of the first singlet excited state can be expressed quantitatively in terms of the radiative and non-radiative deactivation rates (from that state) of the molecule as shown in Equation 1.1, where k_f is the rate constant for fluorescence, k_{ISC} is

$$\tau = \frac{1}{k_f + k_{IC} + k_{ISC} + k_{nr}} \tag{1.1}$$

the rate of ISC, k_{IC} is the rate of internal conversion, and k_{nr} is the rate of other non-radiative deactivation processes, e.g. photoisomerization discussed later. An analogous expression (Equation 1.2) can be written for the lifetime of the triplet state, where k_{ph} is the rate of phosphorescence and k_{nr}^{T} is the rate of all non-radiative deactivation processes from the triplet state.

$$\tau_T = \frac{1}{k_{ph} + k_{nr}^{T}} \tag{1.2}$$

In addition to lifetime, fluorophores are also described via their fluorescence quantum yield, ϕ_f, a property that describes what fraction of absorbed photons is emitted as radiation. Also relevant, the quantum yield of intersystem crossing, ϕ_{ISC}, is defined as the fraction of absorbed photons that enter the triplet state. Together, the quantum yields for all possible deactivation processes must add up to unity—including the quantum yields of internal conversion, ϕ_{IC}, and non-radiative deactivation, ϕ_{nr} (Equation 1.3).

$$\phi_f + \phi_{IC} + \phi_{ISC} + \phi_{nr} = 1 \tag{1.3}$$

These quantities are the probabilities of a molecule relaxing via a particular deactivation pathway. The quantum yield of fluorescence and ISC can be expressed in terms of the deactivation rate constants and, hence, the lifetime (Equations 1.4 and 1.5). In

$$\phi_f = \frac{k_f}{k_f + k_{IC} + k_{ISC} + k_{nr}} = k_f \tau \tag{1.4}$$

$$\phi_{ISC} = \frac{k_{ISC}}{k_f + k_{IC} + k_{ISC} + k_{nr}} = k_{ISC} \tau \tag{1.5}$$

Equation 1.5 the lifetime is the average lifetime of the first singlet excited state. The phosphorescence quantum yield and intersystem crossing rate from triplet to singlet state, shown in Equation 1.6 and 1.7, depend on the rate constants (and lifetime) of the triplet state, however.

$$\phi_{ph} = \frac{k_{ph}}{k_{ph} + k_{IC}^{T} + k_{ISC}^{T} + k_{nr}^{T}} = k_{ph}\tau_{T} \tag{1.6}$$

$$\phi_{ISC}^{T} = \frac{k_{ISC}^{T}}{k_{ph} + k_{IC}^{T} + k_{ISC}^{T} + k_{nr}^{T}} = k_{ISC}^{T}\tau_{T} \tag{1.7}$$

1.3 Background Photophysics of Cyanine Dyes

Cyanine dyes are amongst the most popular fluorophores in use today for bulk and single molecule fluorescence measurements; their photophysical behavior is the primary focus of this dissertation. The structural backbone of the cyanine dye is a conjugated polymethine chain consisting of an odd number of carbon atoms, which connects two nitrogen atoms, as shown in Figure 1.2[31]. Symmetric cyanines have the same substituent on the nitrogen atoms—and are referred to as cyanines—while hemicyanines have different substituents on the two nitrogens. In their most stable form cyanines have indole, quinoline, benzoxazole, or benzothiazole substituents. Cyanines with indole substituents—called indocarbocyanines—are the basis for Cy3 and Cy5, two of the most commonly used fluorophores in fluorescence today (Figure 1.2). The use of the term "Cy" for these dyes began in the late 1980s; the accompanying number refers to the number of carbon atoms in the polymethine chain[32, 33]. The dyes shown in Figure 1.2 have sulfonate substituents to increase solubility and prevent aggregation, and have a

succinimidyl ester group for conjugation to biomolecules. Maleimide groups are also used for conjugation purposes. Due to the sulfonate groups these dyes are charged (single negative charge), however the dyes used for DNA labeling—by companies such as Integrated DNA Technologies, Inc.—do not have sulfonates (solubility no longer being an issue) and possess a single, positive charge.

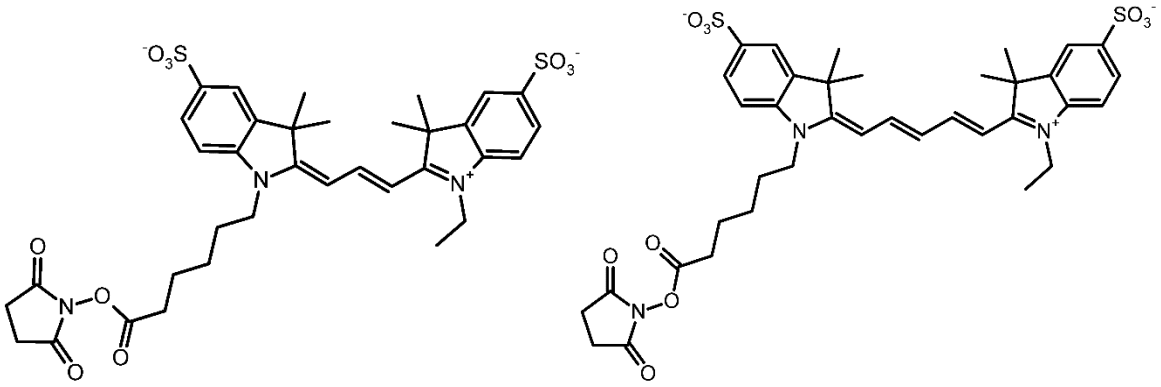


Figure 1.2: Structure of Cy3 and Cy5. The succinimidyl esters of Cy3 (left) and Cy5 (right) are shown here; both dyes possess two sulfonate groups.

Cy3 and Cy5 are part of a large family of cyanine dyes, which absorb in various ranges of the electromagnetic spectrum. The primary absorption band is determined by the length of the conjugated polymethine chain; short chain dyes absorb in the UV and blue regions, while long chain dyes absorb in the red and infrared. Cy3's primary absorption band is at 550 nm while Cy5 absorbs at 649 nm; they have emission maxima at 570 nm and 670 nm, respectively (these values apply to the succinimidyl esters shown in Figure 1.2, as provided by data sheets from GE Healthcare LifeSciences, Marlborough, MA). These dyes have high extinction coefficients, too: for Cy3 $\varepsilon^{\max} = 150{,}000 M^{-1}cm^{-1}$ and for Cy5 $\varepsilon^{\max} = 250{,}000 M^{-1}cm^{-1}$. The absorption and emission spectra of Cy3 and Cy5 are shown in Figure 1.3, as collected by the author for these studies. Cy3 has a short

fluorescence lifetime, measured to be as low as 180 ps in Tris buffer[34] and 210 ps in solutions containing magnesium and manganese cations[35]. Correspondingly, the fluorescence quantum yield of Cy3 is low at 0.09[34] and 0.04[36] at room temperature. Cy5 has a longer lifetime reported at 1.0 ns from single molecule measurements[37] and a fluorescence quantum yield of 0.28 (GE Healthcare). Cyanine dyes have been the focus of numerous studies over the years. A brief review of their photophysical behavior follows.

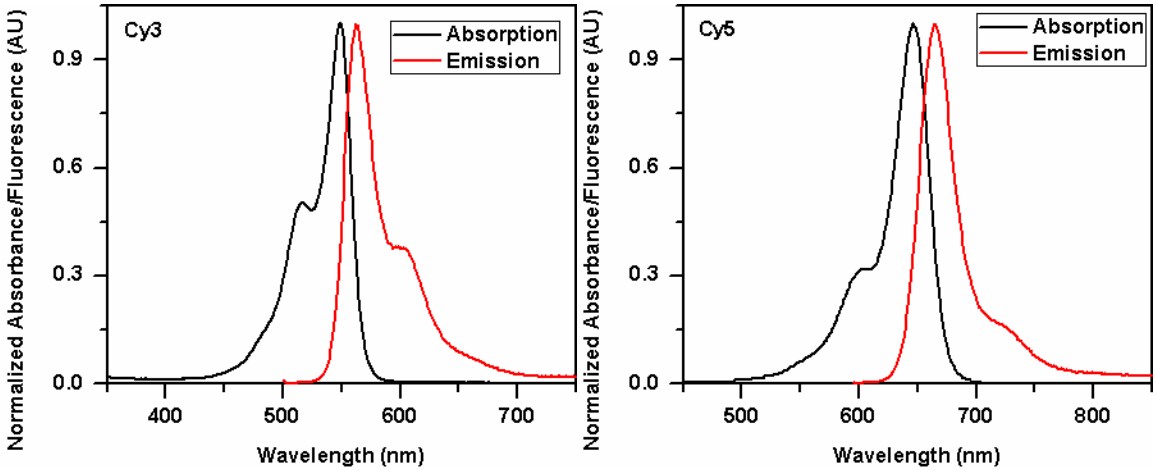


Figure 1.3: Absorption and Emission Spectra of Cy3 and Cy5. These are the absorption and emission spectra of the succinimidyl esters of Cy3 and Cy5 in water.

The photophysical behavior of cyanines is explained in terms of the ground (S_0) and excited (S_1) state potential energy surfaces shown in Figure 1.4, below; this model was first proposed by Rulliere[38]. Due to the conjugated polymethine chain, cyanines can rotate about those carbon-carbon double bonds to form different isomers. In the ground state the *trans*- isomer—symbolized by "N" in the rates and energy barriers in Figure 1.4—is most stable, meaning the substituents on the nitrogen atoms point in the same direction, away from the polymethine chain[39-41]. The potential energy, E, of the ground and excited state surfaces varies with the torsion angle, θ, the angle between the two

heterocycles on either end of the polymethine chain. Upon photon absorption a cyanine dye can deactivate via fluorescence, internal conversion, intersystem crossing into the triplet state, or photoisomerization (isomerization from the excited state). The rates of these processes are designated by k_f, k_{IC}, and k_{ISC}, respectively. Photoisomerization is a two-step process, designated by rates k_{Nt}, and k_{tP}, which are described later.

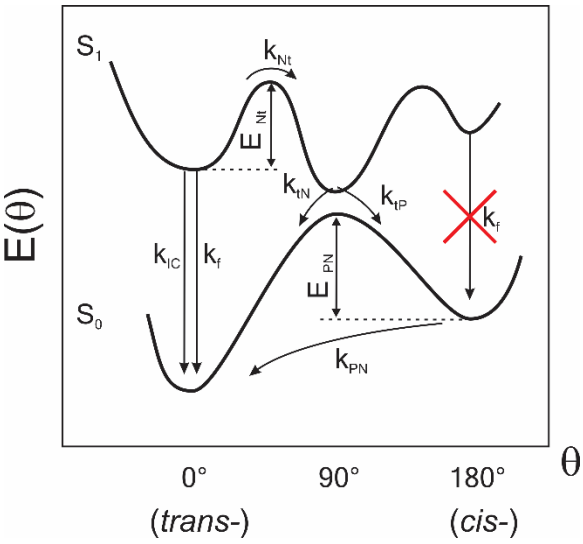


Figure 1.4: Potential Energy Surfaces for Cy3. The potential energy, E, as a function of the torsion angle, θ, of the first two singlet electronic states, S_0 and S_1 is shown along with the dominant relaxation pathways for Cy3-like cyanines. The rate constants and energies depicted in the figure are discussed in detail in the text.

The dominant deactivation pathway for carbocyanines—cyanines with three carbon atoms in the polymethine chain, analogous to Cy3—is via photoisomerization (discussed in detail below) causing the fluorescence lifetime and quantum yield to be low. For example, the fluorescence quantum yield, ϕ_f, of diethylindocarbocyanine in propanol is only 0.028, with a corresponding fluorescence lifetime of 162 ps[42, 43]. At 77 K, ϕ_f is almost unity for dimethylindocarbocyanine[44]. Both parameters are strongly affected by solvent viscosity: a variety of carbocyanines experience doubled and even

tripled lifetimes with doubled solvent viscosity[45, 46]. Isomerization requires the molecule to undergo a large movement, which is made difficult in highly viscous solvents, increasing the probability of fluorescence as a relaxation pathway. Temperature also plays a role; as discussed below, photoisomerization is an activated process. Low temperatures decrease the non-radiative deactivation rate(s) forcing the dye to fluoresce more efficiently[43, 47-49]. Solvent polarity, on the other hand, does not have a significant effect on the fluorescence lifetime of these dyes[50, 51]. Conjugation and binding to biomolecules also increases the fluorescence lifetime of short cyanines[52-55]. The quantum yield of internal conversion, ϕ_{IC}, for dimethylindocarbocyanine is estimated at 0.06 at 77 K when no isomerization occurs[44], while for the succinimidyl ester shown in Figure 1.2 it is estimated at 0.15[34, 36]. At high solvent viscosity—which also precludes isomerization—internal conversion becomes the dominant relaxation pathway with a ϕ_{IC} of 0.66 for dimethylindocarbocyanine, in contrast to the value at low temperatures[56]. The quantum yield of intersystem crossing (ISC), ϕ_{ISC}, is negligible, even in comparison to ϕ_f for these dyes. For diethylindocarbocyanine in propanol ϕ_{ISC} is less than 0.005[42]. While for dimethylindocarbocyanine in ethanol ϕ_{ISC} is less than 0.01[44]. The succinimidyl ester, Cy3, has ϕ_{ISC} of 0.03; the *trans*- isomer triplet state has maximum absorption at 580 nm and an extinction coefficient measured at 40,770 M^{-1} cm^{-1} [57]. Diethylthiacarbocyanine—a cyanine dye with benzothiazole substituents rather than indole—is reported to have an ISC quantum yield of less than 0.001 in butanol[58].

As stated above, the dominant relaxation pathway for short cyanines—cyanines with three carbon atoms in the polymethine chain (five total carbon atoms between the

nitrogen atoms)—is via photoisomerization. In the case that an excited cyanine dye does not fluoresce, undergo internal conversion, or intersystem crossing, it can overcome an energy barrier in the excited state, E_{Nt}, leading to what is known as a "twisted intermediate" (symbolized by "t" in the rate constants and energy barriers of Figure 1.4). The rate of photoisomerization depends on many factors, among them solvent viscosity, temperature, and the identity of the substituents at the *meso*- position of the polymethine chain[59]. The quantum yield of overcoming the energy barrier in the excited *trans*- state to enter the twisted intermediate state, ϕ_{Nt}, has been measured at 0.9 for diethylindocarbocyanine[42]. Increasing solvent viscosity hinders rotation about the carbon-carbon double bonds reducing k_{Nt} and the photoisomerization rate; the energy barrier, E_{Nt}, has been measured at 5 kJ/mol in methanol and increases to 18 kJ/mol in hexanol[43]. Further experiments determined a viscosity independent barrier height of 7.5 kJ/mol[47]; the viscosity of methanol adds 7.6 kJ/mol to the barrier, while that of dodecanol adds 21.6 kJ/mol[46]. The origin of a viscosity dependent energy barrier is discussed later. The rate of isomerization is also affected by temperature. High temperature increases the energy available to the dye to overcome the energy barrier for twisting, resulting in a greater photoisomerization rate. At high temperatures there is also a decrease in solvent viscosity, further increasing the isomer population[43, 46, 47, 60]. The succinimidyl ester of Cy3 has an energy barrier, E_{Nt}, of 19 kJ/mol[34]. At the torsion angle for the twisted intermediate a conical intersection is formed with the ground state allowing the dye to relax to the ground state[50, 61]. However, the dye can either return to the *trans*- form (N) or to the *cis*- form (symbolized by "P" in the rate constants and energy barriers of Figure

1.4)[50, 61]. The branching ratio ($k_{tP}:k_{tN}$) is a measure of which isomer is favored in deactivation from the twisted intermediate. For dimethylindocarbocyanine the branching ratio is 2:1 in ethanol with the *cis*- state favored[44]. The *cis*- form is proposed to be formed via rotation about only one carbon-carbon double bond—to create a mono-*cis* isomer[46, 59]. The *cis*- state can revert to the *trans*- form by overcoming an energy barrier, E_{PN}, which separates the two forms in the ground state; this process is referred to as a thermal back-isomerization. Rulliere found an Arrhenius law dependence for the rate of deactivation (k_{PN}) of the photoisomer[38]. This process has been investigated extensively—the isomer can be directly observed with techniques such as transient absorption—and found to be a first-order reaction whose rate depends on solvent viscosity[48, 49, 59]. The energy barrier in the ground state, E_{PN}, is reported to be 45 kJ/mol for diethylindocarbocyanine in propanol[42]. The cyanine photoisomer itself is referred to as a "dark" state due to its negligible fluorescence quantum yield; the large, red "x" in Figure 1.4 indicates that k_f is several orders of magnitude lower than other deactivation rates for the excited *cis*- state. This value is negligible for short and long cyanines [42, 46, 62-64]. The rate of back isomerization does not depend on solvent polarity[50].

The fluorescence quantum yield, ϕ_f, (and lifetime) of cyanines is significantly increased in situations where bond rotation is restricted, for example in solvents of high viscosity[46, 56, 65]. Bulky substituents on the nitrogen atoms also hinder rotation and increase fluorescence quantum yield compared to dyes with smaller substituents[59, 66]. Conjugation to biomolecules, such as proteins and DNA, also creates a sterically hindered environment for the dye decreasing the rate of photoisomerization, k_{Nt}, as

studied by researchers and the Levitus lab[52-54]. To eliminate the photoisomerization deactivation pathway the dye must be prevented from rotating; for Cy3 this has been accomplished via chemical rigidization to form the dye Cy3B, which possesses similar spectral properties to Cy3, but has a longer lifetime (reported at 2.7 ns and 2.8 ns) and greater fluorescence quantum yield (0.85 and 0.67 reported)[34, 36]. The structure of the succinimidyl ester of Cy3B is in Figure 1.5, below.

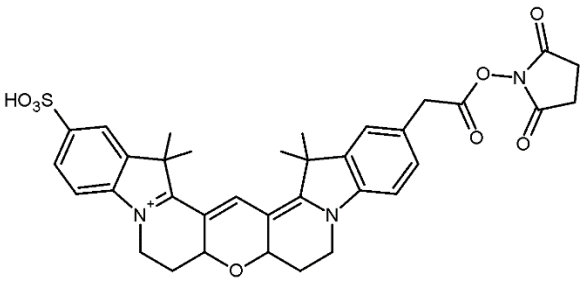


Figure 1.5: Structure of Cy3B. This is the succinimidyl ester of Cy3B; note the Cy3-like structure of polymethine chain connecting two indole substituents.

The longer cyanines, precursors to the succinimidyl ester of Cy5 (Figure 1.2, right), have higher fluorescence quantum yields and longer lifetimes. For diethylindodicarbocyanine ϕ_f in propanol is 0.24[42], while for dimethylindodicarbocyanine it is 0.21 at room temperature in ethanol with a lifetime of 0.98 ns; at -196°C ϕ_f increases to 0.98 with a lifetime of 2.4 ns[59]. Intersystem crossing into the triplet state is as rare as for the short cyanines; ϕ_{ISC} is reported as < 0.005 for diethylindodicarbocyanine and < 0.003 for dimethylindodicarbocyanine[42, 59]. Chibisov *et al.* also report the maximum of triplet-triplet absorption at 690 nm, and a triplet state lifetime, τ_T, of 60 μs[59]. The succinimidyl ester of Cy5 is reported to have a triplet-triplet absorption at 625 nm with τ_T of 35 μs[37]. Internal conversion has a quantum yield of 0.11 for

dimethylindodicarbocyanine, estimated from measurements at low temperature, when photoisomerization is not possible[59]. As for the short cyanines, photoisomerization is still the main deactivation pathway. Based on the values provided above for ϕ_f, ϕ_{ic}, and ϕ_{ISC} for dimethylindodicarbocyanine, ϕ_{Nt} is approximately 0.68. However, unlike the short cyanines, the probability of forming the *cis*- isomer from the twisted intermediate, ϕ_{tP}, is only 0.038[59]. This indicates a branching ratio of 1:17—formation of the *trans*- state is highly favored; it has been proposed that the twisted intermediate minimum on the excited state surface does not meet the twisted intermediate maximum on the ground state surface, but rather is located on the *trans*- side of the ground state maximum (see Figure 1.6)[59]. The energy barrier in the excited state, E_{Nt}, is reported to be 21 – 37 kJ/mol

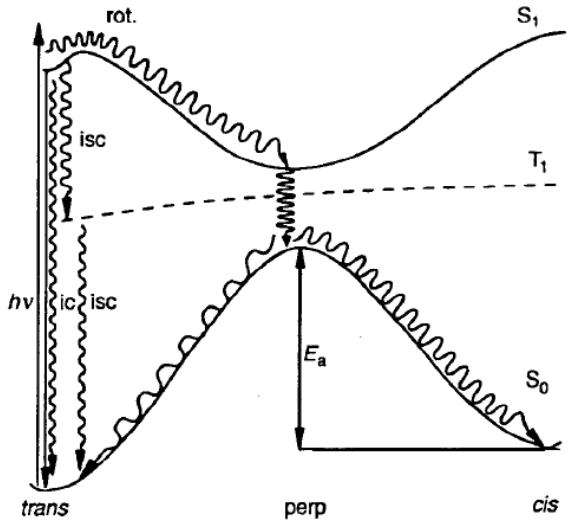


Figure 1.6: Suggested Potential Energy Surfaces for Long Cyanines. The minimum in S_1 is shown as occurring to the left of the maximum in the ground state for the perp form. Reproduced from Reference 58 with permission of The Royal Society of Chemistry (http://dx.doi.org/10.1039/FT9969204917).

depending on the solvent, while the barrier in the ground state, E_{PN}, is 51 – 57 kJ/mol[49, 59]. For diethyloxadicarbocyanine—a cyanine with benzoxazole substituents—the energy

barrier in the excited state is reported at 11 kJ/mol and 57.3 kJ/mol in the ground state[67].

Studies of cyanine photoisomerization often focus on the effects of solvent, i.e. what effect varying the viscosity of the solvent has on the rate of the ground and excited state isomerization reactions, k_{PN} and k_{Nt}, respectively. Several studies cited here (references 46, 49, and 67) attempt to use Kramers theory to model the dependence on viscosity of the isomerization rates. The rate of crossing an energy barrier is typically modeled by transition state theory; however, this theory neglects solvent effects, e.g., it does not provide for a dependence of the rate on solvent viscosity. Kramers' theory is based on a model of a Brownian particle passing a one-dimensional potential barrier. Unlike transition state theory Kramers model assumes re-crossings of the barrier are possible due to the presence of the frictional forces exerted on the activated complex by the solvent[68]. Neglecting re-crossing events in transition state theory leads to an overestimation of the rate for reactions taking place in solvated media. The Kramers rate expression for one-dimensional reactions taking place in condensed media is given by Equation 1.8, below, where k is the rate of barrier crossing, ω_R and ω_b are the harmonic frequencies of the reactant and barrier wells, respectively, ξ is the friction coefficient, E_a is the size of the energy barrier, R is the gas constant, and T is the temperature. This

$$k = \frac{\omega_R}{2\pi\omega_b}\left(\left(\frac{\xi^2}{4}+\omega_b^2\right)^{1/2}-\frac{\xi}{2}\right)\exp\left(-E_a/RT\right) \qquad (1.8)$$

form of the rate expression is valid at intermediate values of friction, while at low friction Equation 1.9 is applied, where the low frictional force is proportional to the rate. At high values of friction Equation 1.10 is valid. The friction is typically related to the solvent

viscosity via Stokes law, Equation 1.11, where η is the viscosity, R is the hydrodynamic radius of the particle (molecule) undergoing the reaction, and M is the mass of the particle. Substituting Equation 1.11 into Equation 1.10 shows that at high friction the rate is proportional to $1/\eta$. Equation 1.10 is known as the Smoluchowski limit. Data

$$k = \frac{\omega_R}{2\pi}\xi \exp\left(-E_a / RT\right) \tag{1.9}$$

$$k^{SL} = \frac{\omega_R \omega_b}{2\pi\xi} \exp\left(-E_a / RT\right) \tag{1.10}$$

$$\xi = \frac{6\pi\eta R}{M} \tag{1.11}$$

collected for diethyloxadicarbocyanine for the ground and excited state isomerization rates was unable to be fit to Equation 1.10[67]. Data collected for diethylindocarbocyanine in low viscosity solvents did not fit Equation 1.9, while data in high viscosity solvents did not fit Equation 1.10[46]. Aramendía *et al.* performed a comprehensive study on six short and long cyanines and found the Kramers model to be a good fit only for diethyloxacarbocyanine and diethylthiacarbocyanine[49]. In cases where neither version of Kramers equation reproduces the data it is common to use a power law form of the rate expression (Equation 1.12), where D and b are adjustable parameters. While this equation for the rate has fit many data sets well, its drawback is the lack of a physical interpretation for the parameters[46, 49, 56, 67]. The viscosity is expressed as Equation 1.13 to indicate its temperature dependence, where η_0 and E_η are constants associated with each liquid. This gives the following (Equation 1.14) expression for the rate. The energy barrier of isomerization, or any reaction for that matter, should not change with the environment in which the reaction occurs. Use of the rate expression in Equation 1.12

will yield an intrinsic barrier height of the reaction, E_a, and a viscosity dependent addition to the barrier, E_η. This shows the origin of the viscosity dependent barrier height as reported above for several cyanines (Equation 1.15).

$$k = D\eta^{-b} \exp(-E_a / RT) \tag{1.12}$$

$$\eta = \eta_0 \exp(E_\eta / RT) \tag{1.13}$$

$$k = D\eta_0^{-b} \exp(-bE_\eta / RT)\exp(-E_a / RT) = D\eta_0^{-b} \exp(-(bE_\eta + E_a) / RT) \tag{1.14}$$

$$E_{barrier} = E_a + bE_\eta \tag{1.15}$$

1.4 Instrumentation for Fluorescence Measurements

A. Absorption Spectroscopy

The most basic measurements in the field of fluorescence are the absorption and emission spectra. Both are measured in commercially available benchtop instruments requiring only a few components. A simple spectrophotometer contains a lamp, monochromator, sample and reference cell holder, and a detector. The lamp must have a relatively even output throughout the desired measurement region; UV-VIS spectrophotometers contain two light sources, a tungsten (halogen) lamp for the visible region and a deuterium lamp for the ultraviolet region. The monochromator selects the wavelength of light that enters the sample chamber; this light is split evenly and the two beams pass through the sample and reference solution. The reference solution will contain everything except the fluorophore so that the intensity of light passing through the sample can be compared to that passing through the reference. A detector records the two intensities, and a computer presents the data as an absorption spectrum, absorbance,

A, versus the wavelength, λ.

The mathematical relationship[69] describing the intensity of light absorbed by the sample is given by Equation 1.16, where $I(x)$ is the function describing intensity along the

$$\frac{dI(x)}{dx} = -n\sigma I(x) \tag{1.16}$$

long axis of light entering the solution, the x-axis, and number density (n) and absorption cross-section (σ) are the proportionality constants (the rate of change of the intensity is negative, since it decreases due to being absorbed by the fluorophores). The solution to this differential equation, with initial condition $I(0) = I_0$, is known as the

$$I(x) = I_0 \exp(-n\sigma x) \tag{1.17}$$

Lambert Law, Equation 1.17, where I_0 is the initial intensity. The final intensity passed through a solution (I_f) of thickness l is given in Equation 1.18. The ratio of these two

$$I_f = I_0 \exp(-n\sigma l) \tag{1.18}$$

$$T = \frac{I_f}{I_0} \tag{1.19}$$

intensities gives the transmittance, T, of the solution (Equation 1.19), which is converted to absorbance A, via the logarithm (Equation 1.20). After substituting Equations 1.18

$$A = -\log(T) = -\log\left(\frac{I_f}{I_0}\right) = -\log\left(\frac{I_0 \exp(-n\sigma l)}{I_0}\right) = -\log(\exp(-n\sigma l)) \tag{1.20}$$

$$\exp(-n\sigma l) = 10^{-c\varepsilon l} \text{ when } \varepsilon \cong \frac{\sigma N_A}{2.303} \tag{1.21}$$

and 1.19, the exponential term is changed to a base ten exponential (Equation 1.21)

which gives a linear relationship between absorbance and concentration, c, via the extinction coefficient, ε (Equation 1.22). For a fluorophore with known extinction

$$A = -\log(\exp(-n\sigma l)) = -\log(10^{-c\varepsilon l}) = -(-c\varepsilon l) = c\varepsilon l \qquad (1.22)$$

coefficient the concentration can be calculated from Equation 1.22. This relationship can also be used to determine extinction coefficients, as long as the mass of the fluorophore and volume of the solvent have been accurately measured. The author determined the extinction coefficient of pyrene in 30% acetonitrile in this way: the mass of pyrene was measured with an analytical balance and dissolved in 100% acetonitrile using a volumetric flask (to millimolar concentration). Then, the sample was diluted to micromolar concentration in 30% acetonitrile, using a volumetric flask again to precisely control the volume. Then, the absorption spectrum was measured. The process was repeated three more times and the absorbance versus concentration data was fit to a line,

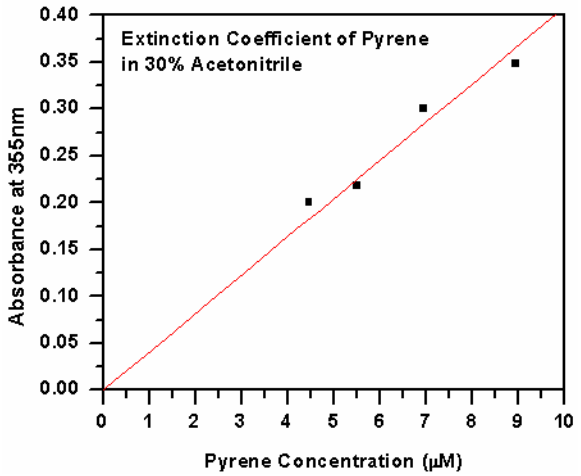


Figure 1.7: Extinction Coefficient of Pyrene. The measured absorbance at 355 nm is plotted versus the known concentration of four independent pyrene samples. The square points are the measured absorbances for the samples. The red line is the best fit line to these points.

the slope of which gave the extinction coefficient of pyrene in 30% acetonitrile,

$\varepsilon = 40{,}900 M^{-1} cm^{-1}$ (Figure 1.7).

B. Steady-State Fluorescence Spectroscopy

Emission spectra are measured in spectrofluorometers, or spectrofluorimeters. The distinction lies in whether the instrument is also designed to measure time resolved data. Since instruments made specifically for the collection of time resolved data are discussed below, here the basic design of a spectrofluorimeter (measures steady-state values) is discussed. Fluorimeters also come in commercially available benchtop models, and are composed of only a few more components than spectrophotometers. A schematic of a fluorimeter is shown in Figure 1.8. Fluorimeters have a light source, an excitation monochromator, a sample chamber, an emission monochromator, and a detector. A typical light source is a xenon or mercury arc lamp; together with the excitation monochromator this allows the user to measure emission spectra at various excitation wavelengths, and also from fluorophores that absorb in various regions of the spectrum, e.g. Cy3 and Cy5. The emission monochromator is placed at 90° to the line from the excitation monochromator to the sample chamber in order to reduce the excitation light that reaches the detector—it may be scattered towards the detector when the emission monochromator is set to the excitation wavelength. The excitation light that enters the sample cell first encounters a beam splitter, which splits off a small amount of light (about 4%[70]) to a reference cell. A reference solution is needed to correct for variations in the lamp intensity with wavelength. A good reference solution is highly fluorescent, absorbs all incident light over the wavelength region the fluorimeter is used for, and has an emission peak independent of the wavelength of excitation. The emission intensity of

this solution will vary if the power of the incident light varies; by dividing the sample's fluorescence intensity by the reference's fluorescence intensity the instrument can correct sample spectra for power variations. Such reference solutions are called quantum counters.

The most common detector used for steady state fluorimetry is the photo multiplier tube (PMT). PMTs consist of a photocathode, a photosensitive thin film of

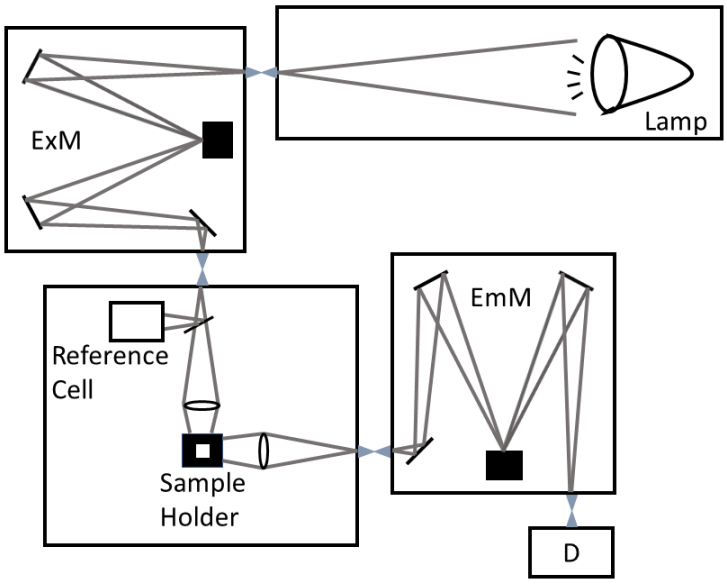


Figure 1.8: Schematic of a Fluorimeter. This schematic is a representation of the fluorimeter used for much of the work in this dissertation. The grey lines show the path of the light, while the light blue "bow-ties" represent optics allowing the light to pass from section to section of the instrument. The excitation and emission monochromators are represented by "ExM" and "EmM", respectively. The detector is represented by "D".

metal that releases electrons in response to incident photons. The photocathode's electron emission efficiency is dependent upon the incident wavelength; the metal used must be appropriate (according to the photoelectric effect) for the emission region of the fluorophore(s) used. PMTs are available in the UV, visible, and near-IR regions. The emitted photoelectron is then accelerated via an electric field towards a series of

dynodes—electrodes which eject electrons upon impact. The photoelectron will produce about five to 20 electrons upon collision with the first dynode[70], which will proceed towards the next dynode, and so on, for about eight to 14 dynodes[70-72]. Each dynode is held at a voltage more positive than the previous electrode to accelerate the generated electrons forward. After the last dynode the single photoelectron (generated from a single photon) has become 10^5 to 10^8 electrons[70, 71]—a highly amplified current pulse that arrives at the anode. This current can be detected in analog or photon counting mode. Analog mode records an average of the current pulses allowing a greater dynamic range of signal to be detected, which can be adjusted by adjusting the voltage on the PMT, but the signal-to-noise ratio (SNR) for weak signals can be low. In photon counting mode a discriminator (an electronic component) is set to a predetermined current above which it produces an output pulse. For signals below that current no output is produced. This provides a higher SNR than analog detection for very weak signals. In PMTs noise may come from electrons produced within the dynode chain (not from a photoelectron produced at the first dynode), which would cause a signal smaller than the discriminator's predetermined current, thus allowing the noise to be undetected. Photon counting mode, however, is unsuitable for high signals due to the phenomenon of "pulse pile up"; it takes approximately 5 ns for an amplified signal to reach the anode[70]. During this time, if another photon arrives at the photocathode, the PMT is unable to distinguish the signal from the two photons.

Fluorimeters are used to measure steady-state emission and excitation spectra, as well as the steady-state anisotropy. Emission spectra are measured with a fixed excitation wavelength, while the emission monochromator varies the emission

wavelength. Conversely, for excitation spectra the excitation monochromator varies the excitation wavelength and the emission monochromator is fixed. For reasons described in the previous section, emission spectra are usually independent of excitation wavelength. Excitation spectra—theoretically expected to look just like absorption spectra—and emission spectra are impacted by fluctuations in the lamp intensity (which the quantum counter may not be able to perfectly correct for), transmission efficiency of the monochromators, and optical density of the sample (reabsorption of emitted light may occur at high concentrations).

I. Steady-State Fluorescence Anisotropy

Fluorescence anisotropy is a measure of a fluorophore's rotational mobility. The probability of a molecule absorbing incident light (P_A) is dependent upon the angle (θ_A) between the molecule's transition dipole moment and the polarization of the light's electric field (Equation 1.23). After absorption the molecule remains in the excited state

$$P_A \propto \cos^2(\theta_A) \tag{1.23}$$

for the duration of its excited state lifetime. During this time the molecule is undergoing Brownian motion in solution allowing it to change orientation. For the case where the absorption and emission transition dipole moments are parallel—absorption to and emission from the S_1 state, for example—this motion causes the radiation to be emitted in a different orientation. Other sources of depolarization include non-parallel absorption and emission transition dipole moments, torsional vibrations, and energy transfer, e.g., emitted light from one molecule could be re-absorbed by another before finally being re-emitted and detected. For samples without energy transfer and parallel transition

moments anisotropy is a measure of how much the molecule has moved during its excited state lifetime, and is determined from a measure of the emitted light's polarization.

Steady-state anisotropy is calculated from four measurements. The intensity of horizontally and vertically polarized emission from vertically polarized excitation light, and the G-factor—a ratio of horizontally and vertically polarized emission from horizontally polarized light (Equation 1.24), where r is the anisotropy, G is the G-factor, and I is the intensity where the first subscript refers to the excitation polarization and the second refers to the emission polarization. Anisotropy measurements require the use of

$$r = \frac{I_{VV} - GI_{VH}}{I_{VV} + 2GI_{VH}} \qquad G = \frac{I_{HV}}{I_{HH}} \tag{1.24}$$

polarizers, which may be inserted into the sample chamber after the excitation and before the emission monochromator. The transmission efficiency of monochromators is highly dependent on the polarization of the light; the purpose of measuring the G-factor is to compensate for any differences in transmission of vertically versus horizontally polarized

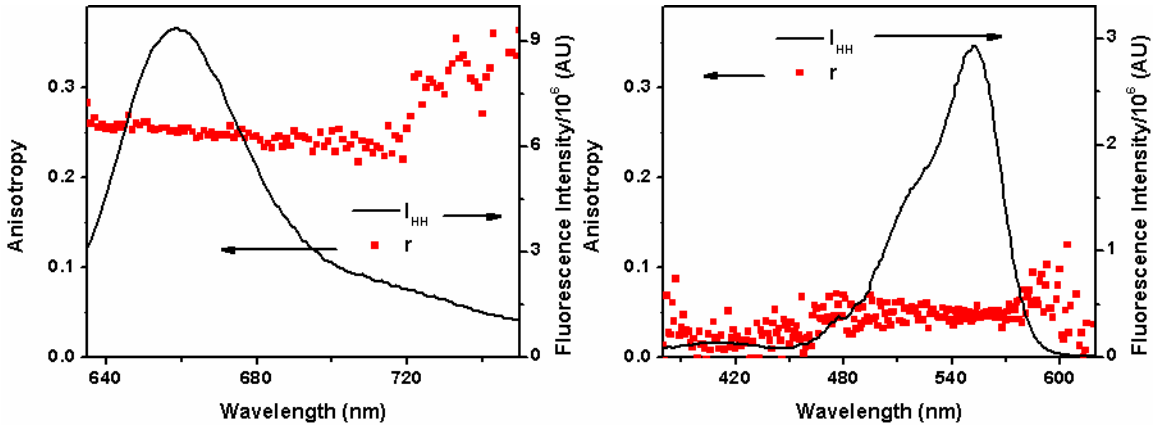


Figure 1.9: Example of Steady State Anisotropy. The emission spectra (I_{HH}, black trace) and anisotropy (red points) of Dy630-dsDNA and tetramethylrhodamine (TMR) are shown in the left and right panels, respectively.

light. In the left panel of Figure 1.9, the emission spectrum of Dy630-dsDNA (I_{HH}) is

shown along with the steady-state anisotropy. It's important to notice that the anisotropy is nearly constant for the transition (645 nm – 675 nm), but varies wildly outside of it (720 nm onwards), likely an artifact of the low fluorescence signal at these wavelengths. Hence, for time-based measurements, when the anisotropy is monitored over a period of time, one should choose an emission wavelength within this flat region.

The value of anisotropy can range from -0.2 (for perpendicular transition moments) to 0.4 (parallel transition moments). The anisotropy measured in Figure 1.9 is the average anisotropy, averaged over the excited state lifetime. Using time-resolved measurements the change in the anisotropy can be observed during the excited state lifetime. For parallel transition moments the anisotropy can be observed to decrease from 0.4 as the fluorophore undergoes motion during the excited state lifetime. Similarly, for perpendicular transition moments the anisotropy will increase from -0.2. Time-resolved experiments allow the measurement of the fundamental anisotropy, r_0, the value of anisotropy in the absence of molecular motion. For instance, Cy3B has an r_0 of 0.38, meaning the absorption and emission transition moments are nearly, but not perfectly, parallel; Cy3B's anisotropy decreases from 0.38 with a rotational correlation time of 380 ps[34]. A measured fundamental anisotropy can be used to calculate the angle between the relevant transition moments, α, using Equation 1.25. For the same absorption and emission transition, larger molecules (such as DNA and proteins) will have a greater

$$r_0 = \frac{2}{5}\frac{3\langle\cos^2(\alpha)\rangle - 1}{2} \tag{1.25}$$

anisotropy as they are bulkier and move slowly; the angle between the absorption and emission transition dipoles will increase slowly allowing most of the absorbed light

(vertically polarized) to be emitted in vertical polarization. For small, highly mobile molecules (organic fluorescent probes) the transition dipole will have rotated much from the absorption dipole, thus emitting mostly horizontally polarized light. This is illustrated in Figure 1.9, where in the right panel the anisotropy values for tetramethylrhodamine—a small organic probe—free in solution are much lower than for Dy630 conjugated to DNA (left panel).

C. Time-Resolved Fluorescence Spectroscopy

The anisotropy measured in a spectrofluorimeter is an average value, meaning it is the average anisotropy of the sample over its fluorescence emission lifetime. To measure the time-dependent anisotropy, as well as the lifetime, the time-correlated single photon counting (TCSPC) technique is used. TCSPC utilizes a pulsed laser for excitation and detects 1% or less of emitted photons; the time from laser pulse to emitted photon detection is measured and stored in a histogram of emission times. The electronics involved in TCSPC measurements, and a typical experimental setup, will be discussed later on. The rate of change of the excited state population is described by the differential equation[73] shown below (Equation 1.26), where $n(t)$ describes the excited state population and k_{all} is the rate of deactivation of the excited state via all possible routes.

This $\frac{dn(t)}{dt} = -k_{all}n(t) \;\; k_{all} = \frac{1}{\tau}$ (1.26)

observed deactivation rate, k_{all}, is the inverse of what is called the lifetime, τ, discussed above. The solution of Equation 1.26 gives the population of the excited state over time (Equation 1.27), which is proportional to the fluorescence intensity (Equation 1.28). The

$$n(t) = n_0 \exp(-\frac{t}{\tau}),\ n(0) = n_0 \tag{1.27}$$

histogram obtained during the experiment (frequency of occurrences versus time to emission) is fit to Equation 1.28 to extract τ. A single exponential intensity decay is

$$I(t) = I_0 \exp(-\frac{t}{\tau}) \tag{1.28}$$

typical of small, unbound fluorophores, but for dyes conjugated to proteins or DNA a multi-exponential fit may be required (Equation 1.29), where the contribution of each lifetime to the intensity is weighted by its fraction, α_i. The average lifetime, $\langle\tau\rangle$, is calculated from the component lifetimes and their weights (Equation 1.30).

$$I(t) = \sum_{i=1}^{m} \alpha_i \exp(-\frac{t}{\tau_i}),\ \sum_{i=1}^{m} \alpha_i = 1 \tag{1.29}$$

$$\langle\tau\rangle = \sum_{i=1}^{m} \alpha_i \tau_i \tag{1.30}$$

The time-dependent anisotropy can be calculated from measurements of the intensity decays, $I_{VV}(t), I_{VH}(t)$, and the G-factor, and Equation 1.24. The resulting anisotropy decay can be described by Equation 1.31, where $r(t)$ is the anisotropy as a function of time, r_0 is the fundamental anisotropy value (r_i is the contribution to the

$$r(t) = r_0 \exp(-\frac{t}{\theta}),\ r(t) = \sum_{i=1}^{m} r_i \exp(-\frac{t}{\theta_i}) \tag{1.31}$$

fundamental anisotropy value for each component in the sample), and θ is the rotational correlation time (θ_i is the rotational correlation time for each component). The rotational correlation time is the time it takes for the anisotropy to decrease to $1/e$ of its initial

value; it is greater for larger molecules, such as DNA and proteins, than for small fluorophores for reasons discussed above. Anisotropy data can also be fitted to determine the initial anisotropy, which will not necessarily equal to the fundamental anisotropy due to instrumental time resolution limits; although highly viscous solvents can be used to slow down molecular motion to measure r_0.

The average anisotropy, $\langle r \rangle$, which is what Equation 1.24 calculates when measuring the steady-state intensities in a fluorimeter, can be calculated from time-dependent data using Equation 1.32. The value from Equation 1.32 should equal what is measured in a steady state experiment. A similar relationship exists for the lifetime (Equation 1.33), but it does not relate to steady-state measurements, it is just a mathematical average of the lifetime of an excited state.

$$\langle r \rangle = \frac{\int_0^\infty r(t)I(t)dt}{\int_0^\infty I(t)dt} \tag{1.32}$$

$$\langle \tau \rangle = \frac{\int_0^\infty tI(t)dt}{\int_0^\infty I(t)dt} \tag{1.33}$$

The equipment requirements for TCSPC measurements are numerous and complex[74]. Today, lasers are the most common excitation source, and so-called "white lasers" are now available: white lasers provide monochromatic light over a wide range of wavelengths, accommodating for those studying fluorophores absorbing from the blue to the red and everywhere in between. There are two stringent requirements for lasers. First, they must have picosecond or shorter pulse duration as this determines the time

resolution of the instrument. Second, the repetition rate must be such that the time between excitation pulses is long enough for the excited state molecule to deactivate. For instance, Cy3B has a lifetime of 2.4 ns, and for a measurement accuracy of 1%, the pulse interval must be about 11 ns, or a 91 MHz repetition rate. The laser used to collect data presented here has a 12MHz repetition rate (much better measurement accuracy). Although the laser pulse rate is high, the actual photon count rate must be much lower to avoid a phenomenon known as "pulse pile-up"[73, 74]. The electronics used for TCSPC do not allow the detection of more than one photon from a single excitation pulse; even the best electronics may have "dead times" in the hundreds of nanoseconds, much longer than the fluorescence lifetime of most dyes. Pulse pile-up causes the photon time arrival histogram to be skewed to shorter times: since emission is a stochastic process governed by Equation 1.28 it follows that after excitation there are more photons emitted from short-lived excited molecules than longer-lived ones. To avoid pulse pile-up the photon count rate is adjusted to be 2% of the pulse rate or less (a 2.4×10^5 count rate for the 12 MHz repetition rate laser). This ensures that the probability of two photons or more arriving at the detector per excitation pulse is negligible, and that the relative error in photon counts is less than 1%[74]. The setup used for experiments discussed here uses a maximum photon count rate of 1.2×10^4, which is 0.1% of the pulse rate. Intensity decays are collected until the most frequent photon detection time (the peak of the histogram) reaches 10^4 counts. For the Cy3B sample to reach 10^4 counts at maximum a total of about 5.8×10^6 photons are collected, which at the count rate mentioned takes about 10 minutes.

The timing electronics are the most complicated part of any TCSPC setup. The

experiment begins with the simultaneous generation of an electrical (from the trigger) and optical (from the excitation source) pulse. The electrical pulse travels to a constant function discriminator (CFD) and a time-to-amplitude converter (TAC). These components function as the START and timer of the experiment. The CFD determines the arrival time of the electrical pulse, while the TAC, which contains a charge capacitor, measures the time elapsed since the START signal. The TAC's capacitor has a linear relationship between voltage accumulated and time, the greater the charge accumulated the more time has passed. The optical pulse, meanwhile, travels to the sample. The laser pulse may travel through several optics before reaching the sample, for example a waveplate to ensure the light is vertically polarized, a filter to ensure monochromatic excitation light, and a focusing lens. Fluorescence from the sample passes through additional optics: an aperture to ensure the photon count rate is much less than 1% of the optical pulse rate, a filter to block out stray excitation light, and a polarizing filter set at an appropriate angle for intensity or anisotropy measurements. For greater control over detection of emission wavelength a monochromator may be used. The detector, a PMT, sends an electrical signal to another CFD, timing the STOP signal, which is sent to the TAC stopping the charge increase on the capacitor. The TAC sends an electrical signal, proportional in amplitude to the voltage in the capacitor, to an analogue-to-digital converter (ADC), which converts the voltage to a time in nanoseconds (the lifetime of the excited state for the photon from that particular molecule). This time value is sent to a data storage device (a computer); collection of these voltage signals from many photons results in the histogram of decay times, which can be fit to extract the mean lifetime of the sample.

One problem with the description above is the operational limitation of the TAC. Before the TAC can accept a new START signal it must be reset to zero; the TAC may operate at a frequency below the repetition rate of the laser, causing many START signals to be missed. To remedy this situation most TCSPC setups operate in "reverse" mode. The emission photon—the STOP signal—is routed to the TAC input for the START signal, while the STOP input receives the signal from the trigger. This creates a "negative" histogram where the photons with "short" times actually arrived at longer times after the excitation pulse. The data processing program then transforms this data into the proper form.

The most crucial aspect of the data analysis is to properly deconvolute the observed intensity decay of the sample from the instrument response function (IRF), the time profile of the excitation pulse, to get the true intensity decay. This is necessary because the excitation pulse has a finite width; while molecules excited by the earlier photons are already emitting, other molecules are still absorbing photons from the tail of the excitation pulse. The IRF may be measured from scattered excitation light (from a colloidal silica solution, like Ludox, or by dissolving coffee creamer in water). The software program used to fit the data must be able to deconvolve the decay from the IRF.

The polarizing filter placed in the emission pathway of the instrument needs to be set at the correct angle for the measurement. Anisotropy measurements require separate measurements of the $I_{VV}(t)$ and $I_{VH}(t)$ intensity decays, easily accomplished by setting the emission polarizer to 0° and 90° to the polarization direction of the laser (typically vertical). An example of the $I_{VV}(t)$ and $I_{VH}(t)$ decays for Cy5 is shown in the left panel of Figure 1.10. Measurement of the G-factor, to compensate for the uneven transmission

of polarized light through the monochromator, is done using the tail-matching method (not by changing the polarization of the excitation light). In the tail-matching method, the $I_{VV}(t)$ and $I_{VH}(t)$ decays are measured for a standard probe—Cy3B for the green-absorbing region and Cy5 for the red-absorbing region. Then, this data is plugged into the formula in Equation 1.34 (the time-dependent version of Equation 1.24), and an

$$r(t) = \frac{I_{VV}(t) - GI_{VH}(t)}{I_{VV}(t) + 2GI_{VH}(t)} \tag{1.34}$$

arbitrary value of G is chosen. As discussed above, small molecules will have low average anisotropy values, and, correspondingly, their time-dependent anisotropy will decay rapidly to zero. As such, for the standard probes, at long times the $I_{VV}(t)$ and $I_{VH}(t)$ decays will be equal to zero, which means the numerator in Equation 1.34 is zero. Thus, the value of G is adjusted until the tail of the probe's time-dependent anisotropy

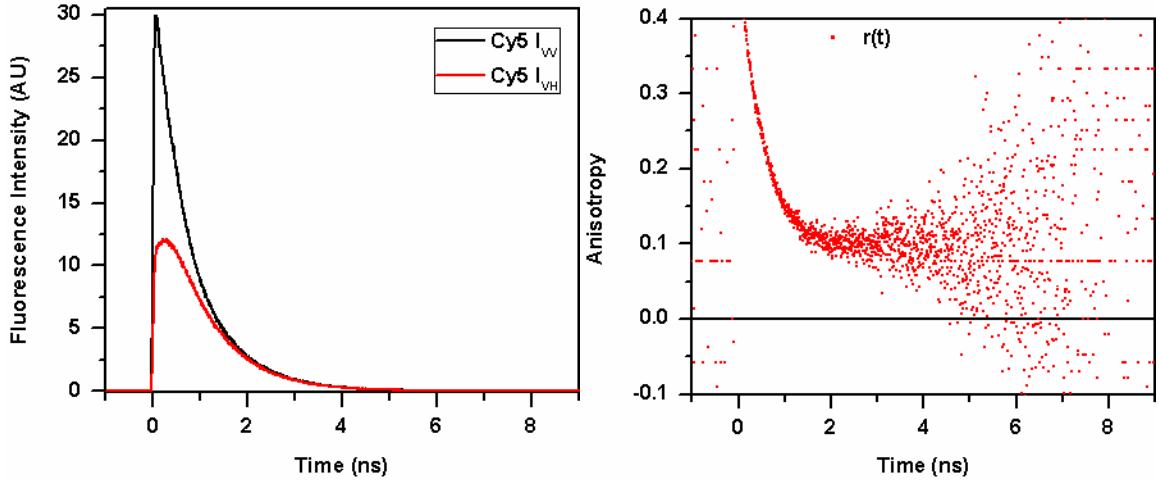


Figure 1.10: Time-resolved Anisotropy of Cy5. The left panel shows the intensity decays of Cy5 measured with the emission polarizer set at 0° (black trace) and 90° (red trace). The right panel shows the anisotropy calculated for an arbitrary value of G. The true value of G is determined when the tail-end of the anisotropy rests along the horizontal line at zero anisotropy.

comes to zero. This value of G is then used to construct $r(t)$ for all samples measured at

the same excitation and emission wavelength. Figure 1.10 (right panel) shows the anisotropy of Cy5 calculated for an arbitrary value of G, which will be adjusted until the tail-end of the anisotropy is at zero.

The measurement of fluorescence lifetime must be done with the emission polarizer set to the magic angle to eliminate the effects of depolarization[75]. As shown in Figure 1.10 (right panel), the anisotropy changes dramatically during the fluorescence lifetime, and setting the polarizer to the magic angle ensures the fluorescence intensity measured is proportional to the total intensity emitted. By convention, emission intensity is characterized with respect to the polarization of the exciting electric field. For an excitation beam that is polarized vertically (along the z-axis in the laboratory frame) the fluorescence with an electric field vector parallel to excitation is called I_{II} (or I_Z) while the fluorescence with an electric field vector perpendicular to excitation is called I_{perp} (or I_X, I_Y). If the excitation beam's electric field is at an angle θ from the vertical the directional intensities are described by Equations 1.35. For fluorescence detection, at a $90°$ from the excitation beam to sample line, a detector placed along either axis (x or y) can detect only two components of the emission ($I_{II} + I_{perp}$), while a detector along the z-axis will only detect twice the perpendicularly polarized fluorescence ($2I_{perp}$). The total fluorescence, however, is $I_{Tot} = I_{II} + 2I_{perp}$. If a polarizer is placed before the detector at

$$\begin{aligned} I_X &= I_{II}\sin^2\theta + I_{perp}\cos^2\theta \\ I_Z &= I_{II}\cos^2\theta + I_{perp}\sin^2\theta \\ I_Y &= I_{perp} \end{aligned} \qquad (1.35)$$

an angle ϕ with respect to the z-axis, then the observed fluorescence (I_{obs}) along the x-axis, for example, is shown in Equation 1.36. Substituting the expressions from Equation

$$I_{obs} = I_Y \sin^2 \phi + I_Z \cos^2 \phi \quad (1.36)$$

1.35 and rearranging so that there are two terms corresponding to the parallel and perpendicular intensities, gives Equation 1.37. The observed intensity must equal

$$I_{obs} = I_{perp} \sin^2 \phi + (I_{II} \cos^2 \theta + I_{perp} \sin^2 \theta) \cos^2 \phi$$

$$I_{obs} = I_{II} \cos^2 \theta \cos^2 \phi + I_{perp} (\sin^2 \phi + \sin^2 \theta \cos^2 \phi) \quad (1.37)$$

the total intensity, which happens when Equation 1.38 is satisfied. For a vertically polarized excitation beam ($\theta = 0°$) this gives an angle, ϕ, of $54.7°$ for the emission polarization filter. This is known as the magic angle in fluorescence polarization measurements.

$$2\cos^2 \theta \cos^2 \phi = \sin^2 \phi + \sin^2 \theta \cos^2 \phi \quad (1.38)$$

D. Transient Absorption Spectroscopy

To measure the lifetime, and hence the deactivation rate, of the triplet state the technique of transient absorption (TA) spectroscopy is used. In fact, this technique is used to measure the lifetime of any species present that has a lifetime longer than the fluorescent lifetime of the molecule. In TA spectroscopy the fluorophore is excited by a pulsed laser source populating the first singlet excited state. From here, the fluorophore relaxes to the ground state; most molecules will fluoresce, however, some will enter into longer lived states, e.g. the triplet state. The principle of this technique lies in the fact that these transient states also absorb light. The sample under study is illuminated with a

lamp, which excites the transient species into higher energy transient states. By measuring the absorption of the sample before and after the initial laser pulse one can detect the presence of these transients.

Transient absorption spectroscopy employs a pulsed laser source operating at a repetition rate that allows the fluorophore to relax to the ground state before another excitation pulse. A schematic of the transient absorption instrument used for measurements in this dissertation is shown in Figure 1.11. The probe source is typically a broad spectrum lamp. The excitation laser will be set to the maximum absorption wavelength of the sample, and it should illuminate as much as possible of the sample in the cuvette—the higher the population of the excited state, the more transient will be produced. The beam from the lamp must overlap the excitation beam closest to its entrance (the two light sources enter the sample at 90° to each other). This configuration maximizes the transient signal as the population of excited molecules decreases with the laser beam's distance inside the sample; molecules closest to the laser beam's entrance absorb and decrease the intensity encountered by the remaining molecules. The probe source must be able to monitor many wavelengths in order to find the absorbing transient, hence the need for a lamp. The transient absorption is monitored one wavelength at a time through the use of monochromators and/or filters. A monochromator placed after the lamp, or a set of filters, may be used to select the probe wavelength. Neutral density filters may also be used to prevent sample photobleaching from the high lamp intensity. A monochromator must be used after the sample to select the monitoring wavelength, and more importantly, to reject the lamp excitation light (filters that allow only the region around the probe wavelength to pass may also help to reduce excitation light and stray

fluorescence). Lenses are placed as needed to focus the lamp light into the cuvette and into the monochromator entrance. A photodetector is placed after the detection monochromator; the observed signal is displayed on an oscilloscope and passed to a computer for analysis. In certain instances, the intensity from the monochromator may be too great for the photodetector (as was the case for the author's measurements), in that case an attenuator is used to decrease the magnitude of the signal to the detector.

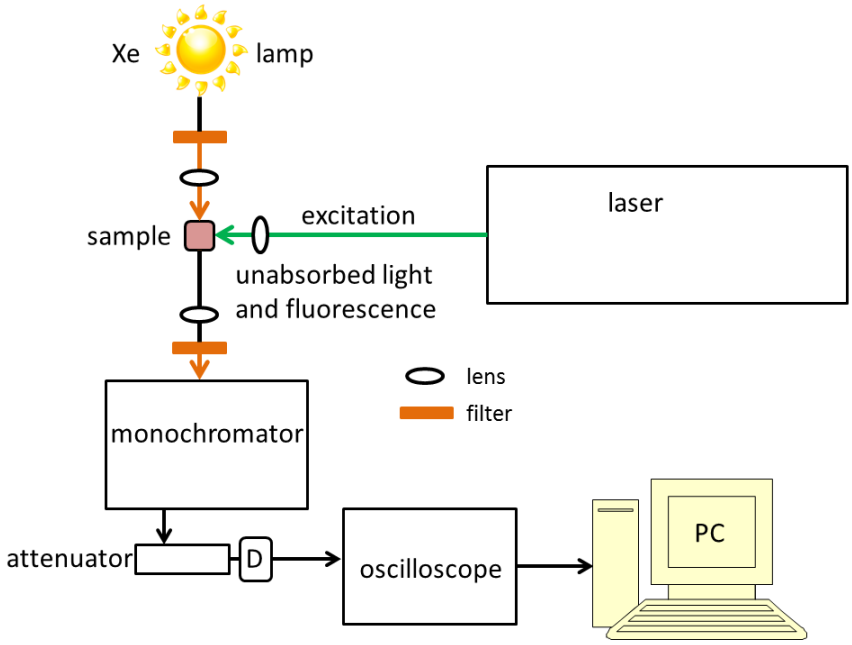


Figure 1.11: Schematic of Transient Absorption Equipment. This figure shows a representation of one of the TA setups used for measurements in this dissertation. A detailed explanation of components is in the text. The filters show the selection of probe wavelength. The "D" signifies the photodetector.

The photodetector used must have a time resolution short enough to observe the transient signal immediately after excitation and long enough to observe the signal decay to zero (depending on the type of transient observed the signal may last from nanoseconds to milliseconds). A particular concern is the contamination from the pulsed laser source and fluorescence. At probe wavelengths close to the excitation wavelength

the detection monochromator may not effectively filter out scattered light from the excitation source; similarly, when probing wavelengths that overlap with the emission spectrum of the fluorophore there is no way for a single monochromator to separate the fluorescence from the unabsorbed lamp light. Such contamination is seen in Figure 4a; the kinetic trace at 630 nm possesses a "spike" in signal at short times due to the strong fluorescence of Cy3B. The fluorescence lifetime of Cy3B is 2.4 ns, however, the photodetector used is unable to recover from the saturating intensity and the effect of fluorescence can be seen on the microsecond timescale.

The signal observed in TA spectroscopy is a difference in absorption of the transient state before and after the excitation pulse[76]. The intensity detected by the photodetector is described by Equation 1.39 (following the treatment of absorption spectroscopy in Equations 1.19 and 1.22), where $I(t,\lambda)$ is the intensity detected as a function of time and probe wavelength, $I_{in}(\lambda)$ is the intensity entering the sample (it varies with wavelength based on the characteristics of the lamp), and $A(t,\lambda)$ is the absorbance as a function of time and wavelength. Before the excitation pulse there is no population in the excited state, and thus, no, or very little, population in the transient state to absorb the lamp light; the initial absorbance of the transient(s) is represented by $A_0(\lambda)$. The excitation pulse populates any transient states present causing a change in the absorbance of the lamp light, $A_0(\lambda)+\Delta A(t,\lambda)$. Equation 1.39 may be simplified by recognizing that the first term represents the initial detected intensity, $I_0(\lambda)$, yielding

$$I(t,\lambda)=I_{in}(\lambda)10^{-A(t,\lambda)}=I_{in}(\lambda)10^{-A_0(\lambda)-\Delta A(t,\lambda)} \quad (1.39)$$

$$I(t,\lambda)=I_0(\lambda)10^{-\Delta A(t,\lambda)} \quad (1.40)$$

Equation 1.40, which is Equation 1.41 in logarithmic form. The intensity may also be described as undergoing a change, $I(t,\lambda) = I_0(\lambda) + \Delta I(t,\lambda)$, and substitution of this relationship leads to Equation 1.42, which relates the differential absorbance to the observed change in intensity. The differential absorbance data is two-dimensional and

$$\Delta A(t,\lambda) = -\log\left(\frac{I(t,\lambda)}{I_0(\lambda)}\right) \tag{1.41}$$

$$\Delta A(t,\lambda) = -\log\left(1+\frac{\Delta I(t,\lambda)}{I_0(\lambda)}\right) \tag{1.42}$$

may be studied at either fixed time or fixed wavelength. Following the excitation pulse the population in the transient state is probed, i.e. excited. As the transient relaxes back to the ground state the population that may be excited to higher energy transient states decreases. Thus, the change in the intensity detected is high right after the laser pulse, and slowly decreases to zero over time (the differential absorbance starts high and decreases to zero). This is represented in Figure 1.12 below (left panel), which shows the differential absorbance time (or kinetic) traces of Cy3B with Mn^{2+} at 630 and 550 nm. The excitation pulse occurs at time zero populating the triplet state—which absorbs at 630 nm—causing a large increase in absorbance by the triplet at 630 nm, hence the large positive signal. The triplet state molecules eventually relax to the ground state of Cy3B decreasing the triplet state population and, hence, the absorbance at 630 nm. The large negative differential absorbance at 550 nm is due to the "photobleaching" of Cy3B at its ground state absorption wavelength. The excitation pulse depletes the ground state population, thus when the probe lamp is set to wavelengths where the ground state dye absorbs the population after the excitation laser is less than before making the differential

absorbance negative. This is referred to as "photobleaching". A transient absorption spectrum is made from kinetic traces of many wavelengths; the differential absorbance at a particular time after the laser pulse is plotted versus the probe wavelength of that kinetic trace resulting in the right panel of Figure 1.12. Here, the entire transient absorption spectrum is shown at four different time snapshots after the pulse.

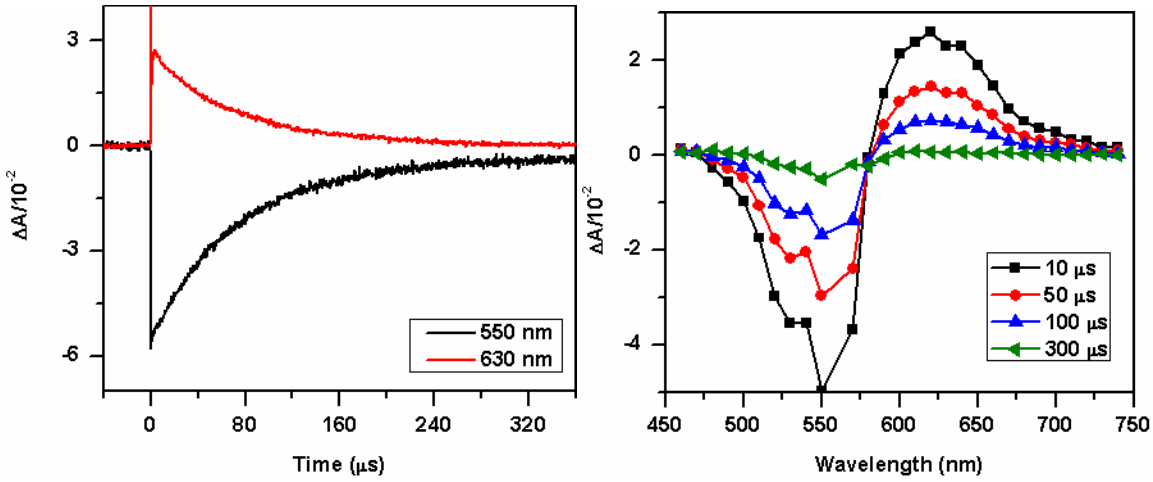


Figure 1.12: Examples of Transient Absorption Data. This is data collected for Cy3B in the presence of Mn^{2+}. The left panel shows kinetic traces at 550 nm (black) and 630 nm (red); they represent the ground state repopulation and triplet state depletion, respectively. The right panel shows the difference spectrum of Cy3B/Mn^{2+} at four different time snapshots.

A variation on transient absorption is pump-probe spectroscopy, which embodies the same concept on much shorter (picosecond) timescales. This is accomplished by using a pulsed laser source for the probe light—femtosecond lasers of pulse duration from 20 to 200 fs are ideal. In fact, the same laser can be used to generate both pump and probe pulses: the initial pulse (at the excitation wavelength) is split into two beams, one of which serves as the pump, while the other is passed through additional optics for white continuum generation and serves as the probe. Bandpass filters are used for probe wavelength selection, and a delay line is installed along the pulse beampath to control the

time separation between pump and probe pulses. Pump-probe instruments require only two photodetectors to monitor the probe beam intensity before and after the sample; the delay line eliminates the need for time-resolved detection.

E. Fluorescence Correlation Spectroscopy

The aforementioned techniques provide measurements of "bulk" variables, meaning any variation present on the molecular level are averaged out. In contrast, fluorescence correlation spectroscopy (FCS) is a single molecule technique. While samples for bulk measurements are on the micromolar concentration scale (involving about 10^{13} molecules) FCS requires concentrations no greater than nanomolar; the source of the intensity will be from the diffusion of 10 to 100 molecules through the observation volume. At lower concentrations, at picomolar values, the intensity will result from the passage of one molecule through the observation volume. Other single-molecule techniques, such as total internal reflection fluorescence (TIRF) spectroscopy, require that molecules be immobilized so that they may be observed one at a time. TIRF spectroscopy will be discussed in detail in Appendix III.

The ability to detect fluorescence from only a handful of molecules comes from restricting the observation volume of the sample. In FCS the exciting laser beam is directed with optics into an objective lens that focuses the laser to a diffraction-limited spot within the sample. A schematic of an FCS instrument is shown in Figure 1.13. The sample is placed onto a coverslip inside of a perfusion chamber (to limit evaporation during measurement) that fits about 50 μL; the objective lens is beneath the sample stage and is raised until the laser is focused inside. The illuminated volume is on the order of a

few femtoliters. The fluorescence passing through the objective is reflected by a dichroic (to exclude excitation light) towards a confocal pinhole and optics that focus onto the detector. The confocal pinhole excludes fluorescence from above and below the focal plane, limiting the volume; a typical pinhole is 50 microns in diameter.

While it is possible to use PMTs for detection most FCS setups use single-photon counting avalanche photodiodes (SPC-APDs). The primary benefit of SPC-APDs over PMTs is their high quantum efficiency, up to 60% in the visible compared to 20% for PMTs. In addition, such detectors have low dark count rates, similar to cooled PMTs,

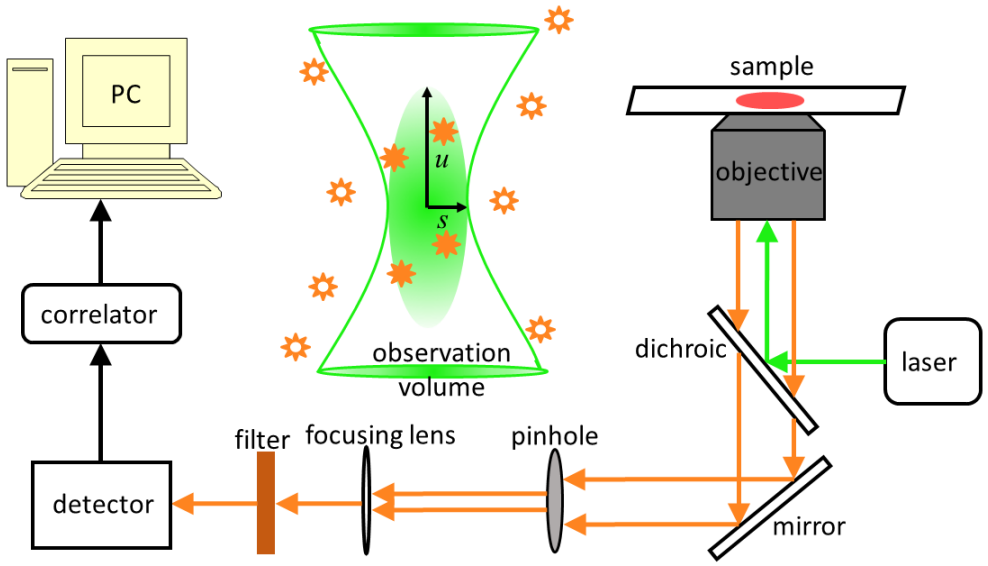


Figure 1.13: Schematic of an FCS Instrument. The major components of an FCS instrument are shown. Light from the laser is directed by the dichroic into the objective, which focuses the light onto the sample. Fluorescence from the sample is collected by the same objective and directed by the mirror through a pinhole, a focusing lens, and a filter onto the active area of a detector. From the detector the signal goes to a correlator and a PC for analysis. The observation volume is shown in the center of the figure; the conical outline represents the outline of a focused laser. The oval, with dimensions indicated by "u" and "s" represents the Gaussian shape from Equation 50.

even while operating at room temperature. One drawback to SPC-APDs is the very small

active area of the sensor, just under 200 microns in diameter. PMTs, for comparison, have photocathodes with up to 1 cm^2 active area. The confocal pinhole and additional optics help focus the fluorescence to the small sensor area, which, due to its size, acts as an additional pinhole, only detecting the light from the chosen focal plane.

With the confocal optics the excitation source creates an illumination volume the shape of an elongated ellipsoid. Molecules within the laser beam are excited and emit fluorescence. The fluorescence intensity fluctuates as molecules drift in and out of the observation volume. The theory underlying FCS is built on Poisson statistics. The Poisson equation states that the probability, $P(n)$, of finding n molecules in the observation volume depends on n and the average number of molecules in the observation volume, N, i.e. the concentration, as shown in Equation 1.43. For a 1 nM

$$P(n) = \frac{N^n}{n!} e^{-N} \tag{1.43}$$

solution, and an observation volume of 1 fL, the average number of molecules is 0.6, and $P(0) = 0.55$, $P(1) = 0.33$, and $P(2) = 0.10$. For values of $n \geq 3$, the probability of finding three or more molecules in the observation volume simultaneously is even smaller. Thus, for 88% of the time there will only be 1 molecule or less in the observation volume. For a 10 nM solution, the average number of molecules is 6, and 89% of the time there will be between 3 and 10 molecules in the observation volume. As the average number of molecules increases the observation volume will have more and more molecules present at any one time. The more molecules are in the observation volume the smaller the increases/decreases (fluctuations) in fluorescence intensity as molecules enter/exit the laser beam. The standard deviation of a Poisson distribution is

$\sqrt{n}$, and when concentrations are too high, the intensity fluctuations are no longer detectable. Thus, FCS is best suited for dilute solutions, from 10 pM to about 50 nM.

The direct observable in FCS experiments is the fluorescence intensity, $F(t)$, which is compared with the intensity at a later time, called the lag time τ, $F(t+\tau)$. How the two intensity values compare, whether they are similar or different, depends on how quickly the fluorophore is diffusing. Mathematically, the autocorrelation function is used to quantitate any similarity; the autocorrelation is calculated from the average value of the product of the two intensity values (Equation 1.44), or from the integral of the products over the data collection time, T. The fluorescence intensity can be written in terms of its average value, $\langle F(t)\rangle$, and the fluctuations about the average, $\delta F(t)$, in

$$R(\tau) = \langle F(t)F(t+\tau)\rangle = \frac{1}{T}\int_0^T F(t)F(t+\tau)dt \tag{1.44}$$

$$F(t) = \langle F(t)\rangle - \delta F(t) \tag{1.45}$$

Equation 1.45. This definition of intensity gives the autocorrelation function of the fluorescence intensity (Equation 1.46), which is normalized by the average intensity squared. Expanding the numerator gives Equation 1.47. Since the average of a sum is equal to the sum of averages, and because the average of the fluctuations is zero

$$G'(\tau) = \frac{\left\langle \left(\langle F(t)\rangle - \delta F(t)\right)\left(\langle F(t+\tau)\rangle - \delta F(t+\tau)\right)\right\rangle}{\langle F\rangle\langle F\rangle} \tag{1.46}$$

$$G'(\tau) = \frac{\left\langle \langle F(t)\rangle\langle F(t+\tau)\rangle + \delta F(t)\delta F(t+\tau) - \delta F(t)\langle F(t+\tau)\rangle - \delta F(t+\tau)\langle F(t)\rangle\right\rangle}{\langle F\rangle^2} \tag{1.47}$$

($\langle \delta F\rangle = 0$) Equation 1.47 can be simplified to Equation 1.48, where t is replaced with

zero because only the time difference, τ, between two intensity values is relevant. Depending on preference, some authors choose to ignore the one in Equation 1.48 and work only with Equation 1.49, called the autocorrelation function of fluorescence

$$G'(\tau) = \frac{\langle\langle F(t)\rangle\langle F(t+\tau)\rangle\rangle}{\langle F\rangle^2} + \frac{\langle \delta F(t)\delta F(t+\tau)\rangle}{\langle F\rangle^2} = 1 + \frac{\langle \delta F(0)\delta F(\tau)\rangle}{\langle F\rangle^2} \tag{1.48}$$

$$G(\tau) = \frac{\langle \delta F(0)\delta F(\tau)\rangle}{\langle F\rangle^2} \tag{1.49}$$

fluctuations. Physically, the fluorescence intensity is a function of the fluorophore's brightness, B, the instrument's collection efficiency function, $CEF(r)$, the excitation intensity at each position, $I(r)$, and the concentration distribution of the fluorophores, $C(r,t)$, as shown in Equation 1.50. The brightness depends on the fluorophore's excitation cross section, σ_{exc}, the fluorescence quantum yield, ϕ_f, and the instrument's efficiency of photon detection, Q, which includes the performance of the optics and filters, the solid angle of light collection, and the detector's quantum yield of detection[77]. The product of the collection efficiency function and excitation intensity is referred to as the molecular detection efficiency, or point-spread function, $p(r)$, and takes the

$$F(t) = B\int CEF(r)I(r)C(r,t)dV \tag{1.50}$$

$$p(r) = I_0 e^{\frac{-2(x^2+y^2)}{s^2}} e^{\frac{-2z^2}{u^2}} \tag{1.51}$$

mathematical form shown in Equation 1.51 when the laser focus has a Gaussian intensity profile, where I_0 represents the maximum intensity, x, y, and z are the Cartesian coordinates, and s and u are the distance from the center of the laser focus in the radial

and axial dimension, respectively, as shown in Figure 1.13. The autocorrelation for the intensity fluctuations is given in Equation 1.52, where r is the fluorophore

$$G(\tau) = \frac{B^2 \iint p(r)\, p(r') \langle \delta C(r,0) \delta C(r',\tau) \rangle dV dV'}{\left| BC \int p(r) dV \right|^2} \tag{1.52}$$

position at $t = 0$, r' is its position at $t = \tau$, and C is the mean concentration. Thus, the correlation of the concentration fluctuations needs to be determined in order to calculate the correlation functions of the intensity fluctuations. For translational diffusion the correlation of the concentration fluctuations is given in Equation 1.53, where D is the diffusion coefficient. Substitution of Equations 1.51 and 1.53 into Equation 1.52 gives the correlation function for diffusion in three dimensions (Equation 1.54); $G(0)$ is the amplitude of the function at $\tau = 0$ and it is equal to the inverse of the number of molecules (N) present in the observation volume. A fit of autocorrelation data

$$\langle \delta C(r,0) \delta C(r',\tau) \rangle = \frac{C}{(4\pi D\tau)^{3/2}} e^{-\frac{|r-r'|^2}{4D\tau}} \tag{1.53}$$

$$G(\tau) = G(0)\left(1 + \frac{4D\tau}{s^2}\right)^{-1}\left(1 + \frac{4D\tau}{u^2}\right)^{-1/2} \qquad G(0) = \frac{1}{N} \tag{1.54}$$

to Equation 1.54 provides an independent measure of the concentration as long as the observation volume is known. The shape of the observation volume is determined by $p(r)$, which is only assumed to be Gaussian. In reality, the intensity profile of the laser, and the detection optics are not Gaussian. A best estimate of the observation volume is made from the measurement of a standard solution of known concentration and diffusion coefficient. A fit to the standard's data will yield the value of the radial parameter, s, that can be used for fitting subsequent data sets. The value of the axial parameter, u, is

taken to be about five times the value of s; the fit is insensitive to the value of the axial parameter, which cannot be determined from the Levitus lab FCS setup as the laser beam has no boundary along the z-axis. The value of $G(0)$ from the standard's fit will give the number of molecules in the observation volume, and, combined with the known concentration, the true observation volume. Fits of sample data will yield N, which combined with the determined observation volume will give the concentration of the samples under study.

The correlation function, $G(\tau)$, is typically plotted with lag time on a logarithmic scale, and will decrease from its maximum value, $G(0)$, to zero as lag time increases. This is due to the decreasing similarity in fluorescence fluctuations as the fluorophore diffuses farther from its initial position; a fluorophore will fluoresce with similar characteristics when it has only moved a small distance inside the observation volume (high correlation). However, its fluorescence will have a very different pattern when it

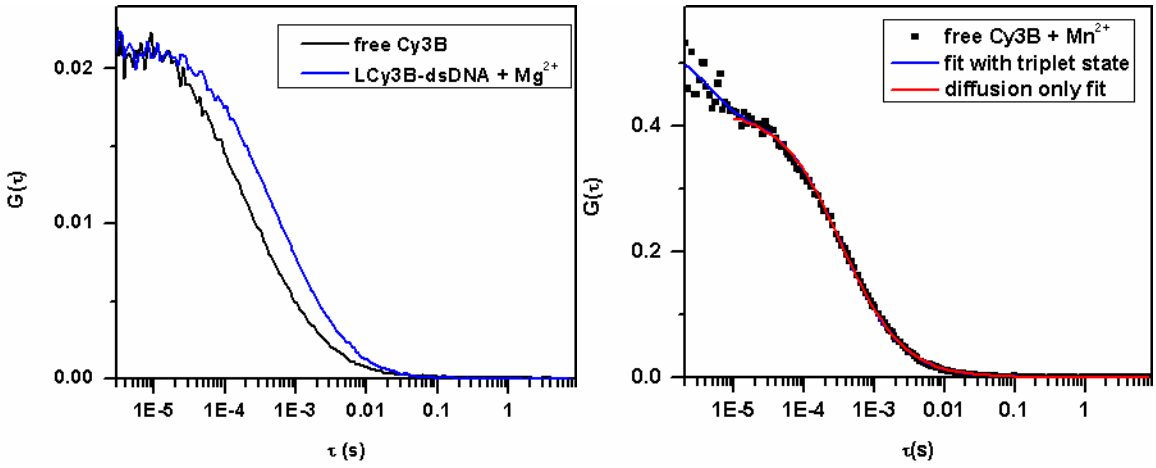


Figure 1.14: Examples of Fluorescence Correlation Spectroscopy Data. The left panel shows $G(\tau)$ for free Cy3B (black trace) and when conjugated to DNA (blue trace). The right panel shows $G(\tau)$ for Cy3B/Mn^{2+} (black points) and two possible fits to the data (blue and red traces).

has moved a great distance, for example from the center to the edge of the laser beam (low correlation). How large, and hence, how quickly a molecule diffuses will influence how rapidly the correlation decreases. An example of $G(\tau)$ for a free fluorophore, and when it is attached to DNA, is shown in Figure 1.14 below (left panel). The DNA is obviously larger, and slower, than the free Cy3B, and thus, its correlation decay is shifted to longer times.

Determination of the diffusion coefficient, D, is the goal of many FCS experiments. The diffusion coefficient is a measure of how large the fluorescent species is, and thus, how quickly it diffuses through solution. For example, in Figure 1.14 (left panel) Cy3B has a diffusion coefficient of 440 $\mu m^2 s^{-1}$[78] while for the DNA it is 195 $\mu m^2 s^{-1}$(based on the radial parameter from a fit of Cy3B's data). The diffusion coefficient is a molecular property of the sample under investigation; it can be related to the diffusion time, τ_D, via Equation 1.55. The diffusion time is the time for a fluorophore

$$\tau_D = \frac{s^2}{4D} \tag{1.55}$$

to pass through the observation volume; since τ_D depends on the size of the radial parameter it will vary from instrument to instrument. The FCS technique has been used to study the stoichiometry of oligomeric proteins: RuBisCo activase (Rca), for instance, was studied by a fellow group member[79] in order to determine the assembly mechanism. Individually labeled Rca monomers were mixed with an excess of unlabeled monomers. As monomers became dimers, hexamers, and larger units the apparent diffusion coefficient of the mixture decreased. An analysis of the change in the correlation functions allowed the concentration profiles to be determined for assumed assembly

mechanisms. Other fellow group members used FCS in single-molecule mode to study the dissociation kinetics of DNA processivity clamps[80]. In single-molecule mode the concentration of the fluorescent probe is reduced to pM levels; at such low concentrations the observation volume is empty 99% of the time (1fL volume at 10 pM concentration). When a fluorescent molecule enters the laser beam a burst of fluorescent photons is released. The β-clamp, a homodimeric protein, was labeled with two TAMRA dye molecules at the interface—one on each subunit. At such short distance from one another the dyes can form nonfluorescent dimers, which fluoresce very little or not at all when transiting the observation volume. Over time, the (protein) dimers dissociate, the dyes function as single dyes again, and more fluorescent bursts are observed.

The right panel of Figure 1.14 shows an example of an FCS decay for free Cy3B in the presence of Mn^{2+} at high laser power. Cyanines are known to have a low quantum yield of triplet state formation,[62 58] however, high excitation intensities are also known to increase the intersystem crossing rate, which is discussed below. A molecule that enters the triplet state is "dark", unable to fluoresce, and is thus, invisible in the experiment. The triplet states of cyanine dyes have lifetimes on the order of microseconds,[59, 81, 82] which is longer than the time required to diffuse through the observation volume. Therefore, the fluctuation in fluorescence intensity due to triplet state population can be observed in FCS data; since diffusion and triplet state dynamics occur on different timescales an FCS decay for a sample with a significant triplet population possess increased correlation values on the microsecond timescale as is seen in Figure 1.14 (right).

The presence of a triplet state fluctuation alters the shape of an FCS decay, which

can now be fit to Equation 1.56, where $\overline{T}$ is the average fraction of molecules in the observation volume that are in the triplet state at any one time, and τ_R is the singlet-triplet relaxation time. Equation 1.56 is merely the product of the diffusion and triplet

$$G(\tau) = G(0)\left(1+\frac{4D\tau}{s^2}\right)^{-1}\left(1+\frac{4D\tau}{u^2}\right)^{-1/2}\left(1+\frac{\overline{T}}{1-\overline{T}}e^{-\tau/\tau_R}\right) = G_D(\tau)G_T(\tau) \quad (1.56)$$

correlation functions; this is a valid simplification for the case where intersystem crossing occurs faster than diffusion and there is no change in the diffusion coefficient of the fluorophore when in the triplet state. The red and blue curves in the right panel of Figure 1.14 are the fits to the data with Equation 1.54 and 1.56, respectively. The red curve clearly does not fit the additional microsecond fluctuation; the best fit to the data (blue) is given only when using the additional terms introduced in Equation 1.56. It is important to understand that τ_R is distinct from τ_T, the triplet state lifetime introduced earlier. Equations 1.58 and 1.59 give the dependence of $\overline{T}$ and τ_R on the rate constants of photophysical processes introduced earlier and k_{01}, the rate of transition from the ground to first excited singlet state. This rate will depend on the molecule's absorption cross-section, σ, and the excitation intensity, I_{ex} (Equation 1.57). The singlet-triplet

$$k_{01} = \sigma I_{ex} \quad (1.57)$$

$$\overline{T} = \frac{k_{01}k_{ISC}}{k_{01}(k_{ISC}+k_{ISC}^T)+k_{ISC}^T(k_{ISC}+k_f)} = \frac{\sigma I_{ex}k_{ISC}}{\sigma I_{ex}(k_{ISC}+k_{ISC}^T)+k_{ISC}^T(k_{ISC}+k_f)} \quad (1.58)$$

$$\frac{1}{\tau_R} = k_{ISC}^T + \frac{k_{01}k_{ISC}}{k_{01}+k_f} = k_{ISC}^T + \frac{\sigma I_{ex}k_{ISC}}{\sigma I_{ex}+k_f} \quad (1.59)$$

relaxation time depends on both intersystem crossing rates, the excitation rate, and the

rate of fluorescence, and is thus, not the triplet state lifetime, τ_T, which depends only on the deactivation rates from the triplet state (Equation 1.2). The fraction of molecules in the triplet state, $\overline{T}$, depends on I_{ex} and explains why, in FCS, high excitation intensities make a more pronounced contribution to the correlation function from the triplet state.

The following chapters will detail the use of these techniques to the study of cyanine photophysics in various solution (Chapter 2) and protein (Chapters 3 and 4) environments.

CHAPTER TWO

CYANINE PHOTOBLEACHING AND TRIPLET BLINKING IN THE PRESENCE OF MN^{2+}

2.1 Introduction and Motivation

Occasionally, interesting photophysical phenomena are discovered during completely unrelated investigations. The photophysical study of 5-carboxytetramethylrhodamine (TAMRA) dye in the presence of Mn^{2+} was motivated by the Levitus lab's observations of fluorescence intensity fluctuations in fluorescence correlation spectroscopy (FCS) measurements of TAMRA-labeled DNA interacting with RAG proteins in a Mn^{2+} buffer.[83] The FCS data showed a sub-ms intensity fluctuation present for samples in Mn^{2+} buffer, but absent in Mg^{2+} buffer. The complete characterization of TAMRA-dsDNA in 2.5 mM Mn^{2+} buffer revealed an increased intersystem crossing (ISC) rate, which creates an increased population of the triplet—"dark"—state[83]. Once in the long lived (on the order of μs) triplet state the excited state dye has more opportunity to react with reactive oxygen species (ROS), thus decreasing the total population of dye, and, hence, its photostability. Dissolved oxygen, at a concentration of 0.29 mM at room temperature and atmospheric pressure,[84] forms the basis for formation of ROS in buffer solutions. Molecular oxygen—a triplet in its electronic ground state—can undergo energy exchange with excited fluorophores in their triplet states. This results in the ground state fluorophore and singlet oxygen, a highly reactive intermediate,[85] which is known to react with cyanine dyes at the base of the polymethine chain.[86] Hydrogen peroxide, another ROS, caused higher energy absorption bands to appear in the

absorption spectra of two long-wavelength absorbing cyanines upon irradiation—with the concomitant decrease in the dye's primary absorption band.[87] The appearance of an absorption band at short wavelengths indicates the formation of molecules with shorter chromophores that can form from the long-chain parent. Other ROS intermediates implicated in photobleaching are superoxide[88, 89] and the hydroxyl radical.[90] The hydroxyl radical can be formed in solution via the Fenton reaction: iron(II) reacts with hydrogen peroxide to produce iron(III), hydroxide, and the hydroxyl radical.[91] This reaction is doubly destructive as the hydroxyl radical reacts with hydrogen peroxide to produce superoxide. Thus, triplet states cause two problems for fluorophores as they can enable the formation of ROS and, due to their long lifetimes, can react with ROS.

To prevent the formation of ROS intermediates buffers for single molecule measurements are deoxygenated, either by bubbling argon or nitrogen through the solution or through use of an enzymatic oxygen scavenging system.[92-96] The drawback to oxygen removal is the increased lifetime of the dark, triplet state—as oxygen is a triplet quencher. An alternate pathway to triplet quenching, in the absence of oxygen, is through electron transfer reactions that form a reducing and oxidizing system (ROXS).[97-99] Once in the triplet state the dyes can be quenched by either an oxidant (to yield a radical cation, assuming the ground state is neutral) or a reductant (to yield a radical anion). In this state, the dye is again vulnerable to photobleaching reactions; depending on the fluorophore one of these three states (triplet, radical anion, radical cation) may be more prone to photobleaching. Additionally, these radical states are, like the triplet state, non-fluorescent, but have longer lifetimes up to milliseconds.[58, 100] To return the intermediate radical anion or cation back to the ground state an oxidant or reductant,

respectively, is used. Thus, the ROXS system comprises some form of oxygen removal along with a reductant and oxidant.

Even if no reaction occurs while the dye is in an intermediate state, the dye is still unavailable for its ns absorption-emission cycle while "shelved" in that particular dark state. In FCS, fluctuations in intensity due to presence of a dark state will show up in the timescale associated with the lifecycle of that dark state in addition to the ms timescale fluctuations from diffusion (lifecycle refers to the time for creation and deactivation of that dark state). For dark states due to ISC an additional μs fluctuation will be seen in the FCS decay. Since conformational changes in proteins occur on the nanosecond to second timescale this is a problem as what is a simple photophysical behavior can be misinterpreted for dynamics in biological molecules. As such, a greater understanding of how a fluorophore's photophysical processes are affected by their environment is necessary.

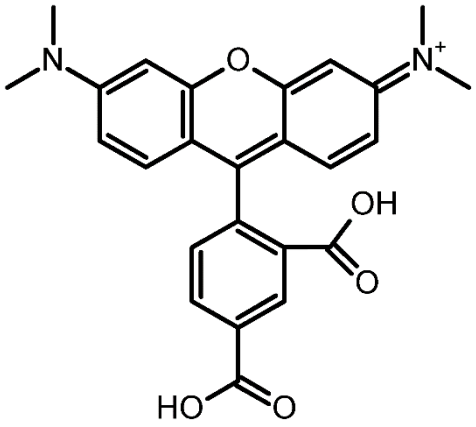


Figure 2.1: Structure of TAMRA Dye. This is the structure of 5-carboxytetramethyl-rhodamine.

In the TAMRA-Mn^{2+} study, the TAMRA dye was attached, via a 6-carbon linker, to the DNA backbone, which acts as a scaffold to bring the cation into close proximity to

the dye, allowing it to affect the dye's photophysics. It is not unrealistic, then, to assume that if other fluorescent probes are brought close to Mn^{2+} they, too, may be affected in the same way. This chapter presents the work done to determine whether Mn^{2+} affects other single molecule dyes. Several cyanine dyes (Cy3, Cy3B, and Cy5) were chosen for the study because they are commonly used in the single molecule community and are commercially available. Also, their base chromophore structure (see Figures 1.2 and 1.5) is different from TAMRA (see Figure 2.1), and rhodamines in general; a positive response to Mn^{2+} indicates this effect is not restricted to rhodamine dyes.

The initial experiments for this project were done without DNA, using dioctyl sulfosuccinate sodium (AOT) reverse micelles (RMs) to force the dye and dication into close proximity with each other. Figure 2.2 shows the lifetime of TAMRA encapsulated in RMs in the presence of Mg^{2+} or Mn^{2+}. The presence of manganese(II) quenches the fluorescence of TAMRA; TAMRA-Mg^{2+} has a mean lifetime of 3.0 ns while TAMRA-Mn^{2+} has a mean lifetime of 2.3 ns. The lifetimes measured by Stennett et al.[83] of TAMRA-dsDNA are 3.0 ns (with Mg^{2+}) and 2.7 ns (Mn^{2+}). This preliminary result indicated that the interaction between dye and dication is facilitated by distance and not by the presence of DNA. In fact, at high concentrations of dication, it is not necessary to use a construct (DNA, micelles) to bring dye and dication together. The right panel of Figure 2.1 shows lifetime measurements for free TAMRA dye in Mg^{2+} and Mn^{2+} buffers; there is a noticeable difference in lifetime, 2.3 ns (Mg^{2+}, single exponential) compared to 2.0 ns (Mn^{2+}, double-exponential). Henceforth, the photophysical studies on cyanines were conducted in free dye conditions. The goal of this study was to determine the underlying cause of the shortened lifetime, i.e., is it also due to an increased ISC rate as

for TAMRA? Transient absorption (TA) measurements were performed to identify the transient state, and FCS measurements were performed to determine whether the presence of manganese(II) would cause measurable μs fluctuations that could interfere with data interpretation. This study has been published in a peer-reviewed journal[35].

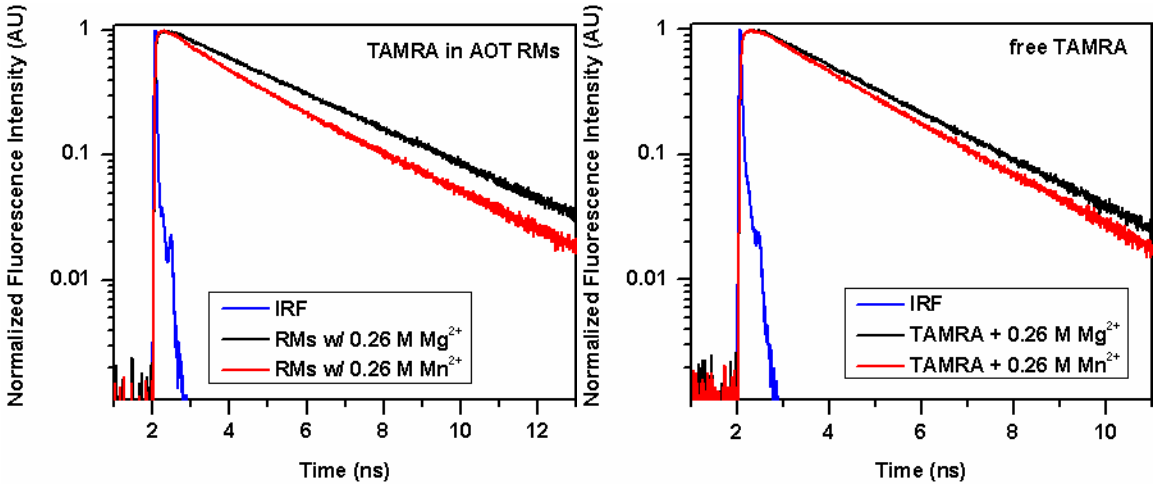


Figure 2.2: Lifetime of TAMRA in the Presence of Dications. The left panel shows lifetimes of TAMRA inside RMs with Mg^{2+} (black trace) or Mn^{2+} (red trace). The right panel shows lifetime measurements on TAMRA with the same dications, but without the RM construct.

2.2 Materials and Methods

A. Materials

Cy3B NHS ester, Cy3 NHS ester, and Cy5 NHS ester were purchased from GE Healthcare (Piscataway, NJ). Magnesium chloride hexahydrate was purchased from EMD Millipore (Billerica, MA). Manganese(II) chloride tetrahydrate, ≥98%, was purchased from Sigma-Aldrich. Zinc chloride, ≥98%, was purchased from Fluka Analytical. 4-Hydroxy-2,2,6,6-tetramethyl-1-piperidin-1-yloxy (TEMPOL), 98+%, free radical was purchased from Alfa Aesar. 1,3,5,7-cyclooctatetraene (COT), 98%, was

purchased from VWR. Sodium iodide (Ultra Pure grade) was purchased from Bio-world. The sequence of Cy3-labeled ssDNA (single-stranded DNA) used for photobleaching experiments was 5'-/5Cy3/AAG AAG AGT TTA CTG TGA-3', where the /5Cy3/ denotes a non-sulfonated Cy3 molecule attached to the 5' end of the DNA via a 3 carbon linker; labeled DNA was purchased from Integrated DNA Technologies (Coralville, IA) and purified via HPLC. DNA samples were dissolved in 10 mM TRIS buffer, pH = 7.4.

B. Photobleaching Experiments

Photobleaching experiments were performed in the cuvette using a PTI QuantaMaster-4/2005SE spectrofluorimeter (a schematic of this instrument is shown in Figure 1.8). The instrument consists of a 75 Watt Xenon arc lamp, two monochrometers for excitation and emission wavelength selection, and a detector. Fluorescence emission was monitored at a fixed wavelength over a period of at least one hour. Cuvettes used had quartz SUPRASIL windows (HellmaAnalytics); solutions were continuously stirred with a magnetic stirrer. The dyes Cy3 and Cy3B were excited at 532 nm, while the emission was recorded at 561 nm and 578 nm, respectively. For Cy5 excitation was at 640 nm, and emission detected at 662 nm. The adjustable slits of the monochromators were set such that the maximum amount of excitation light could be used without overwhelming the detector. Typical slit settings for the emission monochromator were between 1 and 2 half turns (1 nm/half turn), while for the excitation monochromator slits were opened between 8 and 20 half turns—a neutral density filter of OD=2 was placed before the emission monochromator for samples with μM dye concentrations. Dye concentrations were 100 nM (for the low concentration photobleaching experiments) in

pure water (resistivity of 18.2 MΩ-cm at 25°C). Dication concentrations were 0.25 M. For the high concentration photobleaching experiments dye concentrations were: 5 μM (Cy3), 6 μM (Cy3B), and 3 μM (Cy5). Absorption spectra were measured before and after photobleaching using a Shimadzu UV-1700 PharmaSpec spectrophotometer. Cy3-DNA samples were dissolved in a solution of 10 mM TRIS (pH = 7.4), dye-DNA concentration was 100 nM. COT and TEMPOL were used at 20 mM and 6 mM concentration, respectively.

C. Lifetime Measurements

Lifetime measurements were made using the time-correlated single photon counting (TCSPC) technique, described elsewhere[101]. In brief, the excitation source is a Fianium SC450—a fiber supercontinuum laser with a 6 ps pulsewidth—operating at 20MHz. The laser's output is passed through a Fianium acousto-optical tunable filter (AOTF) for wavelength selection. The selected wavelength is vertically polarized prior to entering the sample. Fluorescence emission is polarized 54.7° with respect to excitation; emission is detected at 90° using a Jobin-Yvon, Gemini-180 monochromator (double-grating) and a Hamamatsu microchannel plate photomultiplier tube (model R3809U-50). Data is acquired using a Becker-Hickl single photon counting card (SPC-830). The instrument response function (IRF) was measured from scattering of a Ludox (colloidal silica in water) solution at the excitation wavelength; it has a FWHM of 50-60 ps. Samples (from 0.2 - 0.9 μM were excited at 545 nm (Cy3), 532 nm (Cy3B), and 640 nm (Cy5). Emission was detected at 570 nm (Cy3), 578 nm (Cy3B), and 667 nm (Cy5). The appropriate interference filters for excitation and long band pass filters for the

emission were used. Fluorescence intensity decays were fitted with a sum of exponentials (the IRF was used for deconvolution). Fitting was done with ASUFIT, in-house written software (available at www.public.asu.edu/~laserweb/asufit/asufit.html).

D. Transient Absorption Experiments

Transient absorption was used to detect long lived transients on the μs timescale. These experiments were conducted on equipment belonging to the Devens Gust lab (a schematic of this setup is shown in Figure 1.11). Samples were held in a quartz cuvette and laser excited via an optical parametric oscillator (OPO) pumped by the third harmonic of an Ekspla NT342B Tunable Nd:YAG laser operating at 10 Hz with a pulse width of about 4 to 5 ns. Excitation wavelength was 560 nm (Cy3B), 550 nm (Cy3), and 650 nm (Cy5). The probing light source—situated at 90° to the excitation laser—was a Spectra-Physics 50-500 W Xenon arc lamp. Appropriate glass color filters were used before (after the Xe lamp) and after the sample to select probe and emission wavelength. A Spectral Products 1/4m Digikrom monochromator is used for specific wavelength monitoring. Output is collected by a photodiode, amplified, sent to a digital oscilloscope, and finally to a computer. The probe and detection arm of the instrument was manufactured by Ultrafast Systems; Proteus 3.3.2 is the data collection program. The instrument response function has a FWHM of about 4.8 ns. Data analysis was carried out using locally written software (ASUFIT) developed under a MATLAB environment. Dye concentrations were 6 μM (Cy3B), 4 μM (Cy3 and Cy5). Dication concentrations were 1 M, iodide was used at 50 mM concentration, COT at 20 mM, and TEMPOL was used at concentrations indicated in the figures.

E. Fluorescence Correlation Spectroscopy Experiments

Fluorescence Correlation Spectroscopy experiments were performed on a home built confocal setup (a schematic of this setup is shown in Figure 1.13). Excitation was achieved with a Compass 215M-10 532 nm CW laser (Coherent GmbH, Germany); laser output was attenuated with a gradient neutral density filter as desired. Output of the laser is expanded, collimated, and directed, via a dichroic lens, into an Olympus PlanApo 100X/1.4NA Oil objective. Samples were placed into silicone perfusion chambers (Grace Biolabs, Bend, OR) attached to Fischerbrand microscope coverglass, that rests atop the objective. Fluorescence from samples was collected via the objective, separated from excitation light through the dichroic, and reflected into a 50 μm pinhole. The emission was split using a 50/50 beamsplitter and directed into two independent avalanche photodiodes (Perkin-Elmer Optoelectronics, SPCM-AQR14). Bandpass filters were used before the detectors to minimize unwanted light (Omega 3RD560-620). The recorded fluorescence signals from the two detectors were cross-correlated using an ALV7002 USB-25 correlator (ALV, Germany). This procedure eliminates the anomalously high correlation at times less than 2 μs due to detector afterpulse. The cross-correlation measured by two detectors is identical to the auto-correlation measured by one detector above 2 μs. The autocorrelation, $G(\tau)$, is defined as in Equation 48. FCS experiments were performed only with Cy3B (at 10 nM concentration) with 1 M Mn^{2+} or Mg^{2+} in pure water.

2.3 Results

A. Lifetime Measurements

Lifetimes of Cy3, Cy3B, and Cy5 in the presence of various dications (and at various concentrations) were measured with the TCSPC technique. In Figure 2.3 the variation of Cy3 lifetime with Mg^{2+} (left panel) and Mn^{2+} (right) concentration is seen.

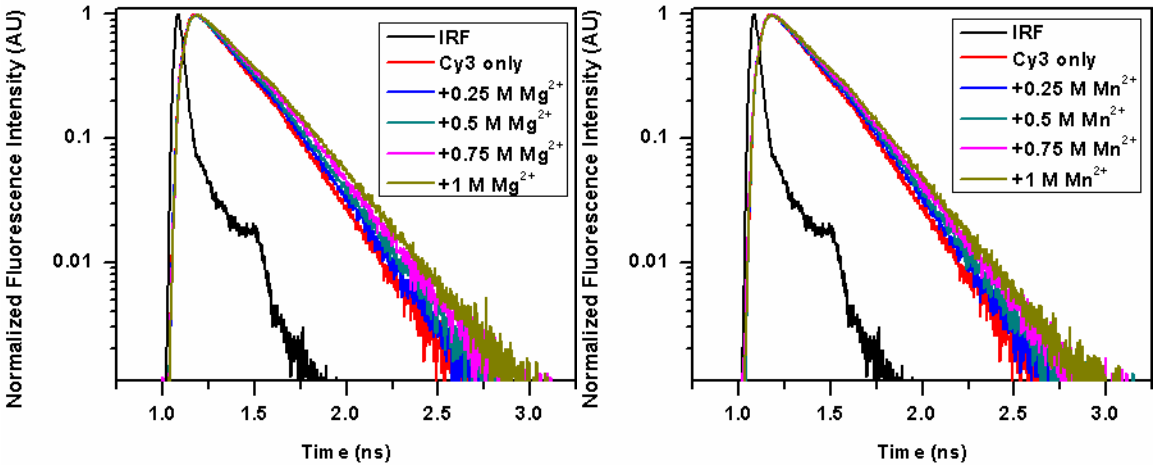


Figure 2.3: Cy3 Lifetime in the Presence of Dications. The lifetime of Cy3 is shown to vary with the concentration of Mg^{2+} or Mn^{2+} present.

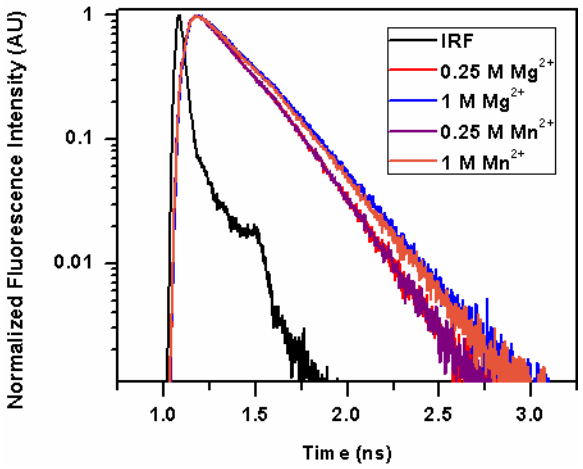


Figure 2.4: Comparison of Cy3 Lifetimes in the Presence of Dications. Cy3/Mg^{2+} and Cy3/Mn^{2+} samples plotted together for 0.25 M and 1 M dication concentrations. There is no significant difference in lifetimes for both samples at the same dication concentration.

The lifetime of Cy3 increases from no dication present to 1 M dication for both Mg^{2+} and Mn^{2+}. A comparison of dication samples at the same concentration, in Figure 2.4, shows no significant effect due to Mn^{2+} presence, i.e., Cy3 with the same amount of dication will have the same lifetime. Cy3B, on the other hand, shows no change in lifetime with Mg^{2+} concentration, but an obvious decrease with increasing Mn^{2+} concentration (Figure 2.5). Table 2.1 shows the resulting parameters from the mono- and double-exponential fits of the lifetimes shown in Figure 2.5. Magnesium has no effect on the lifetime of Cy3B, while Mn^{2+} reduces it with increasing concentration. Figure 2.6 (left panel) shows the effect of Zn^{2+} and the paramagnetic cation, TEMPOL on the lifetime of Cy3B. It is difficult to tell from this figure, however, the only dication which affects the lifetime is Mn^{2+}. The difference in lifetime between Cy3B alone/Zn^{2+}/Mg^{2+} or with Mn^{2+} is small, but significant. On the other hand, TEMPOL dramatically decreases the lifetime (Table

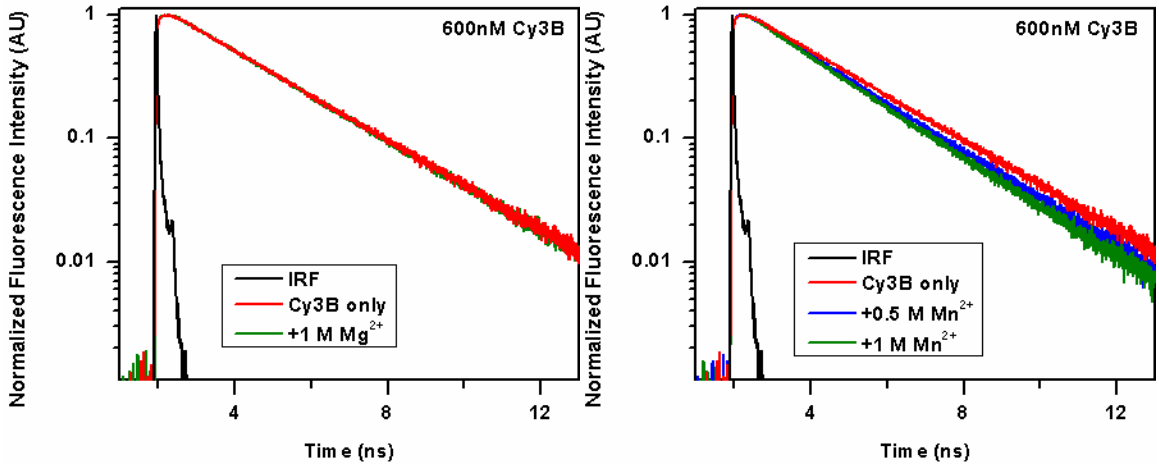


Figure 2.5: Cy3B Lifetime in the Presence of Dications. The left panel shows no change in Cy3B lifetime even with 1 M Mg^{2+} present in the buffer. The right panel shows a marked decrease (red to green trace) in lifetime of Cy3B as more Mn^{2+} is added.

2.1). The right panel shows the lifetime of Cy5 with these same buffer conditions. Cy5 has practically no response to Zn^{2+} or Mn^{2+}, but, as for Cy3B, experiences a large

decrease in lifetime in the presence of paramagnetic TEMPOL. The results from the lifetime fits are in Table 2.1. Increasing the concentration of Mn^{2+}, up to 1 M, does increase the lifetime of Cy5 (Figure 2.7, right panel), however the increase in lifetime is the same as for 1 M Mg^{2+} (Figure 2.7, left panel and Figure 2.8). From this data, it appears that Cy3B is the dye most susceptible to changes in its photophysical behavior due to Mn^{2+}. Manganese(II) decreases the lifetime of Cy3B indicating that dyes which would typically have a longer fluorescence lifetime are now deactivating via another pathway. It was suspected that this is via the triplet state, a long-lived (on the order of microseconds) electronic state. If true, this would increase the photobleaching rate of the dye.

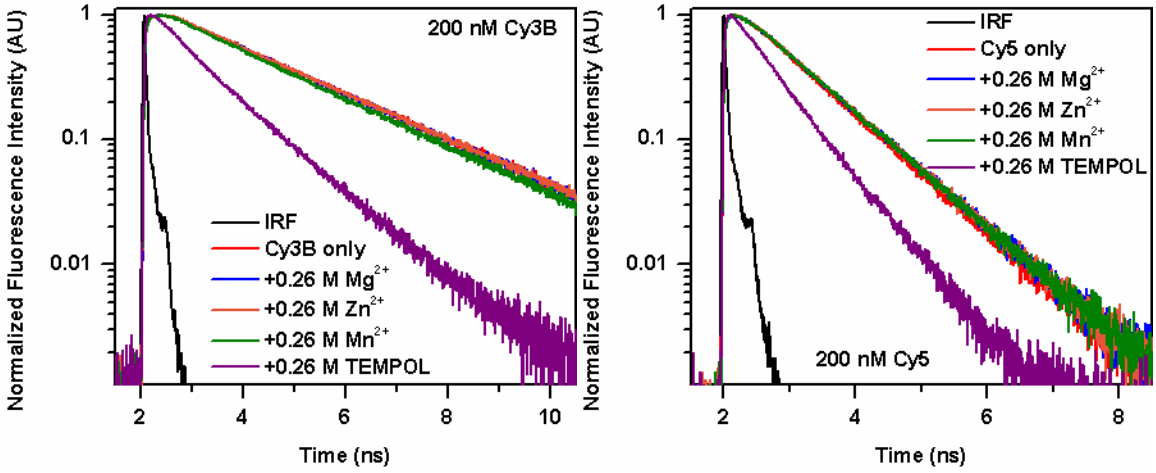


Figure 2.6: Lifetimes of Cy3B and Cy5 with Dications and TEMPOL. Lifetimes of Cy3B (left panel) and Cy5 (right panel) were measured in the presence of 0.26 M Mg^{2+}, Zn^{2+}, Mn^{2+}, and the paramagnetic cation TEMPOL. The lifetime of both dyes is significantly decreased by TEMPOL.

Table 2.1: Lifetimes of Cy3B and Cy5 in the Presence of Cations

Sample	τ_1/ns	$\%\alpha_1$	τ_2/ns	$\%\alpha_2$	$\langle\tau\rangle$/ns
Cy3B only	2.4	100			
+ 0.26 M Mg^{2+}	2.4	100			
+ 1 M Mg^{2+}	2.4	100			
+ 0.26 M Zn^{2+}	2.4	100			
+ 0.26 M Mn^{2+}	1.9	35	2.4	65	2.2
+ 0.5 M Mn^{2+}	1.5	15	2.3	85	2.2
+ 1 M Mn^{2+}	1.6	23	2.2	77	2.1
+ 0.26 M TEMPOL	0.37	36	1.2	64	0.92
Cy5 only	0.90	100			
+ 0.26 M Mg^{2+}	0.93	100			
+ 0.5 M Mg^{2+}	0.96	100			
+ 1 M Mg^{2+}	1.0	100			
+ 0.26 M Zn^{2+}	0.93	100			
+ 0.26 M Mn^{2+}	0.93	100			
+ 0.5 M Mn^{2+}	0.95	100			
+ 1 M Mn^{2+}	1.0	100			
+ 0.26 M TEMPOL	0.18	38	0.65	62	0.49

Table 2.1: Lifetimes of Cy3B and Cy5 in the Presence of Cations. These are the lifetimes of Cy3B and Cy5 samples shown in Figures 2.5, 2.6, 2.7, and 2.8. The table shows the results of single-exponential fits and double-exponential fits when necessary. τ_1 and τ_2 refer to the lifetime from the fit, and $\%\alpha_1$ and $\%\alpha_2$ refer to the weight of each lifetime. For double-exponential fits the average lifetime is in the last column, $\langle\tau\rangle$.

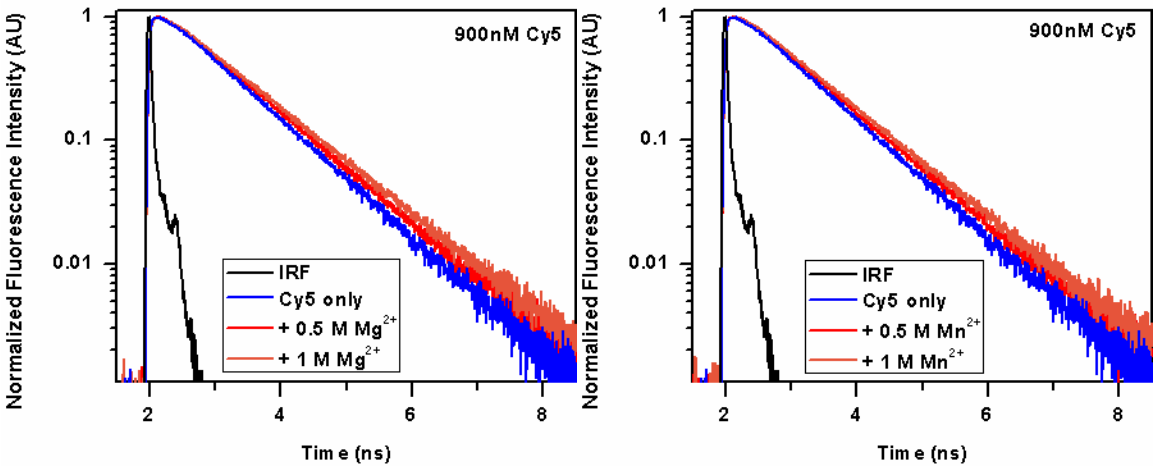


Figure 2.7: Cy5 Lifetime in the Presence of Dications. Cy5 lifetimes measured in the presence of Mg^{2+} (left panel) and Mn^{2+} (right panel).

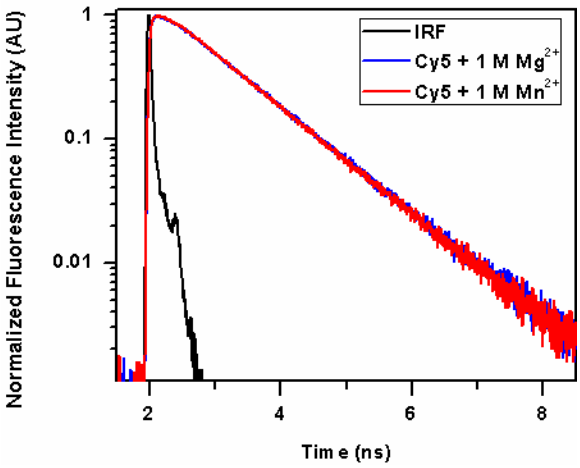


Figure 2.8: Comparison of Cy5 Lifetimes in the Presence of Dications. Lifetime of Cy5 in 1 M Mg^{2+} compared to that in 1 M Mn^{2+}. No significant difference is observed.

B. Photobleaching Experiments

I. Cy3B

Photobleaching experiments were performed in the cuvette—in a fluorimeter—with an excitation intensity determined by the size of the opening between excitation monochromator and sample chamber (as described in the experimental section). The

opening was large in order to have an excitation intensity high enough for photobleaching; the solutions were continuously stirred because the rate of diffusion would not replace bleached fluorophores fast enough from the lamp's path. Results from the photobleaching experiments on Cy3B are shown in Figure 2.9; the left panel shows the experiment at a low (100 nM) concentration of dye, while on the right are the results from the high concentration experiment (6.5 μM). It is clear that Mn^{2+} causes photobleaching of Cy3B (the small decrease in fluorescence intensity for Cy3B alone or

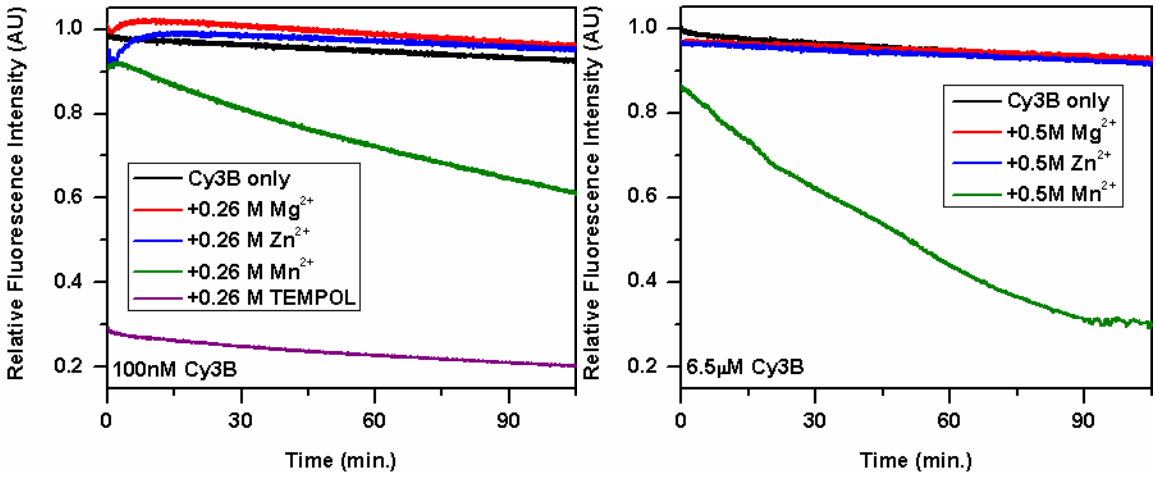


Figure 2.9: Photobleaching of Cy3B in the Presence of Cations. The left panel shows photobleaching traces for 100 nM Cy3B in the presence of 0.26 M Mg^{2+}, Zn^{2+}, Mn^{2+}, and TEMPOL. The right panel shows the same experiment performed at higher Cy3B concentration. A marked increase in the photobleaching rate of the Cy3B/Mn^{2+} sample is seen for both experiments.

with Zn^{2+} or Mg^{2+} is negligible over the course of the almost two-hour long experiment. The presence of TEMPOL seems to quench the fluorescence, but not affect Cy3B's photobleaching rate. The benefit of performing the photobleaching experiment at high concentration is to measure the absorption spectra of the samples before and after exposure to high intensity light. The absorption spectra of the Mn^{2+} and Mg^{2+} samples are shown in Figure 2.10 in the left and right panels, respectively. It is obvious that the

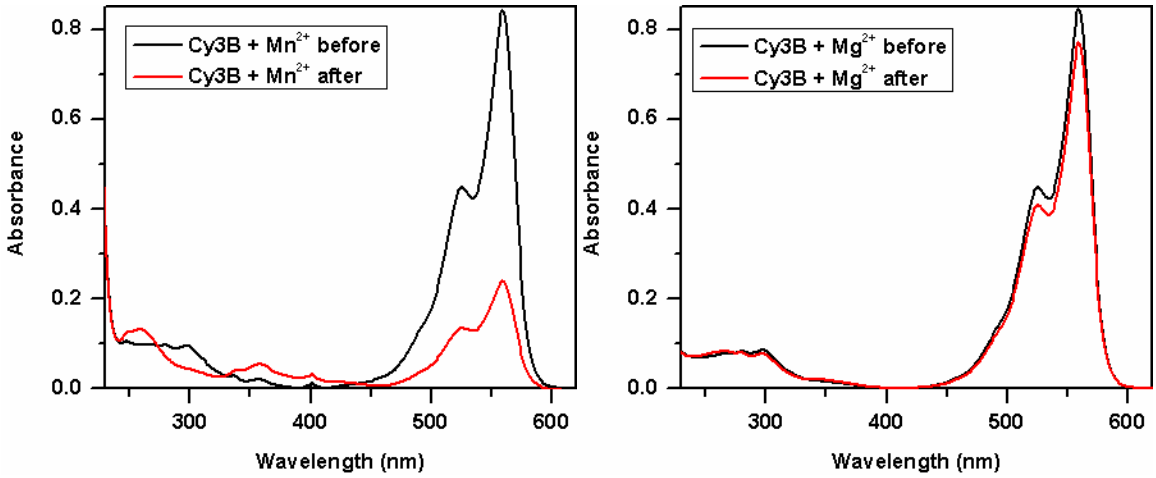


Figure 2.10: Absorption Spectra of Cy3B Pre- and Post-Photobleaching. The left panel shows the absorption spectra of the Cy3B/Mn^{2+} sample; the primary absorption band decreases significantly. The right panel shows the same measurement for Cy3B/Mg^{2+}.

absorption band of Cy3B decreased significantly after photobleaching, while at the same time there is an increase in absorbance around 275 nm and 350 to 400 nm. The absorption spectra for the Mg^{2+} sample show only a minor decrease in absorbance at the dye peak corresponding to the small decrease in fluorescence intensity over the irradiation time. The absorption spectra for the other samples (Cy3B alone and with Zn^{2+}) match that of the Mg^{2+} sample (data not shown). As a control for this photobleaching experiment a separate aliquot of these samples (high concentration) was kept in the dark for the same amount of time; their absorption spectra, measured before and after, did not change (data not shown).

Additional photobleaching tests were conducted in order to determine the source of the increased photobleaching. Cyclooctatetraene (COT), a known triplet quencher, and azide (N_3^-), known to quench singlet oxygen, were added to Cy3B solutions containing Mn^{2+} and irradiated (Figure 2.11). Azide had no effect on the photobleaching rate, however COT decreased the photobleaching rate implicating the triplet state in the

photobleaching mechanism of Mn^{2+}. The photobleaching experiment was also carried out in deuterium oxide buffer: D_2O increases the lifetime of singlet oxygen (Figure 2.11, right panel). The rate of photobleaching did not increase for Cy3B alone in D_2O compared to H_2O, however there was a minor increase in the rate for Cy3B with Mn^{2+}.

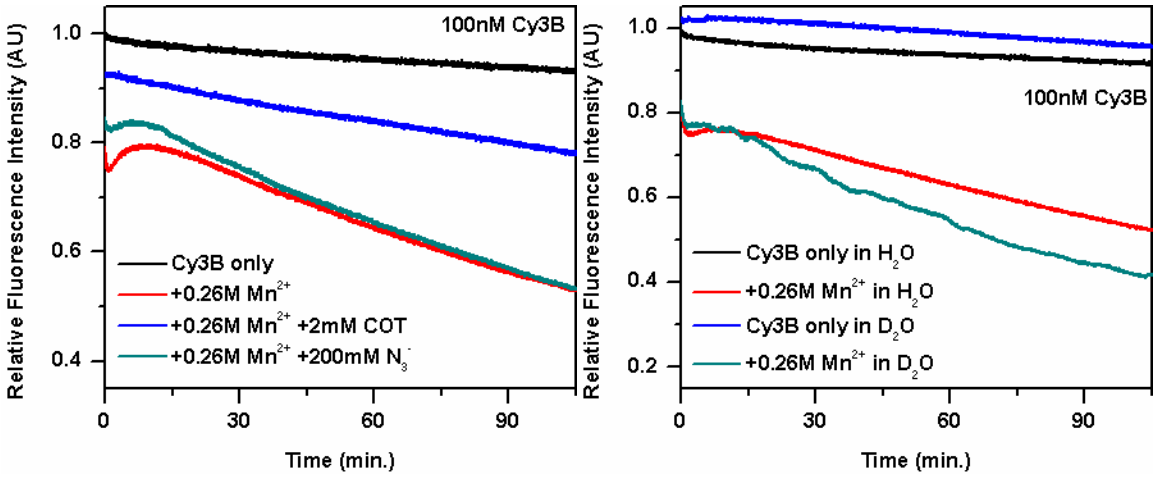


Figure 2.11: Photobleaching of Cy3B with COT, Azide, and D_2O. Photobleaching experiments were repeated on Cy3B/Mn^{2+} with COT (a triplet quencher) and azide (a singlet oxygen quencher) in the left panel, and in heavy water (increases the lifetime of singlet oxygen) in the right panel.

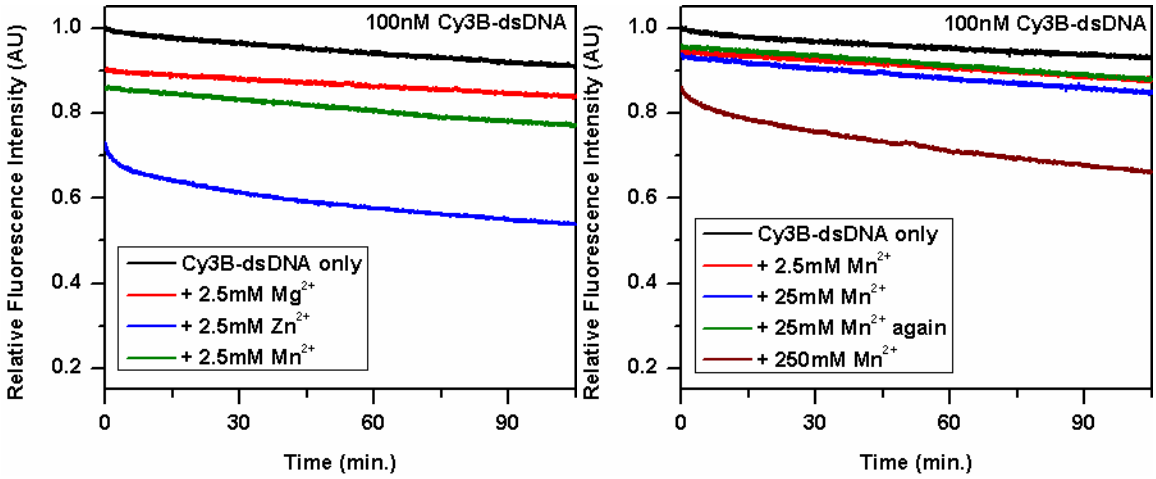


Figure 2.12: Photobleaching of Cy3B-dsDNA in the Presence of Cations. Left panel shows the effect Mg^{2+}, Zn^{2+}, and Mn^{2+} have on the photobleaching rate of Cy3B-dsDNA. The right panel shows the effect of various concentrations of Mn^{2+}. The measurement for the 25 mM Mn^{2+} sample was done twice to ensure reproducibility.

The photobleaching rates of free Cy3B were compared to that of Cy3B-dsDNA as a comparison to the work done by Stennett et al.[83] Low concentrations of Mn^{2+} have no effect on photobleaching rates (Figure 2.12), and even an increase to 25 mM Mn^{2+} (ten times the Mn^{2+} concentration shown by Stennett to affect photostability) yields no effect. It took up to 0.25 M Mn^{2+} to achieve an increased photobleaching rate of Cy3B on DNA—though the more pronounced effect is quenching (Figure 2.12, right panel). Interestingly, a low Zn^{2+} concentration caused more quenching than a high Mn^{2+} concentration.

II. Cy5

The same experiments were performed on Cy5 to assess its response to the metal dications. Manganese(II) and TEMPOL both increased the initial photobleaching rate of Cy5 (Figure 2.13, left) in addition to quenching the fluorescence. Magnesium and Zn^{2+},

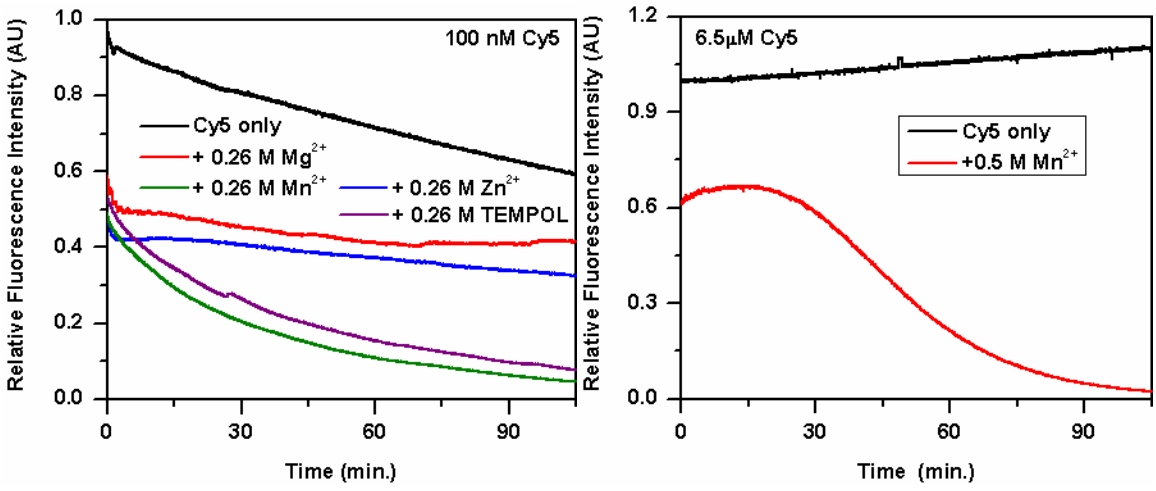


Figure 2.13: Photobleaching of Cy5 in the Presence of Cations. The left panel shows the effect of Mg^{2+}/Mn^{2+}/Zn^{2+} and TEMPOL on the photobleaching rate of Cy5. The right panel shows the same experiment repeated for sample Cy5/Mn^{2+} but at a higher dye concentration.

although quenching the fluorescence, appear to significantly decrease photobleaching. In the right panel of Figure 2.13 is the photobleaching experiment for a much higher concentration of Cy5. The fluorescence of the Cy5 only sample increases during irradiation; the Mn^{2+} sample also experiences an increase in fluorescence, but only during the first 15 minutes. This is due to the inner filter effect: due to the high concentration of fluorophores present emitted light is reabsorbed by the sample preventing it from reaching the detector. Once photobleaching happens, the concentration of dye decreases, and more emission can reach the detector. There is enough photobleaching occurring in the Mn^{2+} sample that after 15 minutes the detected fluorescence begins to decrease; the rate of photobleaching for the Cy5 only sample is so low that few fluorophores are removed from the system, and during the experiment time only an increase in fluorescence is observed. In any case, the photobleaching rate for Cy5 with Mn^{2+} is dramatically greater than for Cy5 alone. The absorption spectra for the Cy5 samples

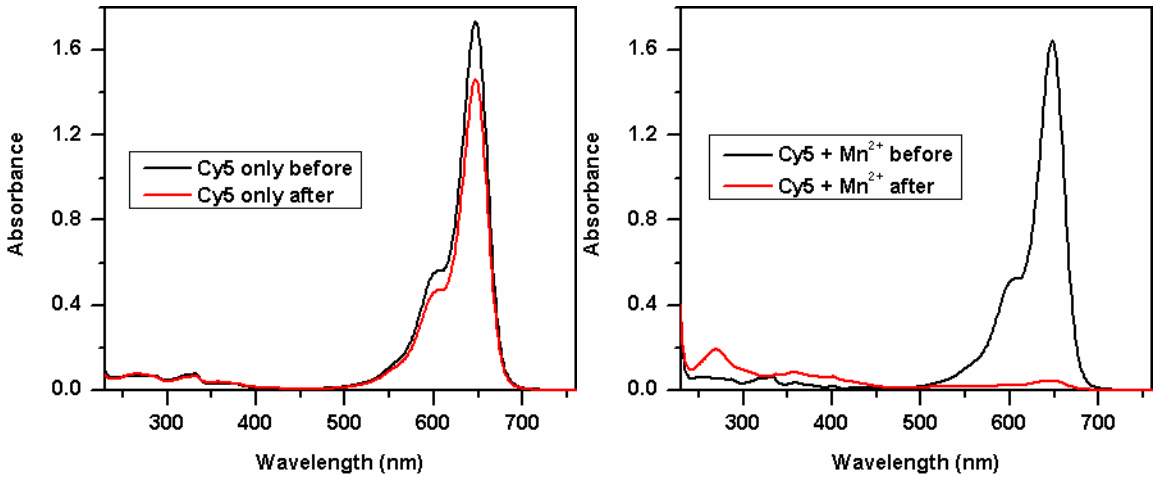


Figure 2.14: Absorption Spectra of Cy5 Pre- and Post-Photobleaching. These spectra were collected for the Cy5 only and Cy5/Mn^{2+} samples before and after photobleaching for the experiment shown in Figure 2.13 (right panel). A significant decrease in the primary absorption band of Cy5 is seen for the Cy5/Mn^{2+} sample (right panel).

before and after irradiation are shown in Figure 2.14. As for Cy3B, there is a decrease in

absorbance of the primary absorption band of Cy5, and an increase in absorbance at short wavelengths. Also, the absorption spectra of Cy5 alone and with the dications under study was measured before and after a bleaching in the dark session of the same length as for the irradiation experiments. The spectra revealed no changes in the absorption spectrum (data not shown).

The photobleaching rate of free Cy5 exposed to atmosphere was also compared to an argon degassed solution. In Figure 2.15 below the left panel shows that there is minimal difference in the photobleaching rate of Cy5 alone when oxygen is removed

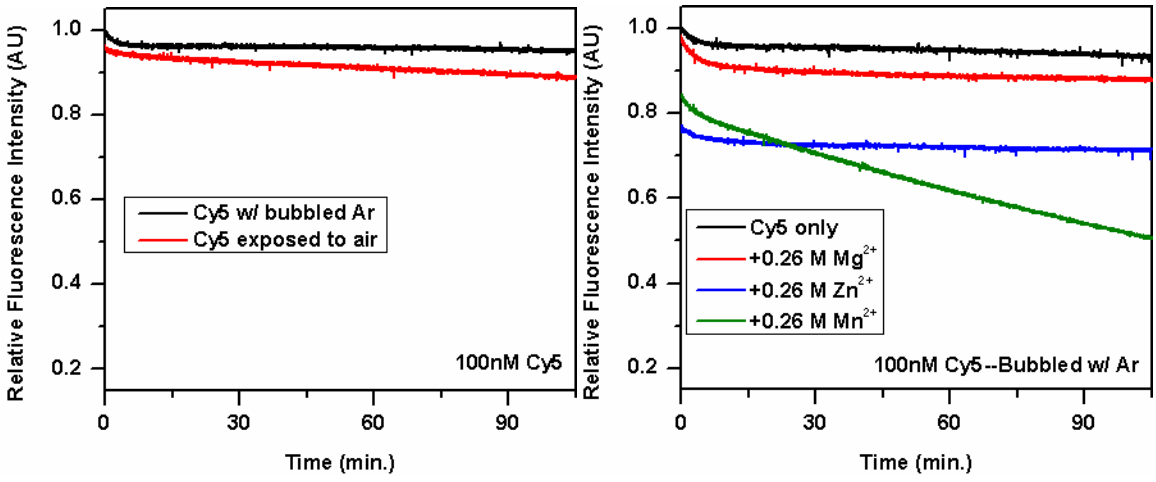


Figure 2.15: Photobleaching of Cy5 in Argon. The left panel shows a comparison of bleaching rates for a Cy5 only sample compared to the same sample degassed with argon. The right panel shows the photobleaching experiment with dications in degassed solution.

from the solution. Addition of Mg^{2+} and Zn^{2+} to the degassed Cy5 solution does not alter bleaching, however, Mn^{2+} still causes a significant increase in photobleaching rate, even after the removal of oxygen.

Due to the presence of trace amounts of iron in the manganese(II) used in these experiments, the effect of iron(II) on the photobleaching rate was also investigated. As shown in Figure 2.16 below, the addition of micromolar amounts of iron(II) does not

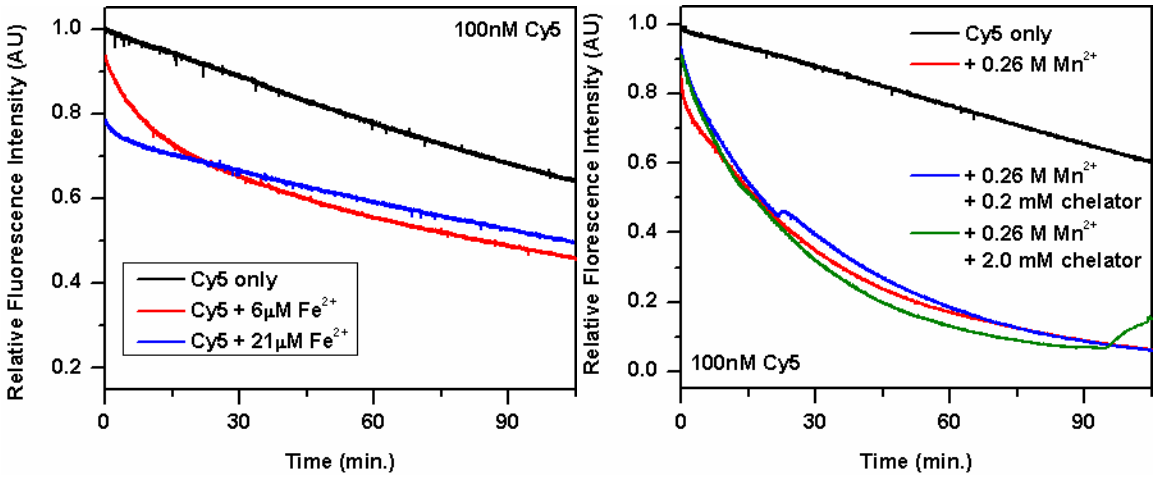


Figure 2.16: Photobleaching of Cy5 with Iron(II). Cy5 is photobleached with Fe^{2+} (left panel) and with Fe^{2+} and an iron chelator (right panel). The results in the right panel indicate iron(II) is not responsible for the photobleaching seen in Mn^{2+} samples.

affect the rate of Cy5 photobleaching, although there appears to be quenching (left panel). Another way to test for iron involvement in photobleaching is to use Mn^{2+} with an iron chelator present. The right panel of Figure 2.16 shows the results of adding deferoxamine mesylate, and iron(II) chelator, to Cy5/Mn^{2+} solutions. The chelator, even when used in a 400-fold excess to the iron(II) impurity, has no effect on the photobleaching rate.

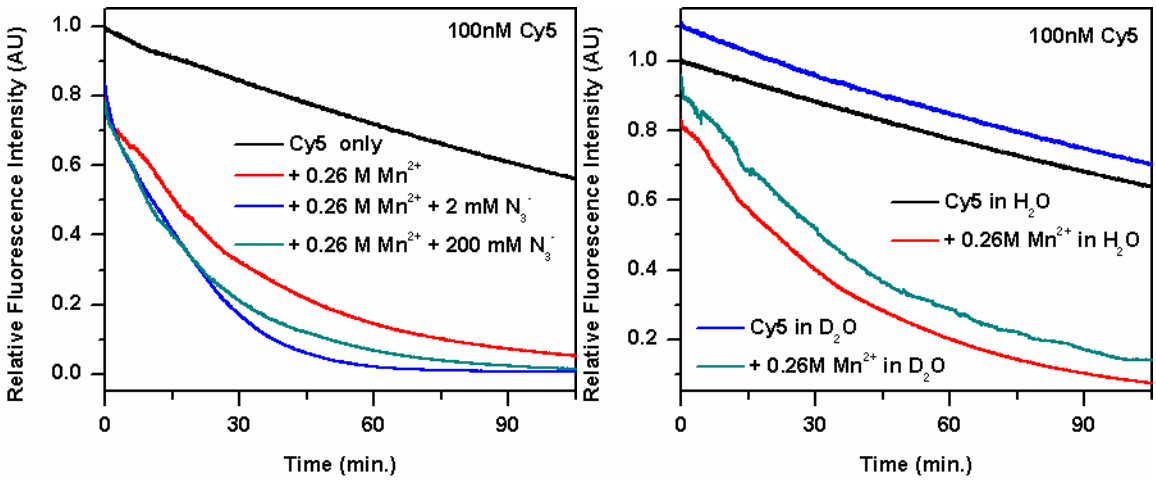


Figure 2.17: Photobleaching of Cy5 with Azide and D_2O. The left panel shows the effect of azide on the rate of photobleaching of Cy5/Mn^{2+}. The right panel shows the effect of photobleaching of Cy5/Mn^{2+} in heavy water. Neither substance has an impact.

As for Cy3B, azide and deuterated water had no impact on photobleaching rate of Cy5 (Figure 2.17), however COT does decrease the photobleaching rate of Cy5/Mn^{2+} to levels seen for Cy5 only; there is, however, noticeable quenching (Figure 2.18).

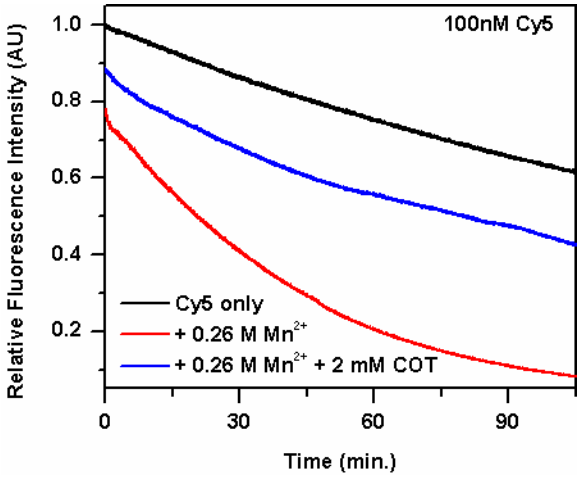


Figure 2.18: Photobleaching of Cy5 with COT. Photobleaching experiment on Cy5/Mn^{2+} with triplet quencher COT. COT decreases the rate of photobleaching.

The photobleaching rate of Cy5 was also investigated when conjugated to DNA. The DNA sample used here contains an internal modification: the Cy5 is attached to both 3' and 5' ends of the DNA backbone placing it between two bases, rather than on the end of the strand. Because the modification is internal the sample is referred to as iCy5-dsDNA. This sample was irradiated in the presence of the four dications investigated and at various concentrations of iron(II) (Figure 2.19). As for the free dye, Mn^{2+} increased the photobleaching rate noticeably, and Zn^{2+} caused far more photobleaching than even the Mn^{2+} (left panel). In contrast to Cy3B-dsDNA, the iCy5-dsDNA sample did not experience the initial fluorescence quenching. Iron(II) concentrations of 100 nM and 1 μM had no effect on photobleaching rate, while 10 μM Fe^{2+} quenched Cy5 fluorescence by approximately 10-15%. The highest concentration of iron(II) tested, 100

μM, quenched at least 80% of iCy5-dsDNA fluorescence at the onset of irradiation (right panel). Again, to be sure that Mn^{2+} is the sole cause of the increased photobleaching, a 99.99% pure source of Mn^{2+} was used; it confirmed the previous results (left).

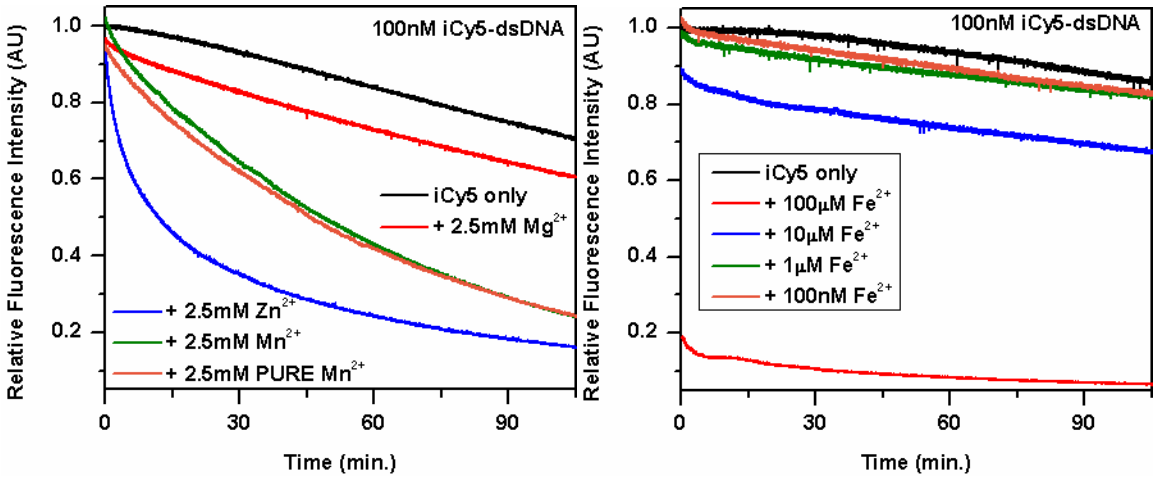


Figure 2.19: Photobleaching of iCy5-dsDNA in the Presence of Dications. Photobleaching experiment on iCy5-dsDNA sample. Mn^{2+} has the same effect as on free Cy5, however Zn^{2+} greatly increases the photobleaching rate (the cause of this is unkown). In the right panel the effect of iron(II) is investigated; Fe^{2+} appears to cause quenching, but only at high concentrations (blue and red traces).

The final test performed on free Cy5 involves the oxidant, methylviologen (MV), and reductant, ascorbic acid (AA) to detect the involvement of radical cation and/or anion states in the photobleaching process. According to the results in Figure 2.20, addition of the oxidant increases photobleaching dramatically, akin to the Mn^{2+} effect. The reductant has no effect on the photobleaching, whereas the combination results in a stable fluorescence level over the experiment duration with quenching—at the experiment's end the Cy5/ROXS sample fluorescence is only about 13% less than that of Cy5 alone.

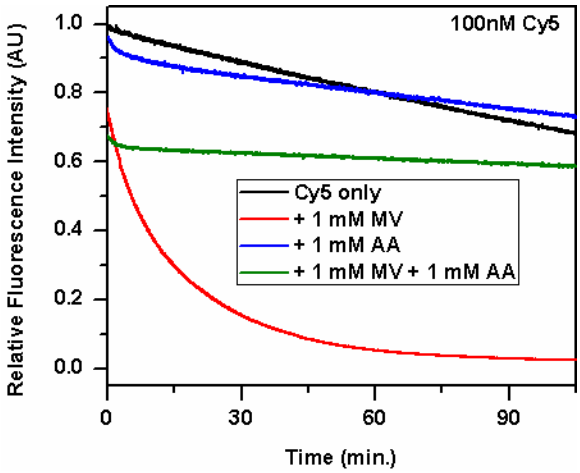


Figure 2.20: Photobleaching of Cy5 in the Presence of ROXS. Photobleaching of Cy5 was performed with methylviologen (MV) and ascorbic acid (AA). The combination of oxidant and reductant produced a stable level of fluorescence (green trace).

III. Cy3

Photobleaching experiments on free Cy3 yielded less interesting results. There is no difference in photobleaching rates between samples with Mg^{2+} or Mn^{2+} (Figure 2.21). At low concentrations, shown in the left panel, both dications increase the

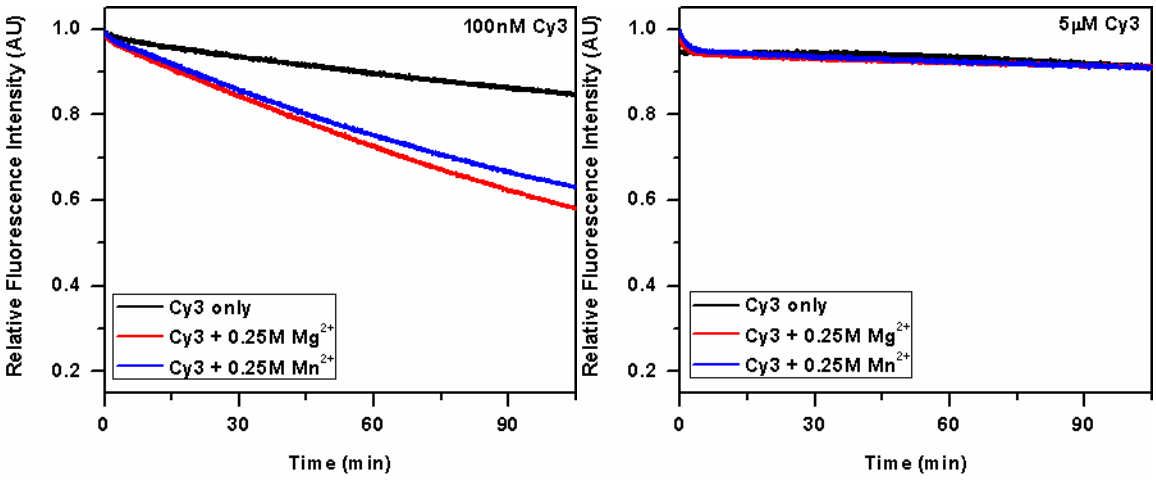


Figure 2.21: Photobleaching of Cy3 in the Presence of Dications. Left panel shows the photobleaching experiment at low Cy3 concentration. The experiment shown on the right was performed at high Cy3 concentration. There is no difference in the photobleaching rates caused by the dications. Experiment performed by David Kanno.

photobleaching rate of Cy3, but the difference in rate between the two is negligible. On the other hand, at high concentrations (right panel), there is no impact on photobleaching rate with dications as compared to the dye alone. The absorption spectra from the high concentration experiment confirms this (Figure 2.22). Although, both Mg^{2+} (left) and Mn^{2+} (right) samples cause the dye's absorbance at the primary absorption band to decrease, the decrease is small and neither sample shows an increase in absorbance at short wavelengths. The photobleaching in the dark experiment, as for Cy3B and Cy5, showed no change in the absorption spectrum over time (data not shown).

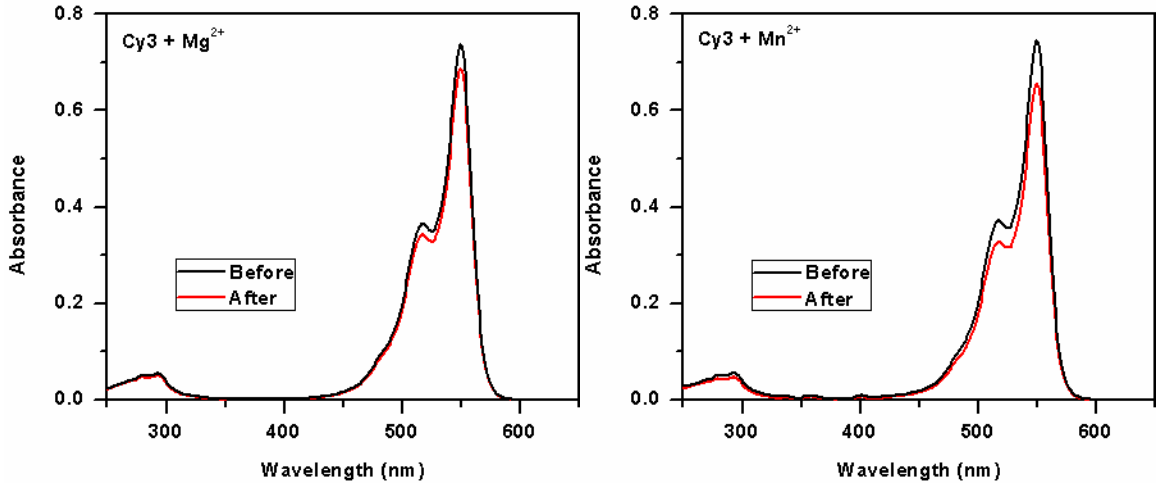


Figure 2.22: Absorption Spectra of Cy3 Pre- and Post-Photobleaching. The absorption spectra of Cy3/Mg^{2+} (left panel) and Cy3/Mn^{2+} (right panel) measured before and after photobleaching are shown here. Neither sample shows significant changes. This experiment was performed by David Kanno.

However, significant photobleaching is observed for Cy3 conjugated to DNA. In Figure 2.23 below, the photobleaching experiment was conducted in steps meaning that a a solution of pure Cy3, or Cy3-dsDNA, was measured, and then, after about ten minutes, the dication was added to the solution. The left panel of Figure 2.23 compares the addition of Mg^{2+} to Mn^{2+} to free Cy3; neither dication has a significant effect on the rate

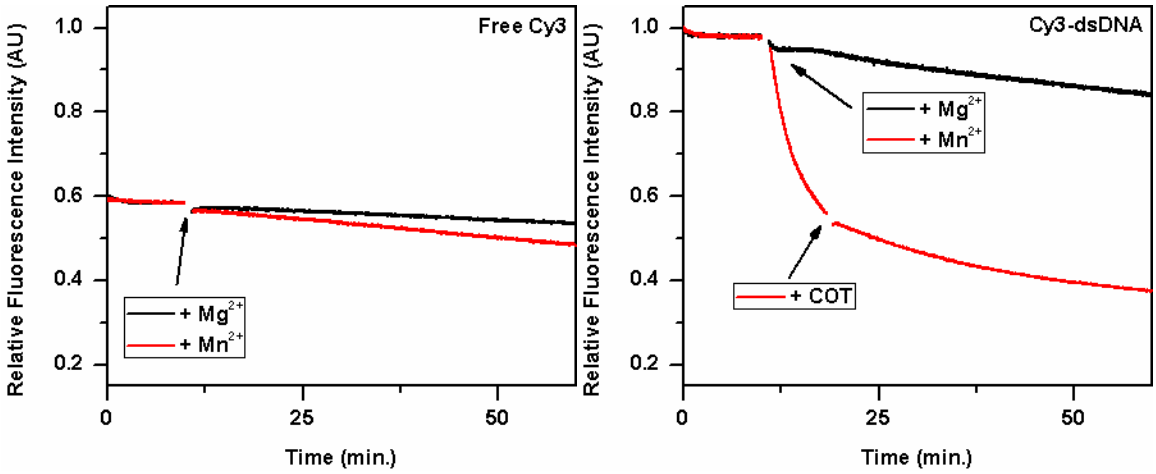


Figure 2.23: Free Cy3 vs. Cy3-dsDNA: Photobleaching in the Presence of Dications. A step-wise version of the photobleaching experiment is conducted for free Cy3 (left) and Cy3-dsDNA (right). Cy3 on DNA is more susceptible to photobleaching in the presence of Mn^{2+}. Triplet quencher COT slows the rate of photobleaching (right). Measurement by David Kanno. Adapted from Reference 35. Copyright © 2013 WILEY-VCH Verlag.

of photobleaching. In the right panel Cy3-dsDNA is irradiated for ten minutes, then the dications are added to solution. The rate of photobleahing is unchanged for the Mg^{2+} sample, but the fluorescence intensity of the Mn^{2+} sample decreases dramatically.

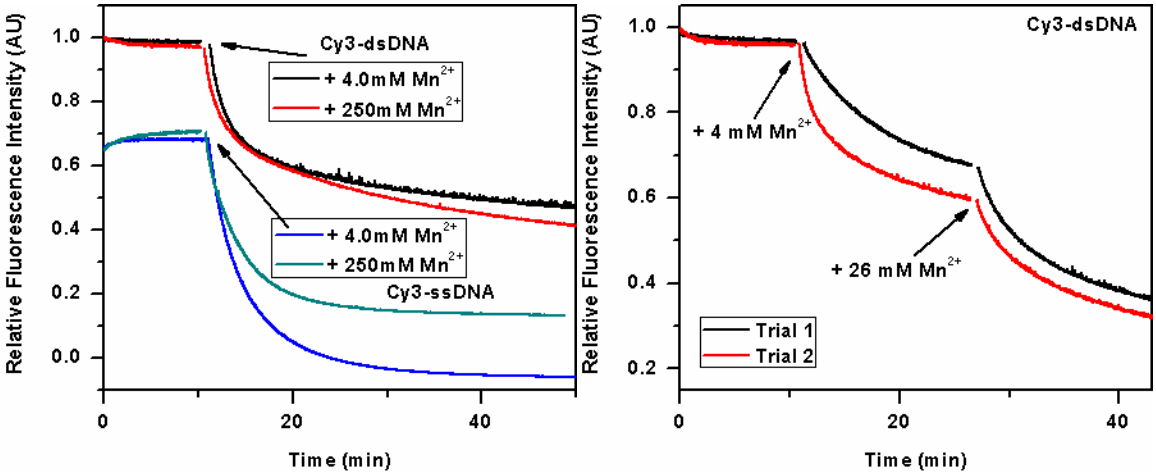


Figure 2.24: Photobleaching of Cy3 on DNA with Varying Mn^{2+} Concentration. The left panel shows a comparison of photobeaching rates of Cy3 on single-stranded DNA (blue and green) and Cy3 on double-stranded DNA (black and red). Two different Mn^{2+} concentrations are tested. The right panel shows another experiment on Cy3-dsDNA comparing the photobleaching rate with an intermediate Mn^{2+} concentration. Experiment performed by David Kanno.

Addition of COT, about five minutes later, reduces the photobleaching rate almost to the original rate. The photobleaching rate of Cy3 conjugated to single-stranded DNA is compared to Cy3-dsDNA in Figure 2.24, on left. The initial photobleaching rate, immediately after Mn^{2+} addition, is similar for Cy3-ssDNA and Cy3-dsDNA, as well as for the low and high concentrations of Mn^{2+}. The right panel of Figure 2.24 compares photobleaching rates for two different concentrations of Mn^{2+}. There appears to be no difference in initial photobleaching whether 4 or 26 mM Mn^{2+} is added.

C. Transient Absorption Experiments

I. Cy3B

Transient absorption measurements on the microsecond timescale were conducted in order to unequivocally ascribe the increased photobleaching in Mn^{2+} samples to an increased intersystem crossing rate. Samples were deoxygenated using argon gas to decouple the Mn^{2+} effect from quenching expected due to dissolved oxygen. The difference spectrum of Cy3B in the presence Mn^{2+} is shown at four selected times after the laser pulse (Figure 2.25, left panel). The negative signal from 500 to 580 nm is due to singlet ground state absorption, while the positive signal from 600 to 700 nm is caused by the presence of Mn^{2+} and is assigned to triplet-triplet absorption—control experiments that prove the assignment of this band follow below. The right panel shows the kinetic traces from 550 nm (the maximum ground state absorption) and 630 nm (the maximum triplet absorption); the data points in the left panel are from the specified time points of the kinetic traces. The difference spectrum for the Cy3B/Mn^{2+} sample, but with 20 mM

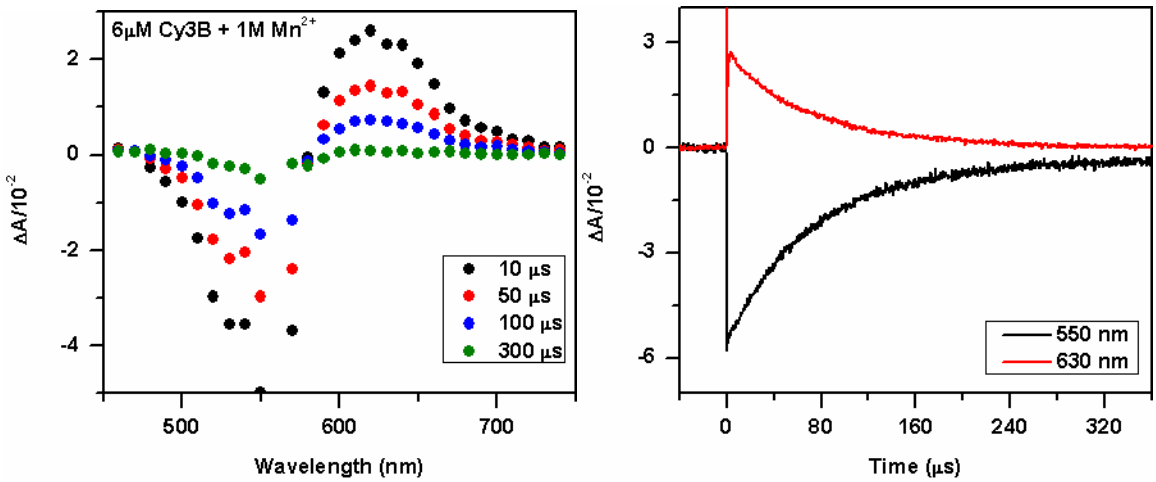


Figure 2.25: Difference Spectrum and Kinetic Traces of Cy3B/Mn^{2+}. The difference spectrum of Cy3B/Mn^{2+} at four times after the laser pulse are shown in the left panel; kinetic traces at two relevant wavelengths are shown in the right panel.

COT added (still in argon saturated solution), is shown in Figure 2.26 (left) on the same axes for direct comparison with Figure 2.25 (left). Selected kinetic traces are shown in the right panel and in both panels of Figure 2.27, and are compared to the kinetic traces from the Cy3B/Mn^{2+} sample at those same probe wavelengths. The presence of COT

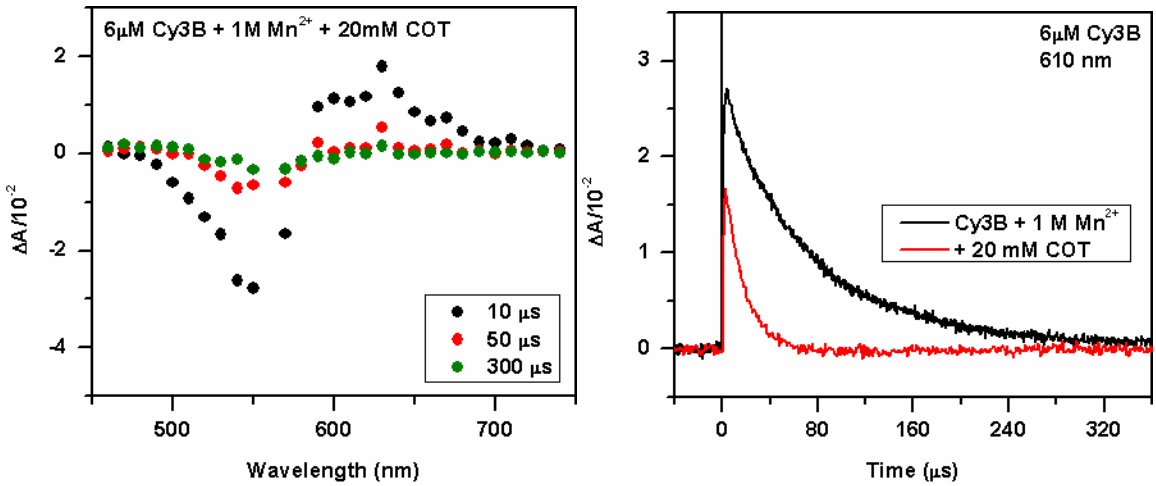


Figure 2.26: Difference Spectrum and Kinetic Traces of Cy3B/Mn^{2+}/COT. The difference spectrum of Cy3B/Mn^{2+}/COT is shown in the left panel for three selected times after the laser pulse. The right panel compares the kinetic trace at 610 nm of Cy3B/Mn^{2+} (from Figure 2.25) with Cy3B/Mn^{2+}/COT.

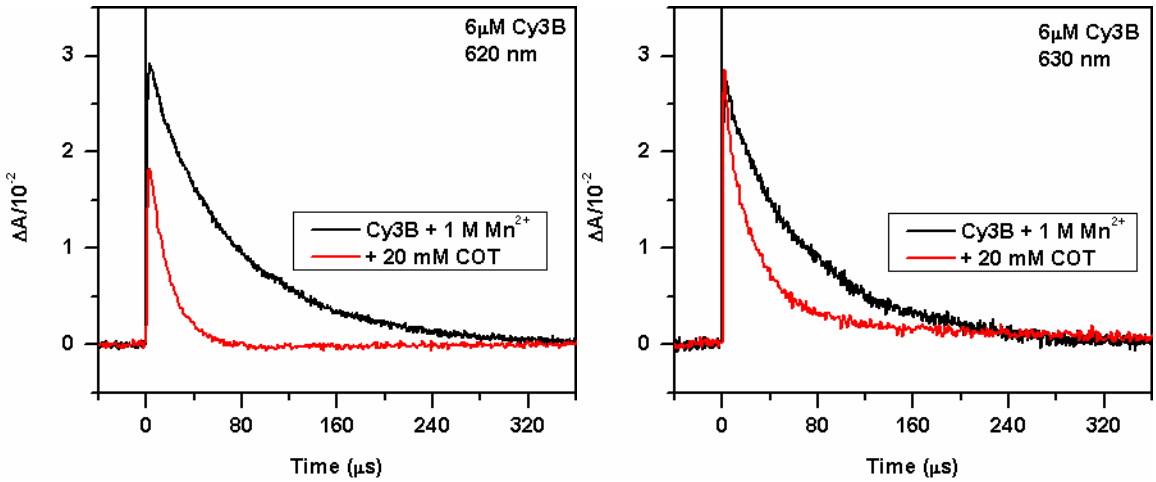


Figure 2.27: Cy3B/Mn^{2+}/COT Kinetic Traces Compared with Cy3B/Mn^{2+}. The kinetic traces of Cy3B/Mn^{2+}/COT are compared to those of the Cy3B/Mn^{2+} sample at 620 and 630 nm. The lifetime of the transient is clearly shorter in the Cy3B/Mn^{2+}/COT sample. Adapted from Reference 35. Copyright © 2013 WILEY-VCH Verlag.

decreases the signal, in amplitude and lifetime: the kinetic trace at 630 (Figure 2.27, right) shows the same initial amplitude for both samples, however the lifetime of the triplet is clearly shorter in the presence of COT. The traces at 610 nm (Figure 2.26, right) and 620 nm (Figure 2.27, left) show a decrease in triplet lifetime and amplitude for the COT sample.

The full spectrum of the Cy3B/Mg^{2+} sample was also measured under argon and is shown in Figure 2.28, below, where the spectrum at 10 μs after the flash is presented on the same axes as the previous two spectra. The Cy3B/Mg^{2+} sample has no signal in the triplet region and only a small negative signal for the ground state absorption of the dye; thus, the triplet-triplet absorption is caused by the presence of Mn^{2+}. A few kinetic traces from the T-T absorption region are shown in Figure 2.28 (right panel) on the same scale as above for comparison. Additional reagents, TEMPOL and gadolinium(III), were tested and compared to Mg^{2+} at 610 and 620 nm probe wavelengths in Figure 2.29

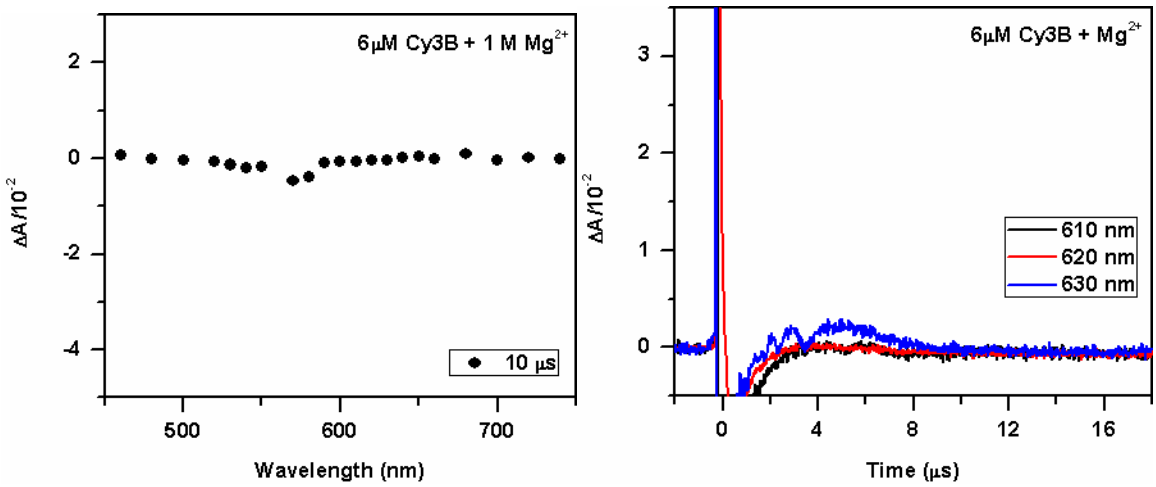


Figure 2.28: Difference Spectrum and Kinetic Traces of Cy3B/Mg^{2+}. The difference spectrum of Cy3B/Mg^{2+} shows no signal in the T-T absorption region (left). Several kinetic traces from this region are shown (right).

(under argon). Only TEMPOL, at a concentration of 10 mM, gives a strong, but short-lived signal. Figure 2.30 below also shows the comparison of Mg^{2+} and TEMPOL signals to Zn^{2+}. As it turns out, there is no increased triplet population in the presence of

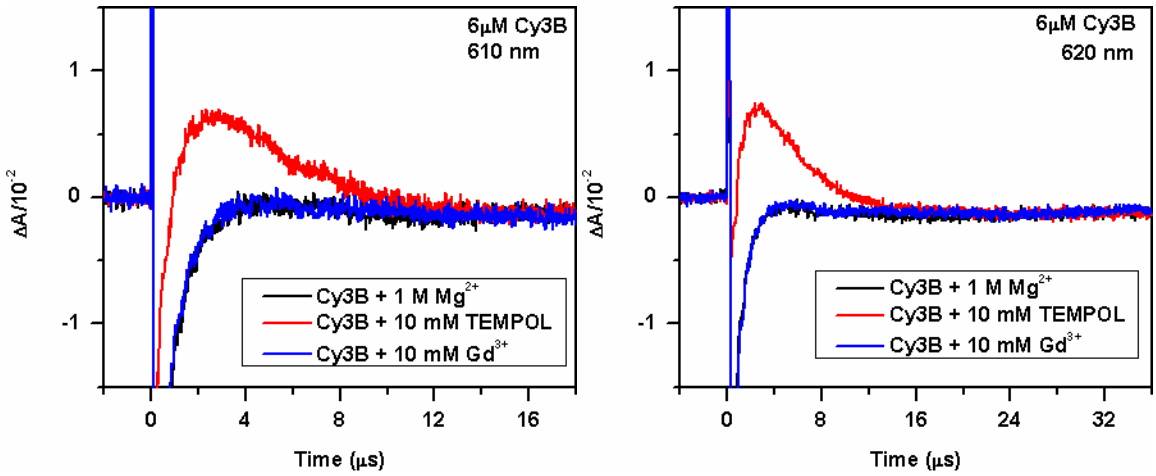


Figure 2.29: Kinetic Traces of Cy3B in the Presence of Cations. Kinetic traces at 610 nm (left) and 620 nm (right) are shown for Cy3B with Mg^{2+} (black), with TEMPOL (red), and with gadolinium(III) (blue). Only the Cy3B/TEMPOL sample shows an appreciable signal.

Zn^{2+}. The effect of TEMPOL concentration on amplitude and lifetime of the triplet signal is shown in Figure 2.31 (left panel). TEMPOL concentrations from 1 mM to

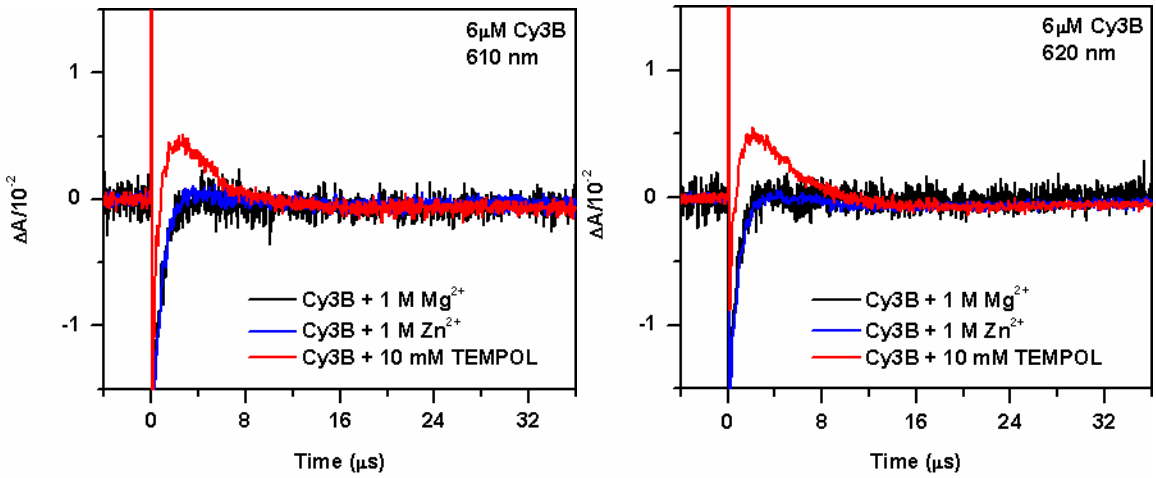


Figure 2.30: Kinetic Traces of Cy3B in the Presence of Zinc(II). Kinetic traces at 610 nm (left) and 620 nm (right) comparing the Cy3B/Zn^{2+} (blue) sample to the Cy3B/Mg^{2+} (black) and Cy3B/TEMPOL (red) samples. Cy3B/Zn^{2+} shows no signal.

20 mM were tested. As the concentration of TEMPOL increases the amplitude of the triplet-triplet absorption increases, however the lifetime of the triplet state decreases indicating that TEMPOL, in affecting the ISC rate, also has influence over the return

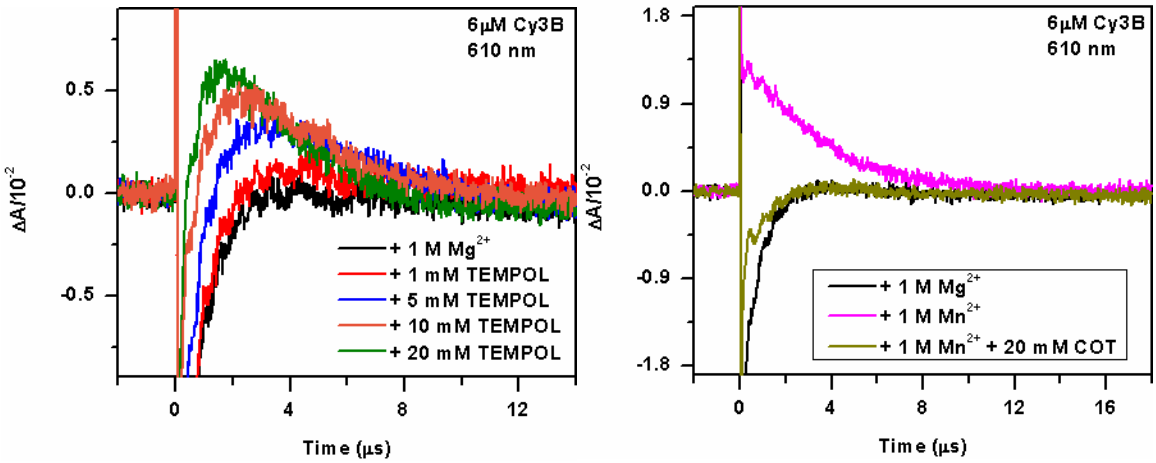


Figure 2.31: Kinetic Traces of Cy3B in the Presence of TEMPOL and Mn^{2+}. The left panel shows kinetic traces of Cy3B in the presence of 1 M Mg^{2+} and four different concentrations of TEMPOL. These samples were degassed prior to measurement. The presence of TEMPOL induces ISC into the triplet state. The signal increases in amplitude and decreases in lifetime with concentration of TEMPOL. The right panel shows Cy3B samples (not degassed). The presence of Mn^{2+} induces triplet formation, which is quenched by COT. Adapted from Reference 35. Copyright © 2013 WILEY-VCH Verlag.

rate, k_{ISC}^{T}. Since all previous transient absorption spectra/kinetic traces for Cy3B were collected from deoxygenated samples, Figure 2.31 (right panel) shows the effect of dissolved oxygen. The Cy3B/Mn^{2+} triplet lifetime is greatly reduced, and in the presence of COT no appreciable triplet is formed.

II. Cy5

Cy5 with various dications was studied using transient absorption spectroscopy as well. The difference spectra of Cy5 with Mn^{2+} and Mg^{2+} are shown in Figure 2.32, left and right panels, respectively. Both spectra were collected from deoxygenated samples, however they cannot be directly compared since the dye concentration is different. Regardless, the Cy5 spectrum shows the same qualitative features that were pointed out for Cy3B: the strong negative signal is due to the ground state absorption. The strong positive signal is due to photoisomer formation (only, in Cy5/Mg^{2+}) and an overlap of

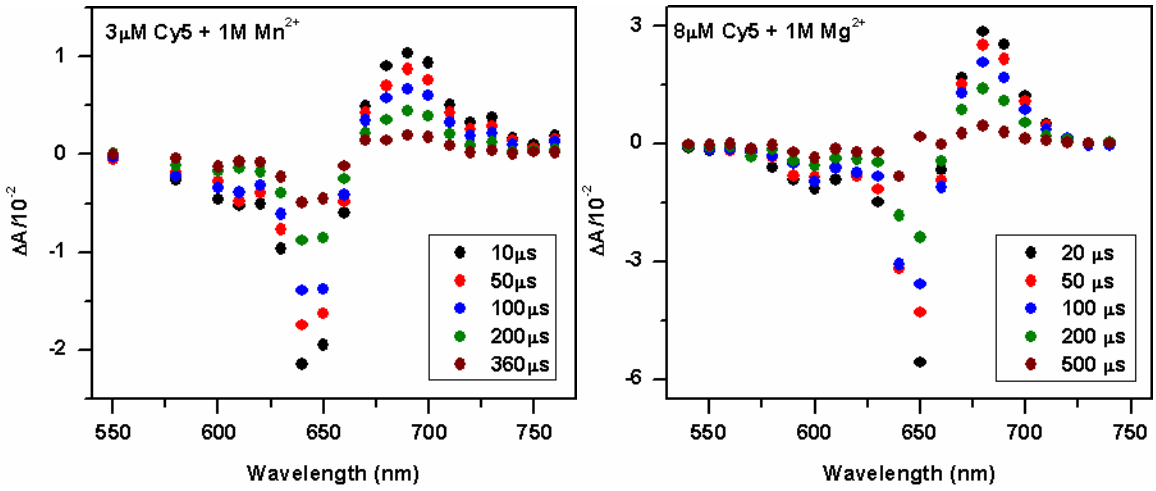


Figure 2.32: Difference Spectra of Cy5 in the Presence of Mn^{2+} and Mg^{2+}. Difference spectra of Cy5 with Mn^{2+} (left) and Mg^{2+} (right) at five different times after the laser pulse. Samples were degassed prior to measurement.

photoisomer and triplet state absorption (in Cy5/Mn^{2+}). The spectrum of Cy5/Mg^{2+} in

oxygen saturated solution clearly shows the distinction between samples with and without triplet-triplet absorption (Figure 2.33, left). In the red part of the spectrum Cy5/Mg^{2+} has zero signal immediately after the laser pulse, however Cy5/Mn^{2+} clearly

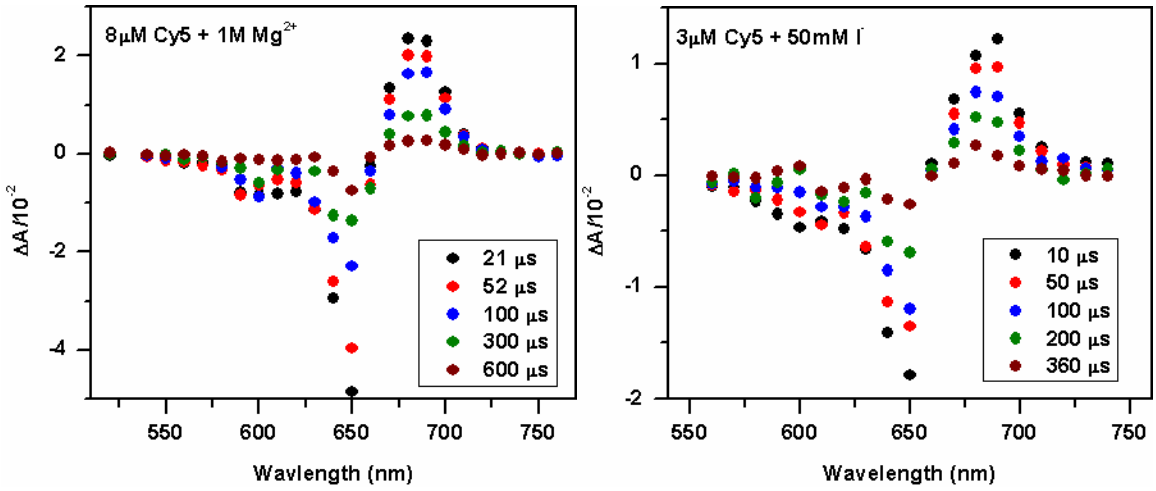


Figure 2.33: Difference Spectra of Cy5 in the Presence of Mg^{2+} and Iodide. Difference spectrum of Cy5/Mg^{2+} in oxygen saturated solution (left). Difference spectrum of Cy5 in the presence of iodide (right). Difference spectra measured at five times after laser pulse.

has a positive signal at 730 – 760 nm. A control sample, Cy5/iodide, also has a positive signal in the red wavelengths like the Mn^{2+} sample (Figure 2.33, right). A more direct comparison is seen in Figure 2.34, below. The kinetic traces at 700 nm (left panel) and 730 nm (right) for four different samples (measured on the same day, under argon) are shown on the same scale. At 700 nm every sample has a positive signal, however, at 730 nm the Cy5/Mg^{2+} sample has no absorbance. The Cy5/iodide sample has a short-lived signal, while the transient generated in the Mn^{2+} samples has a much longer lifetime. Also noteworthy, the signal in the red is much weaker. In one final test, the effect of β-mercaptoethanol—another triplet quencher—was compared to COT. Figure 2.35 (under argon, data was collected in one day) shows the kinetic traces of Cy5 with the specified buffer conditions at 730 nm and 740 nm probe wavelengths. The addition of

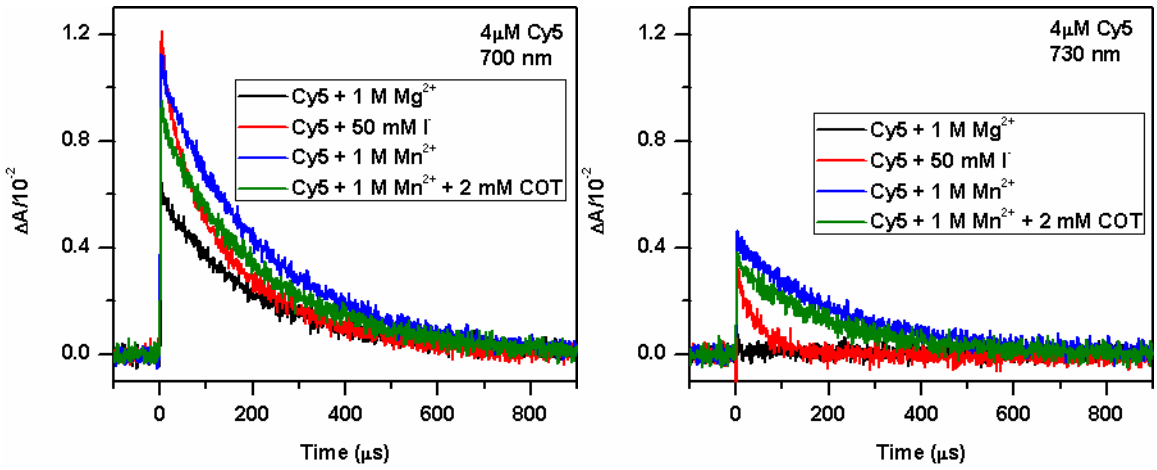


Figure 2.34: Kinetic Traces of Cy5 in the Presence of Ions and COT. The kinetic traces at 700 nm (left) and 730 nm (right) are shown for four samples of Cy5 with Mg^{2+} (black), iodide (red), Mn^{2+} (blue), and Mn^{2+}/COT (green).

β-mercaptoethanol does not significantly alter the amplitude or lifetime of the Cy5/Mn^{2+} sample, while COT decreases its lifetime. At the 730 nm probe wavelength there is no appreciable signal from either the Mg^{2+} or TEMPOL samples. The same trends are observed at the 740 nm probe wavelength although the amplitudes are lower. Since the Cy5/TEMPOL sample shows no signal at 730 nm, the measurement at 740 nm

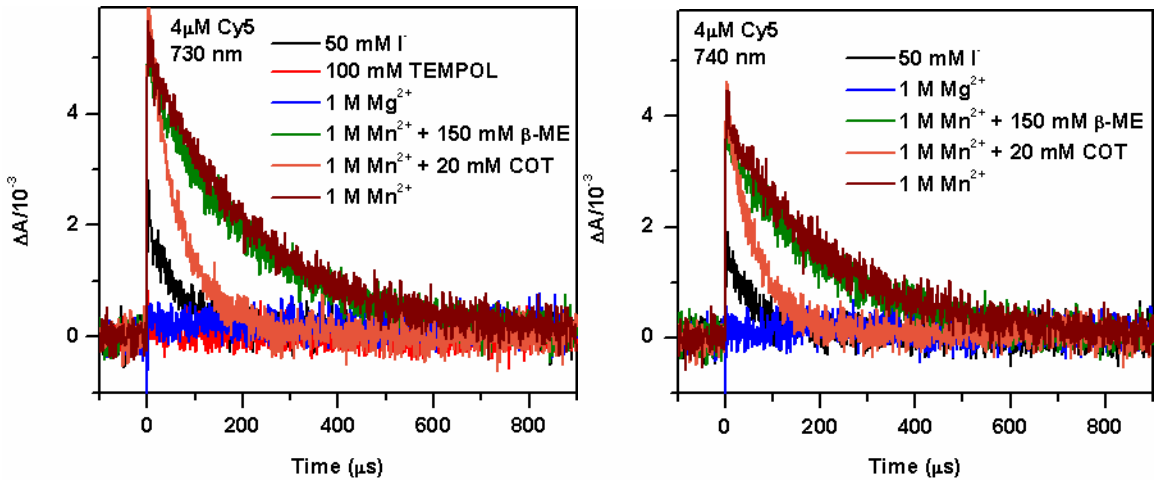


Figure 2.35: Kinetic Traces of Cy5 in the Presence of Ions and Triplet Quenchers. Kinetic traces of Cy5 samples measured under Ar at probe wavelengths 730 nm (left) and 740 nm (right). Conditions are as indicated in the figures. The kinetic trace for TEMPOL at 740 nm was measured on a different timescale and is shown in Figure 2.36.

was collected on a shorter timescale (Figure 2.36), and, indeed, the signal is insignificant. The same samples were also measured under oxygen saturated conditions (Figure 2.37). Again, the trends seen are the same.

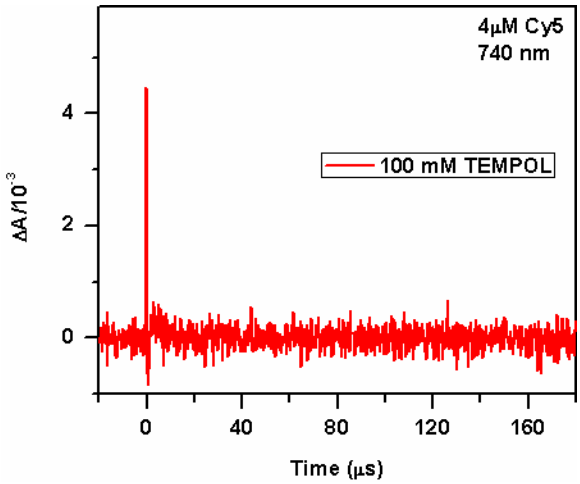


Figure 2.36: Kinetic Trace of Cy5 in the Presence of TEMPOL. An argon degassed solution of Cy5/TEMPOL was measured at 740 nm probe wavelength.

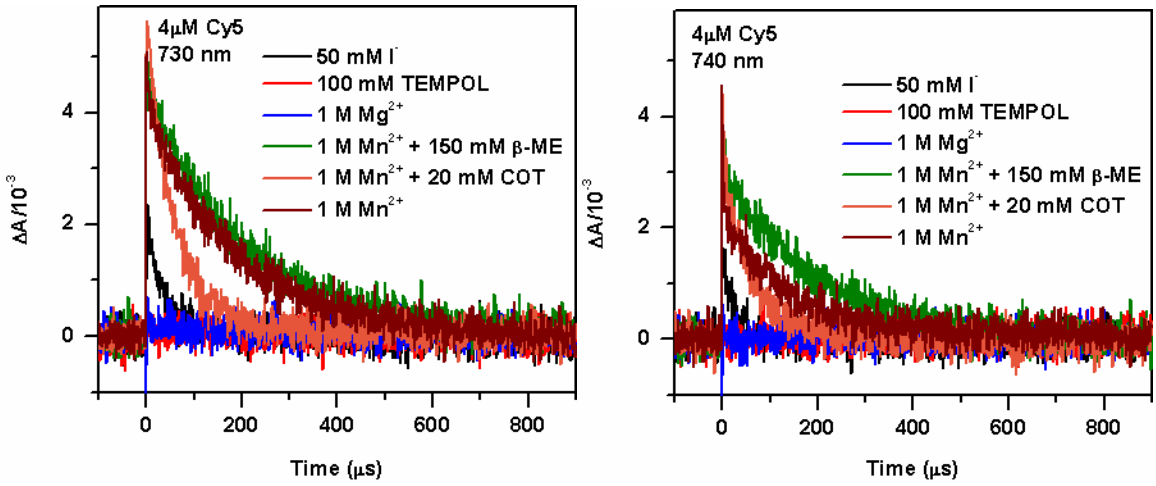


Figure 2.37: Kinetic Traces of Cy5 in Oxygen Saturated Solution. Same samples measured in oxygen saturated conditions. The lifetime of the triplet state does not significantly change.

III. Cy3

The same transient absorption experiments were conducted on Cy3 samples. In Figure 2.38, below, the samples were tested on the same day under an argon atmosphere. The left panel shows kinetic traces at 570 nm probe wavelength, the approximate peak of Cy3 emission, and all samples appear to have the same transient lifetime. At the 620 nm

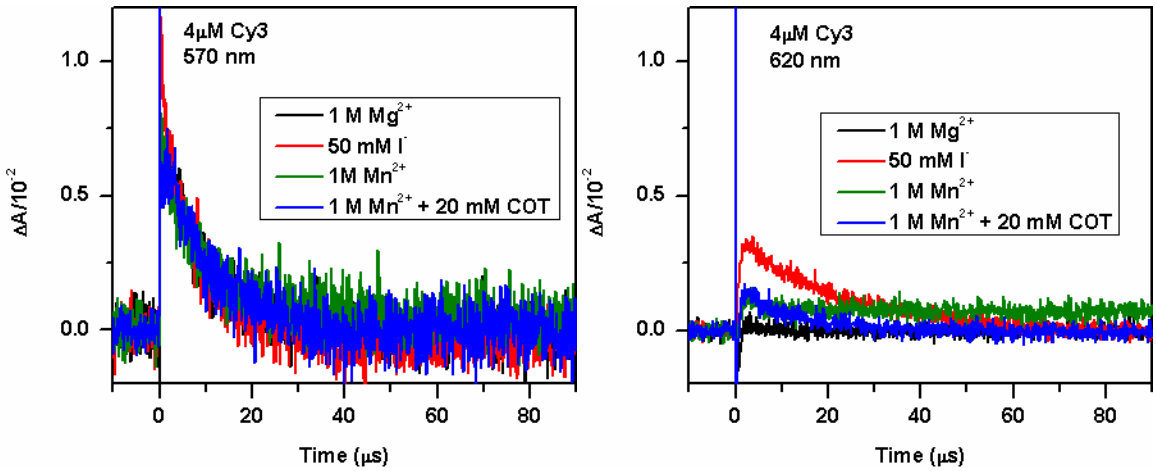


Figure 2.38: Kinetic Traces of Cy3 in the Presence of Ions and COT. Kinetic traces of Cy3 samples measured under Ar at probe wavelengths 570 nm (left) and 620 nm (right). Conditions as indicated in the figures. Adapted from Reference 35. Copyright © 2013 WILEY-VCH Verlag.

probe wavelength (right panel) the Cy3/Mg^{2+} sample shows no absorption, while the other three samples show a weak signal. The iodide sample has a clear signal, while the Cy3/Mn^{2+} sample has a low, but long-lived absorption—which does not decay on the timescale of data collection. Upon addition of COT the Cy3/Mn^{2+} signal becomes very short-lived, decaying to zero by 30 μs after the laser flash. Changing the data collection timescale to 900 μs allows observation of the Cy3/Mn^{2+} until it decays appreciably (Figure 2.39). The Cy3/iodide signal is stronger than Cy3/Mn^{2+}, but very short-lived. The triplet quencher (COT) decreases the transient lifetime so much that the Cy3/Mn^{2+}/COT sample resembles the Cy3/iodide sample, but with smaller amplitude.

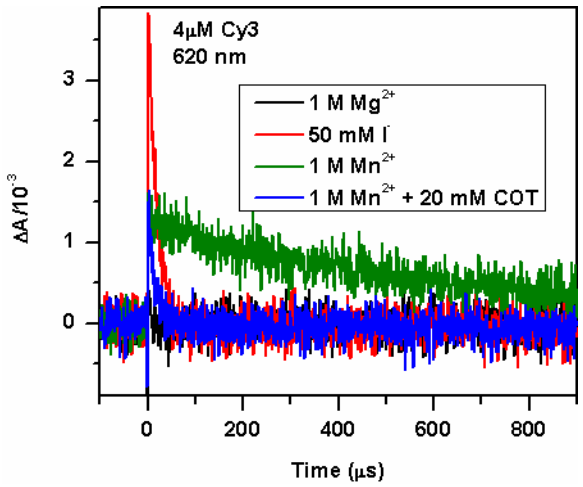


Figure 2.39: Kinetic Traces of Cy3 at Long Times. Kinetic traces of the same Cy3 samples as in Figure 2.38, but observed on a longer timescale. Adapted from Reference 35. Copyright © 2013 WILEY-VCH Verlag.

D. Fluorescence Correlation Spectroscopy Experiments

Finally, the single molecule dyes were measured via FCS to see if a fast fluctuation due to triplet blinking is detectable. Figure 2.40, below, shows the autocorrelation decays of three Cy3B samples, alone, with Mg^{2+}, and with Mn^{2+}. The

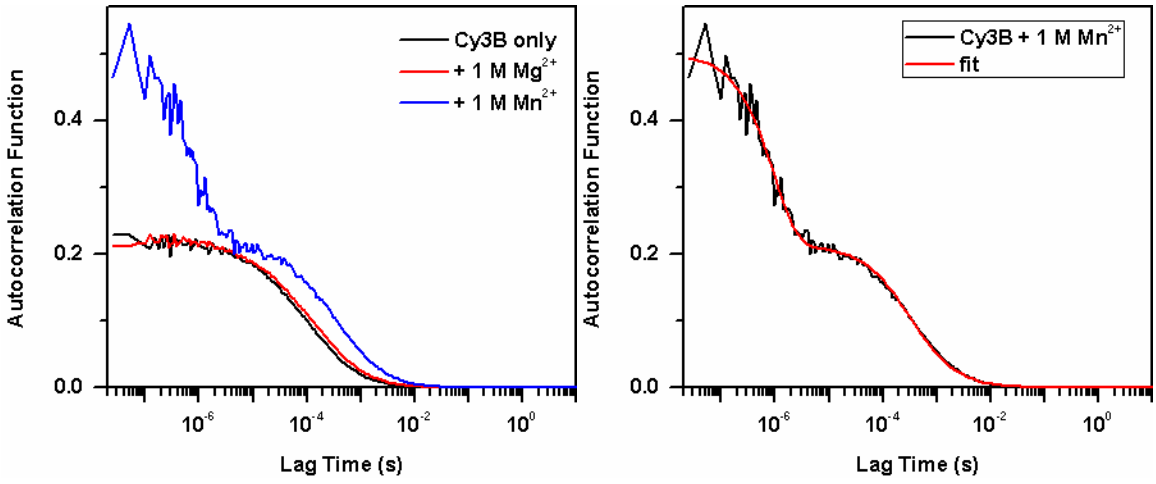


Figure 2.40: FCS Decays of Cy3B in the Presence of Cations. The left panel shows the FCS decays of Cy3B with Mg^{2+} (red), Mn^{2+} (blue), and alone (black). The laser power used was 570 μW, dye concentration was 10 nM. The right panel shows a fit to the Cy3B/Mn^{2+} samples using Equation 1.56. Adapted from Reference 35. Copyright © 2013 WILEY-VCH Verlag.

Cy3B/Mn^{2+} sample displays a prominent fluctuation in the microsecond timescale, while the other two samples appear to be standard diffusion only autocorrelation decays. However, even the decays displaying no additional fluctuation could not be fit with the standard diffusion only model (Equation 1.54). Instead, Equation 1.56 was used as the fitting model; Table 2.2 shows the parameter values from the fit. Even the Cy3B only and Cy3B/Mg^{2+} samples have almost 20% population in the triplet state. The

Table 2.2: Fit Parameters for FCS Decays of Cy3B

	$G(0)$	r_0/μm	$\bar{T}$	τ_R/μs
Cy3B only	0.062 ± 0.001	0.47 ± 0.01	0.16 ± 0.01	9 ± 1
Cy3B/Mg^{2+}	0.131 ± 0.001	0.54 ± 0.01	0.19 ± 0.01	14 ± 1
Cy3B/Mn^{2+}	0.213 ± 0.002	0.75 ± 0.02	0.58 ± 0.01	0.97 ± 0.03

Table 2.2: Fit Parameters for FCS Decays of Cy3B. Best fit parameters of Equation 55 used to fit FCS decays of Cy3B, Cy3B/Mg^{2+}, and Cy3B/Mn^{2+} samples. Error shown is from the fit.

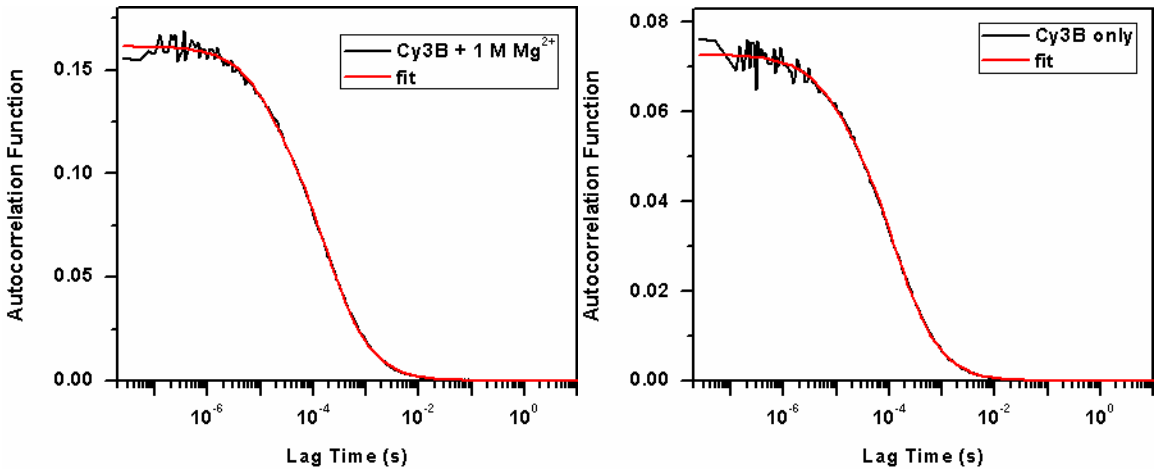


Figure 2.41: FCS Decays of Cy3B with Fit Results. The fit of Equation 55 is shown in red for Cy3B/Mg^{2+} (left) and for Cy3B only (right).

Cy3B/Mn^{2+} sample, however, has almost 60% of its population in the triplet state. The fits of the Cy3B alone and the Cy3B/Mg^{2+} samples to Equation 1.56 are shown in Figure 2.41.

2.4 Discussion

A. Determining the Cause of Photobleaching

From the lifetime results presented initially, it's clear that Cy3B is most affected by the presence of Mn^{2+}, which decreases its lifetime from 2.4 ns to 2.2 ns—at 0.5 M Mn^{2+}, that is. Increasing the Mn^{2+} concentration to 1 M decreases the lifetime further to 2.1 ns. TEMPOL, however, has an even greater effect on Cy3B's lifetime decreasing it to 0.92 ns. As for Cy3B, TEMPOL decreases Cy5's lifetime from 0.90 ns to 0.49 ns, although Cy5 lifetime increases in the presence of Mn^{2+} to 1.0 ns (Table 2.1). These results suggest that paramagnetism may be the effect behind the altered photophysics. In aqueous solution Mn^{2+} exists in the high spin complex $Mn(H_2O)_6^{2+}$ with five unpaired electrons. TEMPOL, on the other hand, has only one unpaired electron; it appears the strength of the interaction is not directly related to the magnetic field of the paramagnetic

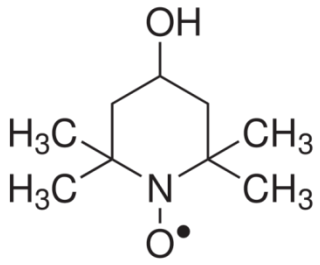


Figure 2.42: Structure of TEMPOL. Structure of 4-Hydroxy-2,2,6,6-tetramethyl-1-piperidin-1-yloxy. TEMPOL is a radical, possessing one unpaired electron.

ion/molecule. Additionally, due to the lack of influence of Mn^{2+} on Cy3 and Cy5, lifetime may play a role in this interaction: a longer lifetime may be necessary to provide the dye molecule—dication complex enough time for the interaction to occur. If this is indeed the case it would explain why there is no lifetime change with Mn^{2+} for Cy3 (normally 0.2 ns), a small change for Cy5 (normally 0.90 ns), and a significant change in

lifetime for Cy3B (2.4 ns lifetime when alone). Interestingly, the cations Mg^{2+} and Mn^{2+} cause the same increase in lifetime for Cy5. In the photobleaching experiments, however, Cy5 fluorescence intensity is strongly quenched by both Mn^{2+} and TEMPOL, however only the Cy5/TEMPOL sample experiences a significantly shorter lifetime. There is also significant quenching for the Mg^{2+} and Zn^{2+} samples, but only a minor increase in Cy5 lifetime (Figure 2.13, left).

The photobleaching experiments for Cy3B show a marked increase in the bleaching rate when in the presence of Mn^{2+}, and large (about 70%) quenching in the presence of TEMPOL (Figure 2.9, left). The photobleaching experiment conducted at high dye (6.5 μM) concentration allowed the measurement of absorption spectra of the samples before and after irradiation. The absorption spectrum of the Cy3B/Mn^{2+} sample showed significant changes after irradiation: the main absorption band of Cy3B (around 550 nm) decreased dramatically, while there's an increase in absorbance at the short wavelengths around 250 – 270 nm and 350 – 400 nm (Figure 2.10). These two observations indicate that Cy3B is undergoing a reaction that destroys its chromophore structure—the polymethine chain—resulting in smaller molecule fragments, which absorb higher energy wavelengths. The same results were observed for the Cy5 photobleahing experiment at high concentration (Figure 2.14).

The DNA photobleaching experiments were performed as a comparison to Stennett et al.'s work on TAMRA-labeled DNA[83] which showed that low (millimolar) concentrations of Mn^{2+} are enough to cause photobleaching of TAMRA-dsDNA. Low concentrations of Mn^{2+} (2.5 mM) did not cause any increase in photobleaching of Cy3B-dsDNA, although the Cy3B-dsDNA/Zn^{2+} sample was significantly quenched (Figure

2.12, left); it is not known what the origin of this behavior is. A Mn^{2+} concentration as high as 0.25 M was required to alter the behavior of Cy3B-dsDNA, and it caused quenching of the dye rather than an increase in photobleaching rate (Figure 2.12, right). For Cy5, however, the low 2.5 mM concentration of Mn^{2+} is enough to cause a significant increase in photobleaching rate compared to iCy5-dsDNA alone. However, as for Cy3B-dsDNA, Zn^{2+} alters the behavior of iCy5-dsDNA, which experiences a photobleaching rate greater than that of iCy5-dsDNA/Mn^{2+} (Figure 2.19, left). Low concentrations of Mn^{2+} also cause significant photobleaching for Cy3-ssDNA and Cy3-dsDNA (Figure 2.24, left). This is due to the ability of the Mn^{2+} to chelate to the negatively charged phosphate backbone of the DNA; once chelated the dication is closer to the dye than it would be in solution allowing the dication-dye interaction to affect the dye's behavior.

Given these results, the next set of photobleaching experiments aimed to determine the cause of the accelerated photobleaching rate. As explained in the introduction to this chapter, singlet oxygen is a reactive intermediate often responsible for the loss of dye molecules in solution. The Cy5 photobleaching experiments in Figure 2.15 (left panel) showed no difference in photobleaching rate of Cy5 in deoxygenated solution versus oxygen saturated solution indicating that the presence of oxygen has no bearing on the photobleaching rate of Cy5. The photobleaching experiment on Cy5 with dications in deoxygenated solution (Figure 2.15, right) indicates that Mn^{2+} causes a significant increase in photobleaching rate, but not through a singlet oxygen path, i.e., reaction of the dye with singlet oxygen may not be the cause. Other tests for singlet oxygen include adding azide (N_3^-) to the buffer, and making the buffer with heavy

water—deuterium oxide (D_2O). Azide, the single oxygen quencher, had no effect on the rate of photobleaching: Cy3B/Mn^{2+}/N_3^- and Cy3B/Mn^{2+} bleached at the same rate (Figure 2.11, left) as did Cy5/Mn^{2+}/N_3^- and Cy5/Mn^{2+} (Figure 2.17, left). Increasing the concentration of azide from 2 mM to 200 mM did not alter the photobleaching kinetics of Cy5/Mn^{2+} either. Deuterium oxide, in which singlet oxygen has a longer lifetime—it increases an order of magnitude from H_2O to D_2O[102]—was expected to increase the photobleaching rate for the dyes in Mn^{2+}. For Cy3B/Mn^{2+} in D_2O there is a slight increase in photobleaching rate as compared to Cy3B/Mn^{2+}/H_2O (teal vs. red traces in Figure 2.11, right). However, it's unclear how significant this increase is since the initial photobleaching rates are the same, and because the fluorescence intensity is not "smooth" during that trial (may be due to variations in the lamp intensity). For Cy5 the photobleaching rate is the same whether the Cy5/Mn^{2+} is in heavy water or not, but the fluorescence intensity is greater for the deuterated buffer (Figure 2.17, right). Also interesting to note is that the intensity of Cy5 and Cy3B is greater in D_2O (compare black and blue traces in Figures 2.11 and 2.17, right).

The presence of the Fenton reagent, iron(II), was tested for due to its potential presence in the source of Mn^{2+} used, which may then be the actual reagent responsible for the increased photobleaching rates. In tests with Cy5 (Figure 2.16, left) the 6 μM Fe^{2+} sample experienced an initial increase in photobleaching rate for Cy5, while the 21 μM Fe^{2+} sample only showed a quenching effect. Due to the inconclusive nature of this test an iron(II) chelator was also used in Cy5/Mn^{2+} samples. The chelator, desferoxamine mesylate, will chelate any iron(II) impurity from the source of manganese(II), which is a chloride tetrahydrate at least 98% pure. The chelator was used in 0.2 mM and 2.0 mM

concentrations, whereas the iron impurity is up to 5 ppm, which translates into a concentration of about 5 μM iron, whether that is iron(II) or iron(III) was not detailed in the specification sheet from Sigma-Aldrich. In any case, the iron(II) chelator was used in up to a three order of magnitude higher concentration; the presence of the chelator made no difference in the photobleaching rate of Cy5/Mn^{2+} (Figure 2.16, right). The effect of impurities was also investigated on internally-labeled Cy5 DNA (iCy5-dsDNA). An extremely pure version of manganese(II) was used (99.99% pure on a trace metals basis from Sigma-Aldrich); iCy5-dsDNA photobleached at the same rate for both sources of manganese(II) used (Figure 2.19, left). Various concentrations of iron(II) were tested with iCy5-dsDNA (Figure 2.19, right) and only quenching effects were observed with 10 μM Fe^{2+} (100 times the concentration of DNA, about 15% quenching) and 100 μM Fe^{2+} (1000 time the concentration of DNA, about 80% quenching). Although these tests do not conclusively rule out ROS as the cause of the increased photobleaching, they suggest that the reaction with ROS is not the rate determining step in the photobleaching reaction.

Cy5's photobleaching behavior was also studied with the ROXS reagents MV (methylviologen, the oxidant) and AA (ascorbic acid, the reductant) in Figure 2.20. The Cy5/MV sample photobleached completely, while the Cy5/AA sample experienced only a minor decrease in fluorescence intensity. This suggests that the radical anion form of Cy5 is long-lived in solution, and, hence, susceptible to chemical attack, which depletes the chromophore. The unaltered photobleaching rate of The Cy5/AA sample indicates the radical cation form of Cy5 may be too short-lived for any reaction to occur. When used in conjunction, the ROXS reagents (MV and AA) quench the fluorescence of Cy5 by about 30% initially, but output of the dye remained stable for the duration of the

experiment. This experiment indicates that the presence of Cy5's radical anion is the cause of photobleaching, however an oxidant would have to present in solution for Cy5 to form the radical cation form. The ROXS system is a good method for mitigating the radical cation's effects.

Finally, tests for the triplet state were conducted using cyclooctatetraene (COT), a known triplet quencher.[103] Solutions of Cy3B/Mn^{2+}/COT and Cy5/Mn^{2+}/COT photobleached at a much lower rate than solutions of Cy3B/Mn^{2+} and Cy5/Mn^{2+} (Figure 2.11, left and Figure 2.18), thus providing tangible proof that the accelerated photobleaching observed in Mn^{2+} solutions proceeds through the triplet state. Cy3 does not display a difference in photobleaching rate between Mg^{2+} and Mn^{2+} samples (Figure 2.21 and Figure 2.23, left panel), however on DNA Mn^{2+} dramatically increases the photobleaching rate of Cy3 (Figure 2.23, right panel), and COT slows the photobleaching of Cy3 back to the initially observed rate. Thus, transient absorption (TA) spectroscopy was employed to directly observe the triplet state in Mn^{2+} samples.

B. Direct Measurement of the Triplet State

The TA spectrum—also called the difference spectrum—of Cy3B/Mn^{2+} shows a strong positive absorption to the red of the singlet ground state absorption (Figure 2.25, left), which is assigned to triplet-triplet absorption since the difference spectrum of Cy3B/Mg^{2+} shows no signal in that region (Figure 2.28, left), and since addition of COT shows a much weaker signal (Figure 2.26, left). The same is seen in Figure 2.31 (right panel) where the same experiment was conducted, but the solutions are oxygen saturated; although much shorter-lived the Cy3B/Mn^{2+} sample produces a clear positive signal at

610 nm (the peak of the triplet band of Cy3B) which decays to zero by 10 μs (in argon saturated solution the signal decays to zero by 300 μs). The Mg^{2+} sample produces no signal, while the Cy3B/Mn^{2+}/COT sample also produces no signal—the COT effectively quenches the short-lived triplet state produced in oxygen saturated solution.

For Cy5 and Cy3 the understanding of the difference spectrum is more complicated since both dyes can rotate about the carbon-carbon double bonds in the polymethine chain. Once in the first singlet excited state the dye can either fluoresce, deactivate via internal conversion, photoisomerize into the *cis*- ground state, or undergo intersystem crossing to enter the triplet state. Both triplet and *cis*- states can be probed for in transient absorption, however, for cyanine dyes the absorption of the photoisomer and triplet states overlap.[58, 104] In the difference spectrum of Cy5/Mg^{2+} (Figure 2.32, right) the strong positive signal to the red of the photobleach (ground state absorption) is the absorption of the photoisomer(s). The difference spectrum of Cy5/Mn^{2+} (Figure 2.32, left) looks almost identical with the exception of the small positive signal at 730 nm and longer wavelengths—the Cy5/Mg^{2+} shows no signal in that region even though the dye is at a much higher concentration, thus this weak absorption band is due to the triplet state. This is corroborated by the difference spectrum of Cy5/iodide (Figure 2.33, right) which shows a slight positive signal in the red-most region of the spectrum. The individual kinetic traces in Figure 2.34 show the overlap of photoisomer and triplet absorption at 700 nm (left panel), where the Cy5/iodide signal is greater than the Cy5/Mg^{2+} signal. At 730 nm (right panel), there is no absorption due to photoisomer (Cy5/Mg^{2+} trace is at zero) but the triplet has a clear signal (Cy5/iodide and Cy5/Mn^{2+}). Figure 2.35 shows the effect of triplet quenchers COT and β-mercaptoethanol on kinetic traces at 730 and 740

nm: COT is effective at decreasing the lifetime of the triplet state, while β-mercaptoethanol has no effect even though it's used at more than seven times the concentration of COT. At these probe wavelengths Cy5/Mg^{2+} has no absorption while Cy5/iodide has a clear signal meaning this absorption is due solely to the triplet state. In oxygen saturated solution (Figure 2.37) the trends are similar with the notable exception that Cy5/Mn^{2+}/β-ME has a larger triplet signal (at 740 nm) than Cy5/Mn^{2+}. This could be due to the triplet quenching effect of oxygen—able to reduce the triplet population in Cy5/Mn^{2+}; why having two triplet quenchers (oxygen and β-mercaptoethanol) does not reduce the signal at 740 nm for Cy5 is unclear.

Transient absorption data for Cy3 supports the same conclusions. Cy3 has a shorter polymethine chain than Cy5, but can still rotate about its carbon-carbon double bonds to form the *cis*-isomer. The maximum of Cy3's difference spectrum is at probe wavelength 570 nm, where, in Figure 2.38 (left), all samples absorb identically. The photoisomer absorption dies away by 620 nm, where Cy3/Mg^{2+} has no signal, and Cy3/iodide has a relatively strong (up to 0.3 x 10^{-2}), but short-lived signal (decays to zero by 70 μs) (right panel). A better comparison of the Cy3/Mn^{2+} to Cy3/Mn^{2+}/COT signals is in Figure 2.39; the triplet formed by Mn^{2+} is long-lived, decaying to zero more than 900 μs after the initial laser pulse. COT reduces its lifetime by more than a tenth.

C. Triplet Observation by Fluorescence Correlation Spectroscopy

The final test of manganese(II)'s triplet forming ability came in an FCS experiment. The sub-ms fluctuation in intensity observed for Cy3B/Mn^{2+} is in stark contrast to that for the Mg^{2+} and dye only samples (Figure 2.40, left), which appear to

have the form of a diffusion only decay. The high laser power used for the experiment (570 μW, I_{ex} in Equation 1.58) contributes to the large triplet state population (almost 60%) and low singlet-triplet relaxation time (Equation 1.59). Most interestingly, however, is the apparent increase in the size of radial parameter of the observation volume, r_0, which increases from 465 nm—for the dye only sample—to 746 nm for the Cy3B/Mn^{2+} sample. This increase is due to the optical saturation effect: a virtual increase in the observation volume—and, concomitantly, a decrease in the diffusion time (coefficient)—when the excitation intensity exceeds the maximum excitation rate of the molecule as defined by its photophysical properties.[105-108]

I. Optical Saturation Effect in FCS

The maximum excitation rate, known as the saturation rate, is determined by the rates of fluorescence and of populating and depopulating any dark states present; when the dark state is the triplet state it is given by Equation 2.1[109], below, where k_{10} is the

$$k_{sat} = \frac{k_{10}}{1 + k_{ISC} / k_{TS}} \tag{2.1}$$

rate of fluorescence, and k_{TS} is the rate of transition from the triplet state to the ground singlet state. For the simplified case of no dark states the saturation rate is equivalent to the fluorescence rate. As an example, let's assume Cy3B with lifetime of 2.4 ns, has no potential dark state. In this case Cy3B has a saturation rate of 4.2×10^8 s^{-1}. For 532 nm excitation and laser power of 100 μW the excitation rate is 2.6×10^7 s^{-1}, below saturation, meaning if the laser power is to be increased there will be an accompanying increase in the fluorescence intensity of the sample. Once the excitation rate surpasses the saturation

rate—which occurs at about 1585 μW of laser power—the sample will no longer increase in fluorescence intensity. These values are calculated from the simple relationships below for energy of a photon (Equation 2.2), power (in photons/s Equation 2.3), intensity (Equation 2.4) and excitation rate (Equation 2.5). The absorption cross section, σ, is calculated in Equation 2.6 from an extinction coefficient, ε, of 130,000 M^{-1} cm^{-1}. Equation 2.4 also assumes the radial parameter of the observation volume is 0.400 μm.

$$E_{ph} = \frac{hc}{\lambda} = \frac{(6.626\times10^{-34}\,J\cdot s)(2.997\times10^{8}\,m/s)}{532\times10^{-9}\,m} = 3.7\times10^{-19}\,J/photon \tag{2.2}$$

$$P = \frac{laserpower}{energy/photon} = \frac{100\times10^{6}\,J/s}{3.7\times10^{-19}\,J/photon} = 2.7\times10^{14}\,photons/s \tag{2.3}$$

$$I = \frac{P}{\pi r^{2}} = \frac{2.7\times10^{14}\,photons/s}{\pi(400\times10^{9}\,m)^{2}} = 5.3\times10^{26}\,photons/m^{2}/s \tag{2.4}$$

$$k_{ex} = \sigma I_{ex} = (5.0\times10^{-20}\,m^{2})(5.3\times10^{26}\,photons/m^{2}/s) = 2.6\times10^{7}\,photons/s \tag{2.5}$$

$$\sigma = \frac{2.303\varepsilon}{N_A} = \frac{2.303(130000\,M^{-1}cm^{-1})}{6.022\times10^{23}\,mol^{-1}}\frac{0.1\,cm\cdot m^{2}}{L} = 5.0\times10^{-20}\,m^{2} \tag{2.6}$$

For the case experienced in this study, where Equation 2.1 applies, the rates of the singlet-triplet transition significantly affect the saturation rate of Cy3B. Unfortunately, values for k_{ISC} and k_{TS} for Cy3B have not been reported in the literature, however it is the ratio of the two rates (k_{ISC}/k_{TS} defined as r below) which determines k_{sat}. Taking this ratio into account the fluorescence rate is given by Equation 2.7, which is normalized by the fluorescence rate at infinite excitation rate to give Equation 2.8. A plot showing the effect of different dark state population/depopulation ratios, r, is shown below (Figure 2.43). As the ratio, r, increases the excitation rate at which saturation is reached

decreases.

$$k_f = \frac{\phi_f k_{ex}}{1+(k_{ex}/k_{10})(1+r)} = \frac{\phi_f k_{ex}}{1+(k_{ex}/k_{sat})} \tag{2.7}$$

$$k_f = \frac{1}{\frac{k_{10}}{k_{ex}(1+r)}+1} \tag{2.8}$$

To illustrate the optical saturation effect assume the triplet state population/depopulation ratio is 100 (green curve in Figure 2.43). The point-spread function, $p(r)$ shown in Equation 1.51, is well represented by a Gaussian when the laser's excitation intensity is below the molecule's saturation intensity; the excitation intensity experienced by the sample is greatest in the center of the observation volume

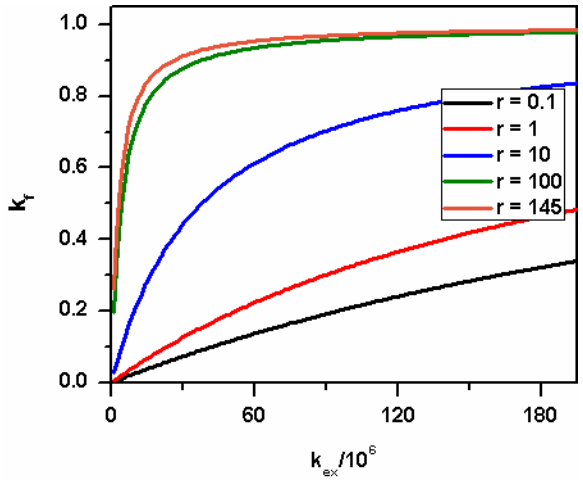


Figure 2.43: Fluorescence Saturation Rate Model. The fluorescence rate, k_f, is plotted versus the excitation rate, k_{ex}, for several values of r, the dark state population/depopulation ratio, according to the relationship in Equation 2.8.

and decreases away from the center following the Gaussian function. Below the saturation rate a molecule in the center of the observation volume and one at an outermost point (in the radial direction, for instance) may experience fluorescence rates on the "lower" part of the fluorescence rate curve. As the excitation intensity is increased

beyond the saturation rate a molecule in the center of the observation volume may have a fluorescence rate on the "upper" part of the curve whereas a molecule farther from the center may have a rate on the "lower" part. Since the center of the observation volume is at saturation any increase in the laser power will not bring an increase in fluorescence rate. At the outer perimeter, however, an increase in laser power will increase the fluorescence rate. This leads to a "top-hat" shape of the point spread function, $p(r)$, as illustrated in Figure 2.44, below, and is the cause of the larger s parameter required to fit the autocorrelation function, making the observation volume appear larger. Thus, higher-than-saturation laser power increases the observation volume "virtually" but not

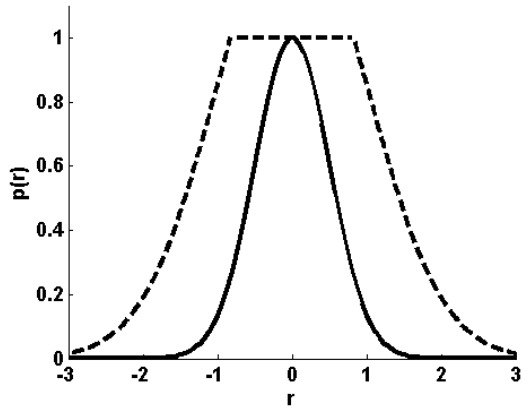


Figure 2.44: FCS Point-Spread Function at Saturation. The black curve shows the point-spread function, $p(r)$, at fluorescence rates below saturation. The dashed curve is a model of what the point-spread function looks like once molecules in the center of the observation volume reach saturation.

physically as the laser radius remains the same; the laser's greater excitation rate merely increases the probability of excitation on the laser beam's edge, causing more fluorescence to be observed from that region.

For Cy3B k_{ISC} is expected to be similar to values reported for analogous cyanines: quantum yields of less than 0.01 dimethylindocarbocyanine[44], 0.005 for

diethylthiacarbocyanine[82], and 0.03 for the succinimidyl ester of Cy3[57] have been reported. The data presented here in Figure 2.28 concurs with these low values as no triplet state was observed for Cy3B. This gives an estimated value of 4.2×10^{6} s^{-1} (from Equation 1.5, assuming ϕ_{ISC} is 0.01). This estimate, however, applies only to Cy3B alone, and will be affected by the presence of Mn^{2+}. The heavy atom effect is known to increase both population and depopulation rates, as shown in the left panel of Figure 2.31: more TEMPOL increases the rise in the signal (k_{ISC})—due to triplet state population—and increases k_{TS}—seen as a decrease in the lifetime (compare 10 mM and 20 mM TEMPOL samples). Thus, in the conditions used for FCS Cy3B's rate of ISC must be larger than the estimate given from literature. Assuming that Mn^{2+} increases the population rate by an order of magnitude gives k_{ISC} of 4.2×10^{7} s^{-1}. The rate for depopulation of the triplet state, k_{TS}, is unknown for Cy3B in its natural state. In the presence of Mn^{2+} and oxygen, however, the triplet state lifetime is approximately 3.4 μs, thus k_{TS} is 2.9 $\times10^{5}$ s^{-1} (from the right panel of Figure 2.31). These estimates give a ratio, r, of 145 (orange line, Figure 2.43). At 570 μW the excitation rate is approximately 150 MHz, at the center of the illuminated sample. This is "high" enough on the fluorescence excitation rate curve where saturation occurs, and this is the cause of the abnormally high r_0 value (0.75 μm) for the Cy3B/Mn^{2+} sample.

2.5 Conclusion

The purpose of this project was to determine whether the proximity of the paramagnetic cation Mn^{2+} to cyanine dyes will increase the intersystem crossing rate

resulting in photobleaching and increased blinking due to triplet state formation. Indeed, the photobleaching experiments show an increase in the photobleaching rate for Cy3B and Cy5 in buffers containing Mn^{2+}; chemical tests show that COT, a triplet quencher, can slow the rate of photobleaching down to levels when no Mn^{2+} is present. Transient absorption experiments performed on Cy3B/Mn^{2+} and Cy5/Mn^{2+} prove that the transient present is the triplet state. The triplet is also observed for Cy3/Mn^{2+} samples, but the dye's photobleaching rate is not altered unless it is conjugated to DNA. This is the result of the dye's short lifetime. Cy3B and Cy5 have longer lifetimes allowing for Mn^{2+} to alter the ISC rate significantly. Thus, proximity and excited state lifetime are the two deciding factors in whether a dye's ISC rate will be enhanced by Mn^{2+}. The triplet state of Cy3B/Mn^{2+} is also prominently seen in FCS decays at high laser power. The high laser power used combined with the enhanced ISC rate created ideal conditions for the optical saturation effect in which the observation volume is virtually enlarged by the saturation of the fluorescence rate.

These results show that the ISC rate enhancement caused by Mn^{2+} does not depend on a particular chromophore structure; Mn^{2+} has the same effect on rhodamine dyes[83]. Beyond the photophysics, these results have implications for biophysical studies: manganese(II) is involved in biochemistry as an enzyme cofactor and is sometimes used as a substitute for Mg^{2+} to study enzyme-nucleic acid interactions[110-113]. Fluorescence studies of biological systems that use Mn^{2+} must have carefully designed controls to ensure signals observed are due to biophysics rather than photophysics of cyanine, and rhodamine, probes.

Furthermore, the ability to use something as simple as a divalent cation to force a

dye to enter the triplet state may be exploited for super-resolution imaging purposes. In fact, the first experiments which overcame the diffraction barrier in fluorescence microscopy used triplet states to "optically shelve" the fluorophores.[114] Localization microscopy actually works better when more stable dark states are chemically generated from triplet states[97, 115, 116]. The cation's ability clearly has pros and cons. The interaction between Mn^{2+} and organic fluorophores should be investigated further for optical shelving purposes. While a probe's photophysics needs to be carefully considered when in the presence of this cation.

CHAPTER THREE

CHARACTERIZING THE PHOTOPHYSICS OF CY3 BEHIND PROTEIN INDUCED FLUORESCENCE ENHANCEMENT

3.1 Introduction and Motivation

Protein Induced Fluorescence Enhancement (PIFE) is a term coined by Prof. Sua Myong[117] now at Johns Hopkins University, to describe the observed increase in fluorescence intensity of a probe in close proximity to a protein. The PIFE technique is an alternative to Förster Resonance Energy Transfer (FRET), which requires a donor and acceptor molecule to report on the distance between the target biomolecules under study. With PIFE only a single fluorophore is necessary. This greatly simplifies the experimental design for studying nucleic acid-protein interactions as it is unnecessary to label the protein—a difficult, time consuming process involving mutations, which inherently change the behavior of the protein. Labeling the DNA, on the other hand, is efficient and cheap. Additionally, the problem of acceptor photophysics is eliminated; Cy5, amongst other red-absorbing dyes, experiences blinking, which has been mistaken for nucleosome dynamics in FRET experiments[118].

The removal of the second dye is the primary drawback to the PIFE technique. The Forster distance for many donor-acceptor pairs has been characterized, and is related to the distance between the donor-acceptor pair through the transfer efficiency equation[119, 120]. The efficiency measured in an experiment allows the determination of the distance between any FRET pair without the need to characterize the donor and acceptor for each system under study. The PIFE technique, although sensitive on

distances comparable to FRET, still requires that Cy3's fluorescent response be characterized for each protein studied. The Myong lab characterized the distance sensitivity of PIFE with BamHI (on dsDNA) and RIG I (on RNA-DNA duplexes), and found the fluorescence intensity of Cy3 will vary differently for each protein[117]. Myong and co-workers also used PIFE in further studies of RIG I,[121] Rad51,[122] the POT1-TPP1N complex,[123] and many others[124,125,126], and have authored reviews on the subject[127,128].

PIFE, however, was observed before the acronym was coined in *E. Coli* UvrD translocation,[129] binding of T7 DNA polymerase,[130] and transcription initiation by T7 RNA polymerase[131]. An "anomalous" increase in fluorescence of covalently bound (as compared to free) Cy3 and Cy3.5 was also reported[53]. Since 2009, the popularization of PIFE as a single-molecule technique has resulted in many publications focused on protein interactions with nucleic acids[132-141]. PIFE is typically used in conjuction with sm-FRET measurements to monitor protein binding,[132, 133] which can allow for a measurement of K_D,[136, 141] orientation[138], and kinetics[135]. PIFE has also been observed in bulk measurements[134, 140, 141]. Fluorescence enhancement due to protein proximity is not unique to Cy3; PIFE was observed for fluorescein in RNA binding studies of influenzavirus[137].

Despite the common occurrence of PIFE in empirical observations, there is a lack of understanding of the mechanism involved. There has been speculation, but no proof, that in Cy3 the bulkiness of the protein hinders the dye's rotation about the carbon-carbon double bonds in the polymethine chain, thus forcing the excited state dye to deactivate via other means rather than the preferred photoisomerzation, hence increased fluorescence[127]. In order to test this theory E.M.S. Stennett and the author used Cy3-

labeled DNA and the Klenow fragment (KF) as the experimental system. The Klenow fragment is the larger (approximately 68 kDa out of 103 kDa total mass), C-terminal part of DNA polymerase I (Pol I) from *E. Coli*, that carries out two out of the three enzymatic activities of pol I: 5'-3' polymerase (*pol*) and 3'-5' exonulease (*exo*). KF binds to double stranded DNA (dsDNA). For dsDNA with an overhang (the terms overhang, primer, and template are defined in Figure 3.1) the *pol* activity will add deoxynucleotide triphosphates (dNTPs) to the primer DNA strand, obeying complementarity, until the DNA is fully double stranded (see Figure 3.1). In the event the KF encounters a

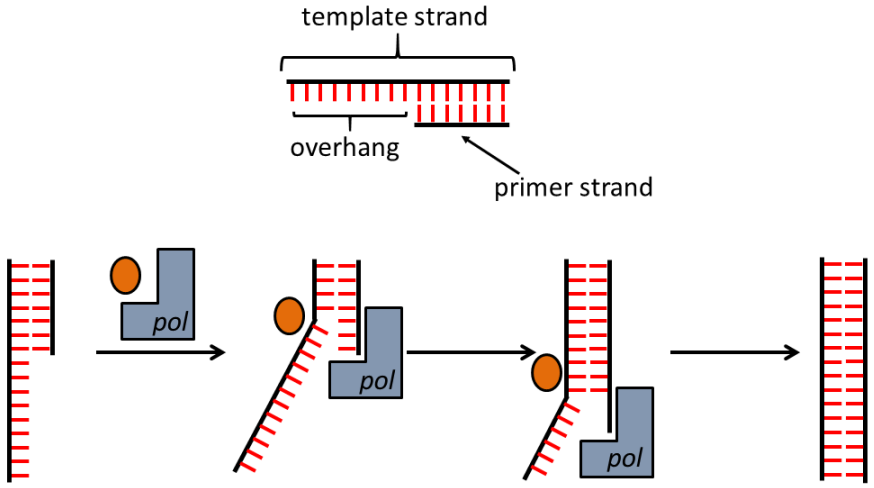


Figure 3.1: Schematic Representation of Polymerase Function of Klenow Fragment. The Klenow fragment consists of two domains, the *pol*- and *exo*- domains represented by the blue and orange shapes, respectively, in the cartoon. The *pol*- domain adds bases to the primer strand based on complementarity to the template strand (the long strand at the beginning of the process).

mismatched base pair—in the base duplex of the primer strand—the *exo* function will remove the incorrect base. This function, however, applies only to the terminal pair in the duplex region—if the first pair is correct but the second one is mismatched, the error will not be fixed. It is also known that the *pol* and *exo* functions are physically separated

in KF by approximately 30 Å[142, 143]. This study utilized two mutants of KF. One is the commercially available mutant (henceforth referred to as KFcom) that has the mutations D355A and E357A, which prevent activity and binding at the *exo* site[144, 145]. The second mutant has the mutation D424A, which prevents activity, but allows DNA binding at the *exo* site[144, 145]; this mutant was a gift from the lab of David Millar, and is henceforth referred to as KF. The DNA sample utilized in this study consists of a 6-base primer strand, labeled with Cy3 on the 5' end, and a 15-base complementary strand. The 6-bp (base pair) double-stranded region is composed of cytosine and guanosine bases (to ensure the two strands do not dissociate). This choice of experimental system was inspired by work done by Millar and co-workers studying the shuffling behavior of KF on DNA (discussed in detail below)[146].

The goal of this study was to directly observe the photoisomer of Cy3 with, and without, KF present. Time-dependent lifetime and anisotropy measurements were used to detect differences in Cy3's photophysical behavior and the binding of KF to the DNA, respectively. Transient Absorption (TA) measurements were performed as a direct measurement of the photoisomer population. As expected, the samples with protein formed approximately half the amount of photoisomer as compared to samples without it. This chapter presents the author's data for this project, which is complementary to data presented by E.M.S. Stennett in her doctoral dissertation[147]. This study has been published in a peer-reviewed journal[148]. It should be mentioned that an intensity enhancement of Cy3 has also been observed by the author in nucleic acid systems in the presence of hRPA (human replication protein A); this data is presented in Appendix I.

3.2 Material and Methods

A. Materials

Individual primer and template DNA strands were purchased from Integrated DNA Technologies. The primer was 5' labeled with Cy3: 5'-Cy3/CGC-CGC. The template strand was longer: 5'-CCC-GGA-ATT-GCG-GCG. Due to the short double-stranded region DNA was annealed in 10 mM Tris-HCl (pH 7.4) buffer with 10 mM $MgCl_2$ (the template strand was added at a 25% excess). The DNA was heated to 80°C, and after 5 minutes slowly cooled to room temperature. Annealing process was performed by E.M.S. Stennett.

Two versions of the Klenow fragment (KF) were utilized in this study. A commercial version, with mutations D355A and E357A, referred to as comKF, was purchased from New England Biolabs (catalog #: M0212M). A version of KF with mutation D424A was provided as a gift from Prof. David Millar (The Scripps Research Institute); it was expressed and purified as described previously[149].

DNA samples were mixed with a 25% excess of KF in New England Biolabs's buffer 2 and equilibrated on the bench for 30 minutes prior to measurement. DNA concentrations were 1 μM for TCSPC experiments and 3 μM for transient absorption experiments.

B. Time-Resolved Fluorescence and Anisotropy Measurements

Lifetime and anisotropy measurements were made using the time-correlated single photon counting (TCSPC) technique, as described in Chapter 2. The instrument response function (IRF) was measured at excitation wavelength from scattering of a

Ludox (colloidal silica in water) solution; it has a FWHM of 50-55 ps. The appropriate interference filters for excitation and long band pass filters for the emission were used. Cy3B was used as the standard and excited at 532 nm. Cy3-dsDNA and protein samples were excited at 532 nm; emission was collected at 570 nm. Fluorescence intensity decays were fitted with a sum of exponentials (the IRF was used for deconvolution) using ASUFIT (in-house written software). The time-resolved fluorescence anisotropy decays were calculated from experimental data according to $r(t) = (F_{VV} - F_{VH}\,G)/(F_{VV} + 2\,F_{VH}\,G)$, i.e. no deconvolution was performed. The G-factor was determined via the tail matching method with a solution of free Cy3B in water.

C. Transient Absorption Measurements

Transient absorption of the cis isomer was measured with a multichannel pump-probe transient absorbance spectrometer (EOS, Ultrafast Systems, Sarasota, FL). The system utilizes a photonic fiber-based continuum generator to create probe light between 360 – 914 nm. To create excitation pulses at 530 nm an Optical Parametric Amplifier was pumped by a kilohertz regenerative amplifier system (Tsynami, Spitfire, IROPA, Spectra-Physics). Data from this instrument has a spectral resolution of approximately 1 nm and sub-nanosecond time resolution. Samples were measured in a 2.0 mm path length cuvette and continuously mixed by a magnetic stir bar. A high concentration (3 μM) was used due to low signal-to-noise ratio. The time-resolved spectra were background corrected at each wavelength. Measurements were collected over a 40 ns time window (using 450 time points). The transient spectra shown in this chapter represent averages of spectra measured in the 13-33 ns time window after excitation.

Data for the Klenow fragment provided by David Millar was measured by Elana M. S. Stennett.

3.3 Results

A. Emission Spectra

An emission spectrum was measured of the Cy3-DNA sample on its own and in the presence of KF (in approximate 40% excess). In the presence of KF the fluorescence intensity is almost double that of the Cy3-labeled DNA alone (Figure 3.2). The KF does not shift the fluorescence spectrum, nor does it cause any changes in shape, hence the fluorescence characteristics of Cy3 are not altered by KF.

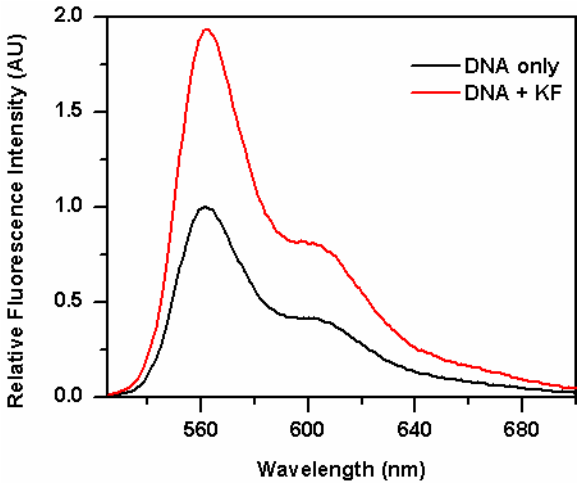


Figure 3.2: Emission Spectrum of Cy3-dsDNA with Klenow Fragment. The emission spectra of the Cy3-DNA primer/template sample was measured on its own (black trace) and in the presence of KF (red trace). Besides the almost two-times enhancement in the intensity there is no effect on the emission spectrum of Cy3. These spectra were measured by Elana M. S. Stennett.

B. Lifetimes and Anisotropies

Lifetime measurements on the primer DNA with and without KF indicate a significant change in the environment of Cy3. As seen in Figure 3.3 (left panel), the presence of KF increases the average lifetime of the dye from 0.65 ns to 0.74 ns (see Table 3.1). Lifetime data was fit with three exponential terms reflecting the contribution to the average lifetime from the dye itself—a very short 200-300 ps—and two terms for the dye's interaction with DNA. The shortest lifetime component changes little with KF, decreasing from 0.28 ns to 0.25, while the second lifetime increases from 0.77 ns to 0.82 ns. The longest lifetime component is most affected by the presence of the protein, increasing from 1.5 ns to 2.0 ns (the relative contribution of each lifetime to the average does not vary significantly). This means the contribution to the average lifetime has switched from the dye and its interaction with DNA to the dye's interaction with the protein; the long lifetime represents the dye interacting with the KF. Interestingly, the

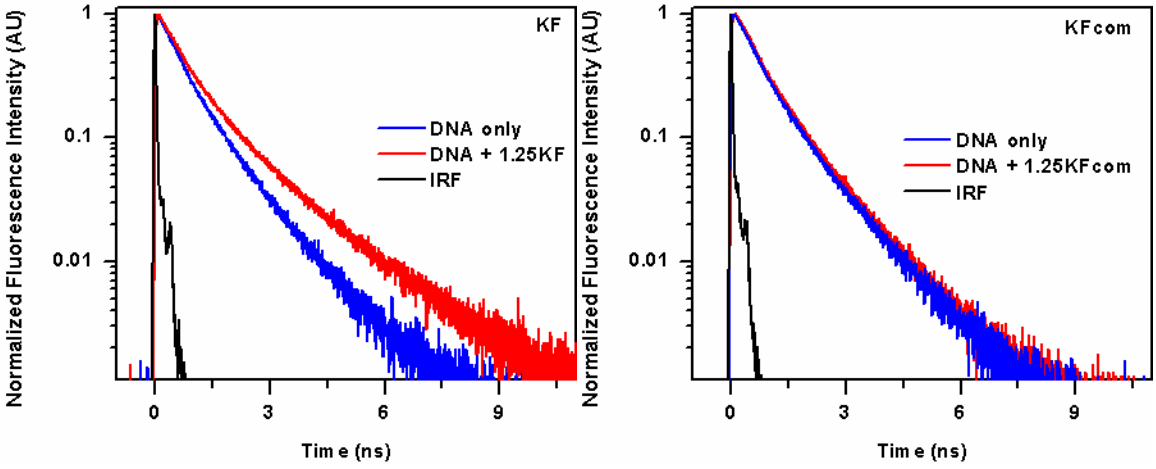


Figure 3.3: Lifetimes of Cy3-dsDNA with Klenow Fragment. The left panel shows the intensity decays for Cy3-DNA with (red trace) and without (blue trace) KF present. The lifetime increases significantly in the presence of KF. The right panel shows the same measurement for the commercial version of KF. No change in lifetime is observed. A 25% excess of KF/KFcom was used; using more equivalents of the Klenow fragment did not further increase the lifetime, i.e., at 25% excess the DNA is saturated with KF.

Table 3.1: Lifetimes of Cy3-DNA in the Presence of Klenow Fragment

	τ_1/ns	α_1	τ_2/ns	α_2	τ_3/ns	α_3	$\langle\tau\rangle$/ns
Cy3-DNA only	0.28	0.43	0.77	0.44	1.5	0.13	0.65
+ KF	0.25	0.41	0.82	0.46	2.0	0.13	0.74
+ KFcom	0.30	0.44	0.83	0.46	1.6	0.10	0.67

Table 3.1: Lifetimes of Cy3-DNA in the Presence of Klenow Fragment. These are the results of individual lifetime fits for Cy3-dsDNA on its own, with KF, and with KFcom. The lifetime components, τ_i, and their weights, α_i, are listed, along with the average lifetime, $\langle\tau\rangle$.

same experiment with the commercial version of the protein, KFcom, yields very different results, shown in the right panel of Figure 3.3. KFcom has nearly no effect on the average lifetime of the dye (Table 3.1) despite being identical in size.

Anisotropy measurements were also performed on the two protein samples yielding very interesting results. In Figure 3.4, below, the left panel shows the anisotropy for the Cy3-DNA in blue. Upon addition of a 25% excess of KFcom the rotational correlation time of the samples increases; this is due to the "bulk" of the protein, which slows down the movement of the tagged dsDNA causing less depolarization of the fluorescence. The right panel of Figure 3.4 shows the anisotropy results when using fully functional KF. In the presence of 25% excess of KF the anisotropy shows a "dip-and-rise" behavior—as observed by Millar for similar samples[146]. The anisotropy decreases at short timescales (0 to 2 ns after the laser pulse) just like the dsDNA only sample, but then it increases from 2 to 6 ns before it begins to level off. In either case, data from both experiments proves the protein is binding to the dsDNA, as evidenced by the increase in rotational correlation time. The difference in the anisotropy decays—for the dsDNA/protein systems—also points towards a difference in environment for Cy3 in the

presence of the two different KF proteins. This difference in environment may stem from the differing activity of the two protein versions. KFcom has only one location with binding activity—the *pol* site—while KF can also bind at the *exo* site. Binding at the *exo* site may cause the dye (Cy3) to experience a different environment leading to what is called an associated anisotropy decay (red, right panel). Associated anisotropy is discussed briefly below and in detail in Appendix I.

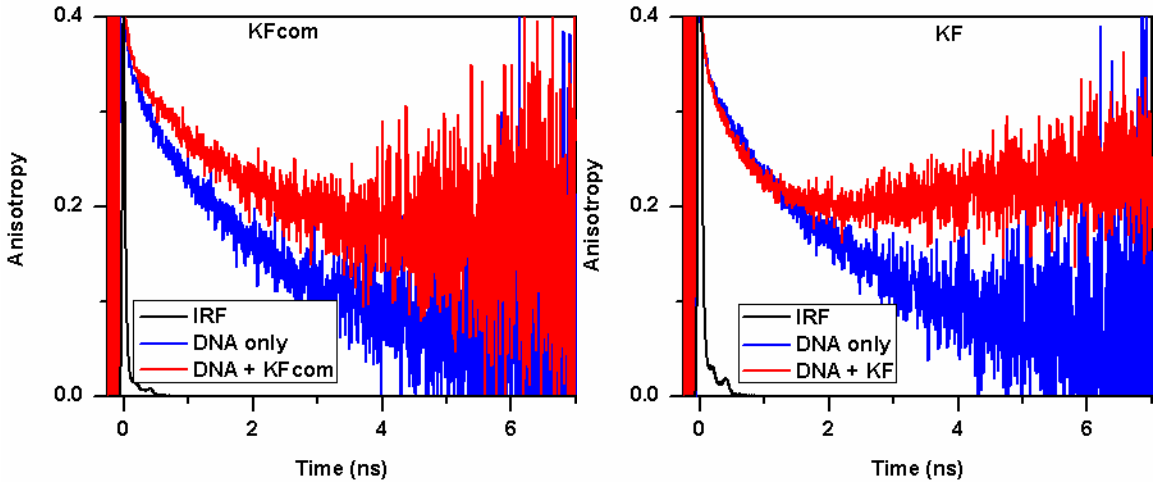


Figure 3.4: Anisotropy of Cy3-DNA in the Presence of Klenow Fragment. Anisotropy of Cy3-DNA alone (blue traces), with KFcom (red trace, left), and with KF (red, right). The Cy3-DNA/KF sample in the right panel shows "dip-and-rise" behavior.

C. Transient Absorption Measurements

Transient absorption measurements also support the theory that the dye experiences different environments depending on which protein binds to the DNA. The left panel of Figure 3.5 below shows the transient absorption spectra of Cy3-DNA on its own (black trace) and with a 40% excess of KFcom (red trace); both measurements were made with independent samples. A small amount of a protein degrader (protease) was added to the Cy3-DNA/KFcom samples (blue trace) to investigate whether the long

measurement duration (about 90 minutes) affects the concentration of the sample, i.e., photobleaching may be a factor. What is seen, however, is that the signal from the protease sample is nearly identical to that of the Cy3-DNA/KFcom sample, with an insignificant difference at the peak. Thus, photobleaching does not appear to be an issue in these measurements. The three samples measured in this set have nearly identical difference spectra featuring a prominent positive signal from 560 – 590 nm, a region associated with the *cis*-photoisomer of Cy3.

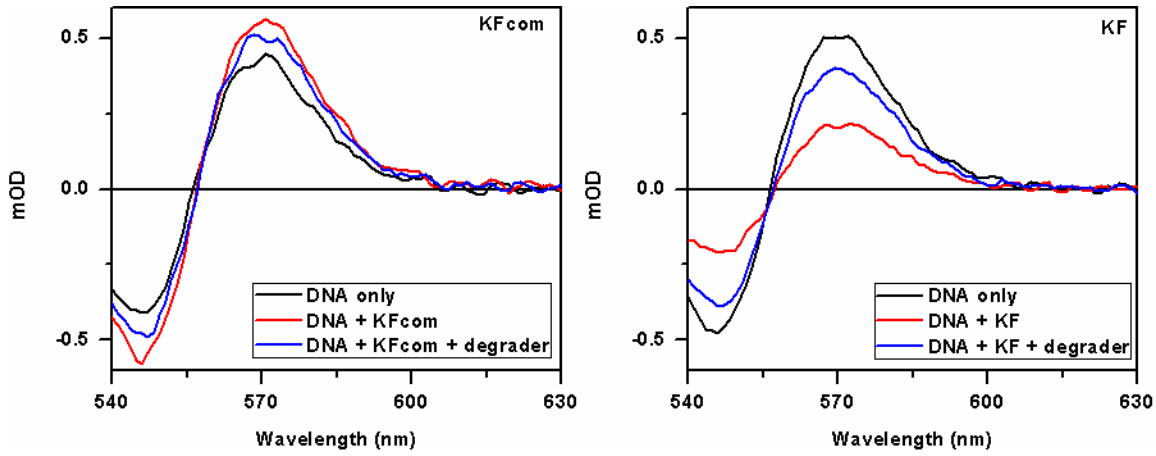


Figure 3.5: Difference Spectra of Cy3-DNA in the Presence of Klenow Fragment. The left panel shows the difference spectra of Cy3-DNA in the presence of the commercial version of KF, while the right panel shows the difference spectra with Millar's KF. KFcom has no effect on the population of photoisomer formed in Cy3-DNA, while KF decreases the isomer population (black to red) by approximately half. The protein degrader is used to show no significant photobleaching of Cy3 occurred during the measurement. Data in the right panel was measured by E.M.S. Stennett.

The right panel of Figure 3.5 shows the transient absorption spectra for the dsDNA sample interacting with the noncommercial version of 40% excess of KF (red trace). Here, there is a significant difference in signal between the Cy3-DNA (black trace) and the Cy3-DNA/KF samples. It appears that the presence of KF decreases the population of the *cis*-photoisomer. The Cy3-DNA/KF sample was then degraded with a

protease (blue trace); the difference between the black and blue traces indicates that the protein does indeed have a significant effect on isomer formation: once the protease degrades the KF the signal increases—almost to the level of the dsDNA only sample—the difference may be due to pipetting errors: the two samples may not have contained an equal amount of DNA to begin with. The cause of the different spectra—comparing KFcom and KF samples—must have to do with the different binding modes of the proteins.

3.4 Discussion

A. Explanation for "Dip-and-Rise" Anisotropy Shape

An associated anisotropy decay—with "dip and rise" shape—was observed by Millar and colleagues for a similar DNA sample in the presence of KF (with mutation D424A, non-commercial version), while a standard anisotropy decay was observed for the same DNA sample in the presence of KFcom (D355A, E357A, commercial version).[146] The probe used by the authors, dansyl chloride, is a derivative of aminonaphthalensufonate (ANS), which is an environmentally sensitive probe. Some derivatives of ANS are barely fluorescent in aqueous solution, but experience high fluorescence when bound to proteins or dissolved in organic solvents. Some ANS derivatives have been used for detecting conformational changes in protein specifically due to this photophysical property[150]. Associated anisotropy decays are the result of the fluorescent probe existing in more than one environment—as long as the environment wherein the dye with the shortest correlation time also has the shortest fluorescence lifetime. As mentioned above, KF has binding activity at the *exo* site while KFcom does

not, meaning a DNA sample exposed to KF could be bound to it through either the *pol* or *exo* sites, while a sample exposed to KFcom could only be bound at the *pol* site. This is the explanation used by Millar and colleagues to explain the difference between their two anisotropy results. Their DNA sample consisted of a labeled 17 base strand annealed to a 20-base complement; the dye is located on the eighth base from the three-base overhang. The authors propose that the primer strand binds to the pol site of KF via its 3' end; in this position the part of the DNA labeled with the probe is still outside of the protein allowing the dye to experience a solvent environment. However, getting the 3' end of the primer to the *exo* site requires the protein to travel 8 bases upstream on the DNA, pulling the dye-labeled base into the protein itself. Here the dye experiences a protein environment, altering its fluorescence characteristics.

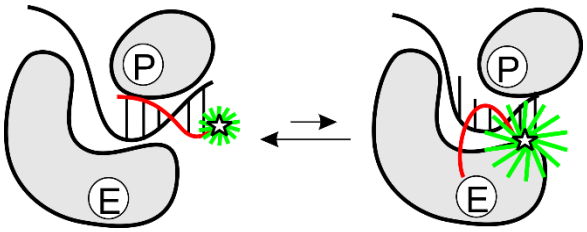


Figure 3.6: DNA Binding to Klenow Fragment. This is a cartoon representation of the two binding modes of KF (from Millar) used for these experiments. When bound at the *pol* site (left) Cy3 remains outside the protein in the solution environment. Binding at the *exo* site (right) pulls the primer strand (along with the Cy3) into the protein interior, where the dye fluoresces more efficiently. Adapted with permission from Stennett, E. M. S.; Ciuba, M. A.; Lin, S.; Levitus, M., Demystifying PIFE: The Photophysics Behind the Protein-Induced Fluorescence Enhancement Phenomenon in Cy3. *Journal of Physical Chemistry Letters* **2015,** *6* (10), 1819-1823. Copyright © 2015 American Chemical Society.

A similar explanation is applied to the anisotropy results seen here. Analysis of the lifetime results for the Cy3-DNA/KF samples shows a considerable effect on Cy3's photophysics due to conjugation and exposure to the proteins. Cy3 has a single, short

lifetime when dissolved on its own in aqueous solution, about 200 ps. The measurements show that conjugation to the 5' end of the dsDNA sample used in this work results in a multi-exponential decay (Table 3.1) requiring three lifetimes. In the presence of KFcom, the two longest lifetimes are impacted, however minimally, such that the fluorescence decay is indistinguishable from the dsDNA only sample. The presence of KF (from Prof. Millar) significantly increases the longest lifetime from 1.5 ns to 2.0 ns, increasing the average lifetime to 0.74 ns (from 0.65 ns for dsDNA only). The dramatic difference in lifetime between the two samples clearly indicates Cy3 experiences a different environment within the two proteins, a consequence of the additional *exo* binding activity present in KF, the non-commercial version (see Figure 3.6). Binding at the *exo* site requires upstream movement of the protein from the 3' to the 5' end of the DNA. With the 3' end separated from the Cy3-labeled 5' end by only six bases, upstream movement of KF for binding at the *exo* site will force the Cy3 to move into the interior of the protein; the dye is no longer in a solvent exposed environment, and, hence, no longer has the photophysical characteristics of the solvent environment (this accounts for the much longer 2.0 ns lifetime).

The effect of the 3' end of the primer binding to the *exo* site is clearly visible in the "dip-and-rise" shape of the anisotropy in Figure 3.4 (right panel). An associated anisotropy decay is the result of the measured probe existing in more than one environment. In this case the 5' attached Cy3 is either solvent exposed (binding at the *pol* site) or inside the protein (binding at the *exo* site). While the lifetime results do not make clear whether KF (Millar) forces binding exclusively at the *exo* site, the anisotropy results—specifically the "dip-and-rise" shape—show that the dsDNA sample binds at

both sites for this protein. The "dip-and-rise" shape only results when the dye's fluorescence characteristics of the two environments are very different.

B. Simulating the Associated Anisotropy of Dy3-DNA/KF

The concept of associated anisotropy is discussed in detail in Appendix I, however, here is a conceptual overview. A sample with the probe in two different environments will emit florescence that is characteristic of the probe in each of those environments. The overall anisotropy from the sample will be a linear combination of the anisotropy from the probe in these two environments; the coefficients are determined by the probe's fluorescent lifetime in its respective environments, and are time-dependent. For example, imagine a probe that has a short lifetime in a solution environment and a long lifetime in a protein environment. At short times after the laser pulse, the anisotropy will be a mixture of anisotropies from the probe in both environments, however, at long times after the laser pulse the environment with the short lifetime will no longer contribute to the fluorescence, nor the anisotropy, and the anisotropy will consist mainly of that from the other (in this case protein) environment. While at short times there may be a decrease in anisotropy as the anisotropy decreases from the short-lived fluorescence environment, as time passes the overall anisotropy will be dominated by the long-lived fluorescence environment, and may increase if that state's anisotropy is greater at times just past the short lifetime. Such a situation gives rise to the "dip-and-rise" shape seen in Figure 3.4 (right panel). The mathematical description of this concept is reviewed in Appendix I.

Such is the case in the Cy3-DNA/KF sample: the two binding modes cause Cy3 to

be in a solution environment—short lifetime, high initial, but rapidly decreasing anisotropy—and in a protein environment—longer lifetime, gradually changing anisotropy. This accounts for the rapid initial decrease (from 0 to 2 ns) and the gradual increase (2 to 6 ns) before the anisotropy decays again. To determine quantitatively what linear combination gives this shape it is necessary to have lifetime and anisotropy measurements of the two pure environments: in this case of the solution exposed dye and of the dye within the protein. The latter sample was not measured, as it was outside the scope of this study, however, assuming binding at the *exo* site pulls the dye completely into the environment of the KF we also assume that within the protein the dye motion is restricted such that photoisomerization, and hence, formation of the *cis*-isomer, is not possible. Under this assumption, the anisotropy of the protein enclosed dye can be approximated by the fundamental anisotropy of Cy3B (the Cy3 analogue which is chemically prevented from rotating about the carbon-carbon double bonds in its polymethine chain) which is 0.38. The anisotropy is assumed to be unchanging during the measurement. Thus, using the lifetime and anisotropy of the solution exposed Cy3 (from the Cy3-DNA only sample) and the lifetime of the dye in its protein environment (from the Cy3-DNA/KF sample) and Cy3B anisotropy we see the resulting associated anisotropy is a close approximation of the experimental anisotropy measured for dsDNA/KF (Figure 3.7). This use of Cy3B's anisotropy value provides more evidence for the idea that the protein restricts the dye's ability to photoisomerize.

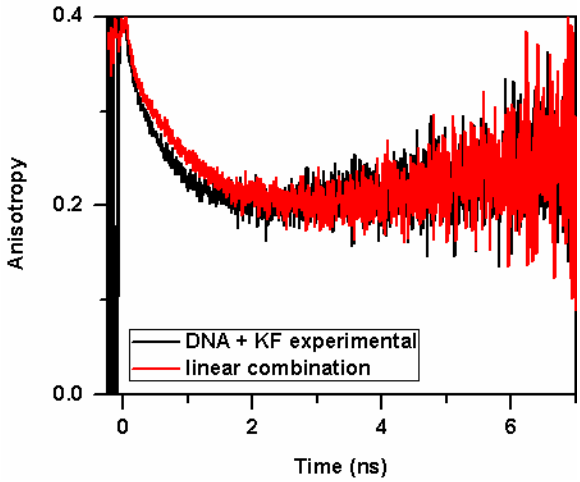


Figure 3.7: Comparison of Simulated and Measured Anisotropy for Cy3-DNA/KF. The experimentally measured anisotropy decay of Cy3-DNA/KF is compared to the anisotropy calculated from the experimental intensity and anisotropy decays of Cy3-DNA, the experimental intensity decay of Cy3-DNA/KF, and the experimental anisotropy of Cy3B, as described in the text.

C. Direct Evidence of Decreased Photoisomerization

The irrefutable evidence for photoisomerization restriction comes from the transient absorption (TA) experiments. Figure 3.5 (left panel) shows no difference in signal whether the sample is Cy3-DNA only or in the presence of KFcom (compare red and black traces). This agrees with the fact that KFcom has binding activity only at the *pol* site, hence the Cy3-labeled 5' end will always be solution exposed, even when KFcom is bound to the dsDNA. On the other hand, the Cy3-DNA sample with KF (Millar) has a clear decrease in TA signal (right panel), indicating less isomer formation when KF binds. A decrease in TA signal only makes sense if there is a reduction in photoisomer formation, which is the case when the primer binds at the *exo* site pulling the Cy3 into the protein interior, inhibiting rotation about the polymethine chain. Thus, this

is conclusive evidence that the Protein Induced Fluorescence Enhancement (PIFE) effect is nothing more than steric hindrance—due to the protein's bulk—making deactivation via photoisiomerization less likely, leading to an increase in Cy3's fluorescence rate. The TA signal decreases by about 50% from the dsDNA sample upon KF addition indicating that some photoisomerization is still occurring; in agreement with lifetime and anisotropy data (see part B) and binding activity at the *pol* site for KF (Millar). Since the KF was in 40% excess, each dsDNA could potentially be bound by a protein; especially considering the dissociation constant (K_D) is approximately 4 – 8 nM[133, 146, 151]. The TA results suggest some of the dsDNA sample was bound at the *pol* site.

D. Determining Fraction of DNA at the *exo* Site

Determining conclusively what fraction of DNA is bound at the *pol* site versus the *exo* site is no easy task. Millar and co-workers estimate a 12% population at the *exo* site for a 17-base primer conjugated to a 20-base complementary strand with no mismatches[146]; their estimate is based on an associated anisotropy analysis similar to what is shown here. In a later study, the same research group found that DNAs with two to four mismatched baser pairs forced almost exclusive binding at the *exo* site (95%), while matched DNAs have between 7 – 14% *exo* population[149]. Other researchers, using circular dichroism spectroscopy, largely confirm these results, finding that three consecutive mismatches located at the end of the primer allow for exclusive *exo* site binding, whereas fully matched DNA will have populations at both binding sites[152]. With the same technique in another study, those researchers determined a 43% *exo* population for fully matched DNA, and a 61% *exo* population for a single mismatch at the

primer/template junction[153]. On the other hand, surface plasmon resonance measurements show a 97% *pol* population for fully matched DNA[154], and single molecule experiments reveal no *exo* site binding for fully matched DNA[133]. As mentioned above a mismatched DNA sample was not used for this project as the primary goal of this study was to prove the mechanism behind PIFE, not determine the partitioning of DNA between KF's *pol* and *exo* sites. Without a mismatched sample a proper determination of the fraction of *exo*-bound DNAs cannot be determined from the anisotropy data.

However, the transient absorption data collected for this study can potentially be used to calculate the yield of photoisomer: a comparison of isomer yields from the Cy3-DNA only and Cy3-DNA/KF samples can estimate the fraction of *exo*-bound DNA. From the difference spectra shown in Figure 3.5 (right panel) the amounts of photoisomer formed in the Cy3-DNA, Cy3-DNA/KF, and Cy3-DNA/KF/degrader samples can be determined. The OD is measured on the y-axis, the path length is known (section 3.2, part C), only the extinction coefficient of the isomer is unknown. The extinction coefficient of the Cy3 isomer has not been reported in the literature, although the red-absorbing analogues of Cy5 have been a frequent target for photoisomer investigations in commonplace optical[59, 62] and rarer optoacoustic experiments[155, 156]. However, there is one problem with this simple approach, the measured OD is actually a difference absorbance, a difference in absorbance of the transient before and after the laser pulse. We can assume that the initial transient absorbance is identical for the two samples—prior to the pump laser populating the S_1 state there is no isomer formation. Thus, we have Equations 3.1 and 3.2, where OD_i refers to the OD value measured in TA

$$OD_{KF} = A_{fKF} - A_{iKF} = \varepsilon l[iso]_{KF} \quad (3.1)$$

$$OD_d = A_{fd} - A_{id} = \varepsilon l[iso]_d \quad (3.2)$$

spectroscopy for each sample ("KF" is the DNA/KF samples while "d" is the degraded sample), A_f and A_i refer to the final and initial absorbances, ε is the extinction coefficient of the isomer, and l is the path length. When $A_{iKF} = A_{id}$, the difference in isomer concentrations is directly proportional to the difference in OD of the two samples (Equation 3.3). However, without the extinction coefficient the *exo*-bound fraction cannot be determined.

$$[exo-boundDNA] = [iso]_d - [iso]_{KF} = \frac{OD_d - OD_{KF}}{\varepsilon l} \quad (3.3)$$

3.5 Conclusion

The focus of this project was to determine the cause of the fluorescence enhancement experienced by Cy3 in the presence of proteins, a phenomenon coined PIFE (protein induced fluorescence enhancement) by Sua Myong and co-workers[117, 127, 157]. Our hypothesis that bulky proteins can impede Cy3's rotation about its carbon-carbon double bond in the excited state was tested via a variety of bulk measurement techniques utilizing two versions of Klenow fragment as the test protein. For KF with both *pol* and *exo* binding activity the lifetime measurements showed only a minor increase in the lifetime upon KF binding, whereas KFcom caused no change in Cy3's lifetime. The anisotropy measurements confirmed binding, and, for KF (Millar), analysis using associated anisotropy showed that Cy3 was present in two different states when bound to the protein, in the solution and within the protein environment. The transient absorption

experiments proved conclusively that photoisomerization is inhibited when the dye is within the protein. The TA spectra shows a significant decrease in positive signal with the protein as compared to without it. Therefore, PIFE (for Cy3) is nothing more than the protein forcing the dye to deactivate via fluorescence when within the restrictive protein environment, which decreases the rate of photoisomerization.

CHAPTER FOUR

PHOTOPHYSICS OF DY DYES IN SOLUTION AND CONJUGATED TO DNA, AND EVALUATION OF THEIR POTENTIAL AS PIFE PROBES

4.1 Introduction and Motivation

The PIFE (protein induced fluorescence enhancement) effect is not limited solely to Cy3 (Chapter 3). Sua Myong and co-workers also investigated the PIFE ability of red-absorbing Cy5; they prepared a 5'-Cy5 labeled dsDNA sample with BamHI recognition sequence, GGATCC, 1 base pair (bp) away from the base to which the dye is conjugated[117]. The Cy5-1bp DNA was observed under TIRF (total internal reflection fluorescence) spectroscopy with BamHI present in the buffer; single molecule traces show the intensity fluctuate between two states, a brighter and a darker state. These intensities correspond to the bound to DNA (brighter) and unbound (darker) state of BamHI. A histogram of the intensity states observed before photobleaching shows a 1.9-fold increase in Cy5 intensity in the presence of BamHI. This is not as high as the 2.7-fold increase observed for the Cy3 labeled sample, which is unfortunate given the numerous benefits to working in the red—reduced Rayleigh and Raman scattering amongst them. Fortunately, there are other red-absorbing dyes whose PIFE response has yet to be characterized.

In addition to the symmetric cyanine dyes available for fluorescence based research a relatively new set of asymmetric cyanines has been developed for use in life science applications. Czerney and coworkers first report the development of Dy630 and Dy635 in 2001; these are hemicyanine dyes part of the DyLight Fluor dye family sold

primarily by Dyomics GmbH (Germany)[158]. Dy630 and Dy635 (structures shown in Figure 4.1) were created primarily with FCS (fluorescence correlation spectroscopy) needs in mind and for 633 nm excitation: the authors wanted dyes that are water soluble and stable, have a reactive group which can be used for covalent coupling, have high molar absorbances, have high fluorescence quantum yields, have thermal and photostability, and can be charge tuned. In fact, Dyomics sells five Dy630 type dyes: Dy630 is neutral, Dy631 possesses a single negative charge, Dy632 has two negative charges, and Dy634 has three negative charges. The charges are added by adding sulfonate groups to the dye, which also makes the dye more soluble in water. Dy633 also has a single negative charge, but the sulfonate group is attached to a different part of the molecule than in Dy631. The Dy630 dyes absorb at 637 nm and emit at 657 nm in ethanol; the absorption spectra of Dy635 is red-shifted to 647 nm (the emission maximum is at 671 nm). The red shift is accomplished through a minor structural change of connecting the aminoalkyl group to the phenyl ring of the benzopyran group. This

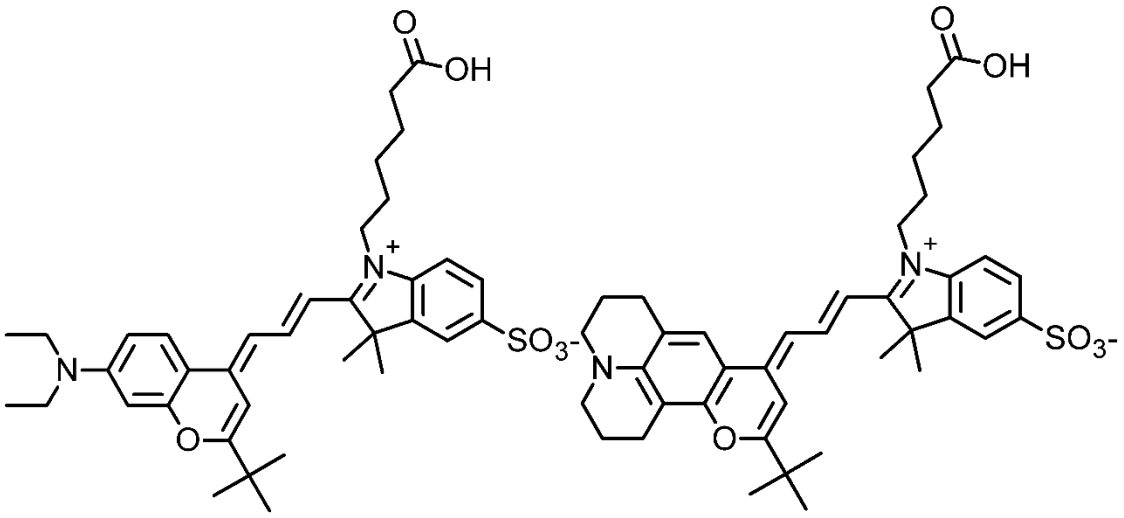


Figure 4.1: Structure of Dy630 and Dy635. The structure of Dy630 is shown in the left panel; the structure of Dy635 is in the right panel. The carboxylic acid modifications of these dyes are shown here.

forces the nitrogen's π-orbital to be parallel to the π-orbitals of the chromophore, thus red-shifting the spectra. Dyomics sells only two versions of Dy635; Dy635 which is neutral and Dy636 which has a negative charge and the same absorption/emission maxima[159].

FCS decays of free Dy630 and Dy635 revealed low count rates for both dyes as compared to free Cy5 in the same conditions; this correlates well with the short lifetimes of Dy630 (0.2 ns) and Dy635 (0.4 ns) and the longer lifetime of Cy5 (0.9 ns)[158]. These authors also observed a dramatic increase in lifetime upon conjugation to ssDNA and bovine serum albumin (BSA); Dy630-DNA has a lifetime of 2.2 ns and 2.6 ns as Dy630-BSA, both lifetimes are monoexponential. Dy635-BSA has a long average lifetime at 2.6 ns (biexponential), but on DNA it is much shorter, and monoexponential, at 1.7 ns. Czerney and co-workers ascribe the longer lifetimes to a decrease in vibrational and rotational degrees of freedom due to the dye's interaction with the charged biomolecule[158].

Markus Sauer and colleagues also studied Dy630 and Dy635 as part of an investigation into spectroscopic properties of commercially available red-absorbing dyes[160]. They observe an increase in the monoexponential lifetime with solvent viscosity and detergent; the 6-fold increase with detergent indicates to the authors a decrease in the internal conversion rate, which suggests decreased rotation about the polymethine backbone. These authors also investigated the FCS behavior of Dy630 and Dy635 as free dyes and conjugated to biotin. The free dyes exhibit fluctuations in the microsecond timescale the same way that symmetric cyanines, such as Cy5, do due to *cis-trans*

photoisomerization. The Dy630-biotin conjugate shows a decrease in diffusion coefficient upon binding to streptavidin; addition of excess biotin to the system does not change the observed diffusion time of Dy630-biotin indicating this conjugate binds nonspecifically to streptavidin[160].

Very limited photophysical data has been reported about dyes from the Dy family, however a group in Spain has used Dy630 for single molecule intensity and polarization measurements. Dy630 was used to study the environment's effect on the dye's population distribution using long silica nanoparticles that possess nanochannels for guests to enter[161]. From the single molecule traces the authors conclude that Dy630 has "strong blinking behavior and weak photostability" when adsorbed onto a glass surface[161]. In the presence of the nanoparticles Dy630 experiences less blinking and is more photostable; this is due to the diminished rotational freedom of the dye when it is confined to the nanochannels of the nanoparticles[161]. Further studies by these authors focused on the photophysics of Dy630 when encapsulated within spherical silica nanoparticles; FCS experiments show a dramatic increase in brightness for Dy630 inside 20 nm and 30 nm particles in the presence of other Dy630 molecules[162]. Single molecule experiments revealed two dye populations within the nanoparticles: there are dyes inside the core and attached to the surface of the silica core, which is then covered by another layer of silica to form a protective shell. The dyes in these two locations experience different lifetime and polarization distributions reflecting the more flexible core interior and rigid outer core environment: Dy630 forms less photoisomer in the outer core then when located in the interior[162].

Other recent literature involving Dy dyes does not delve into their photophysics,

but rather showcases the various applications where Dy dyes are used. Dy630 and Dy635 were used in immunocytochemistry experiments to compare their brightness in the nucleus of human epithelial cells to that of other commercially available green- and red-absorbing dyes[163]. Dy630 was used in flow cytometry to label a neuropeptide rather than Cy5 because Dy630 has a "higher agonistic potency" at the studied receptor[164]. The dye has been used as part of a FRET pair with BODIPY for measuring the dimerization of homodimeric cytochrome b'_{559} in steady state experiments[165]. The conjugate Dy630-biotin has been used in molecular recognition experiments to test the specific/nonspecific binding properties of a new coating for the Langmuir-Blodgett technique[166]. Dy631 has been used in the proof-of-concept of a high-throughput biochip reader that uses dynamic holographic excitation and multiwavelength detection[167]. The ability to dual label core-shell microspheres was demonstrated with Dy630 and GFP (green fluorescent protein); confocal microscopy images show microspheres successfully labeled with both fluorophores can be co-localized[168]. Dy630 has also been used as an acceptor as part of a FRET cascade involving GFP and a rhodamine as an intermediate acceptor[169].

Dy635 has been explored even less. The time resolved anisotropy behavior of Dy635-biotin has been studied; Dy635-biotin displays "dip-and-rise" associated anisotropy decays in the presence of streptavidin[170]. Dy636 has been used for target DNA sequence detection. DNA hairpins of sequence complementary to the target had both ends labeled with Dy636; the non-fluorescent dimers experience a 10-fold increase in intensity when in the presence of the target sequence. The authors also show Dy636 forms a more stable dimer than green-absorbing TMR (tetramethylrhodamine)[171]. Dy636 has also been used in FCS (fluorescence correlation spectroscopy) and confocal imaging

to study the binding of transferrin to FePt nanoparticles and their cellular uptake[172].

In this study, Dy630, Dy632, and Dy635 are investigated to determine whether their PIFE response is more significant than that of Cy5. Dy635 is tested since its spectrum is an almost exact match with Cy5; Dy630 and Dy632 are blue-shifted, but still absorb and emit in the same general region as Cy5. The Dy630/Dy632 pair will be used to investigate the role of charges (Dy630 is neutral, while Dy632 has a double negative charge). The protein used is the commercially available Klenow fragment, the same one used in the PIFE study in Chapter 3, which only has binding activity at the *pol* site. For this study the design of the DNA primer/template pair was borrowed from Millar and coworkers: the primer strand is 11 base pairs (bp) long while the template strand is 20 bp long[146]. The fluorescent label is attached via a six-carbon linker to a modified thymine on the primer strand, one bp away from the primer/template junction (see Figure 4.2). We chose to work with this protein/DNA system due to the extensive work done (by Millar) on KF interacting with this particular DNA sample; the data made available[146] makes for simplified data interpretation. Binding of the primer to the *pol* site will bring

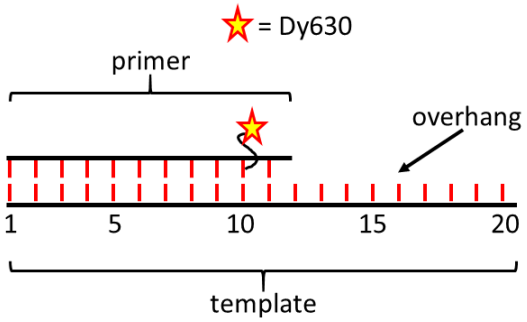


Figure 4.2: Schematic of DNA Samples. In this project the primer strand is 11-bases long, while the template strand is 20-bases long. The dye, whether Dy630, Dy632, or Dy635, is attached via a six-carbon linker to a modified thymine at the indicated position (at position 10 on the primer strand).

the dye into contact with the protein, which is expected to affect the photoisomerization behavior of these asymmetric cyanines. A significant decrease in the formation of the *cis*- isomer will lead to an increase in fluorescence, and hence, PIFE. Time-resolved fluorescence and anisotropy measurements, as well as transient absorption spectra, were collected of Dy630-dsDNA, Dy632-dsDNA, and Dy635-dsDNA and compared to the current red-PIFE standard of Cy5-dsDNA.

4.2 Materials and Methods

A. Materials

DNA primer and template strands were purchased from IBA GmbH (Germany). Primer sequences are 5'-TCG-CAG-CCG-XC-3', where the "X" indicates a modified thymine conjugated to Cy3, Cy5, Dy630, Dy632, or Dy635 via a six-carbon linker. Template strand sequence is 5'-AAA-CCC-TTG-GAC-GGC-TGC-GA-3'. DNA strands were dissolved in 10 mM TRIS buffer, pH = 7.4. Primer and template strands were mixed with a 25% excess of template strand in 10 mM TRIS, heated to 75-90°C, and after 5 minutes slowly cooled to room temperature. Annealing was checked with 20% native PAGE; for incomplete annealing 10 mM Mg^{2+} and 35 mM Na^{2+} was added to the DNA and it was reannealed.

A commercial version of Klenow fragment was used for this study (it has mutations D355A and E357A), and is referred to as KFcom. It was purchased from New England Biolabs (catalog #: M0212M). DNA samples were mixed with an excess of KF in New England Biolabs's buffer 2 and measured immediately. DNA concentrations were 0.8-1.2 μM for TCSPC experiments and 2.5-3 μM for transient absorption

experiments. Deoxynucleotide triphosphates were purchased from New England Biolabs (catalog #: N0440S, N0441S, N0442S, N0443S).

B. Absorption and Emission Measurements

Fluorescence spectra to determine the quantum yield of free Dy630 in ethanol and glycerol were collected using an L-format NanoLog FL3-11 spectrofluorometer (HORIBA Jobin Yvon, NJ) outfitted a CW 450 W Xenon lamp and a thermoelectrically cooled R928 PMT (spectral range 200 nm to 850 nm). The quantum yield of Dy630 was measured in ethanol (at room temperature) and pure glycerol (at 11°C) using oxazine 1 as the standard (φ_f = 0.15[173]). Dilute solutions of Dy630 and oxazine1 were prepared such that the absorbance at 600 nm, the chosen excitation wavelength, was 0.1-0.2 (the chosen wavelength for the measurement in glycerol was 592 nm). The fluorescence quantum yield value (in ethanol) is used as the standard for quantum yield measurements in other solvents and at other temperatures.

Fluorescence spectra to determine the quantum yield of free Dy630 in various solvents and at various temperatures were collected on QM-4/2005SE spectrofluorimeter (PTI, NJ). Temperature was controlled with a water circulation system; the temperature was measured with a calibrated thermocouple, inside the cuvette. Dilute solutions of Dy630 in various solvents were prepared such that the absorbance at 592 nm was 0.1-0.2. The difference in refractive index between sample and reference (Dy630 in ethanol, at room temperature) was taken into account.

Absorption spectra were measured on a Shimadzu UV-1700 PharmaSpec spectrophotometer. Dy630 was dissolved directly into organic solvents; water solutions

of Dy630 were prepared from a highly-concentrated ethanol stock. Dy-labeled DNA was dissolved in 10 mM TRIS (pH = 7.4), or, for PIFE measurements, in a 1x dilution of 10x NEB Buffer #2 (New England Biolabs, Ipswitch, MA).

C. Time-Resolved Fluorescence and Anisotropy Measurements

Lifetime and anisotropy measurements were made using the time-correlated single photon counting (TCSPC) technique, as described in previous chapters. The instrument response function (IRF) was measured at the excitation wavelength (630 nm); it has a FWHM of 50-60 ps. Samples were excited at 630 nm and emission was detected at 670 nm. The appropriate interference filters for excitation and long band pass filters for the emission were used. Fluorescence intensity decays were fitted with a sum of exponentials (the IRF was used for deconvolution). Fitting was done with ASUFIT, in-house written software. The time-resolved fluorescence anisotropy decays were calculated from experimental data according to $r(t) = (F_{VV} - F_{VH}\, G)/(F_{VV} + 2\, F_{VH}\, G)$, i.e. no deconvolution was performed. The G-factor was determined via the tail matching method with a solution of free Cy5 in water.

D. Transient Absorption Measurements

Transient absorption measurements were performed as described in Chapter 3. Excitation pulses were at 630 nm. Samples were measured in a 2.0 mm path length cuvette and continuously mixed by a magnetic stir bar. A high concentration (2.5 – 3 μM) was used due to low signal-to-noise ratio. The time-resolved spectra were background corrected at each wavelength. Measurements were collected over various

time windows from 40 ns to 5 μs (using 450 – 1000 time points). The transient spectra shown in this chapter represent averages of spectra measured in the indicated time windows after excitation.

4.3 Results

A. Absorption, Emission, and Fluorescence Quantum Yield

The absorption spectrum of Dy630 is shown in Figure 4.3 in comparison to Cy5 (left panel); the peak absorption (at 637 nm) of Dy630 is blue shifted from Cy5 by about 15 nm. Dy630 has a shoulder at 600 nm, and a weakly absorbing band centered at about 460 nm. The absorption spectrum of Dy630 in water and ethanol is shown in the right panel; in water the maximum absorbing band shifts to 625 nm. Figure 4.4 (left panel) shows how the absorption spectrum of Dy630 changes upon DNA conjugation; the main band is red-shifted to 634 nm (compared to free Dy630 in water). In the right panel the absorption spectra of Cy5-, Dy630-, Dy632-, Dy635-dsDNA are shown. Cy5-dsDNA

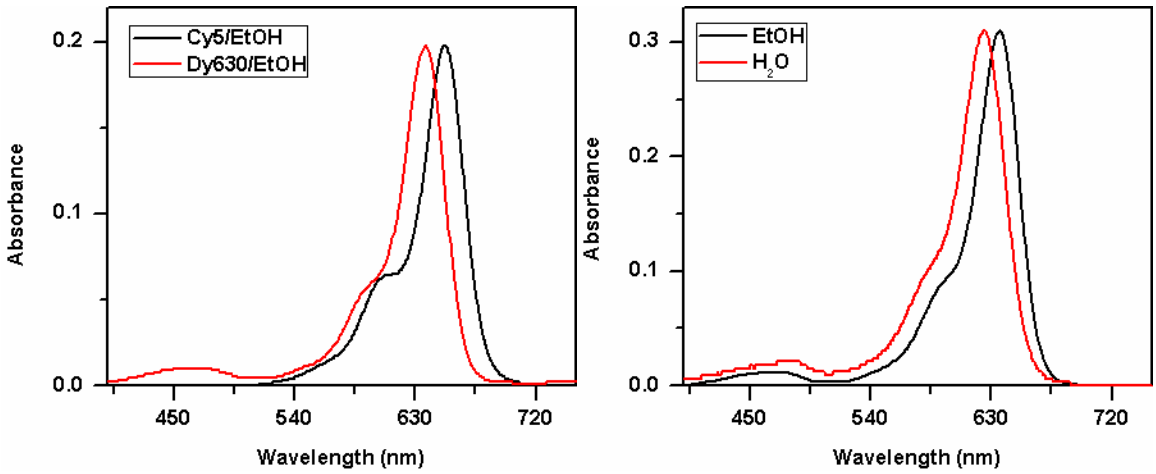


Figure 4.3: Absorption Spectra of Free Dy630. The left panel compares the absorption spectra of free Cy5 and Dy630 in ethanol. The right panel compares the absorption spectrum of free Dy630 in ethanol to water. A blue-shift is seen for the dye in water.

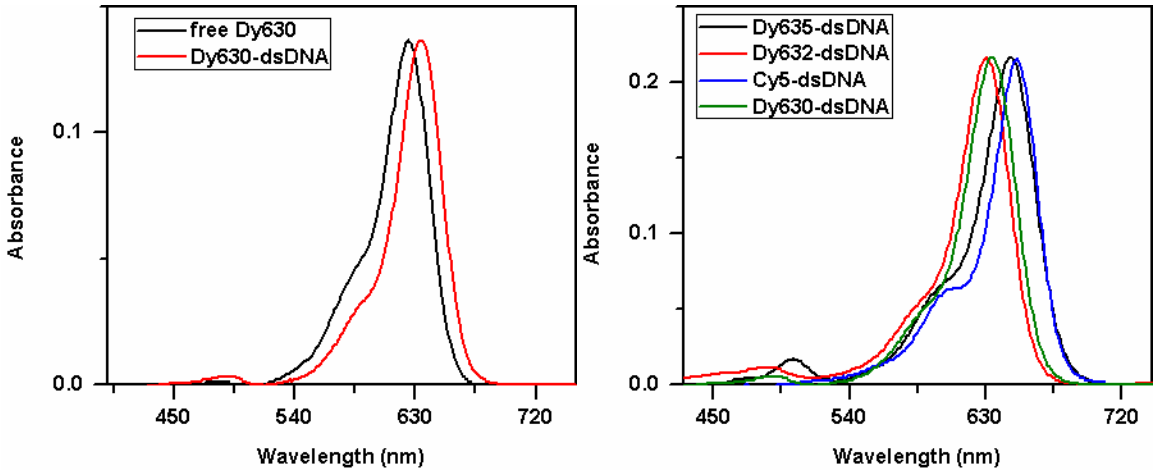


Figure 4.4: Absorption Spectra of Dy Dyes on DNA. The left panel compares the absorption spectra of free Dy630 to that of Dy630-dsDNA, the spectrum red-shifts upon conjugation. The right panel compares the absorption spectra of all Dy-DNA samples to Cy5-dsDNA.

and Dy635-dsDNA overlap in the same wavelength region, while Dy630-dsDNA and Dy632-dsDNA are slightly blue-shifted. Each of the Dy dyes has a weak short-wavelength absorption: Dy635-dsDNA around 505 nm, Dy632- and Dy630-dsDNA around 475 nm and 485 nm, respectively.

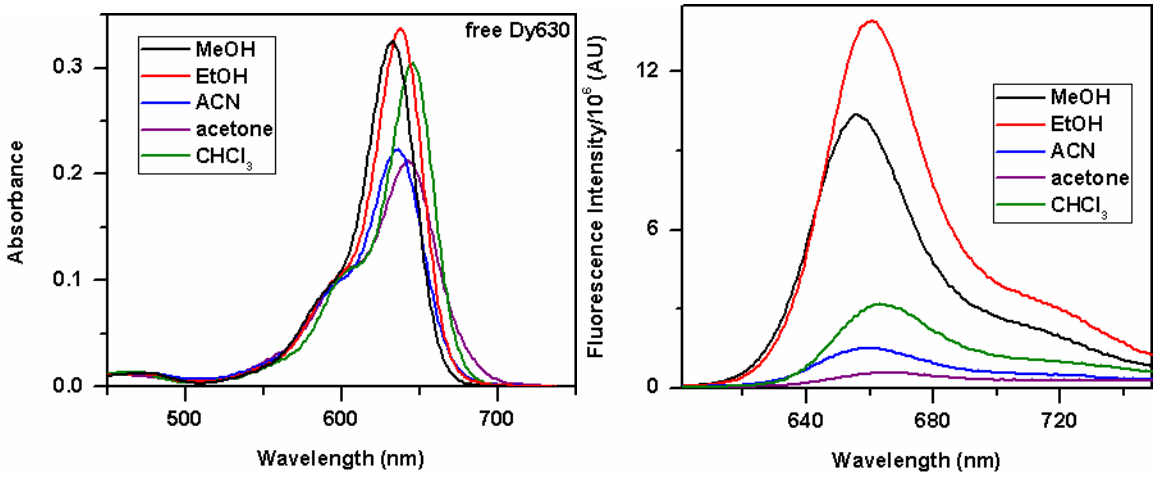


Figure 4.5: Spectra of Free Dy630 in Organic Solvents. Absorption spectra (left) and emission spectra (right) of free Dy630 in organic solvents. Measured by George Brockett.

The absorption spectra of free Dy630 has been measured in a variety of solvents

to determine the dye's sensitivity to viscosity. Figure 4.5 shows the absorption spectra of Dy630 in methanol, ethanol, acetonitrile (ACN), acetone, and chloroform. The right panel of Figure 4.5 shows the corresponding emission spectra. These spectra were recorded for Dy630 samples that had an absorbance between 0.1 – 0.2 at 592 nm, as such the emission spectra accurately show the fluorescence quantum yield of the dye in these solvents. Dy630 becomes more fluorescent as the solvent viscosity increases. In pure glycerol at 11°C Dy630 has a quantum yield of 0.76 (spectra not shown, data collected by Nikita Kumari). In other common solvents (at room temperature), the quantum yield ranges from 0.06 in methanol to 0.01 in acetonitrile (see Table 4.1). The quantum yield of Dy630 at room temperature is as low as the green absorbing cyanine, Cy3, which was measured at 0.09 in tris buffer[34].

Table 4.1: Quantum Yield of Free Dy630

Solvent	ϕ_f	Viscosity (cP at 25°C)
ethanol	0.082	1.074
methanol	0.056	0.544
chloroform	0.024	0.537
acetone	0.011	0.306
acetonitrile	0.005	0.369

Table 4.1: Quantum Yield of Free Dy630. The quantum yield of free Dy630 in organic solvents is shown in the first column; the second column provides the viscosity of these solvents.

The temperature variation of the quantum yield was also investigated and found to vary significantly with temperature. The emission spectra for temperatures from 7 - 72°C is shown in Figure 4.6 (left panel); the shape and peak position of the emission spectrum remains unchanged as temperature varies. The right panel shows the calculated fluorescence quantum yield as a function of temperature. At room temperature (about 21°C) the fluorescence quantum yield of Dy630 is 0.08.

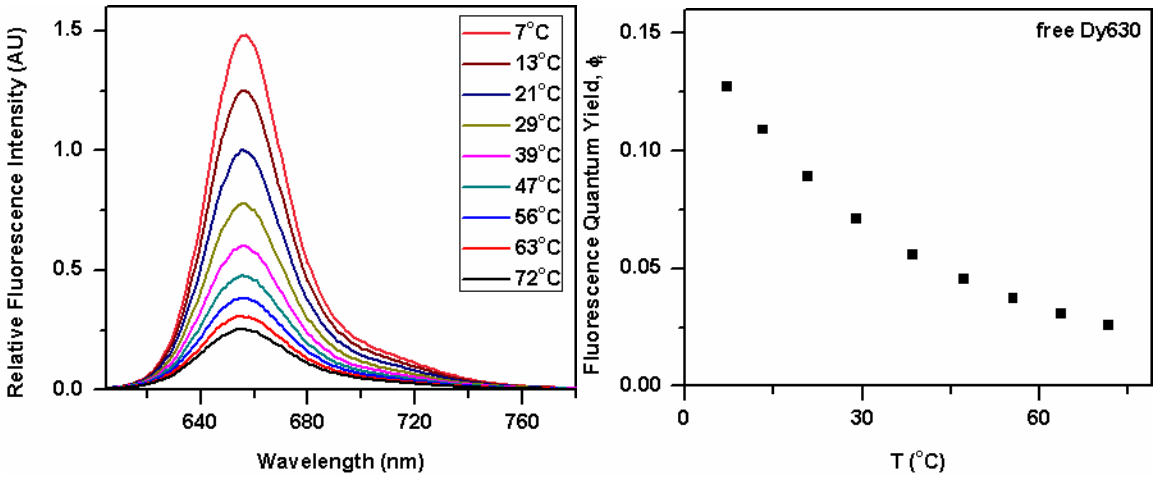


Figure 4.6: Temperature Dependence of Fluorescence Quantum Yield of Free Dy630. Emission spectra of free Dy630 is shown as a function of temperature. The right panel shows the calculated fluorescence quantum yield of Dy630. Measured by Nikita Kumari.

B. Lifetime Measurements

The fluorescence lifetime of free Dy630 was measured in several pure organic solvents, and in 50% ethanol (Figure 4.7, left panel). Dy630 has a short, mono-exponential lifetime of 400 ps in ethanol (Table 4.2). The lifetime of the dye increases with viscosity; the longest lifetime observed, 500 ps in 50% ethanol, corresponds to a high viscosity solvent (2.85 cP). In acetone and acetonitrile the single-exponential fits yield lifetimes close to the temporal response of our setup and may not be accurate. The lifetime increases dramatically upon conjugation to DNA (Figure 4.7, right panel). Dy630-ssDNA has an average lifetime of 2.1 ns, while Dy630-dsDNA has an average lifetime of 2.5 ns (Table 4.3). Conjugation to DNA requires two lifetimes for a satisfactory fit; both DNA samples a minor short component (about 30%) and a longer, major component (70%). On DNA the lifetime is insensitive to changes in viscosity; Dy630-dsDNA in solutions of up to 50% sucrose (15.4 cP) have the same lifetime as in buffer (Figure 4.8, left panel). Putting Dy630-ssDNA in 50% sucrose also shows no

change in lifetime; neither does adding 1 M Na^+ to the solution (Figure 4.9). Dy630-dsDNA is also unaffected by 1 M Na^+ (Figure 4.8, right panel).

Table 4.2: Lifetimes of Free Dy630 in Organic Solvents

Solvent	Viscosity (cP at 25°C)	τ /ns
50% ethanol	2.850 (at 20°C)	0.5
100% ethanol	1.074	0.4
chloroform	0.537	0.4
methanol	0.544	0.2
acetone	0.306	0.1*
acetonitrile	0.369	0.1*

Table 4.2: Lifetimes of Free Dy630 in Organic Solvents. The results of mono-exponential fits to the intensity decays of free Dy630 in various solvents are shown here, along with the solvent viscosity. *These lifetimes are approximately 50% longer than the FWHM of the IRF and cannot be assumed accurate.

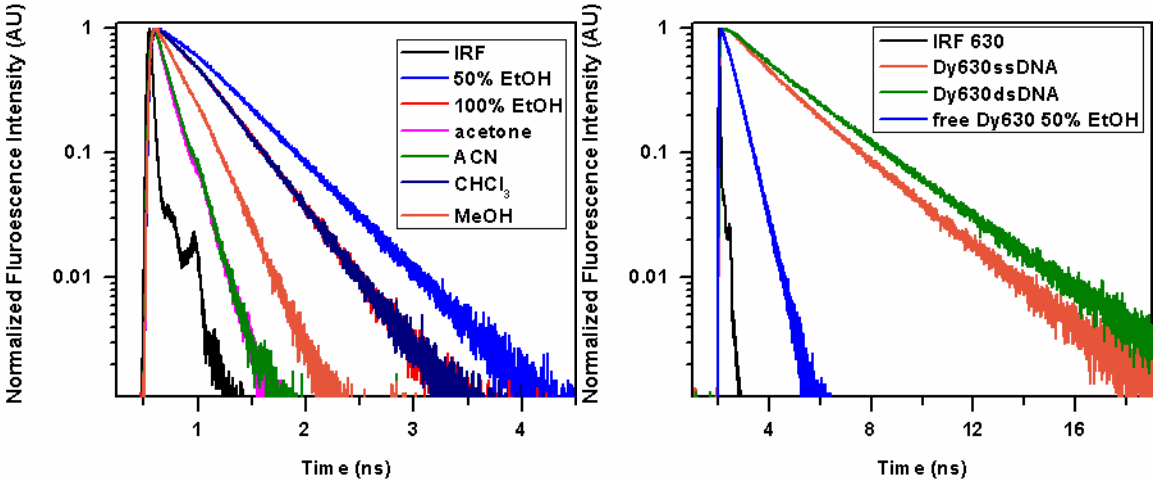


Figure 4.7: Lifetimes of Dy630. The left panel shows intensity decays of free Dy630 in organic solvents; a strong viscosity dependence is seen. The right panel shows intensity decays of Dy630 conjugated to ssDNA and dsDNA.

Table 4.3: Lifetimes of Dy630 Conjugated to DNA

	τ_1 /ns	$\%\alpha_1$	τ_2 /ns	$\%\alpha_2$	$\langle\tau\rangle$ /ns
Dy630ssDNA	1.1	31.9%	2.6	68.1%	2.1
Dy630dsDNA	1.3	27.4%	3.0	72.6%	2.5

Table 4.3: Lifetimes of Dy630 Conjugated to DNA. Two lifetime components were required to produce a fit with random residuals for DNA conjugated Dy630.

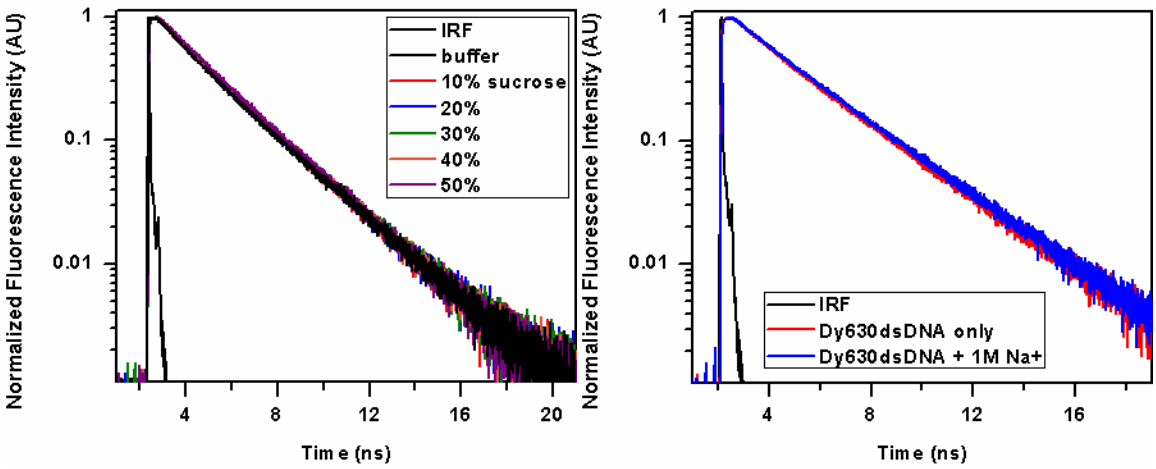


Figure 4.8: Lifetimes of Dy630-dsDNA. The left panel shows intensity decays of Dy630-dsDNA as solvent viscosity is increased. The buffer sample is made from water and is assumed to have its viscosity. The right panel compares the intensity decay to high salt concentration.

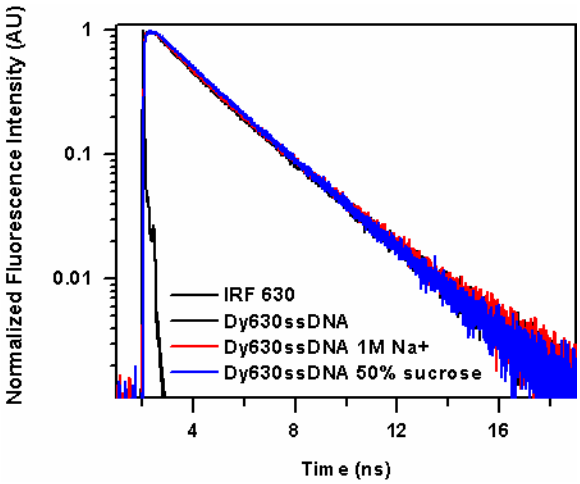


Figure 4.9: Lifetimes of Dy630-ssDNA. Intensity decays of Dy630-ssDNA are shown for high salt and high viscosity condtions.

Dy632, which only differs from Dy630 in the number of sulfonate groups it has, has a shorter lifetime on dsDNA than Dy630 (Figure 4.10). The single-stranded and double-stranded conjugates have the same lifetime visually, however, a biexponential fit gives the average lifetimes to be 2.1 and 2.2 ns, respectively (Table 4.4). Similarly to Dy630-dsDNA, the lifetime of Dy632-dsDNA does not vary with viscosity (Figure 4.10,

right panel). Salt content also has no effect on Dy632-ssDNA (also unaffected by high viscosity) or Dy632-dsDNA (Figure 4.11).

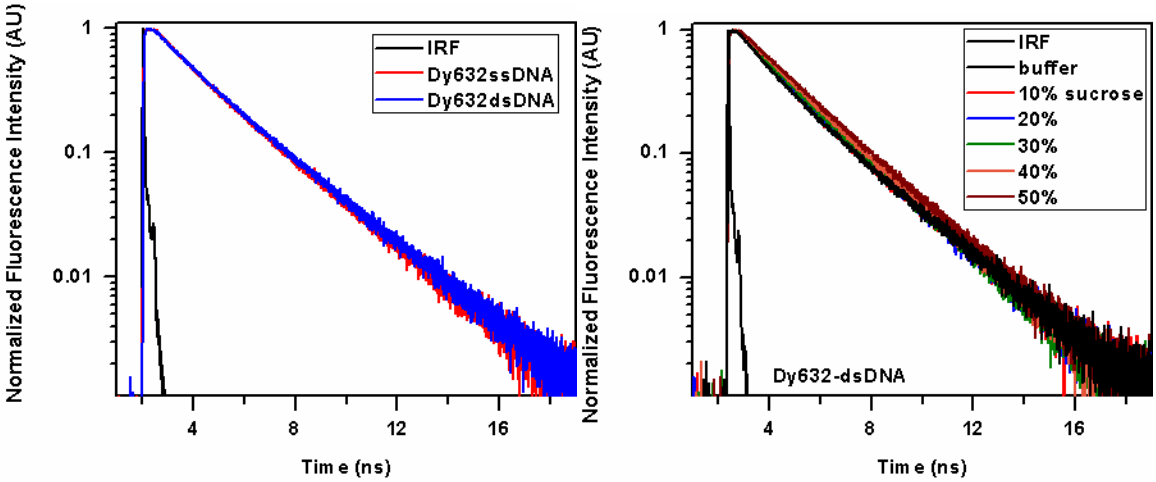


Figure 4.10: Lifetimes of Dy632-dsDNA. The left panel compares the lifetimes of Dy632 on ssDNA to dsDNA. The right panel shows the influence of viscosity on Dy632-dsDNA.

Table 4.4: Lifetimes of Dy632 Conjugated to DNA

	τ_1/ns	$\%\alpha_1$	τ_2/ns	$\%\alpha_2$	$\langle\tau\rangle$/ns
Dy632ssDNA	1.2	33.8%	2.6	66.2%	2.1
Dy632dsDNA	1.1	27.3%	2.6	72.7%	2.2

Table 4.4: Lifetimes of Dy632 Conjugated to DNA. Two lifetime components were required.

The same DNA sample was conjugated with Dy635 and measured in the same conditions. Dy635 conjugated to dsDNA has a longer average lifetime (2.2 ns) than conjugated to ssDNA (2.0 ns); the lifetimes are biexponential (Figure 4.12, left). While Dy635 in both conditions has the same partitioning of the amplitude amongst the short and long components, those components are longer on dsDNA (Table 4.5). The lifetime of Dy635-dsDNA is not sensitive to salt or viscosity (Figure 4.12, right). The same is true for Dy635-ssDNA (Figure 4.13).

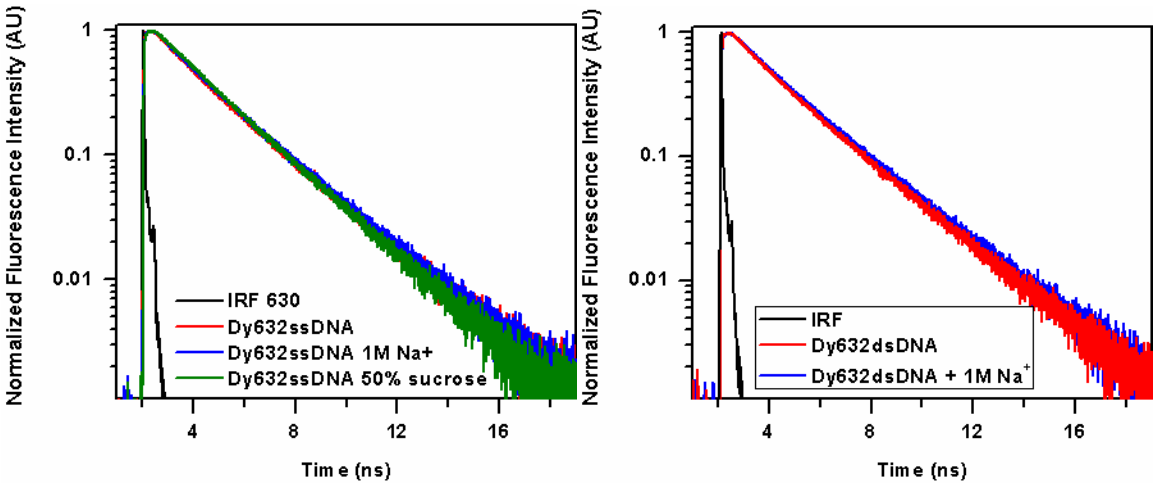


Figure 4.11: Lifetimes of Dy632-DNA with Salt. Variation of Dy632-ssDNA lifetime with salt and viscosity is shown on the left. The right shows the effect of high salt on Dy632-dsDNA.

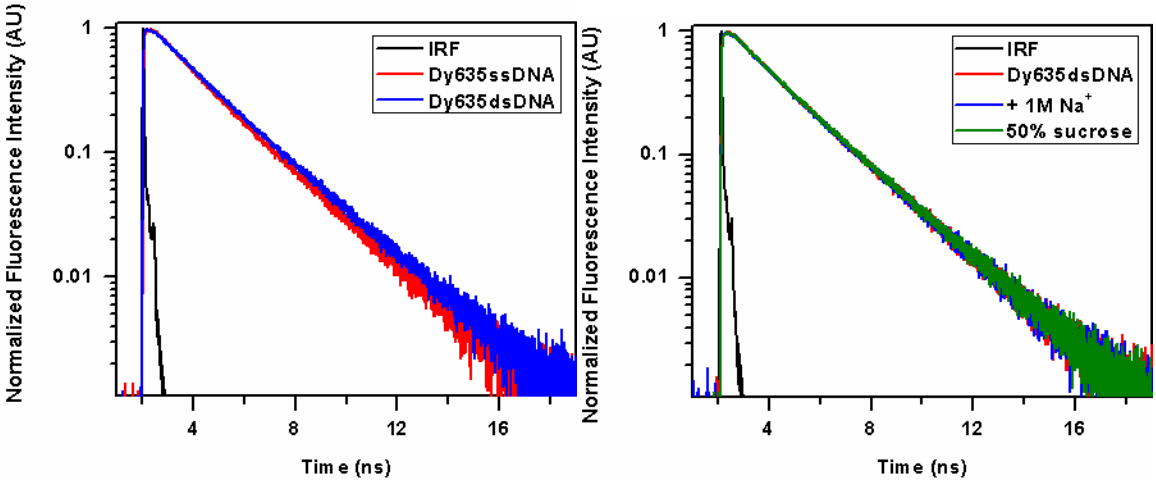


Figure 4.12: Lifetime of Dy635-dsDNA. The left panel compares the lifetime of Dy635 on ssDNA to dsDNA. The right panel shows the effect of high salt and high viscosity on Dy635-dsDNA.

Table 4.5: Lifetimes of Dy635 Conjugated to DNA

	τ_1/ns	%α_1	τ_2/ns	%α_2	$\langle\tau\rangle$/ns
Dy635ssDNA	1.2	28.5%	2.3	71.5%	2.0
Dy635dsDNA	1.3	28.8%	2.5	71.2%	2.2

Table 4.5: Lifetimes of Dy635 Conjugated to DNA. Two lifetime components were required.

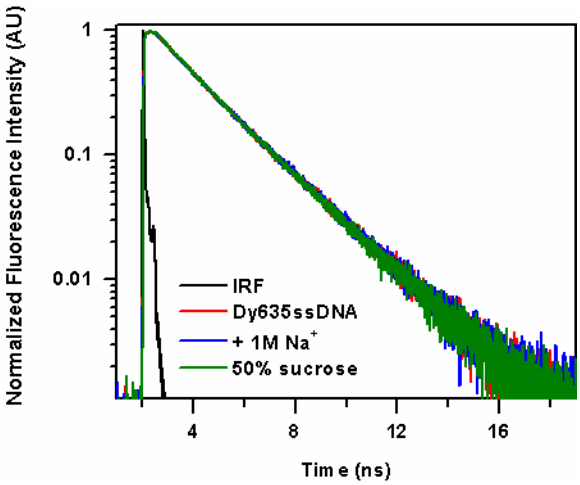


Figure 4.13: Lifetime of Dy635-ssDNA. Lifetime of Dy635-ssDNA is compared in high salt and high viscosity conditions.

Since the purpose of investigating these Dy-dyes is to determine whether they can replace Cy5, i.e., to determine whether they make better PIFE probes than Cy5, the same experiments were performed on Cy5 conjugated to the same primer/template DNA. Free Cy5 is not as sensitive to viscosity as Dy630; it has the longest lifetime in pure ethanol and the shortest in pure water (Figure 4.14, left). Table 4.6 lists the single-exponential lifetimes for free Cy5 and the viscosities of these solvents. From Table 4.6 it can be seen that there is no pattern between lifetime and viscosity for free Cy5. The lifetime increases significantly upon conjugation to DNA (Figure 4.14, right); the lifetime on DNA is biexponential, and is longer for dsDNA than ssDNA (Table 4.7). Cy5-dsDNA has a shorter "short" time and longer "long" time component that on ssDNA, and a greater amplitude of the longer lifetime which contribute to a longer lifetime. The lifetimes of Cy5-ssDNA and Cy5-dsDNA are not affected by high salt concentrations, however Cy5-ssDNA does have a minor increase in lifetime in 50% sucrose—the dsDNA sample is not affected (Figure 4.15). To visually sum up the behavior of Cy5 in

comparison to the Dy-dyes, all ssDNA samples and all dsDNA samples are shown in Figure 4.16. Dy630 and Dy632 have the longest lifetimes on ssDNA (with Dy635 being shorter), however, on dsDNA Dy630 has a longer lifetime than Dy635 and Dy632.

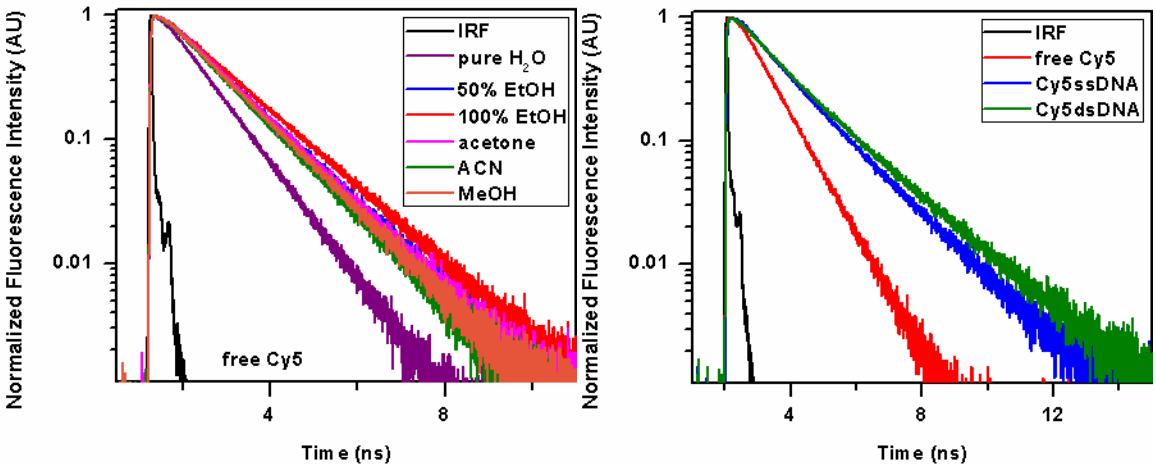


Figure 4.14: Lifetimes of Cy5. The left panel shows intensity decays of free Cy5 in organic solvents. The right panel shows intensity decays of Cy5 conjugated to ssDNA and dsDNA.

Table 4.6: Lifetimes of Free Cy5 in Organic Solvents

Solvent	τ /ns	Viscosity (cP at 25°C)
acetone	1.3	0.306
acetonitrile	1.2	0.369
MeOH	1.2	0.544
water	0.9	0.890
EtOH	1.4	1.074
50%EtOH	1.3	2.850 (at 20°C)

Table 4.6: Lifetimes of Free Cy5 in Organic Solvents. Single-exponential lifetimes of free Cy5 in various organic solvents. No viscosity dependence is seen.

Table 4.7: Lifetimes of Cy5 Conjugated to DNA

	τ_1 /ns	$\%\alpha_1$	τ_2 /ns	$\%\alpha_2$	$\langle\tau\rangle$ /ns
Cy5ssDNA	1.1	48.7%	1.8	51.3%	1.5
Cy5dsDNA	1.0	42.4%	2.0	57.6%	1.6

Table 4.7: Lifetimes of Cy5 Conjugated to DNA. Two lifetime components were required.

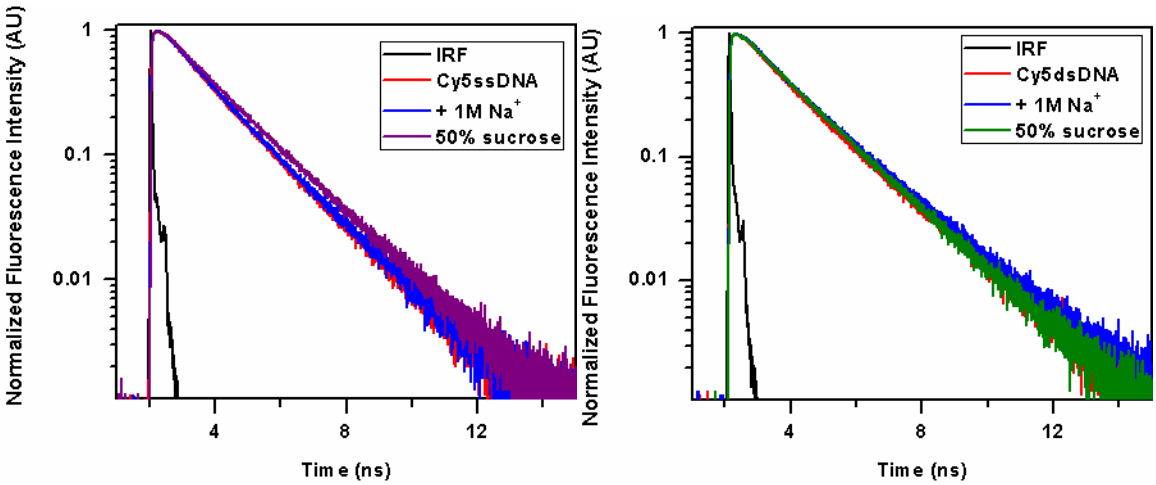


Figure 4.15: Lifetimes of Cy5-DNA in Salt and Sucrose. Variation of Cy5 lifetime with high salt and high viscosity is shown on left for Cy5-ssDNA and on right for Cy5-dsDNA.

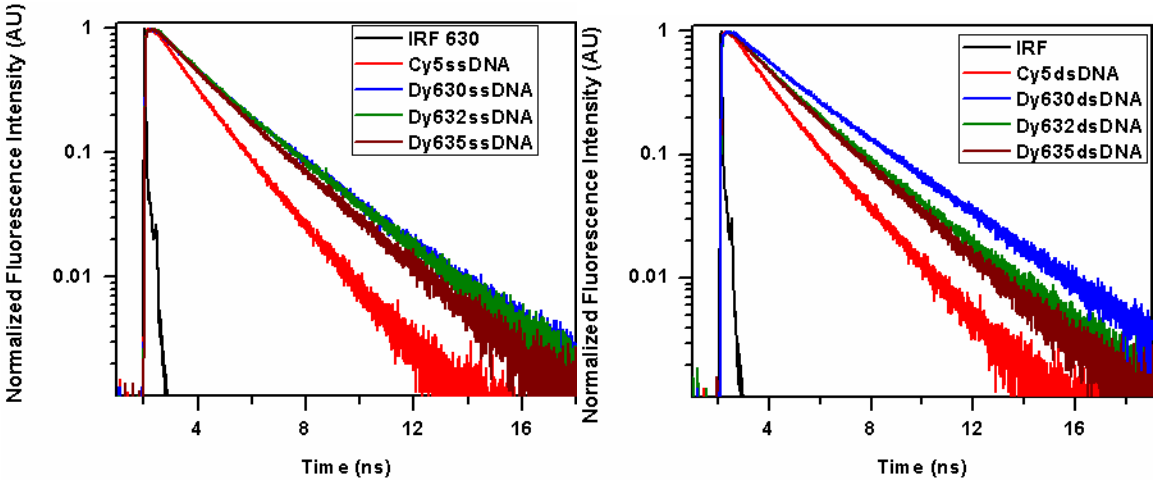


Figure 4.16: Lifetimes of All Samples Compared. Intensity decays of all samples studied in this project are compared. ssDNA samples are compared on the left and dsDNA samples are compared on the right.

C. Lifetimes and Fluorescence Anisotropies with Klenow Fragment

I. Cy5-dsDNA

The behavior of Cy5 in the presence of Klenow fragment (KF) was also characterized fully to compare with the PIFE behavior of the Dy-dyes. Cy5-dsDNA experiences an increase in lifetime with the addition of one equivalent of KF, and a

further increase upon an additional half equivalent addition (Figure 4.17, left). With a total of two equivalents of KF there is only a minor increase in the average lifetime (from 2.1 to 2.2 ns, Table 4.8). The anisotropy of these samples shows an increase due to binding of the protein, and a greater increase for the second equivalent of KF. In this case the anisotropy appears to begin above 0.4, however this is likely due to instrument/laser error; adjusting this decay down to 0.4 still shows the anisotropy decreasing slower in comparison to the other samples (brown trace). The degrader used is a standard protease which degrades the protein leaving the DNA intact in solution. We see from the data that the KF leaves no lasting mark on the sample, i.e. the KF does not alter the behavior of the dye itself.

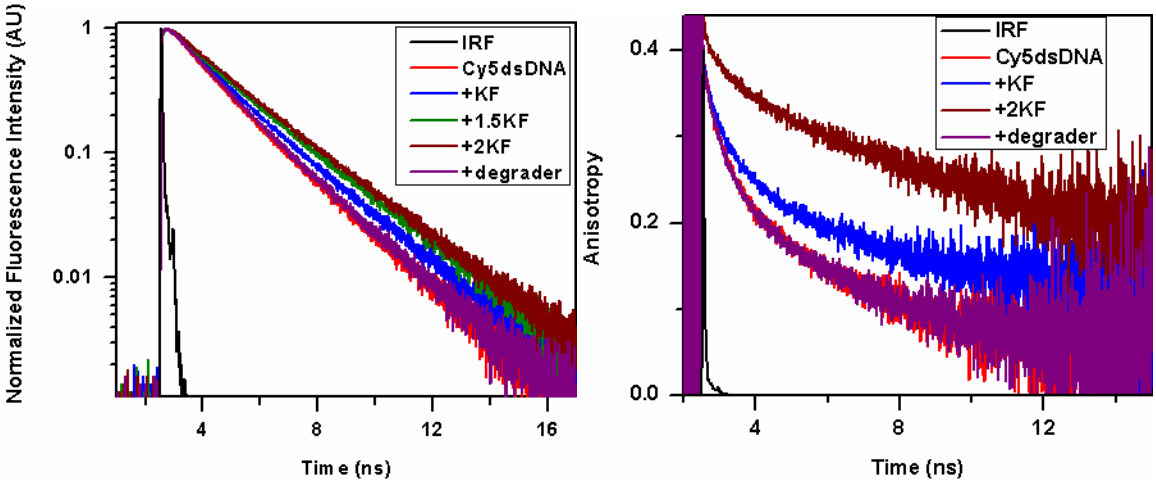


Figure 4.17: Cy5-dsDNA with Klenow Fragment. The left panel shows intensity decays and the right panel shows anisotropy decays of Cy5-dsDNA with varying amounts of KF.

The KF used in this project is the commercial version which only has binding and activity at the *pol* site. In this DNA sample the dye is located on the second to last base of the primer strand; we do not know exactly in what orientation the protein binds at the primer/template junction. Hence, addition of the dNTPs would allow the protein in a

Table 4.8: Lifetimes of Cy5-dsDNA with KF

	τ_1/ns	$\%\alpha_1$	τ_2/ns	$\%\alpha_2$	$\langle\tau\rangle$/ns
Cy5dsDNA only	1.0	38.4	2.1	61.6	1.7
+ KF	1.1	35.4	2.3	64.6	1.9
+ 1.5KF	1.2	33.6	2.5	66.4	2.1
+ 2KF	1.3	29.9	2.6	70.1	2.2
+ degrader	1.2	46.1	2.2	53.9	1.7

Table 4.8: Lifetimes of Cy5-dsDNA with KF. Biexponential fits of intensity decays in the left panel of Figure 4.17.

different orientation, perhaps one which enhances fluorescence. In Figure 4.18 (left panel) the lifetime of Cy5-dsDNA is shown after addition of KF and dNTPs (blue and green traces, respectively). In this case the dNTPs were added all at once to the solution; the polymerase reaction is practically instantaneous, and the lifetime measured is the lifetime of the newly created, fully double stranded DNA. Since the Cy5 is now part of a different sample of DNA it has a different (shorter) lifetime. The addition of dNTPs in a stepwise fashion is shown in the right panel. Adding the KF and the first two dNTPs increases the lifetime—although lifetime of the +dC samples decreases—and adding the

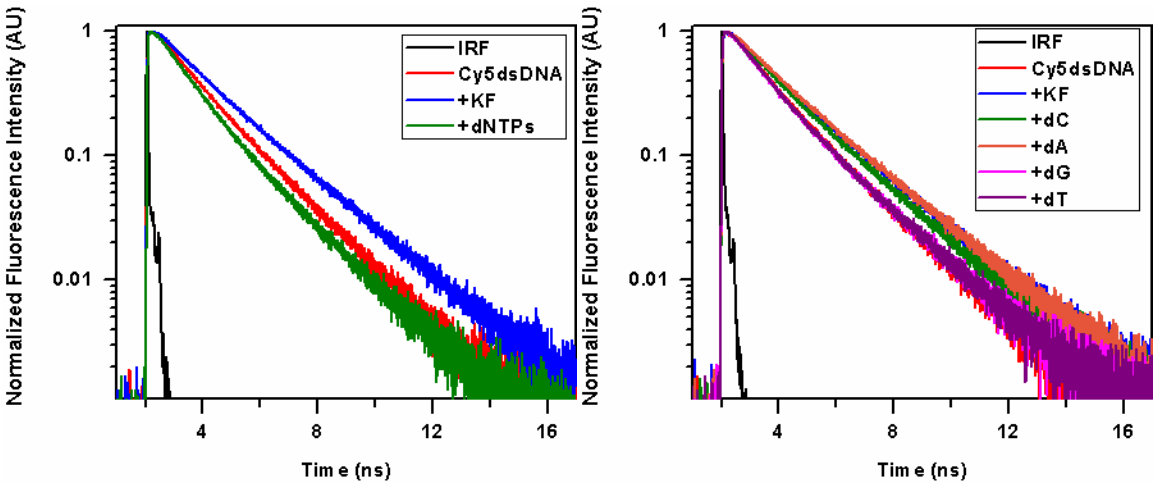


Figure 4.18: Polymerase Reaction on Cy5-dsDNA. These panels show the effect of adding dNTPs all at once (left) and stepwise (right) to Cy5-dsDNA.

remaining two dNTPs decreases the lifetime. The results of biexponential fits to this data are shown in Table 4.9. The ability of KF to perform the polymerase reaction was investigated using denaturing polyacrylamide gel electrophoresis (PAGE). The position of the dye causes no interference to the KF's ability to perform the polymerase reaction (see data in Appendix II). Appendix II also shows the results of titration experiments to determine the K_D of the binding reaction.

Table 4.9: Polymerase Reaction Lifetimes of Cy5-dsDNA

	τ_1/ns	$\%\alpha_1$	τ_2/ns	$\%\alpha_2$	$\langle\tau\rangle$/ns
Cy5-dsDNA	1.0	42%	2.0	56%	1.5
+ KF	1.1	29%	2.3	71%	2.0
+ dC	1.1	37%	2.2	63%	1.8
+ dA	1.1	29%	2.3	71%	2.0
+ dG	1.0	56%	2.2	44%	1.5
+ dT	1.0	56%	2.2	44%	1.5

Table 4.9: Polymerase Reaction Lifetimes of Cy5-dsDNA. Fit results for Cy5-dsDNA samples after the polymerase reaction.

II. Dy635-dsDNA

The lifetime behavior of Dy635-dsDNA, the closest spectral match to Cy5, differs from Cy5-dsDNA in the presence of KF. The lifetime of Dy635-dsDNA increases with a 25% excess of KF; however, unlike for Cy5, there is no further increase in lifetime even when there is an 85% excess of KF in solution (Figure 4.19, left panel). The intensity decays were each fitted with a biexponential; results are in Table 4.10. The anisotropy measurements confirm that KF binds to the DNA as the anisotropy for the KF samples decays at a slower rate than that of the DNA alone (left panel). The anisotropy results for the KF and degrader samples have different time zero values, however, if they are matched to the starting value of the DNA only sample then both Dy635-dsDNA and

degrader samples will have similar rates of decay, whereas the KF samples will clearly have a slower decay rate indicating protein binding.

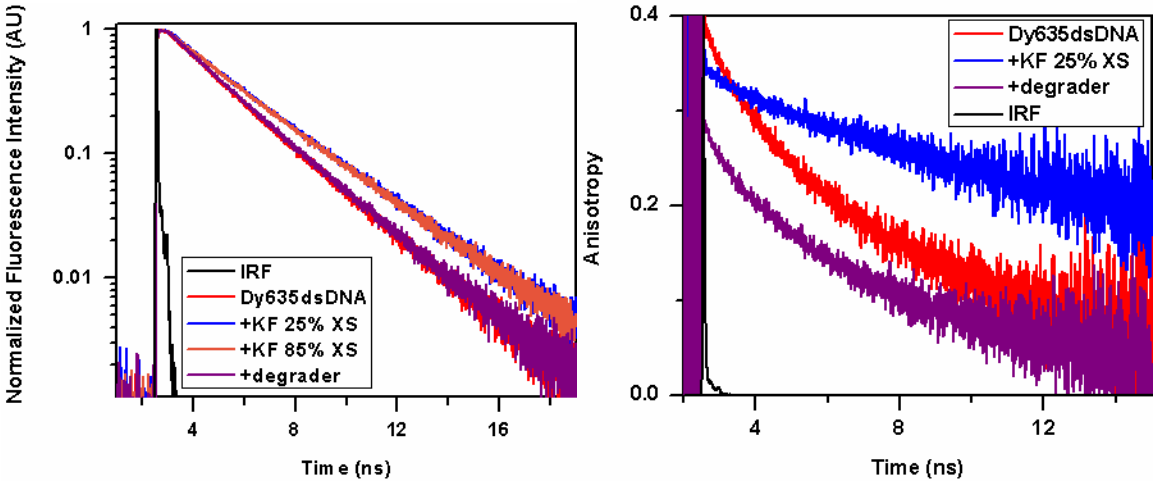


Figure 4.19: Dy635-dsDNA with Klenow Fragment. The left panel shows intensity decays and the right shows anisotropy decays of Dy6355-dsDNA while varying KF.

Table 4.10: Lifetimes of Dy635-dsDNA with KF

	τ_1/ns	$\%\alpha_1$	τ_2/ns	$\%\alpha_2$	$\langle\tau\rangle$/ns
Dy635dsDNA	1.0	13.7	2.4	86.3	2.2
+ KF 25% XS	1.4	18.3	3.0	81.7	2.7
+ KF 85% XS	1.4	20.0	3.0	80.3	2.7
+ degrader	1.0	10.4	2.4	89.6	2.3

Table 4.10: Lifetimes of Dy635-dsDNA with KF. Biexponential fits of the intensity decays in the left panel of Figure 4.19.

The intensity decays also do not follow the same trend for the polymerase reaction on this sample. In Figure 4.20, we see that addition of the first and second dNTPs in the template sequence decreases the lifetime, and addition of dGTP and dTTP decreases the lifetime further. In this sample, the orientation of KF on the DNA does not vary when the protein is adding the first three bases—at least not in such a way as to affect the photophysics of the dye. The discrepancy in lifetime components measured for Dy635-dsDNA and Dy635-dsDNA/KF in the two experiments is due to different time

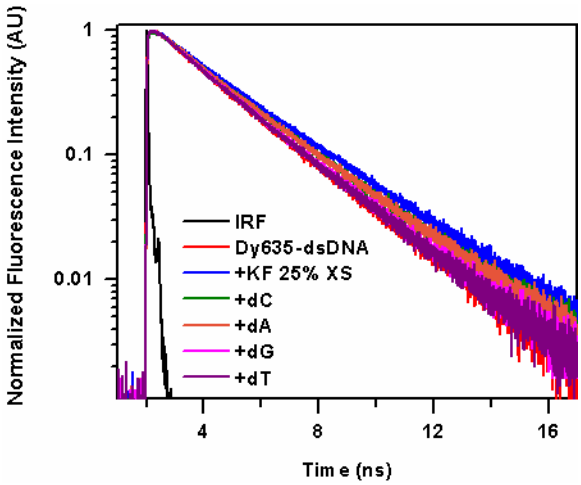


Figure 4.20: Polymerase Reaction on Dy635-dsDNA. Lifetime variation as a function of adding dNTPs in a stepwise fashion.

measurement windows being used for the two sets of data. The results of the lifetime fits are shown in Table 4.11.

Table 4.11: Polymerase Reaction Lifetimes of Dy635-dsDNA

	τ_1/ns	$\%\alpha_1$	τ_2/ns	$\%\alpha_2$	$\langle\tau\rangle$/ns
Dy635-dsDNA	1.3	29%	2.5	71%	2.2
+ KF 25% XS	1.3	23%	2.9	77%	2.5
+ dC	1.4	24%	2.7	76%	2.4
+ dA	1.3	27%	2.7	73%	2.4
+ dG	1.4	30%	2.6	70%	2.2
+ dT	1.4	30%	2.5	70%	2.2

Table 4.11: Polymerase Reaction Lifetimes of Dy635-dsDNA. Fit results for Dy635-dsDNA samples after the polymerase reaction.

III. Dy632-dsDNA

The lifetime of Dy632-dsDNA in the presence of KF reacts similarly as that of Dy635-dsDNA, except that there is a greater increase in lifetime from the DNA only samples to the KF sample. Dy635-dsDNA's lifetime increases from 2.2 ns to 2.5 ns with a 25% excess of KF, but Dy632-dsDNA's lifetime increases from 2.2 ns to 2.8 ns, and

that is with only a one-to-one equivalent of protein (Table 4.12). Adding more KF, up to a 25% excess, does not further increase the lifetime of Dy632-dsDNA (Figure 4.21, left panel). However, that comparison experiment was performed in a standard size cuvette, while the initial experiment (Figure 4.22) was performed in a microcuvette. A KF titration was performed in microcuvettes and shows a steady increase in lifetime up to 80% KF—at 10% excess (110% KF brown trace) no more change is observed (Figure 4.21, right panel). The intensity decays measured for the KF titration were fit globally

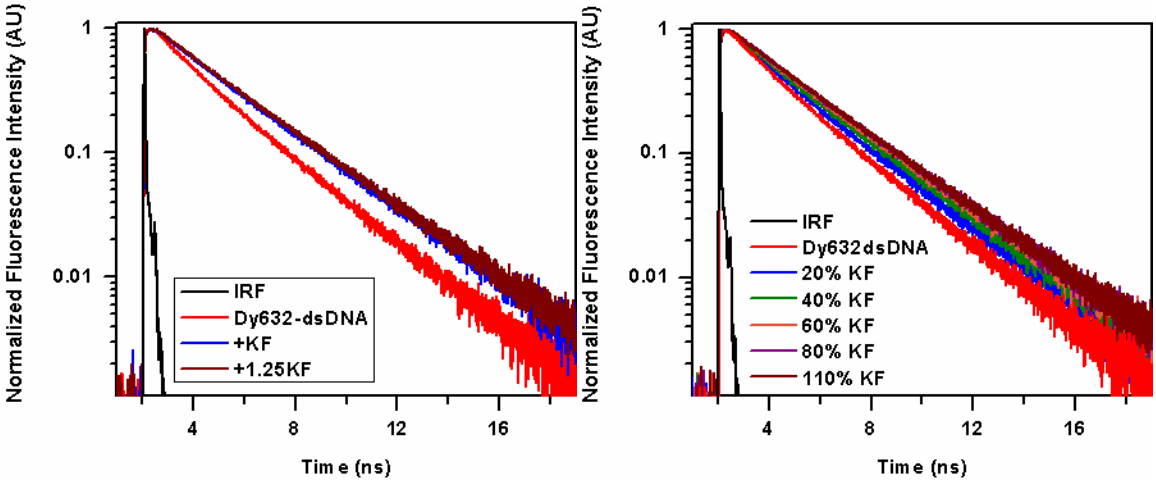


Figure 4.21: Lifetime of Dy632-dsDNA with Klenow Fragment. Left panel shows the lifetimes of Dy632-dsDNA with KF as measured in standard size cuvettes. The right panel shows a KF titration measured in microcuvettes.

Table 4.12: Lifetimes of Dy632-dsDNA with KF Titration

sample	0 KF	+20%KF	+40%KF	+60%KF	+80%KF	+110%KF
τ /ns	amplitudes					
1.7	0.044	0.032	0.023	0.015	0.011	0.010
3.0	0.027	0.038	0.047	0.054	0.058	0.059
$\langle\tau\rangle$ /ns	2.2	2.4	2.6	2.7	2.8	2.8

Table 4.12: Lifetimes of Dy632-dsDNA with KF Titration: Lifetimes of Dy632-dsDNA from the KF titration experiment were fit globally as described in the text.

using two lifetimes, 1.7 ns and 3.0 ns. The amplitudes, and average lifetimes, are shown

in Table 4.12. As KF is added the share of the long lifetime increases, while the share of the short lifetime decreases, thus the increase in average lifetime as KF is added.

As the dNTPs are added the lifetime decreases (Figure 4.22, left); the fully double-stranded sample has a lifetime of 2.1 ns (the lifetime trend with dNTPs is the same regardless of cuvette, data not shown). The anisotropy (Figure 4.22, right panel) shows a clear increase with KF, indicating binding. Some anisotropy traces have time

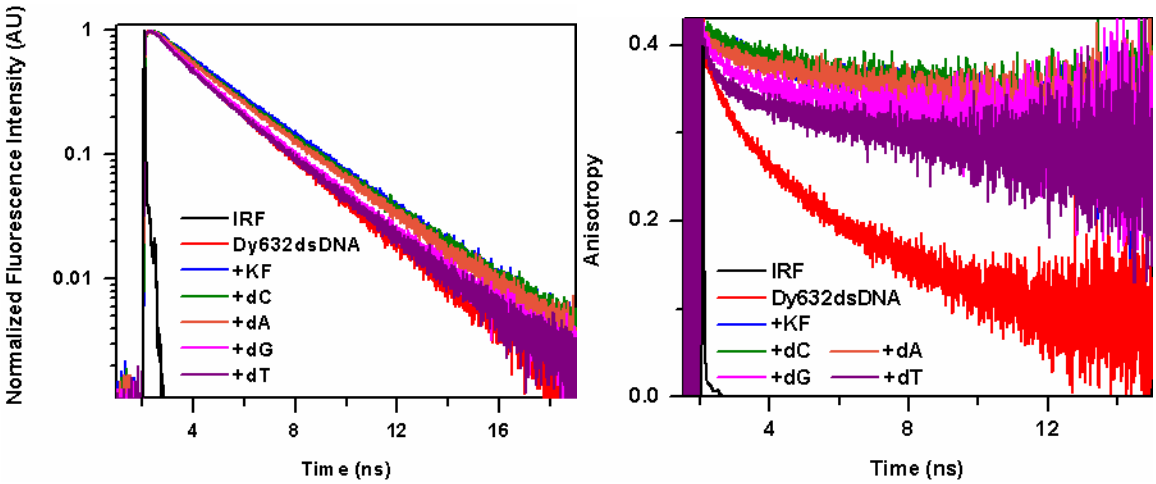


Figure 4.22: Polymerase Reaction on Dy632-dsDNA. Lifetime and anisotropy variation as a function of adding dNTPs in a stepwise fashion.

Table 4.13: Polymerase Reaction Lifetimes of Dy632-dsDNA

	τ_1/ns	%α_1	τ_2/ns	%α_2	$\langle\tau\rangle$/ns
Dy632-dsDNA	1.1	27%	2.6	73%	2.2
+ KF	1.2	8%	2.9	92%	2.8
+ dC	1.4	20%	3.0	80%	2.7
+ dA	1.2	19%	2.9	81%	2.6
+ dG	1.1	30%	2.8	70%	2.3
+ dT	1.0	33%	2.7	67%	2.1

Table 4.13: Polymerase Reaction Lifetimes of Dy632-dsDNA. Fit results for Dy632-dsDNA samples after the polymerase reaction.

zero values above 0.4, however this is most likely due to instrumental errors as discussed for other samples above. The shape of the anisotropy traces for all the protein samples is

similar, however, indicating the position of the KF along the primer does not affect the anisotropy. Lifetime fit results are shown in Table 4.13.

IV. Dy630-dsDNA

The Dy630-dsDNA samples experience less pronounced changes in lifetime with KF. The intensity decays of Dy630-dsDNA alone, with KF, and once the dNTPs have been added appear to decay with the same average lifetime (Figure 4.23, left panel); the biexponential fits reveal an increase from 2.5 ns to 2.8 ns when KF is added (Table 4.14). The addition of the first two dNTPs does not alter the lifetime, while the last two dNTPs decrease the lifetime to 2.7 ns. The amount of KF added in this experiment was in 25% excess to the DNA. The lifetime of the Dy630-dsDNA samples does not change dramatically with KF; a ratio of KF to DNA of 1:4 increases the lifetime only to 2.7 ns, while a ratio of 1.25:1 increases the lifetime to only 2.8 ns (Figure 4.24 and Table 4.15). Dy630-dsDNA is not as sensitive to the presence of KF as Dy632-dsDNA is.

The anisotropy of these samples follows the same trend seen for the Dy632-dsDNA samples: upon KF binding the anisotropy decays significantly slower than for the DNA only sample (Figure 4.23, right panel). In this experiment, the Dy630-dsDNA/KF sample has a lower time zero anisotropy than the other samples, however its rate of decay is clearly slower than that of pure DNA indicating less mobility due to binding. Addition of dCTP and dATP does not affect that rate of decay, but addition of dGTP and dTTP increases the rate of decay.

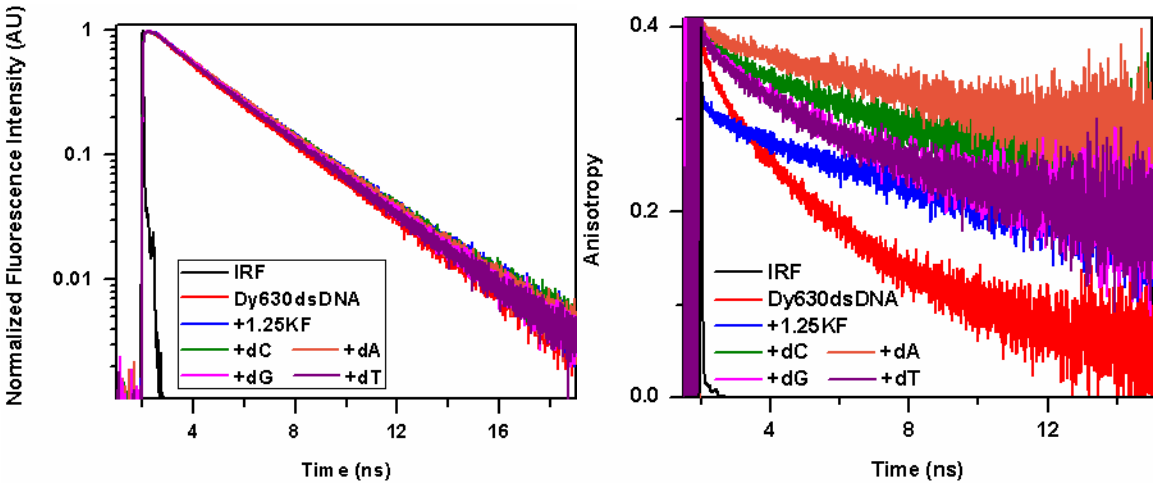


Figure 4.23: Polymerase Reaction on Dy630-dsDNA. Lifetime and anisotropy variation as a function of adding dNTPs in a stepwise fashion.

Table 4.14: Polymerase Reaction Lifetimes of Dy630-dsDNA

	τ_1/ns	%α_1	τ_2/ns	%α_2	$\langle\tau\rangle$/ns
Dy630-dsDNA	1.3	27%	3.0	73%	2.5
+ KF	1.5	23%	3.2	77%	2.8
+ dC	1.4	22%	3.2	78%	2.8
+ dA	1.7	21%	3.1	79%	2.8
+ dG	1.6	26%	3.1	75%	2.7
+ dT	1.6	27%	3.1	73%	2.7

Table 4.14: Polymerase Reaction Lifetimes of Dy630-dsDNA. Fit results for Dy630-dsDNA samples after the polymerase reaction.

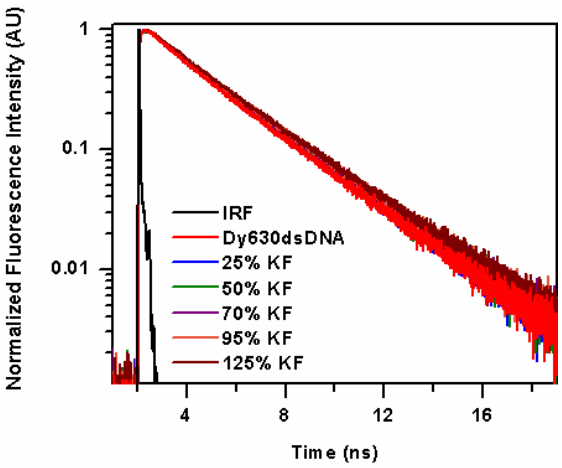


Figure 4.24: Lifetime of Dy630-dsDNA with Klenow Fragment. Change in Dy630-dsDNA lifetime as a function of KF concentration.

Table 4.15: Lifetimes of Dy630-dsDNA with KF Titration

sample	0 KF	+25%KF	+50%KF	+70%KF	+95%KF	+125%KF
τ /ns	amplitudes					
1.7	0.028	0.025	0.023	0.020	0.018	0.017
3.2	0.042	0.045	0.047	0.049	0.051	0.053
$\langle\tau\rangle$ /ns	2.6	2.7	2.7	2.8	2.8	2.8

Table 4.15: Lifetimes of Dy630-dsDNA with KF Titration: Lifetimes of Dy630-dsDNA from the KF titration experiment were fit globally as described in the text.

D. Transient Absorption Measurements

Transient absorption experiments were performed to obtain a direct measurement of the photoisomer. The kinetic traces of several probe wavelengths for free Dy630 in ethanol are shown in Figure 4.25 (left panel). A strong positive signal is seen for wavelengths to the red of the ground state absorption spectrum. The difference spectrum

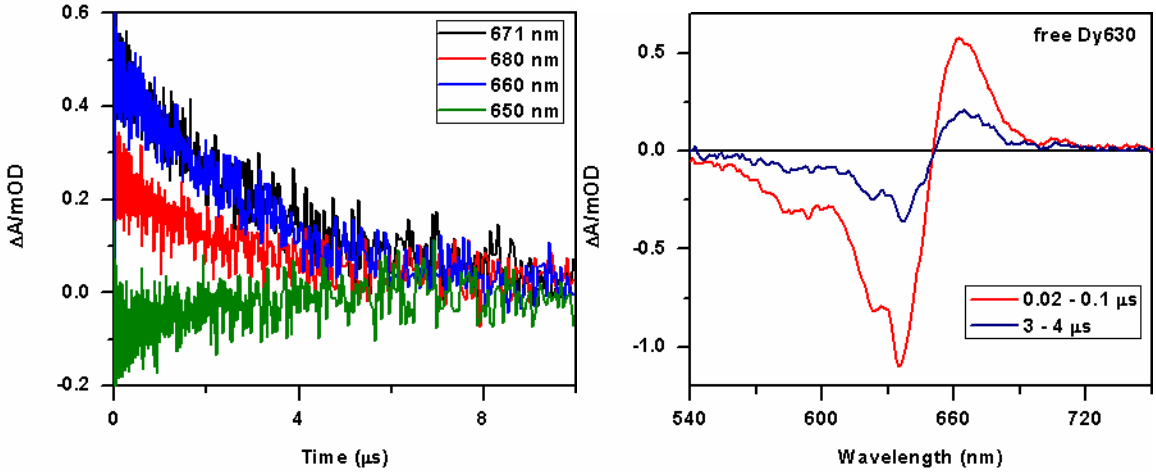


Figure 4.25: Kinetic Traces and Difference Spectra of Dy630. A handful of kinetic traces from the difference spectrum of free Dy630 (on right) are shown in the left panel.

is shown in the left panel; the positive feature from 660 – 690 nm is due to the photoisomer population. The negative signal from 570 – 650 nm is due to ground state absorption.

The Cy5-dsDNA sample was also measured, however, it showed no difference in

isomer signal in the KF sample as compared to the DNA only sample (Figure 4.26, left panel). The degraded sample also appears to have the same isomer population as the KF sample (compare blue and red traces). The strong positive signal for the KF sample at 650 nm is due to scattering by the protein. The KF was used in a 2:1 ratio to the DNA in these experiments. A comparison of kinetic traces at 683 nm probe wavelength (at the isomer maximum) shows no difference between the samples (Figure 4.26, right panel).

Transient absorption measurements were performed on Dy630-, Dy632-, and Dy635-dsDNA, however, no transient signal was detected. The Dy632-dsDNA sample was measured in a solution of 50% glycerol, as well, to "slow down" the isomer, to no avail. Timescales from 50 to 500 ns were probed, but neither sample showed photoisomer formation for DNA only; as such experiments with the KF were not performed.

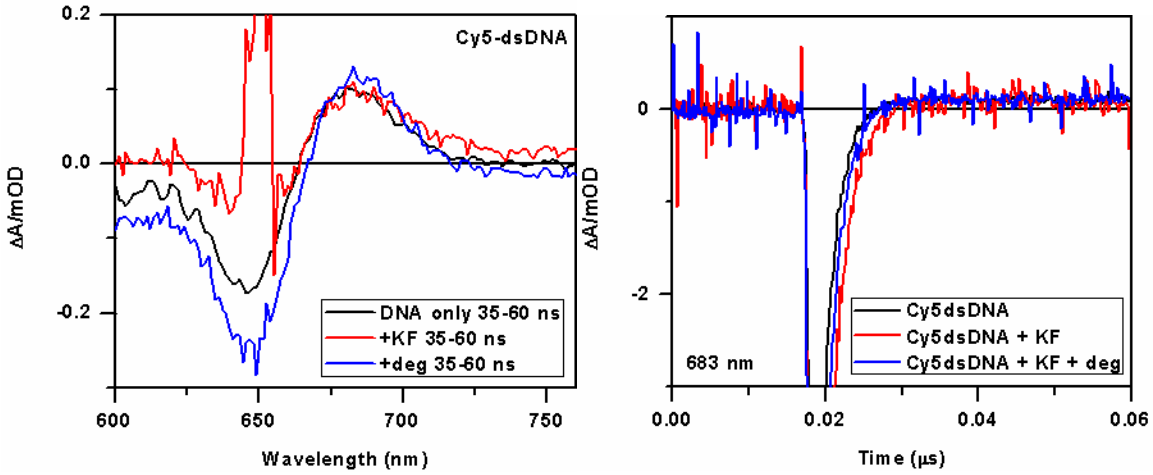


Figure 4.26: Kinetic Traces and Difference Spectra of Cy5-dsDNA. The difference spectrum of Cy5-dsDNA in shown alone, in the presence of KF, and with the protein degrader (left). Kinetic traces of the three sample at 683 nm (the maximum in the spectrum) are shown on the right. No difference is seen between the three samples. The strong positive signal for the Cy5-dsDNA/KF sample (red) is due to scattering from the protein.

4.4 Discussion

A. Dy Dyes Compared to Cy3

The fact that no transient was observed in the difference spectra of the Dy dye labeled DNAs is surprising given the free dye behavior of Dy630 resembles that of Cy3, the highly effective green-absorbing PIFE dye. The viscosity behavior of free Cy3 is shown below (Figure 4.27); while the lifetime does not increase with viscosity—Cy3 in water has the shortest lifetime and its lifetime in methanol is shorter than in acetone—the viscosity of the solvent imparts a significant effect on the lifetime as it does for free Dy630. On DNA, however, the lifetime of Dy630 is impervious to changes in viscosity (and salt concentration, see Figures 4.8 and 4.9), which is why there is only a marginal increase in lifetime in the presence of KF (Figures 4.23 and 4.24). A dye that is unresponsive to viscosity changes in the solvent implies the rate of *cis*- to *trans*-photoisomerization is not changing in response to a more rotation restricted environment (or, that the rate is so small to begin with that any decrease makes it smaller still). This

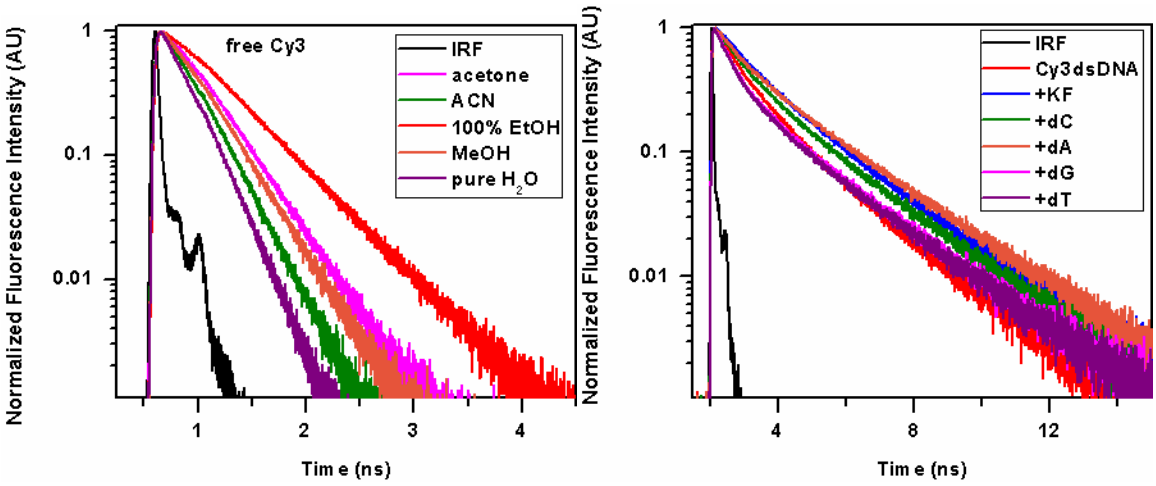


Figure 4.27: Lifetimes of Free Cy3 and Cy3-dsDNA. The left panel shows intensity decays of free Cy3 in organic solvents and in water. The right panel shows the intensity decays of Cy3-dsDNA, with KF, and after the polymerase reaction.

could explain why there is no photoisomer population observed in the difference spectrum of Dy630-dsDNA (and of the other Dy dyes).

The lifetime fit results offer another clue as to the lack of PIFE behavior for Dy630-dsDNA/KF. Figure 4.23 and Table 4.14 show the lifetimes and fit results for the polymerase reaction on Dy630-dsDNA. Each average lifetime is composed of two components, a short lifetime around 1.3 – 1.7 ns and a long lifetime around 3.0 – 3.2 ns. Here is a stark contrast to Cy3's behavior on DNA. A Cy3 labeled sample of the same sequence used for this study was prepared and measured using TCSPC (Figure 4.27, right panel). The fit results are in Table 4.16. In contrast to all Dy dye samples measured here it takes three lifetimes to properly fit this data. The shortest lifetime in each sample is 0.2 ns, which is the approximately the lifetime of free Cy3 in water[34]. Conjugation to DNA does not eliminate this super-short lifetime as it does for all the Dy dyes studied here. The fit results clearly show that when KF is added to the system the contribution of the super-short free dye lifetime is decreased and the contribution of the longest lifetime increases by the same amount. This accounts for the increased lifetime in the presence of

Table 4.16: Polymerase Reaction Lifetimes of Cy3-dsDNA

	τ_1/ns	$\%\alpha_1$	τ_2/ns	$\%\alpha_2$	τ_3/ns	$\%\alpha_3$	$\langle\tau\rangle$/ns
Cy3-dsDNA	0.2	37%	1.0	41%	2.1	22%	0.9
+ KF	0.2	22%	1.1	42%	2.3	36%	1.3
+ dC	0.2	30%	1.0	38%	2.3	32%	1.2
+ dA	0.2	31%	1.0	28%	2.4	41%	1.3
+ dG	0.2	50%	0.8	28%	2.3	22%	0.8
+ dT	0.2	52%	0.9	28%	2.3	20%	0.8

Table 4.16: Polymerase Reaction Lifetimes of Cy3-dsDNA. Fit results for Cy3-dsDNA samples after the polymerase reaction.

KF, the population of Cy3 molecules which fluoresce longer because they cannot deactivate via isomerization.

It is interesting that Cy5 is a better PIFE dye than any of the Dy dyes. Only two components are required to fit the lifetimes of the Cy5-dsDNA samples (Table 4.9); however, the short lifetime is only 0.1 ns longer than Cy5's lifetime in solution, and the fraction of the decay described by the short lifetime decreases significantly upon KF binding. Such a dramatic decrease for the short lifetime is seen only for Dy632-dsDNA (Table 4.13); although this short lifetime is 1.2 ns, which is much longer than the 0.2 ns lifetime of the free Dy632 (the lifetime of free Dy632 was not measured, however given that the only difference between Dy630 and Dy632 is the number of sulfonate groups the lifetime of Dy632 is expected to be similar). The average lifetime of Dy632-dsDNA increases from 2.2 ns to 2.8 ns upon KF binding (Table 4.12); this is a 27% increase compared to Cy5-dsDNA (33%) and Cy3-dsDNA (44%). Also interesting is free Cy5's behavior in various organic solvents (Figure 4.14, left). Unlike Cy3 and Dy630, Cy5 has no lifetime trend with regards to solvent viscosity. Overall, these observations suggest that the presence of a very short lifetime—as a free dye in solution and when conjugated to DNA—is the best predictor of a dye's potential PIFE behavior.

B. DNA Construct Evaluation

The results of this project only show that the Dy dyes do not have the potential to be PIFE dyes when conjugated at the 10 position of the primer strand. No transient signal is observed for any of the Dy-dsDNA samples, however free Dy630 behaves similarly to Cy3 to suggest that it can be a better red-absorbing PIFE dye than Cy5. Free

Dy630 has a very short lifetime of 0.2 ns, it forms a photoisomer (Figure 4.25), and its response to solution viscosity mimics Cy3 (compare left panels of Figures 4.14 and 4.27). The transient absorption results suggest the dye cannot isomerize even in the absence of KF. The dye may be prevented from isomerizing due to stacking interaction between the dye and the last base (in position 11) on the primer strand. Previous work from the Levitus lab has observed an increase in fluorescence quantum yield for Cy3 in the presence of deoxynucleotide monophosphates (dNMPs)[55]. The fluorescence quantum yield of free diethylindocarbocyanine doubles in the presence of 100 mM deoxyguanosine monophosphate (dGMP) and deoxyadenosine monophosphate (dAMP). The pyrimidine bases only increase ϕ_f by 50%. The enhancement is attributed to the interactions between the π-orbitals of the conjugated base and dye, i.e., $\pi - \pi$ stacking interactions. For such an interaction to occur Cy3 must be in a planar conformation and cannot be rotating. Thus, stacking interactions prevent the dye from undergoing photoisomerization. The Levitus lab has also observed these stacking interactions for Cy3 attached covalently to the 5' end of ssDNA[54]. It should be mentioned that the free Dy630 difference spectrum was measured in ethanol. Measurements of Dy630 in water show no transient (data not shown here, measured by Nikita Kumari). This is an interesting, although not yet understood, development, and will be investigated by the Levitus lab in the future.

In the DNA sequence used here, the dye is attached to the modified thymine via a six-carbon linker, which flexible and long enough to allow the dye to stack with the last base of the primer strand. Based on the stacking interactions of Cy3 with nucleobases, it is hypothesized that stacking interactions between the Dy dyes and base 11 prevent the

photoisomerization process. Preliminary data on free Dy630 confirms the validity of this hypothesis. Figure 4.28 shows a six-fold increase in the fluorescence of free Dy630 in the presence of 100 mM dGMP. This suggests that the $\pi - \pi$ stacking interaction is greater for Dy630 than for Cy3. This may be the result of Dy630 having a longer conjugated π system than Cy3—since Dy630 is a red-absorbing dye. Preliminary TIRF measurements on Dy632-dsDNA also show what appears to be two different intensity levels in the single-molecule traces. This, too, suggests the possibility the dye exists in two states in this construct: in one state the dye may be stacked with the DNA bases and have a higher fluorescence intensity, while in the other state the dye may be exposed to solution and have a lower intensity. This data is presented in Appendix III.

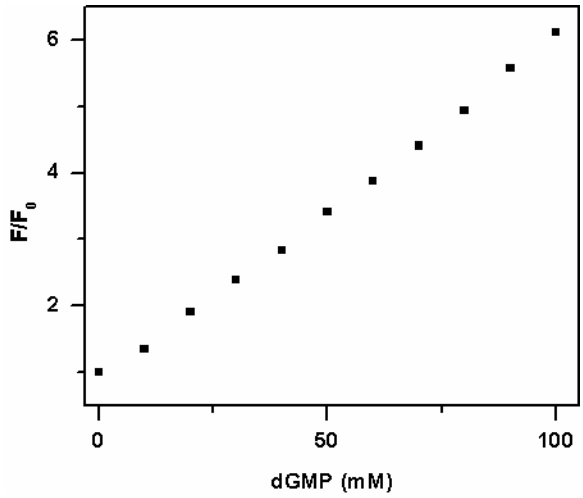


Figure 4.28: Fluorescence Response of Dy630 to dGMP. The relative fluorescence of free Dy630 is measured as dGMP is added. Experiment perfomed by Nikita Kumari.

The sequence also plays a role in stacking interactions. Harvey *et al.* found the lifetime and fluorescence quantum yield of Cy3 vary with up to the first five nucleobases of a 5' labeled ssDNA[54]. It is possible that changing the identity of base 11 of the primer strand, or any of the nearby nucleobases, may reduce the $\pi - \pi$ stacking interactions; this

could potentially allow the Dy dye to be susceptible to steric hindrance from a protein. Alternatively, the length of the linker can be reduced. The Dy dyes are attached to the modified thymine base via a six-carbon linker; reducing the linker to only two carbons, for example, may prevent the dye from stacking with base 11. Similarly, click chemistry—via the copper catalyzed alkyne-azide cycloaddition reaction—may be used to conjugate fluorophores to DNA on short linkers. Precursor uracil bases—with an alkyne functional group—have been effectively conjugated to fluorophores with azide modifications and inserted into oligonucleotides[174]. The alkyne group added to the base can be directly attached or on a several carbon spacer, i.e., the distance of the fluorophore to the base can be controlled.

Attaching the Dy dyes to a different position on the DNA may also result in sample where the Dy dye can still isomerize. For example, the DNA construct used in Chapter 3 could be effective: the dye can be attached to the 5' end of a short (six-base) primer. Based on the previous results, it's expected that such a sample in the presence of the KF (with binding at both *pol* and *exo* sites) would experience increased flouorescence.

4.5 Conclusion

The goal of this project was to evaluate the asymmetric cyanine dyes Dy630, Dy632, and Dy635 as potential PIFE (protein induced fluorescence enhancement) probes, meaning probes which experience enhanced fluorescence in close proximity to a protein. This project used the commercial version of the Klenow fragment (KFcom) that has binding only at the *pol* site, and a DNA construct designed by David Millar for his

studies of KF. The intensity decays show increases in average lifetime for Dy635 and Dy632, but no change for Dy630 in the presence of KFcom. Additionally, the lifetime increases seen for the Dy dyes are modest in comparison to the same DNA construct labeled with Cy5 or Cy3. Detailed analysis of lifetime components also shows that the Dy dyes lose the short lifetime characteristic of the free dye upon DNA conjugation; Cy3 does not and it is this lifetime component which KFcom affects. Transient absorption measurements did not detect the presence of any transient species for the DNA only samples. This implies that the environment of this DNA construct prevents photoisomerization, probably due to $\pi - \pi$ stacking interactions. Hence, the presence of KFcom cannot affect the photoisomerization rate. In order to properly evaluate these dyes for possible fluorescence enhancement a shorter linker (to prevent the dye from stacking with the DNA bases) or conjugation to a different region of the DNA will be investigated in future studies.

CONCLUSIONS

This dissertation focused on photophysical behavior of organic fluorescent probes in a variety of solution and biomolecule environments. In Chapter 2, manganese(II) was found to increase the intersystem crossing (ISC) rate for cyanine dyes. This work was a follow up on work performed by a previous Levitus group member, Elana M. S. Stennett, who observed an increased ISC rate for a rhodamine dye in the presence of manganese(II). Observation of the same phenomenon in cyanines indicates this is a universal effect, i.e., dyes with varied chromophore structures may be susceptible. The formation of the triplet state in Cy3B was observed in fluorescence correlation spectroscopy (FCS) measurements; the timescale of the triplet fluctuation overlaps with the timescale of dynamic biological systems. As such, the triplet fluctuation could be mistaken for biological behavior. On the other hand, the ability to use a simple cation to force the dye into the dark triplet state could be exploited for super-resolution imaging purposes, some of which rely on "shelving" a dye into its dark state.

Chapter 3 explored the mechanism behind protein induced fluorescence enhancement (PIFE) in Cy3. The PIFE technique is used as a qualitative analogue to Forster Resonance Energy Transfer (FRET). Cy3-labeled DNA was observed in the presence of Klenow Fragment (KF). For samples in which Cy3 was solution exposed (remained outside the DNA-bound KF) no change in its photophysical behavior was observed. However, when Cy3 was pulled into the KF interior its fluorescence intensity and anisotropy decays were dramatically altered. Direct measurement of the photoisomer shows that inside the protein Cy3 does not photoisomerize with the same efficiency as in

its solution exposed state. Thus, the fluorescence enhancement in the PIFE technique is due to Cy3's inability to deactivate via photoisomerization, thus increasing its fluorescence rate. This chapter highlights the benefit of a dye's susceptibility to its environment. Understanding how the environment changes the photophysics of a probe makes it a useful reporter of the micro-environment in a biological system.

Chapter 4 investigates a relatively new class of asymmetric cyanines, Dy630, Dy632, and Dy635, and evaluates their potential as red-absorbing PIFE probes. Cy5, like Cy3, can photoisomerize however the fluorescence enhancement observed for Cy5-DNA in the presence of KF is not as significant as for Cy3. The Dy dyes studied here absorb and emit in the same wavelength region as Cy5, and may be suitable alternatives. However, lifetime measurements show insignificant changes with KF, and transient absorption measurements do not detect the presence of a photoisomer for the Dy-DNA samples on their own. Thus, in the DNA construct used here the Dy dye is prevented from photoisomerizing, and this construct does not allow the dye's fluorescence to respond to the environment. Changing the linker length or using a different construct may show these dyes to be decent PIFE probes as they possess extremely short lifetimes as free dyes just like Cy3.

To conclude, understanding the photophysical behavior of fluorescent probes is not only essential to proper data interpretation, but renders the probes useful tools for studying the microscopic behaviors of biological systems.

REFERENCES

1. Lichtman, J. W.; Conchello, J. A., Fluorescence microscopy. *Nature Methods* **2005,** *2* (12), 910-919.

2. Stephens, D. J.; Allan, V. J., Light microscopy techniques for live cell Imaging. *Science* **2003,** *300* (5616), 82-86.

3. Medintz, I. L.; Uyeda, H. T.; Goldman, E. R.; Mattoussi, H., Quantum dot bioconjugates for imaging, labelling and sensing. *Nature Materials* **2005,** *4* (6), 435-446.

4. Lilley, D. M. J.; Wilson, T. J., Fluorescence resonance energy transfer as a structural tool for nucleic acids. *Current Opinion in Chemical Biology* **2000,** *4* (5), 507-517.

5. Klostermeier, D.; Millar, D. P., Time-resolved fluorescence resonance energy transfer: A versatile tool for the analysis of nucleic acids. *Biopolymers* **2001,** *61* (3), 159-179.

6. Klostermeier, D.; Millar, D. P., RNA conformation and folding studied with fluorescence resonance energy transfer. *Methods* **2001,** *23* (3), 240-254.

7. Royer, C. A., Probing protein folding and conformational transitions with fluorescence. *Chemical Reviews* **2006,** *106* (5), 1769-1784.

8. Park, H.; Toprak, E.; Selvin, P. R., Single-molecule fluorescence to study molecular motors. *Quarterly Reviews of Biophysics* **2007,** *40* (1), 87-111.

9. Schuler, B.; Eaton, W. A., Protein folding studied by single-molecule FRET. *Current Opinion in Structural Biology* **2008,** *18* (1), 16-26.

10. Eggeling, C.; Ringemann, C.; Medda, R.; Schwarzmann, G.; Sandhoff, K.; Polyakova, S.; Belov, V. N.; Hein, B.; von Middendorff, C.; Schonle, A.; Hell, S. W., Direct observation of the nanoscale dynamics of membrane lipids in a living cell. *Nature* **2009,** *457* (7233), 1159-U121.

11. Sengupta, P.; Balaji, J.; Maiti, S., Measuring diffusion in cell membranes by fluorescence correlation spectroscopy. *Methods* **2002,** *27* (4), 374-387.

12. Bezanilla, F., The voltage sensor in voltage-dependent ion channels. *Physiological Reviews* **2000,** *80* (2), 555-592.

13. Moerner, W. E.; Kador, L., Optical-detection and spectroscopy of single molecules in a solid. *Physical Review Letters* **1989,** *62* (21), 2535-2538.

14. Moerner, W. E.; Kador, L., Finding a single molecule in a haystack - optical-detection and spectroscopy of single absorbers in solids. *Analytical Chemistry* **1989,** *61* (21), A1217-A1223.

15. Borgia, A.; Williams, P. M.; Clarke, J., Single-molecule studies of protein folding. In *Annual Review of Biochemistry*, Annual Reviews: Palo Alto, 2008; Vol. 77, pp 101-125.

16. Li, G. W.; Xie, X. S., Central dogma at the single-molecule level in living cells. *Nature* **2011,** *475* (7356), 308-315.

17. Marshall, R. A.; Aitken, C. E.; Dorywalska, M.; Puglisi, J. D., Translation at the single-molecule level. In *Annual Review of Biochemistry*, Annual Reviews: Palo Alto, 2008; Vol. 77, pp 177-203.

18. Beechem, J. M.; Brand, L., Time-resolved fluorescence of proteins. *Annual Review of Biochemistry* **1985,** *54*, 43-71.

19. Lakowicz, J. R., Fluorophores. In *Principles of Fluorescence Spectroscopy*, Third ed. ed.; Springer: Baltimore, Maryland, 2006; pp 63-95.

20. Callis, P. R., Electronic states and luminescence of nucleic-acid systems. *Annual Review of Physical Chemistry* **1983,** *34*, 329-357.

21. Tinnefeld, P.; Sauer, M., Branching out of single-molecule fluorescence spectroscopy: Challenges for chemistry and influence on biology. *Angewandte Chemie-International Edition* **2005,** *44* (18), 2642-2671.

22. Ha, T., Single-molecule fluorescence resonance energy transfer. *Methods* **2001,** *25* (1), 78-86.

23. Levitus, M.; Ranjit, S., Cyanine dyes in biophysical research: the photophysics of polymethine fluorescent dyes in biomolecular environments. *Quarterly Reviews of Biophysics* **2011,** *44* (1), 123-151.

24. Ha, T.; Tinnefeld, P., Photophysics of Fluorescent Probes for Single-Molecule Biophysics and Super-Resolution Imaging. *Annual Review of Physical Chemistry, Vol 63* **2012,** *63*, 595-617.

25. Remington, S. J., Fluorescent proteins: maturation, photochemistry and photophysics. *Current Opinion in Structural Biology* **2006,** *16* (6), 714-721.

26. Mehta, S.; Zhang, J., Reporting from the Field: Genetically Encoded Fluorescent Reporters Uncover Signaling Dynamics in Living Biological Systems. In *Annual Review of Biochemistry, Vol 80*, Kornberg, R. D.; Raetz, C. R. H.; Rothman, J. E.; Thorner, J. W., Eds. Annual Reviews: Palo Alto, 2011; Vol. 80, pp 375-+.

27. Giepmans, B. N. G.; Adams, S. R.; Ellisman, M. H.; Tsien, R. Y., Review - The fluorescent toolbox for assessing protein location and function. *Science* **2006,** *312* (5771), 217-224.

28. Arya, H.; Kaul, Z.; Wadhwa, R.; Taira, K.; Hirano, T.; Kaul, S. C., Quantum dots in bio-imaging: Revolution by the small. *Biochemical and Biophysical Research Communications* **2005,** *329* (4), 1173-1177.

29. Chan, W. C. W.; Maxwell, D. J.; Gao, X. H.; Bailey, R. E.; Han, M. Y.; Nie, S. M., Luminescent quantum dots for multiplexed biological detection and imaging. *Current Opinion in Biotechnology* **2002,** *13* (1), 40-46.

30. Michalet, X.; Pinaud, F. F.; Bentolila, L. A.; Tsay, J. M.; Doose, S.; Li, J. J.; Sundaresan, G.; Wu, A. M.; Gambhir, S. S.; Weiss, S., Quantum dots for live cells, in vivo imaging, and diagnostics. *Science* **2005,** *307* (5709), 538-544.

31. Mishra, A.; Behera, R. K.; Behera, P. K.; Mishra, B. K.; Behera, G. B., Cyanines during the 1990s: A review. *Chemical Reviews* **2000,** *100* (6), 1973-2011.

32. Ernst, L. A.; Gupta, R. K.; Mujumdar, R. B.; Waggoner, A. S., Cyanine dye labeling reagents for sulfhydryl-groups. *Cytometry* **1989,** *10* (1), 3-10.

33. Southwick, P. L.; Ernst, L. A.; Tauriello, E. W.; Parker, S. R.; Mujumdar, R. B.; Mujumdar, S. R.; Clever, H. A.; Waggoner, A. S., Cyanine dye labeling reagents - carboxymethylindocyanine succinimidyl esters. *Cytometry* **1990,** *11* (3), 418-430.

34. Sanborn, M.; Connolly, B.; Gurunathan, K.; Levitus, M., Fluorescence properties and photophysics of the sulfoindocyanine Cy3 linked covalently to DNA. *Journal of Physical Chemistry B* **2007,** *111* (37), 11064-11074.

35. Ciuba, M.; Levitus, M., Manganese-Induced Triplet Blinking and Photobleaching of Single Molecule Cyanine Dyes. *Chemphyschem* **2013,** *14* (15), 3495-3502.

36. Cooper, M.; Ebner, A.; Briggs, M.; Burrows, M.; Gardner, N.; Richardson, R.; West, R., Cy3B (TM): Improving the performance of cyanine dyes. *Journal of Fluorescence* **2004,** *14* (2), 145-150.

37. Huang, Z.; Ji, D.; Wang, S.; Xia, A.; Koberling, F.; Patting, M.; Erdmann, R., Spectral identification of specific photophysics of Cy5 by means of ensemble and single molecule measurements. *Journal of Physical Chemistry a* **2006,** *110* (1), 45-50.

38. Rulliere, C., Laser action and photoisomerization of 3,3'-diethyl oxadicarbocyanine iodide (DODCI) - Influence of temperature and concentration. *Chemical Physics Letters* **1976,** *43* (2), 303-308.

39. Wheatley, P. J., The crystallography of some cyanine dyes .2. The molecular and crystal structure of the ethanol solvate of 3,3+-diethylthiacarbocyanine bromide. *Journal of the Chemical Society* **1959,** (DEC), 4096-4100.

40. West, W.; Pearce, S.; Grum, F., Steroisomerism in cyanine dyes-meso-substituted thiacarbocyanines. *Journal of Physical Chemistry* **1967,** *71* (5), 1316-&.

41. Kolesnikov, A. M.; Mikhailenko, F. A., The Conformations of Polymethine Dyes. *Russian Chemical Reviews* **1987,** *56* (3), 275-287.

42. Kuzmin, V. A.; Darmanyan, A. P., Study of sterically hindered short-lived isomers of polymethine dyes by laser photolysis. *Chemical Physics Letters* **1978,** *54* (1), 159-163.

43. Akesson, E.; Sundstrom, V.; Gillbro, T., Solvent-dependent barrier heights of excited-state photoisomerization reactions. *Chemical Physics Letters* **1985,** *121* (6), 513-522.

44. Chibisov, A.; Zakharova, G.; Gorner, H.; Sogulyaev, Y.; Mushkalo, I.; Tolmachev, A., Photorelaxation processes in covalently-linked indocarbocyanine and thiacarbocyanine dyes. *Journal of Physical Chemistry* **1995,** *99* (3), 886-893.

45. Sibbett, W.; Taylor, J. R.; Welford, D., Substituent and environmental-effects on the picosecond lifetimes of the polymethine cyanine dyes. *Ieee Journal of Quantum Electronics* **1981,** *17* (4), 500-509.

46. Korppitommola, J. E. I.; Hakkarainen, A.; Hukka, T.; Subbi, J., An isomerization reaction of a cyanine dye in normal-alcohols - microscopic friction and an excited-state barrier crossing. *Journal of Physical Chemistry* **1991,** *95* (22), 8482-8491.

47. Akesson, E.; Hakkarainen, A.; Laitinen, E.; Helenius, V.; Gillbro, T.; Korppitommola, J.; Sundstrom, V., Analysis of microviscosity and reaction coordinate concepts in isomerization dynamics described by kramers theory. *Journal of Chemical Physics* **1991,** *95* (9), 6508-6523.

48. Sundstrom, V.; Gillbro, T., Viscosity-dependent isomerization yields of some cyanine dyes - a picosecond laser spectroscopy study. *Journal of Physical Chemistry* **1982,** *86* (10), 1788-1794.

49. Aramendia, P. F.; Negri, R. M.; Sanroman, E., Temperature-dependence of fluorescence and photoisomerization in symmetrical carbocyanines - influence of medium viscosity and molecular-structure. *Journal of Physical Chemistry* **1994,** *98* (12), 3165-3173.

50. Ponterini, G.; Momicchioli, F., Trans cis photoisomerization mechanism of carbocyanines - experimental check of theoretical-models. *Chemical Physics* **1991,** *151* (1), 111-126.

51. Sauerwein, B.; Murphy, S.; Schuster, G. B., Dynamics of solute motion - photoisomerization shows linear-dependence on solvent mass. *Journal of the American Chemical Society* **1992,** *114* (20), 7920-7922.

52. Brismar, H.; Trepte, O.; Ulfhake, B., Spectra and fluorescence lifetimes of lissamine rhodamine, tetramethylrhodamine isothiocyanate, texas red, and cyanine-3.18 fluorophores - influences of some environmental-factors recorded with a confocal laser-scanning microscope. *Journal of Histochemistry & Cytochemistry* **1995,** *43* (7), 699-707.

53. Gruber, H. J.; Hahn, C. D.; Kada, G.; Riener, C. K.; Harms, G. S.; Ahrer, W.; Dax, T. G.; Knaus, H. G., Anomalous fluorescence enhancement of Cy3 and Cy3.5 versus anomalous fluorescence loss of Cy5 and Cy7 upon covalent linking to IgG and noncovalent binding to avidin. *Bioconjugate Chemistry* **2000,** *11* (5), 696-704.

54. Harvey, B.; Perez, C.; Levitus, M., DNA sequence-dependent enhancement of Cy3 fluorescence. *Photochemical & Photobiological Sciences* **2009,** *8* (8), 1105-1110.

55. Harvey, B.; Levitus, M., Nucleobase-Specific Enhancement of Cy3 Fluorescence. *Journal of Fluorescence* **2009,** *19* (3), 443-448.

56. Murphy, S.; Sauerwein, B.; Drickamer, H. G.; Schuster, G. B., Spectroscopy of cyanine dyes in fluid solution at atmospheric and high-pressure - the effect of viscosity on nonradiative processes. *Journal of Physical Chemistry* **1994,** *98* (51), 13476-13480.

57. Jia, K.; Wan, Y.; Xia, A.; Li, S.; Gong, F.; Yang, G., Characterization of photoinduced isomerization and intersystem crossing of the cyanine dye Cy3. *Journal of Physical Chemistry a* **2007,** *111* (9), 1593-1597.

58. Chibisov, A. K., Triplet-states of cyanine dyes and reactions of electron-transfer with their participation. *Journal of Photochemistry* **1977,** *6* (3), 199-214.

59. Chibisov, A. K.; Zakharova, G. V.; Gorner, H., Effect of substituents in the polymethine chain on the photoprocesses in indodicarbocyanine dyes. *J. Chem. Soc., Faraday Trans.* **1996,** *92* (24), 4917-4925.

60. Akesson, E.; Sundstrom, V.; Gillbro, T., Isomerization dynamics in solution described by kramers theory with a solvent-dependent activation-energy. *Chemical Physics* **1986,** *106* (2), 269-280.

61. Momicchioli, F.; Baraldi, I.; Berthier, G., Theoretical-study of trans cis photoisomerism in polymethine cyanines. *Chemical Physics* **1988,** *123* (1), 103-112.

62. Dempster, D. N.; Thompson, G. F.; Morrow, T.; Rankin, R., Photochemical characteristics of cyanine dyes .1. 3,3'-diethyloxadicarbocyanine iodide. *Journal of the Chemical Society-Faraday Transactions Ii* **1972,** *68*, 1479-&.

63. Dipaolo, R. E.; Scaffardi, L. B.; Duchowicz, R.; Bilmes, G. M., Photoisomerization dynamics and spectroscopy of the polymethine dye DTCI. *Journal of Physical Chemistry* **1995,** *99* (38), 13796-13799.

64. Duchowicz, R.; Scaffardi, L.; Tocho, J. O., Relaxation processes of singlet excited-state of 3,3'-diethyloxadicarbocyanine iodide (DODCI) photoisomer. *Chemical Physics Letters* **1990,** *170* (5-6), 497-501.

65. Vanderauweraer, M.; Vandenzegel, M.; Boens, N.; Deschryver, F. C.; Willig, F., Photophysics of 2-phenyl-3-indolocarbocyanine dyes. *Journal of Physical Chemistry* **1986,** *90* (6), 1169-1175.

66. Krieg, M.; Redmond, R. W., Photophysical properties of 3,3'-dialkylthiacarbocyanine dyes in homogeneous solution. *Photochemistry and Photobiology* **1993,** *57* (3), 472-479.

67. Velsko, S. P.; Waldeck, D. H.; Fleming, G. R., Breakdown of Kramer theory description of photochemical isomerization and the possible involvement of frequency-dependent friction. *Journal of Chemical Physics* **1983,** *78* (1), 249-258.

68. Kramers, H. A., Brownian motion in a field of force and the diffusion model of chemical reactions. *Physica* **1940,** *7*, 284-304.

69. Tkachenko, N. V., Light absorption in a bulk medium. In *Optical Spectroscopy Methods and Instrumentations*, Elsevier: Amsterdam, 2006; pp 1-5.

70. Lakowicz, J. R., Instrumentation for Fluorescence Spectroscopy. In *Principles of Fluorescence Spectroscopy*, Third ed.; Springer: Baltimore, Maryland, 2006; pp 27-61.

71. Klan, P.; Wirz, J., Light Sources, Filter, and Detectors. In *Photochemistry of Organic Compounds From Concepts to Practice*, Wiley & Sons: United Kingdom, 2010; pp 79-80.

72. Jameson, D. M., Detectors. In *Introduction to Fluorescence*.

73. Lakowicz, J. R., Time-Domain Lifetime Measurements. In *Principles of Fluorescence Spectroscopy*, Third ed.; Springer: Baltimore, Maryland, 2006; pp 98-154.

74. Tkachenko, N. V., Time correlated single photon counting. In *Optical Spectroscopy Methods and Instumentations*, Elsevier: Amsterdam, 2006; pp 151-168.

75. Valeur, B., Appendix: Elimination of polarization effects in the measurement of fluorescence intensity and lifetime. In *Molecular Fluorescence: Principles and Applications*, Wiley-VCH: Weinheim, 2001; pp 196-198.

76. Tkachenko, N. V., Flash-photolysis. In *Optical Spectroscopy Methods and Instrumentations*, Elsevier: Amsterdam, 2006; pp 129-149.

77. Widengren, J.; Mets, U., Conceptual Basis of Fluorescence Correlation Spectroscopy and Related Techniques as Tools in Bioscience. In *Single Molecule Detection in Solution Methods and Applications*, Zander, C.; Enderlein, J.; Keller, R. A., Eds. WILEY-VCH Verlag Berlin GmbH: Berlin, 2002; pp 69-120.

78. Ranjit, S.; Levitus, M., Probing the Interaction Between Fluorophores and DNA Nucleotides by Fluorescence Correlation Spectroscopy and Fluorescence Quenching. *Photochemistry and Photobiology* **2012,** *88* (4), 782-791.

79. Chakraborty, M.; Kuriata, A. M.; Henderson, J. N.; Salvucci, M. E.; Wachter, R. M.; Levitus, M., Protein Oligomerization Monitored by Fluorescence Fluctuation Spectroscopy: Self-Assembly of Rubisco Activase. *Biophysical Journal* **2012,** *103* (5), 949-958.

80. Binder, J. K.; Douma, L. G.; Ranjit, S.; Kanno, D. M.; Chakraborty, M.; Bloom, L. B.; Levitus, M., Intrinsic stability and oligomerization dynamics of DNA processivity clamps. *Nucleic Acids Research* **2014,** *42* (10), 6476-6486.

81. Khimenko, V.; Chibisov, A.; Gorner, H., Effects of alkyl substituents in the polymethine chain on the photoprocesses in thiacarbocyanine dyes. *Journal of Physical Chemistry a* **1997,** *101* (39), 7304-7310.

82. Slavnova, T.; Chibisov, A.; Gorner, H., Photoprocesses of thiacarbocyanine monomers, dimers, and aggregates bound to polyanions. *Journal of Physical Chemistry a* **2002,** *106* (46), 10985-10990.

83. Stennett, E. M. S.; Kodis, G.; Levitus, M., Photobleaching and Blinking of TAMRA Induced by Mn2+. *Chemphyschem* **2012,** *13* (4), 909-913.

84. Murov, S. L.; Hug, G. L.; Carmichael, I., *Handbook of photochemistry*. 2nd ed.; M. Dekker: New York, 1993; p viii, 420 p.

85. Kearns, D. R., Physical and chemical properties of singlet molecular oxygen. *Chemical Reviews* **1971,** *71* (4), 395-&.

86. Byers, G. W.; Gross, S.; Henrichs, P. M., Direct and sensitized photooxidation of cyanine dyes. *Photochemistry and Photobiology* **1976,** *23* (1), 37-43.

87. Barros, T.; Toma, S.; Toma, H.; Bastos, E.; Baptista, M., Polymethine cyanine dyes in beta-cyclodextrin solution: multiple equilibria and chemical oxidation. *Journal of Physical Organic Chemistry* **2010,** *23* (10), 893-903.

88. Vinatier, V.; Guieu, V.; Madaule, Y.; Maturano, M.; Payrastre, C.; Hoffmann, P., Superoxide-induced bleaching of streptocyanine dyes: Application to assay the enzymatic activity of superoxide dismutases. *Analytical Biochemistry* **2010,** *405* (2), 255-259.

89. Clapp, P.; Armitage, B.; OBrien, D., Two-dimensional polymerization of lipid bilayers: Visible-light-sensitized photoinitiation. *Macromolecules* **1997,** *30* (1), 32-41.

90. Renikuntla, B. R.; Rose, H. C.; Eldo, J.; Waggoner, A. S.; Armitage, B. A., Improved photostability and fluorescence properties through polyfluorination of a cyanine dye. *Organic Letters* **2004,** *6* (6), 909-912.

91. Nakagawa, Y.; Hori, H.; Yamamoto, I.; Terada, H., Characteristic bleaching profiles of cyanine dyes depending on active oxygen species in the controlled fenton reaction. *Biological & Pharmaceutical Bulletin* **1993,** *16* (11), 1061-1064.

92. Benesch, R. E.; Benesch, R., Enzymatic removal of oxygen for polarography and related methods. *Science* **1953,** *118* (3068), 447-448.

93. Crawford, D. J.; Hoskins, A. A.; Friedman, L. J.; Gelles, J.; Moore, M. J., Visualizing the splicing of single pre-mRNA molecules in whole cell extract. *Rna-a Publication of the Rna Society* **2008,** *14* (1), 170-179.

94. Englander, S. W.; Calhoun, D. B.; Englander, J. J., Biochemistry without oxygen. *Analytical Biochemistry* **1987,** *161* (2), 300-306.

95. Patil, P. V.; Ballou, D. P., The use of protocatechuate dioxygenase for maintaining anaerobic conditions in biochemical experiments. *Analytical Biochemistry* **2000,** *286* (2), 187-192.

96. Whittaker, J. W., Galactose oxidase. *Copper-Containing Proteins* **2002,** *60*, 1-49.

97. Vogelsang, J.; Steinhauer, C.; Forthmann, C.; Stein, I. H.; Person-Skegro, B.; Cordes, T.; Tinnefeld, P., Make them Blink: Probes for Super-Resolution Microscopy. *Chemphyschem* **2010,** *11* (12), 2475-2490.

98. Stein, I. H.; Capone, S.; Smit, J. H.; Baumann, F.; Cordes, T.; Tinnefeld, P., Linking Single-Molecule Blinking to Chromophore Structure and Redox Potentials. *Chemphyschem* **2012,** *13* (4), 931-937.

99. Vogelsang, J.; Kasper, R.; Steinhauer, C.; Person, B.; Heilemann, M.; Sauer, M.; Tinnefeld, P., A reducing and oxidizing system minimizes photobleaching and blinking of fluorescent dyes. *Angewandte Chemie-International Edition* **2008,** *47* (29), 5465-5469.

100. Korobov, V.; Chibisov, A., Primary processes in photochemistry of rhodamine dyes. *Journal of Photochemistry* **1978,** *9* (5), 411-424.

101. O'Connor, D. V.; Phillips, D., *Time-correlated single photon counting*. Academic Press: London ; Orlando, 1984; p viii, 288 p.

102. Wilkinson, F.; Helman, W. P.; Ross, A. B., Rate constants for the decay and reactions of the lowest electronically excited singlet-state of molecular-oxygen in

solution - an expanded and revised compilation. *Journal of Physical and Chemical Reference Data* **1995,** *24* (2), 663-1021.

103. Frutos, L. M.; Castano, O.; Andres, J. L.; Merchan, M.; Acuna, A. U., A theory of nonvertical triplet energy transfer in terms of accurate potential energy surfaces: The transfer reaction from pi,pi(*) triplet donors to 1,3,5,7-cyclooctatetraene. *Journal of Chemical Physics* **2004,** *120* (3), 1208-1216.

104. Chibisov, A.; Shvedov, S.; Gorner, H., Photosensitized processes in dicarbocyanine dyes induced by energy transfer: delayed fluorescence, trans -> cis isomerization and electron transfer. *Journal of Photochemistry and Photobiology a-Chemistry* **2001,** *141* (1), 39-45.

105. Berland, K.; Shen, G., Excitation saturation in two-photon fluorescence correlation spectroscopy. *Applied Optics* **2003,** *42* (27), 5566-5576.

106. Enderlein, J.; I, G.; Patra, D.; Fitter, J., Art and artefacts of fluorescence correlation spectroscopy. *Current Pharmaceutical Biotechnology* **2004,** *5* (2), 155-161.

107. Nishimura, G.; Kinjo, M., Systematic error in fluorescence correlation measurements identified by a simple saturation model of fluorescence. *Analytical Chemistry* **2004,** *76* (7), 1963-1970.

108. Loman, A.; Dertinger, T.; Koberling, F.; Enderlein, J., Comparison of optical saturation effects in conventional and dual-focus fluorescence correlation spectroscopy. *Chemical Physics Letters* **2008,** *459* (1-6), 18-21.

109. Gregor, I.; Patra, D.; Enderlein, J., Optical saturation in fluorescence correlation spectroscopy under continuous-wave and pulsed excitation. *Chemphyschem* **2005,** *6* (1), 164-170.

110. Hsu, M. T.; Berg, P., Altering specificity of restriction endonuclease - Effect of replacing Mg2+ with Mn2+. *Biochemistry* **1978,** *17* (1), 131-138.

111. Beckman, R. A.; Mildvan, A. S.; Loeb, L. A., On the fidelity of DNA-replication - manganese mutagenesis invitro. *Biochemistry* **1985,** *24* (21), 5810-5817.

112. Yocum, C. F.; Pecoraro, V. L., Recent advances in the understanding of the biological chemistry of manganese. *Current Opinion in Chemical Biology* **1999,** *3* (2), 182-187.

113. Schnabl, J.; Sigel, R. K. O., Controlling ribozyme activity by metal ions. *Current Opinion in Chemical Biology* **2010,** *14* (2), 269-275.

114. Bretschneider, S.; Eggeling, C.; Hell, S. W., Breaking the diffraction barrier in fluorescence microscopy by optical shelving. *Physical Review Letters* **2007,** *98* (21), 4.

115. Hell, S. W., Far-field optical nanoscopy. *Science* **2007,** *316* (5828), 1153-1158.

116. van de Linde, S.; Heilemann, M.; Sauer, M., Live-Cell Super-Resolution Imaging with Synthetic Fluorophores. In *Annual Review of Physical Chemistry, Vol 63*, Johnson, M. A.; Martinez, T. J., Eds. Annual Reviews: Palo Alto, 2012; Vol. 63, pp 519-540.

117. Hwang, H.; Kim, H.; Myong, S., Protein induced fluorescence enhancement as a single molecule assay with short distance sensitivity. *Proceedings of the National Academy of Sciences of the United States of America* **2011,** *108* (18), 7414-7418.

118. Koopmans, W. J. A.; Brehm, A.; Logie, C.; Schmidt, T.; van Noort, J., Single-pair FRET microscopy reveals mononucleosome dynamics. *Journal of Fluorescence* **2007,** *17* (6), 785-795.

119. Forster, T., *Zwischenmolekulare energiewanderung und fluoreszenz. *Annalen Der Physik* **1948,** *2* (1-2), 55-75.

120. Stryer, L., Fluorescence energy-transfer as a spectroscopic ruler. *Annual Review of Biochemistry* **1978,** *47*, 819-846.

121. Myong, S.; Cui, S.; Cornish, P. V.; Kirchhofer, A.; Gack, M. U.; Jung, J. U.; Hopfner, K. P.; Ha, T., Cytosolic Viral Sensor RIG-I Is a 5 '-Triphosphate-Dependent Translocase on Double-Stranded RNA. *Science* **2009,** *323* (5917), 1070-1074.

122. Qiu, Y.; Antony, E.; Doganay, S.; Koh, H. R.; Lohman, T. M.; Myong, S., Srs2 prevents Rad51 filament formation by repetitive motion on DNA. *Nature Communications* **2013,** *4*.

123. Hwang, H.; Buncher, N.; Opresko, P. L.; Myong, S., POT1-TPP1 Regulates Telomeric Overhang Structural Dynamics. *Structure* **2012,** *20* (11), 1872-1880.

124. Bruns, A. M.; Pollpeter, D.; Hadizadeh, N.; Myong, S.; Marko, J. F.; Horvath, C. M., ATP Hydrolysis Enhances RNA Recognition and Antiviral Signal Transduction by the Innate Immune Sensor, Laboratory of Genetics and Physiology 2 (LGP2). *Journal of Biological Chemistry* **2013,** *288* (2), 938-946.

125. Koh, H. R.; Kidwell, M. A.; Ragunathan, K.; Doudna, J. A.; Myong, S., ATP-independent diffusion of double-stranded RNA binding proteins. *Proceedings of the National Academy of Sciences of the United States of America* **2013,** *110* (1), 151-156.

126. Park, J.; Myong, S.; Niedziela-Majka, A.; Lee, K. S.; Yu, J.; Lohman, T. M.; Ha, T., PcrA Helicase Dismantles RecA Filaments by Reeling in DNA in Uniform Steps. *Cell* **2010,** *142* (4), 544-555.

127. Hwang, H.; Myong, S., Protein induced fluorescence enhancement (PIFE) for probing protein-nucleic acid interactions. *Chemical Society Reviews* **2014,** *43* (4), 1221-1229.

128. Qiu, Y. P.; Myong, S., Single Molecule Detection of One, Two and Multiplex Proteins Involved in DNA/RNA Transaction. *Cellular and Molecular Bioengineering* **2011,** *4* (2), 125-137.

129. Fischer, C. J.; Maluf, N. K.; Lohman, T. M., Mechanism of ATP-dependent translocation of E. coli UvrD monomers along single-stranded DNA. *Journal of Molecular Biology* **2004,** *344* (5), 1287-1309.

130. Luo, G.; Wang, M.; Konigsberg, W. H.; Xie, X. S., Single-molecule and ensemble fluorescence assays for a functionally important conformational change in T7 DNA polymerase. *Proceedings of the National Academy of Sciences of the United States of America* **2007,** *104* (31), 12610-12615.

131. Sorokina, M.; Koh, H.-R.; Patel, S. S.; Ha, T., Fluorescent Lifetime Trajectories of a Single Fluorophore Reveal Reaction Intermediates During Transcription Initiation. *Journal of the American Chemical Society* **2009,** *131* (28), 9630-9631.

132. Hwang, W.; Arluison, V.; Hohng, S., Dynamic competition of DsrA and rpoS fragments for the proximal binding site of Hfq as a means for efficient annealing. *Nucleic Acids Research* **2011,** *39* (12), 5131-5139.

133. Markiewicz, R. P.; Vrtis, K. B.; Rueda, D.; Romano, L. J., Single-molecule microscopy reveals new insights into nucleotide selection by DNA polymerase I. *Nucleic Acids Research* **2012,** *40* (16), 7975-7984.

134. Galletto, R.; Tomko, E. J., Translocation of Saccharomyces cerevisiae Pif1 helicase monomers on single-stranded DNA. *Nucleic Acids Research* **2013,** *41* (8), 4613-4627.

135. Marko, R. A.; Liu, H.-W.; Ablenas, C. J.; Ehteshami, M.; Goette, M.; Cosa, G., Binding Kinetics and Affinities of Heterodimeric versus Homodimeric HIV-1 Reverse Transcriptase on DNA-DNA Substrates at the Single-Molecule Level. *Journal of Physical Chemistry B* **2013,** *117* (16), 4560-4567.

136. Maxwell, B. A.; Suo, Z., Single-molecule Investigation of Substrate Binding Kinetics and Protein Conformational Dynamics of a B-family Replicative DNA Polymerase. *Journal of Biological Chemistry* **2013,** *288* (16), 11590-11600.

137. Marc, D.; Barbachou, S.; Soubieux, D., The RNA-binding domain of influenzavirus non-structural protein-1 cooperatively binds to virus-specific RNA sequences in a structure-dependent manner. *Nucleic Acids Research* **2013,** *41* (1), 434-449.

138. Vrtis, K. B.; Markiewicz, R. P.; Romano, L. J.; Rueda, D., Carcinogenic adducts induce distinct DNA polymerase binding orientations. *Nucleic Acids Research* **2013,** *41* (16), 7843-7853.

139. Zawadzki, P.; May, P. F. J.; Baker, R. A.; Pinkney, J. N. M.; Kapanidis, A. N.; Sherratt, D. J.; Arciszewska, L. K., Conformational transitions during FtsK translocase activation of individual XerCD-dif recombination complexes. *Proceedings of the National Academy of Sciences of the United States of America* **2013,** *110* (43), 17302-17307.

140. Craggs, T. D.; Hutton, R. D.; Brenlla, A.; White, M. F.; Penedo, J. C., Single-molecule characterization of Fen1 and Fen1/PCNA complexes acting on flap substrates. *Nucleic Acids Research* **2014,** *42* (3), 1857-1872.

141. Luo, Y.; North, J. A.; Rose, S. D.; Poirier, M. G., Nucleosomes accelerate transcription factor dissociation. *Nucleic Acids Research* **2014,** *42* (5), 3017-3027.

142. Ollis, D. L.; Brick, P.; Hamlin, R.; Xuong, N. G.; Steitz, T. A., Structure of large fragment of Escherichia-coli DNA-polymerase-I complexed with DTMP. *Nature* **1985,** *313* (6005), 762-766.

143. Joyce, C. M.; Steitz, T. A., DNA-polymerase-I - from crystal-structure to function via genetics. *Trends in Biochemical Sciences* **1987,** *12* (8), 288-292.

144. Derbyshire, V.; Freemont, P. S.; Sanderson, M. R.; Beese, L.; Friedman, J. M.; Joyce, C. M.; Steitz, T. A., Genetic and crystallographic studies of the 3',5'-exonucleolytic site of DNA-polymerase-I. *Science* **1988,** *240* (4849), 199-201.

145. Freemont, P. S.; Friedman, J. M.; Beese, L. S.; Sanderson, M. R.; Steitz, T. A., Cocrystal structure of an editing complex of Klenow fragment with DNA. *Proceedings of the National Academy of Sciences of the United States of America* **1988,** *85* (23), 8924-8928.

146. Guest, C. R.; Hochstrasser, R. A.; Dupuy, C. G.; Allen, D. J.; Benkovic, S. J.; Millar, D. P., Interaction of DNA with the Klenow fragment of DNA-polymerase-I studied by time-resolved fluorescence spectroscopy. *Biochemistry* **1991,** *30* (36), 8759-8770.

147. Stennett, E. M. S. Photophysical Properties and Applications of Fluorescent Probes in Studying DNA Conformation and Dynamics. Arizona State University, ProQuest Dissertations & Theses Global, 2015.

148. Stennett, E. M. S.; Ciuba, M. A.; Lin, S.; Levitus, M., Demystifying PIFE: The Photophysics Behind the Protein-Induced Fluorescence Enhancement Phenomenon in Cy3. *Journal of Physical Chemistry Letters* **2015,** *6* (10), 1819-1823.

149. Carver, T. E.; Hochstrasser, R. A.; Millar, D. P., Proofreading DNA - recognition of aberrant DNA termini by the Klenow fragment of DNA-polymerase-I. *Proceedings of the National Academy of Sciences of the United States of America* **1994,** *91* (22), 10670-10674.

150. Onodera, M.; Shiokawa, H.; Takagi, T., Fluorescent-probes for antibody active-sites .1. Production of antibodies specific to N-methyl-2-anilinonaphthalene-6-sulfonyl group in rabbits and some fluorescent properties of hapten bound to antibodies. *Journal of Biochemistry* **1976,** *79* (1), 195-202.

151. Kuchta, R. D.; Mizrahi, V.; Benkovic, P. A.; Johnson, K. A.; Benkovic, S. J., Kinetic mechanism of DNA-polymerase-I (Klenow). *Biochemistry* **1987,** *26* (25), 8410-8417.

152. Datta, K.; Johnson, N. P.; von Hippel, P. H., DNA conformational changes at the primer-template junction regulate the fidelity of replication by DNA polymerase. *Proceedings of the National Academy of Sciences of the United States of America* **2010,** *107* (42), 17980-17985.

153. Datta, K.; Johnson, N. P.; LiCata, V. J.; von Hippel, P. H., Local Conformations and Competitive Binding Affinities of Single- and Double-stranded Primer-Template DNA at the Polymerization and Editing Active Sites of DNA Polymerases. *Journal of Biological Chemistry* **2009,** *284* (25), 17180-17193.

154. Tsoi, P. Y.; Zhang, X. M.; Sui, S. F.; Yang, M. S., Effects of DNA mismatches on binding affinity and kinetics of polymerase-DNA complexes as revealed by surface plasmon resonance biosensor. *Analyst* **2003,** *128* (9), 1169-1174.

155. Bilmes, G. M.; Tocho, J. O.; Braslavsky, S. E., Laser-induced optoacoustic studies of the photoisomerization of the laser-dye 3,3'-diethyloxadicarbocyanine iodide (DODCI). *Chemical Physics Letters* **1987,** *134* (4), 335-340.

156. Bilmes, G. M.; Tocho, J. O.; Braslavsky, S. E., Spectrum, energy content, and relaxation mechanism of the photoisomer of the laser-dye 3,3'-diethyloxadicarbocyanine iodide - laser-induced optoacoustic studies. *Journal of Physical Chemistry* **1988,** *92* (21), 5958-5962.

157. Hwang, H.; Myong, S., Characterization of Single Molecule Protein Induced Fluorescence Enhancement (PIFE) as an Alternative to SmFRET. *Biophysical Journal* **2010,** *98* (3), 590A-590A.

158. Czerney, P.; Lehmann, F.; Wenzel, M.; Buschmann, V.; Dietrich, A.; Mohr, G. J., Tailor-made dyes for fluorescence correlation spectroscopy (FCS). *Biological Chemistry* **2001,** *382* (3), 495-498.

159. Dyomics-GmbH Red Excitation. http://www.dyomics.com/en/products/red-excitation/dy-630.html (accessed February 2017).

160. Buschmann, V.; Weston, K. D.; Sauer, M., Spectroscopic study and evaluation of red-absorbing fluorescent dyes. *Bioconjugate Chemistry* **2003,** *14* (1), 195-204.

161. Cohen, B.; Alvarez, C. M.; Carmona, N. A.; Organero, J. A.; Douhal, A., Single molecule photobehavior of a chromophore interacting with silica-based nanomaterials. *Physical Chemistry Chemical Physics* **2011,** *13* (5), 1819-1826.

162. Cohen, B.; Martin, C.; Iyer, S. K.; Wiesner, U.; Douhal, A., Single Dye Molecule Behavior in Fluorescent Core-Shell Silica Nanoparticles. *Chemistry of Materials* **2012,** *24* (2), 361-372.

163. Berlier, J. E.; Rothe, A.; Buller, G.; Bradford, J.; Gray, D. R.; Filanoski, B. J.; Telford, W. G.; Yue, S.; Liu, J. X.; Cheung, C. Y.; Chang, W.; Hirsch, J. D.; Beechem, J. M.; Haugland, R. P., Quantitative comparison of long-wavelength Alexa Fluor dyes to Cy dyes: Fluorescence of the dyes and their bioconjugates. *Journal of Histochemistry & Cytochemistry* **2003,** *51* (12), 1699-1712.

164. Schneider, E.; Mayer, M.; Ziemek, R.; Li, L.; Hutzler, C.; Bernhardt, G.; Buschauer, A., A simple and powerful flow cytometric method for the simultaneous determination of multiple parameters at g protein-coupled receptor subtypes. *Chembiochem* **2006,** *7* (9), 1400-1409.

165. Volkmer, T.; Becker, C.; Prodohl, A.; Finger, C.; Schneider, D., Assembly of a transmembrane b-Type cytochrome is mainly driven by transmembrane helix interactions. *Biochimica Et Biophysica Acta-Biomembranes* **2006,** *1758* (11), 1815-1822.

166. Jung, S.; Angerer, B.; Loscher, F.; Niehren, S.; Winkle, J.; Seeger, S., Biotin-functionalized cellulose-based monolayers as sensitive interfaces for the detection of single molecules. *Chembiochem* **2006,** *7* (6), 900-903.

167. Glasenapp, C.; Monch, W.; Krause, H.; Zappe, H., Biochip reader with dynamic holographic excitation and hyperspectral fluorescence detection. *Journal of Biomedical Optics* **2007,** *12* (1), 8.

168. Behrendt, J. M.; Nagel, D.; Chundoo, E.; Alexander, L. M.; Dupin, D.; Hine, A. V.; Bradley, M.; Sutherland, A. J., Synthesis and Characterization of Dual-Functionalized Core-Shell Fluorescent Microspheres for Bioconjugation and Cellular Delivery. *Plos One* **2013,** *8* (3).

169. Voss, S.; Zhao, L.; Chen, X.; Gerhard, F.; Wu, Y.-W., Generation of an intramolecular three-color fluorescence resonance energy transfer probe by site-specific protein labeling. *Journal of Peptide Science* **2014,** *20* (2), 115-120.

170. Luschtinetz, F.; Dosche, C.; Kumke, M. U., Influence of Streptavidin on the Absorption and Fluorescence Properties of Cyanine Dyes. *Bioconjugate Chemistry* **2009,** *20* (3), 576-582.

171. Marme, N.; Friedrich, A.; Denapaite, D.; Hakenbeck, R.; Knemeyer, J. P., Single nucleotide polymorphism analysis using different colored dye dimer probes. *Chemical Physics Letters* **2006,** *428* (4-6), 440-445.

172. Jiang, X.; Weise, S.; Hafner, M.; Rocker, C.; Zhang, F.; Parak, W. J.; Nienhaus, G. U., Quantitative analysis of the protein corona on FePt nanoparticles formed by transferrin binding. *Journal of the Royal Society Interface* **2010,** *7*, S5-S13.

173. Rurack, K., Fluorescence Quantum Yields: Methods of Determination and Standards. In *Standardization and Quality Assurance in Fluorescence Measurements I*, Resch-Genger, U., Ed. Springer-Verlag Berlin Heidelberg: Berlin, 2008; pp 101-145.

174. El-Sagheer, A. H.; Brown, T., Click chemistry with DNA. *Chemical Society Reviews* **2010,** *39* (4), 1388-1405.

175. Nardone, G.; George, J.; Chirikjian, J. G., Sequence-specific BamHI methylase - purification and characterization. *Journal of Biological Chemistry* **1984,** *259* (16), 357-362.

176. Newman, M.; Strzelecka, T.; Dorner, L. F.; Schildkraut, I.; Aggarwal, A. K., Structure of restriction-endonuclease BamHI phased at 1.95-Angstrom resolution by MAD analysis. *Structure* **1994,** *2* (5), 439-452.

177. Newman, M.; Strzelecka, T.; Dorner, L. F.; Schildkraut, I.; Aggarwal, A. K., Structure of Bam-HI endonuclease bound to DNA - partial folding and unfolding on DNA-binding. *Science* **1995,** *269* (5224), 656-663.

178. Viadiu, H.; Aggarwal, A. K., The role of metals in catalysis by the restriction endonuclease BamHI. *Nature Structural Biology* **1998,** *5* (10), 910-916.

179. Viadiu, H.; Aggarwal, A. K., Structure of BamHI bound to nonspecific DNA: A model for DNA sliding. *Molecular Cell* **2000,** *5* (5), 889-895.

180. Riccelli, P. V.; Vallone, P. M.; Kashin, I.; Faldasz, B. D.; Lane, N. J.; Benight, A. S., Thermodynamic, spectroscopic, and equilibrium binding studies of DNA sequence context effects in six 22-base pair deoxyoligonucleotides. *Biochemistry* **1999,** *38* (34), 11197-11208.

181. Bochkarev, A.; Pfuetzner, R. A.; Edwards, A. M.; Frappier, L., Structure of the single-stranded-DNA-binding domain of replication protein A bound to DNA. *Nature* **1997,** *385* (6612), 176-181.

182. de Laat, W. L.; Appeldoorn, E.; Sugasawa, K.; Weterings, E.; Jaspers, N. G. J.; Hoeijmakers, J. H. J., DNA-binding polarity of human replication protein A positions nucleases in nucleotide excision repair. *Genes & Development* **1998,** *12* (16), 2598-2609.

183. Iftode, C.; Borowiec, J. A., 5 ' -> 3 ' molecular polarity of human replication protein A (hRPA) binding to pseudo-origin DNA substrates. *Biochemistry* **2000,** *39* (39), 11970-11981.

184. Kolpashchikov, D. M.; Khodyreva, S. N.; Khlimankov, D. Y.; Wold, M. S.; Favre, A.; Lavrik, O. I., Polarity of human replication protein A binding to DNA. *Nucleic Acids Research* **2001,** *29* (2), 373-379.

185. Nguyen, B.; Sokoloski, J.; Galletto, R.; Elson, E. L.; Wold, M. S.; Lohman, T. M., Diffusion of Human Replication Protein A along Single-Stranded DNA. *Journal of Molecular Biology* **2014,** *426* (19), 3246-3261.

186. Zhao, R.; Rueda, D., RNA folding dynamics by single-molecule fluorescence resonance energy transfer. *Methods* **2009,** *49* (2), 112-117.

187. Lamichhane, R.; Solem, A.; Black, W.; Rueda, D., Single-molecule FRET of protein-nucleic acid and protein-protein complexes: Surface passivation and immobilization. *Methods* **2010,** *52* (2), 192-200.

188. Mattheyses, A. L.; Simon, S. M.; Rappoport, J. Z., Imaging with total internal reflection fluorescence microscopy for the cell biologist. *Journal of Cell Science* **2010,** *123* (21), 3621-3628.

APPENDIX I

PIFE WITH BAMHI AND HRPA AND ASSOCIATED ANISOTROPY ANALYSIS

The concept of associated anisotropy is used to describe a heterogeneous probe population. As described briefly in Chapter 3, an environmentally sensitive probe located in different environments within a sample will display a multi-exponential anisotropy decay; the origin of the decay times is not the probe's complex motions, e.g. the probe rotating on a rotating biomolecule, but rather the time-varying intensity of the probe in more than one environment, each of which alters the photophysical properties of the probe. Considering a probe in multiple dissimilar environments the overall anisotropy decay is described by Equation AI.1, where $r_m(t)$ represents the probe's

$$r(t) = \sum_m f_m(t) r_m(t) \tag{AI.1}$$

anisotropy in the respective environment and $f_m(t)$ represents the fractional intensity coming from that environment. The fractional intensity is calculated from the intensity decays, and determines how long each probe environment contributes to the anisotropy (Equation AI.2). Here, τ_m refers to the probe's lifetime in the *m*-th environment and α_m is the amplitude of the *m*-th environment at time zero. The overall anisotropy at any time

$$f_m(t) = \frac{\alpha_m \exp(-t/\tau_m)}{\sum_m \alpha_m \exp(-t/\tau_m)} \tag{AI.2}$$

is an intensity-weighted average of the individual anisotropies at any time from each environment. For a probe in two photophysically distinct environments the anisotropy decay is described by Equation AI.3, below. This clearly shows that the lifetimes from

$$r(t) = \frac{\alpha_1 \exp(-t/\tau_1)}{\sum_m \alpha_m \exp(-t/\tau_m)} r_1(t) + \frac{\alpha_2 \exp(-t/\tau_2)}{\sum_m \alpha_m \exp(-t/\tau_m)} r_2(t) \tag{AI.3}$$

both environments have an impact on how much contribution each environment has to

the overall anisotropy decay.

Put simply, the equations describing associated anisotropies are linear combinations of the individual anisotropies present in the sample. This idea can be expanded to lifetimes: a complex, multi-exponential lifetime observed for a sample with a heterogenous dye population can be expressed as a linear combination of lifetimes of the individual components. Illustrating this concept are the lifetime measurements of BamHI binding to dsDNA.

BamHI is a homodimeric restriction enzyme which binds and cuts double stranded DNA at the recognition sequence GGATCC, requiring only magnesium (Mg^{2+}) as a cofactor[175-179]. This enzyme was originally used for the PIFE project (Chapter 3) since Myong and co-workers also used it for their PIFE measurements[117], however large DNA (and protein) concentrations were required for the transient absorption experiments. Adding BamHI to the sample directly from the commercial stock (which is stored in 50% glycrol) meant that amounts of glycerol up to 15% would be present in the solution and photosiomerization would be restricted not only by the protein, but also by the glycerol. This would complicate data analysis. Elana Stennett performed dialysis, however, most of the protein was lost. Hence, we were unable to obtain a source of BamHI in the necessary micromolar concentrations and in the appropriate buffer forcing us to change to work with the Klenow fragment. Nevertheless, many lifetime and anisotropy measurements had already been collected with the DNA-BamHI system and those results are shown here.

The DNA sample used was 40-bp fully double stranded with Cy3 attached to the 5’ end of the strand with the recognition sequence; the dye and the recognition sequence

are separated by one base pair (labeled strand shown below with recognition sequence in bold). This is the same DNA sample used by Myong and co-workers[117]. This sample is referred to as the 1-bp sample. The complementary strand follows standard Watson-Crick base-pairing rules and is not shown here. A 10-bp sample was also used (where there are 10 bases separating Cy3 from the recognition sequence) to serve as a PIFE control. BamHI was purchased from New England Biolabs (Ipswitch, MA) catalog # R0136.

5'-Cy3-T**GG-ATC-C**AT-AGT-AGC-GTA-GCG-TAG-CGT-AGC-GTA-GCG-TAG-C-3'

5'-Cy3-CGT-ATA-TAC-G**GG-ATC-C**TA-GCG-TAG-CGT-AGC-GTA-GCG-TAG-G-3'

Following lifetime results from the Myong lab[117] the first experiments done with this protein system were lifetime measurements. Figure AI.1 (left panel) shows lifetime results from a BamHI titration of the 1-bp sample. The lifetime of the 1-bp dsDNA sample (black) is for the pure DNA sample only, while the +30 μL trace (green) is the

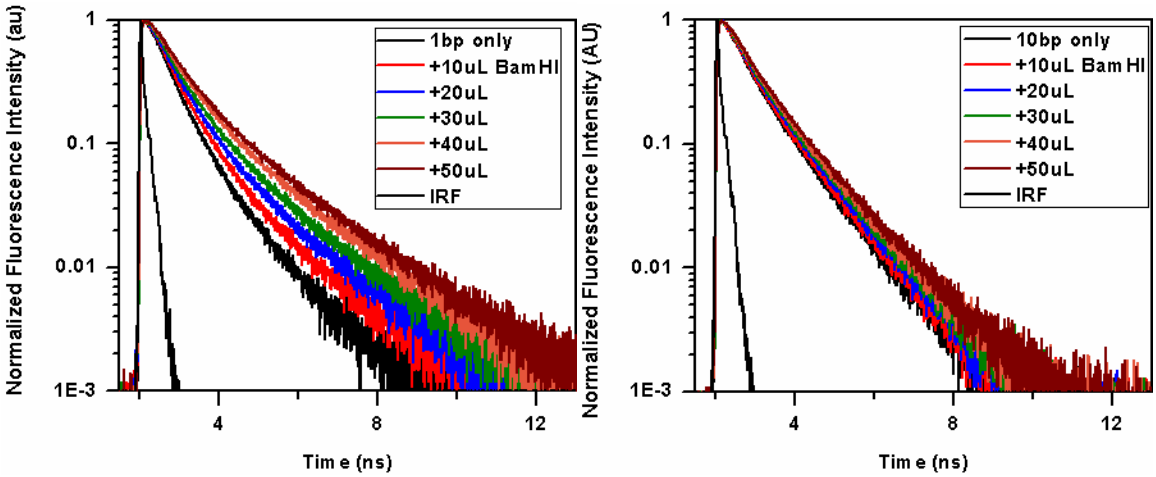


Figure AI.1: Lifetime Results for the 1-bp (left) and 10-bp (right) Samples. BamHI was added in microliter amounts (this indicates how much of the commercial stock was added to the DNA samples which started out at 120 μL in volume at 0.8 μM).

lifetime of the 1-bp dsDNA with an equimolar amount of BamHI (a one-to-one ratio).

More BamHI was added to ensure that each dsDNA in the sample would be bound to the protein. The right panel shows the lifetime results for the 10-bp sample. Lifetimes were fit globally using ASUFit; results for both samples are shown in Tables AI.1 and AI.2. The intensity decays require three lifetimes for random residuals; they have a very short 80 ps lifetime, a 600 ps lifetime that can be described as the "dye on DNA" lifetime, and a longer lifetime. For the 1-bp sample that long lifetime is 1.76 ns, while for the 10-bp it

Table AI.1: Global Fit Results for the 1-bp Sample

sample	τ_1 = 0.08 ns	τ_2 = 0.60 ns	τ_3 = 1.76 ns
1bp only	0.048	0.041	0.002
+10uL BamHI	0.041	0.041	0.005
+20uL	0.038	0.039	0.007
+30uL	0.035	0.037	0.010
+40uL	0.032	0.035	0.014
+50uL	0.030	0.032	0.017

Table AI.1: Global fit results for the 1-bp sample. The variation of the amplitudes for each of the three lifetimes is seen.

is 1.28 ns. For the 1-bp sample the amplitudes of the first (80 ps) and second (600 ps) lifetimes decrease as BamHI is added, while the amplitude of the long lifetime increases. This trend is the same for the 10-bp sample. The increase in the long lifetime is responsible for the overall increase in the lifetimes with BamHI binding. The fact that the lifetime of the 10-bp sample does not increase as dramatically as the 1-bp sample is due to the distance between Cy3 and the recognition sequence. The "bulk" of the protein binds much closer to Cy3 in the 1-bp sample and hinders the dye's ability to photoisomerize much more than in the 10-bp sample. Thus, there is greater fluorescence enhancement in the 1-bp sample.

A standard global fit of these lifetimes is not the only effective way to analyze

Table AI.2: Global Fit Results for the 10-bp Sample

sample	τ_1 = 0.08 ns	τ_2 = 0.60 ns	τ_3 = 1.28 ns
10bp only	0.045	0.032	0.011
+10uL BamHI	0.043	0.031	0.013
+20uL	0.041	0.030	0.015
+30uL	0.040	0.029	0.016
+40uL	0.038	0.028	0.018
+50uL	0.036	0.026	0.020

Table AI.2: Global fit results for the 10-bp sample. The variation of the amplitudes for each of the three lifetimes is seen.

this data, as stated above. As long as data is available for the pure environments the probe experiences, the lifetime of any mixture of environments can be represented as a linear combination of the pure environments' data. In this context pure refers to samples which have homogenous probe populations. For example, the 1-bp only sample provided a measurement of the Cy3 lifetime only on dsDNA, while the 1-bp + 50 uL BamHI sample provided a measurement of the Cy3 lifetime when it's surrounded by the "bulk" of the protein. Since the protein-to-DNA ratio in that sample is greater than one-to-one it can be considered a pure sample (the concentrations used for measurement are above the K_d of the protein so each BamHI is expected to bind). The intensity decays of samples with both populations are described by Equation AI.4, where $I_{DNA}(t)$ and $I_{Bam}(t)$ are the experimental intensity decays in the respective environments, $I(t)$ is the overall intensity decay, and γ is the fraction of the DNA population not bound to BamHI (free DNA).

$$I(t) = \gamma I_{DNA}(t) + (1-\gamma) I_{Bam}(t) \qquad \text{(AI.4)}$$

An excel spreadsheet was used to choose the value of γ such that the residuals between the experimentally observed intensity decays and the calculated intensity decays (from Equation AI.4) were minimized. The resulting γ values are in Table AI.3, below,

and Figure AI.2 shows the results of this fit; the blue traces are the calculated intensity decays, which are compared to the experimentally measured decays, in teal. This linear combination method produces good overlap with experimental data. The same fitting method was used for the 10-bp samples; see Table AI.3 for the γ values and see Figures AI.2, AI.3, AI.4, and AI.5 for the fit results.

Table AI.3: Linear Combination of Lifetimes

1-bp sample			10-bp sample		
Sample	γ	1 - γ	Sample	γ	1 - γ
+10 µL	0.80	0.20	+10 µL	0.69	0.32
+20 µL	0.62	0.38	+20 µL	0.56	0.44
+30 µL	0.47	0.53	+30 µL	0.67	0.33
+40 µL	0.10	0.90	+40 µL	0.42	0.58

Table AI.3: Linear Combination of Lifetimes. Calculated values of γ are shown for the 1-bp and 10-bp samples.

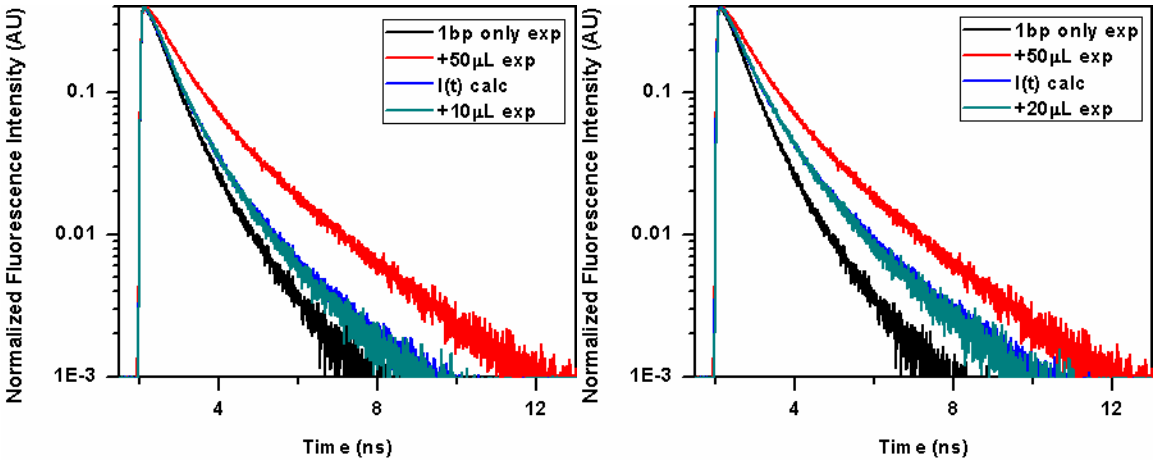


Figure AI.2: Calculated and Experimental Lifetimes Compared for 1-bp Sample. The black and red traces represent the experimental measurements for the pure samples. The teal trace is the experimental measurement for the sample in question; the blue trace is the calculated intensity decay for the sample in question.

The anisotropy of the 1-bp and 10-bp samples was also measured and gave the following results (Figure AI.6). These results clearly show that BamHI is binding to the

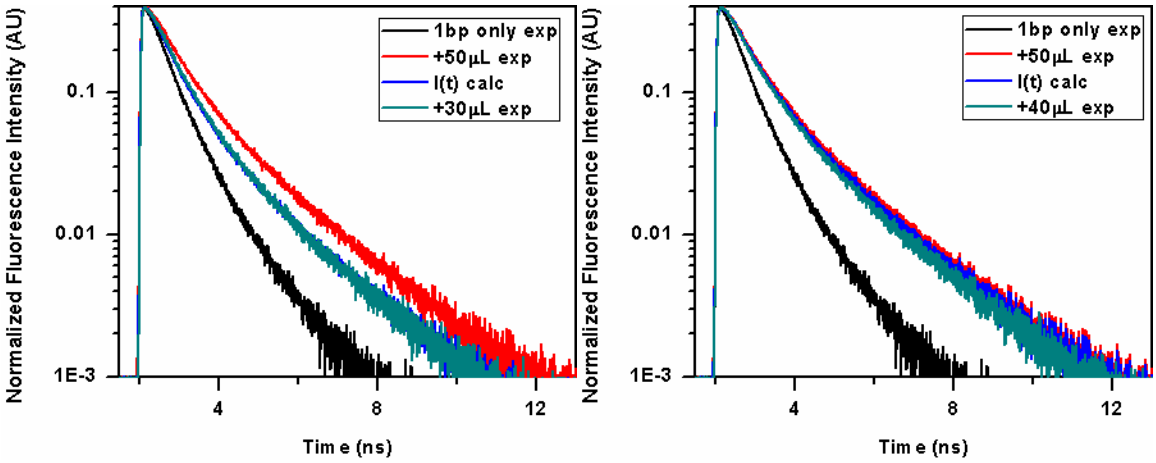


Figure AI.3: Calculated and Experimental Lifetimes Compared for 1-bp Sample

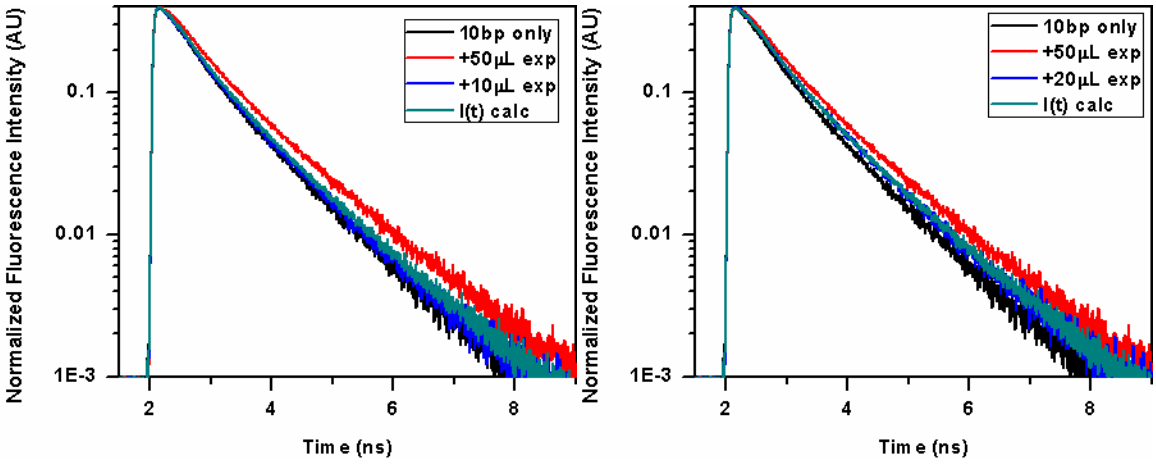


Figure AI.4: Calculated and Experimental Lifetimes Compared for 10-bp Sample

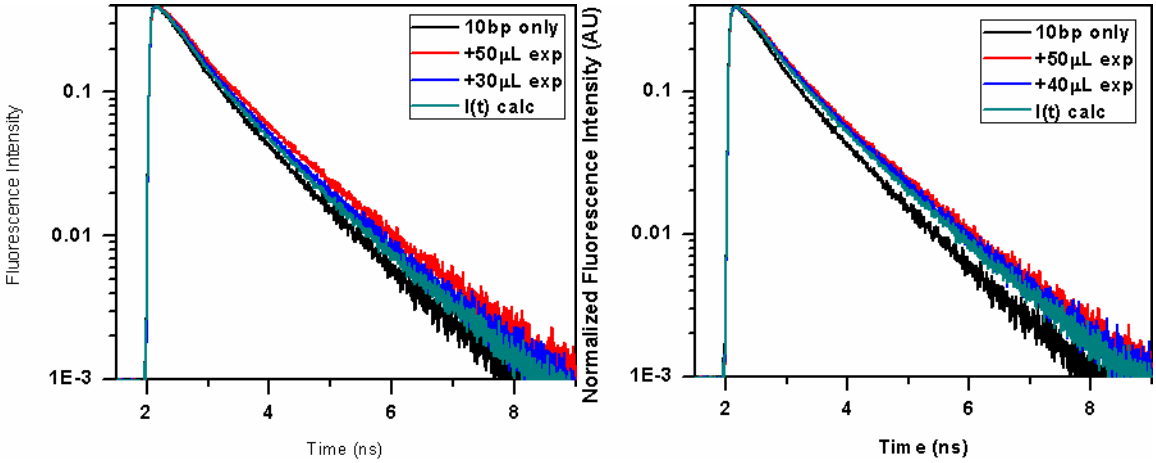


Figure AI.5: Calculated and Experimental Lifetimes Compared for 10-bp Sample

dsDNA as the anisotropy increases with successive additions of the protein. However, the anisotropy increase varies for the two dsDNA samples. There is a greater increase in anisotropy for 1-bp DNA rather than the 10-bp dsDNA sample. This is due to the differing location of the recognition sequence; in the 1-bp sample the recognition sequence is located only 1 base pair away from the Cy3, hence, the dye is forced to interact more with the protein. As more BamHI is added to the solution, a greater fraction of dye is in a protein environment and the characteristic anisotropy of such an

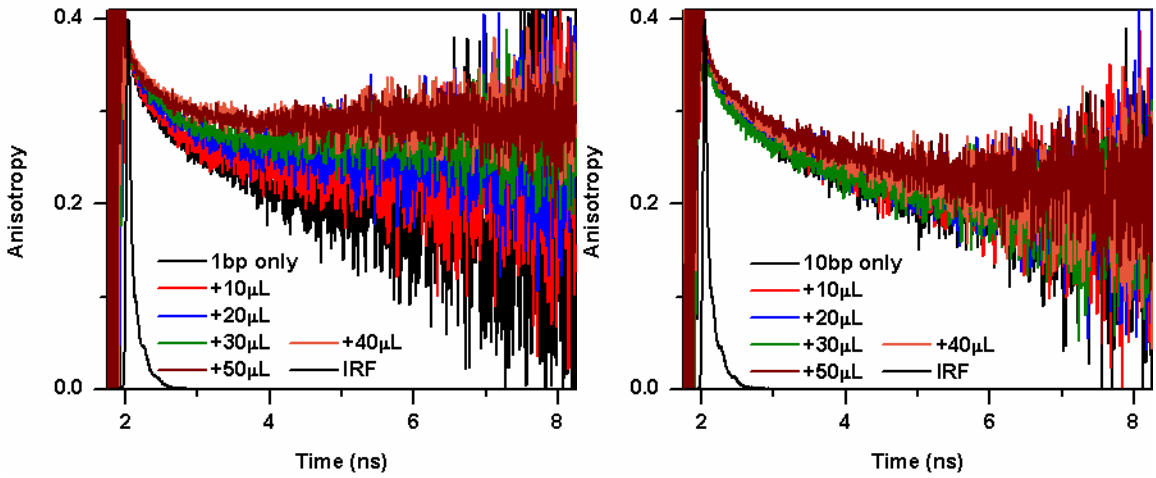


Figure AI.6: Anisotropy Results for the 1-bp (left) and 10-bp (right) Samples.

environment predominates. For the 10-bp samples the dye is 10 base pairs from the recognition sequence; the 10-bp sample shows an increase in anisotropy (Figure AI.6, right panel) with BamHI addition, however, the anisotropy never approaches the high long-time value observed for the 1-bp sample (left panel, brown trace). This data supports the conclusion that the closer a protein is to Cy3 the more the dye's photophysical behavior will be affected. This data suggests the 1-bp sample experiences more PIFE than the 10-bp samples; the same conclusion was reached by Myong and co-workers[117]. The only discrepancy in these samples that ought be mentioned is the

differing anisotropy for the DNA only samples (1-bp only and 10-bp only, black traces). This is due to the different DNA sequences used for the two samples (see above). The 1-bp sequence begins with TGG-ATC, while the 10-bp sequence begins with CGT-ATA; changing the identity of the nearby bases can affect the photophysical properties of Cy3 significantly[54].

Fitting of the anisotropy decays was attempted with Equation AI.5 where r_{01} and r_{02} represent the time zero anisotropy value of Cy3 on DNA alone and with BamHI, respectively, and θ_1 and θ_2 are the corresponding rotational correlational times. The third term accounts for an r_∞ value, meaning an anisotropy value at long times, for samples

$$r(t) = r_{01}\exp(-t/\theta_1) + r_{02}\exp(-t/\theta_2) + (0.38 - r_{01} - r_{02}) \qquad \text{(AI.5)}$$

whose fluorescence does not depolarize on the timescale of the measurement. Data for each sample set was fit globally with four free parameters to determine the correlation times, which were then fixed and the data refit globally to determine the time-zero anisotropy values. The initial fit provided a correlation time of 0.36 ns for the dye's rapid motion and a longer time for the DNA-protein motion (times between 3.6 and 15 ns were used for the second global fit). However, both time-zero anisotropies decreased as BamHI increased in the samples, no matter how long the second correlation time. Furthermore, when a set of parameters fit the BamHI measurements it was not able to satisfactorily fit the DNA only measurements as well.

Applying the theory of associated anisotropy proved to be successful in fitting this data. The anisotropy data was also fit globally in the sense that the lifetimes (fit to Equation AI.1) and the anisotropies (which were fit to Equation AI.3) were fit

simultaneously with the single parameter α_m (from Equations AI.2 and AI.3). The parameter γ, from Equation AI.4, is formally α_m. As for the lifetimes, the goal is to use the DNA only and the +50μL BamHI samples to calculate the anisotropy decay which minimizes the residuals from the experimentally observed decay. The γ values reported in Table AI.3 are actually the α_m values from this lifetime and anisotropy global fit (the Excel spreadsheet was set up to minimize both sets of residuals). Figures AI.7 and AI.8, below, show the results of this fitting procedure for the 1-bp samples; the 10-bp fitting results are in Figure AI.9 and AI.10. In Figures AI.9 and AI.10 the pure sample traces (of the 10-bp only and +50μL BamHI) have been omitted for clarity. With the exception of the +30μL BamHI 10-bp sample (Figure AI.10) the associated anisotropy theory reproduced the experimental data perfectly; the poor match for that sample may be the reason why the α_m value does not follow the trend shown in Table AI.4.

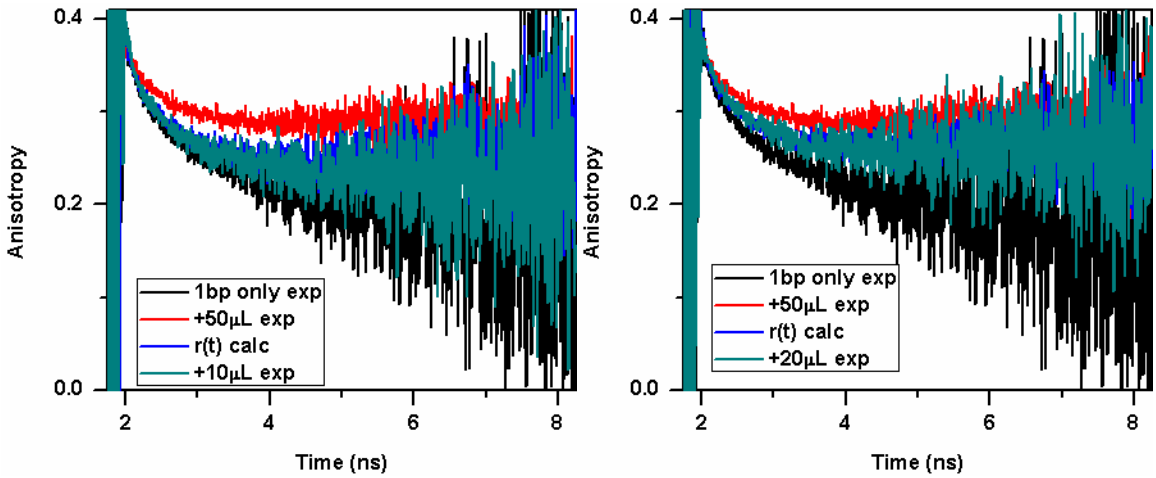


Figure AI.7: Calculated and Experimental Anisotropies Compared for 1-bp Sample. The black and red traces represent the experimental measurements for the pure samples. The teal trace is the experimental measurement for the sample in question; the blue traces are the calculated anisotropy for the sample in question.

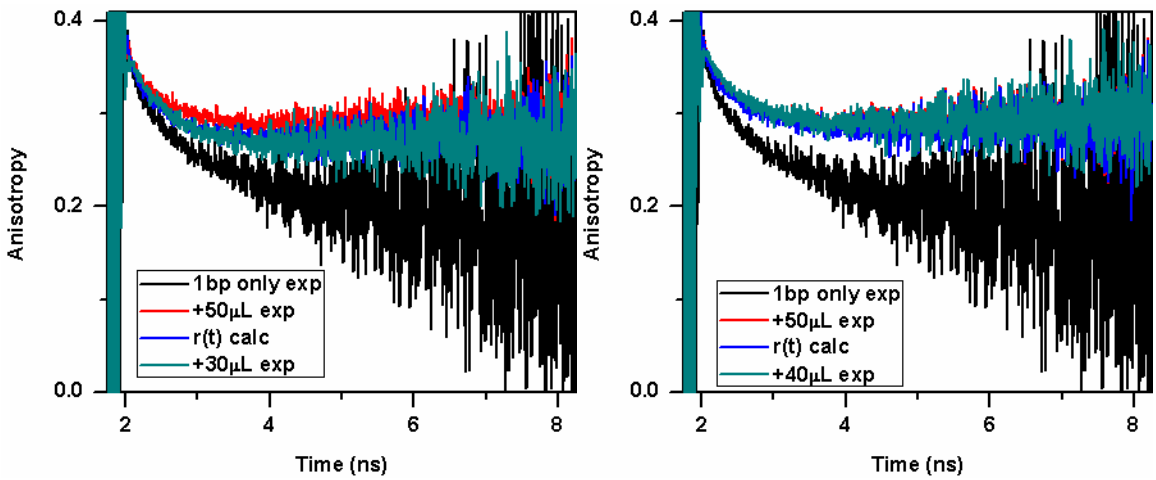


Figure AI.8: Calculated and Experimental Anisotropies Compared for 1-bp Sample.

This method of analysis provides the fraction of free and bound DNA for this DNA-protein system (Table AI.4). The validity of this method depends on having "pure" samples for the two endpoint measurements, without which the extracted parameter α_m could not be accepted as true. For the system studied here the real fraction bound can be estimated from the DNA and protein concentration in the samples. At the micromolar concentrations used for these experiments all BamHI added to the DNA samples was assumed to be bound; the dissociation constant of BamHI is approximately 1-10 nM[180]. The 1-bp samples contained about 96 pmoles of DNA; Table AI.4 contains the amount of protein added to the sample for each measurement. These amounts were calculated based on a reported activity of 8.9 x 10^4 U/mg (NEB website); using this activity the BamHI stock had a concentration of 3.4 μM. The ratio of protein to DNA is calculated and compared to the fraction of bound DNA as determined by the associated anisotropy global fits (Table AI.4). For the both samples the calculated α_m values understate the actual extent of binding in the system. The source of this discrepancy is not known and was not further investigated for this project.

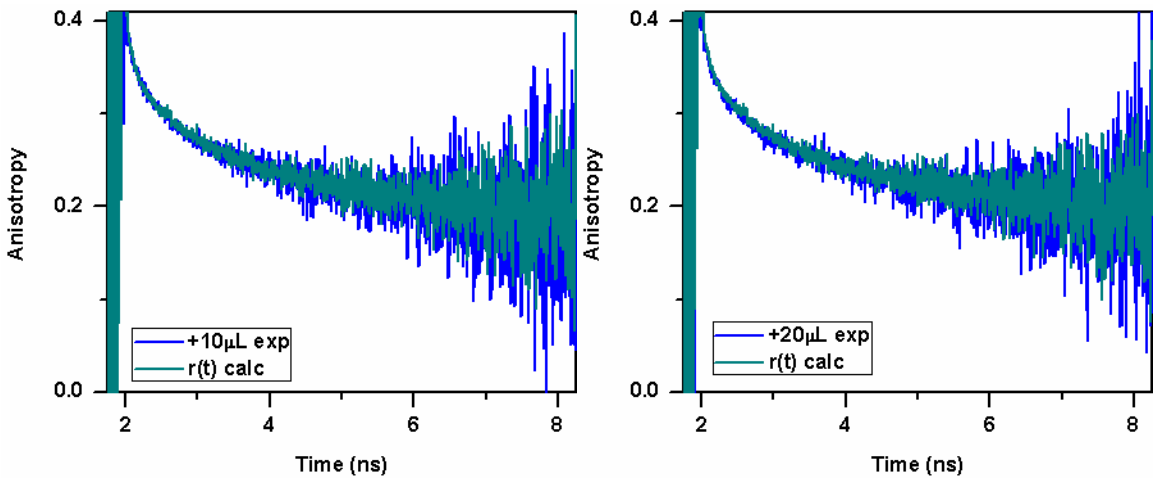


Figure AI.9: Calculated and Experimental Anisotropies Compared for 10-bp Sample.

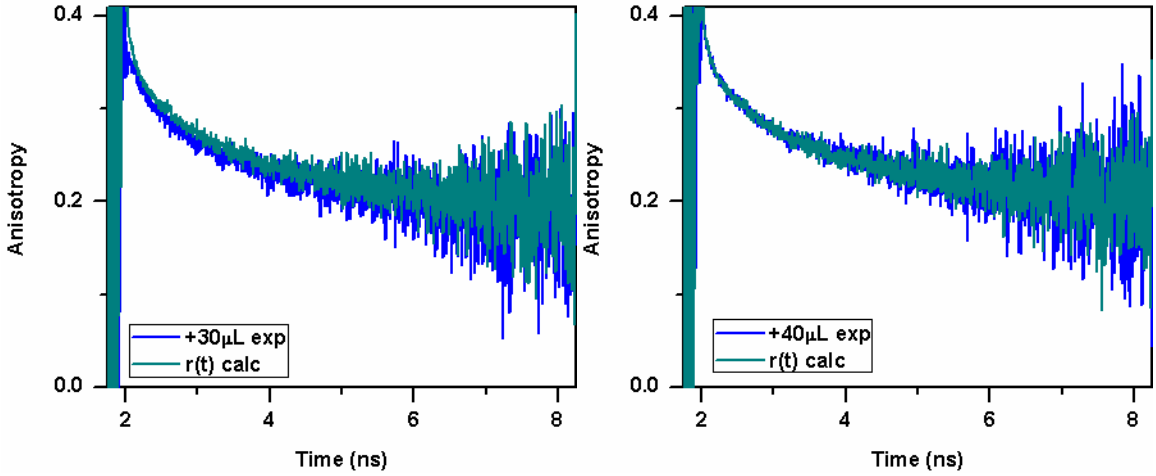


Figure AI.10: Calculated and Experimental Anisotropies Compared for 10-bp Sample.

Table AI.4: Experimental and Calculated Comparison

Sample	BamHI/pmol	BamHI:DNA	α_m 1-bp	α_m 10-bp
+10 µL	34	0.35	0.20	0.32
+20 µL	68	0.71	0.38	0.44
+30 µL	102	1.06	0.53	0.33
+40 µL	136	1.42	0.90	0.58

Table AI.4: Experimental and Calculated Comparison. The first column displays the pmol amount of BamHI added to each sample calculated based on the reported activity. The second column displays the ratio of protein to DNA (based on column one and the amount of DNA initially in the sample). The last two columns show the calculated value of α_m based on the "fit" as described in the text.

Another protein-nucleic acid system studied by the author was human replication protein A (hRPA) and its binding to ssDNA. These measurements were performed for Prof. Timothy Lohman of the Washington University in St. Louis. The DNA sequences studied are shown below (the DNA and protein were provided by Prof. Lohman). Both sequences were labeled with Cy3, however at different ends of the otherwise identical DNA strand. For the sample L1 the Cy3 is on the 3' end of the DNA strand, whereas for L2 the Cy3 is on the 5' end of the strand. The dye is internally attached to the DNA backbone; one thymine is located on one side of the dye, while 30 thymines are on the other side. Results of the lifetime and anisotropy measurements are shown in Figure AI.11. While the lifetime and anisotropy of L1 and L2 are identical when measured

L1: 5'-$(dT)_{30}$-Cy3-dT-3'

L2: 3'-$(dT)_{30}$-Cy3-dT-5'

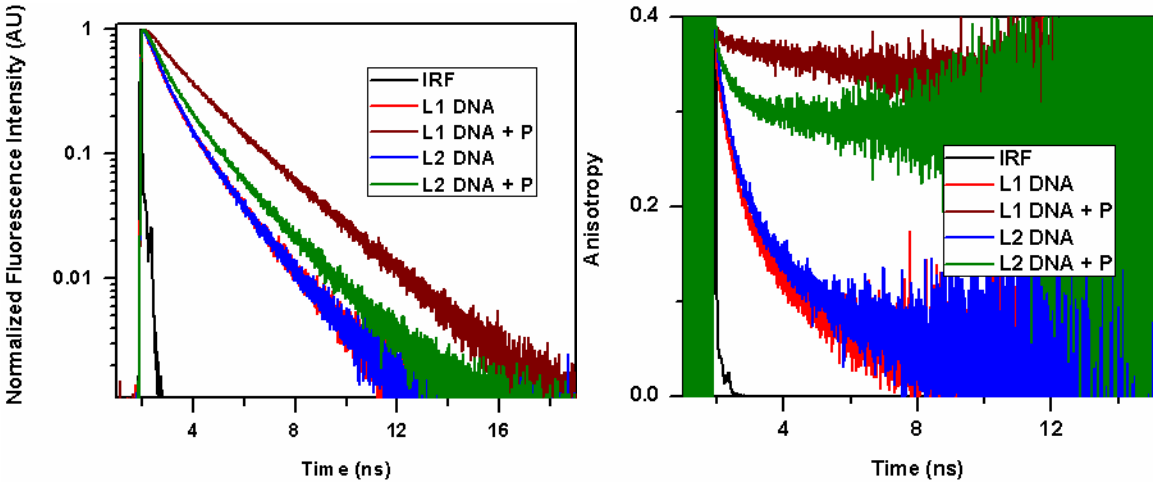


Figure AI.11: hRPA Interaction with DNA. The lifetime measurements for L1 and L2 are shown on the left. L1 (red trace) and L2 (blue) have the same lifetime. The presence of hRPA, however, affects the two samples differently. L1 + P (brown) has a much longer lifetime than L2 + P (green). The anisotropy measurements are shown on the right. The DNA strands have the same anisotropy. The L1 sequence (brown) has a slower anisotropy decay than L2 (green) in the presence of hRPA. The presence of hRPA is indicated by "+ P" in the figure.

separately, the addition of hRPA affects each sample differently. L2 has a modest increase in lifetime while L1 experiences a large increase in the lifetime. Similarly, the L2 sequence has a slower anisotropy decay than L1 in the presence of hRPA. This is a result of the "handedness" of the protein. The protein binds to DNA through two subdomains, which are structurally homologous. Each subdomain binds three nucleotides and two nucleotides occupy the space between the subdomains. The DNA lying inside the protein makes different contacts with the protein based on which subdomain it is in; there are more DNA/protein contacts made by domain A rather than domain B[181]. It is also known that hRPA binds DNA with a preferred polarity. Domain A—the strongly interacting domain of hRPA—is located at the 5' end of the ssDNA-binding region, while the weaker binding domain B is located at the 3' end[182-184]. Furthermore, it has been demonstrated that binding of hRPA to DNA proceeds in a 5' to 3' direction[183, 184]. This information explains why the two DNA sequences, L1 and L2, have different intensity and anisotropy decays in the presence of the protein. Domain A binds DNA at the 5' end, and domain B binds DNA at the 3' end. The strongest intensity and anisotropy enhancement occurs for L1, when Cy3 is at the 3' end of the DNA. This indicates that although the interaction is strongest at domain A, the "bulk" of the protein is at the 3' end of the DNA binding region, obstructing the dye's ability to photoisomerize and tumble (in regards to emission depolarization). In any case, there is a clear polarity for binding of this protein, and fluorescence enhancement of Cy3 has been observed in the presence of hRPA for sequences similar to L1 and L2[185]. For sequences L1 and L2, a simple fluorescence measurement in the cuvette showed an almost 80%

enhancement in fluorescence intensity for L1 (and only 10% enhancement for L2) with hRPA present versus no hRPA in solution (data not shown here). Thus, PIFE is demonstrated in yet another protein-nucleic acid system, and is more complicated due to hRPA's binding polarity.

Experimental details are as follows. The hRPA was received from Prof. Lohman in storage buffer which includes 50% glycerol (200 μL of 10 μM hRPA). The protein stock was dialyzed against the experimental buffer: 10 mM TRIS-HCl, pH 8.1, 0.5 M NaCl, 0.1 mM Na_2EDTA, 1 mM β-mercaptoethanol, at 25°C. Dialysis was performed using a Spectra/Por Micro Float-A-Lyzer microdialysis device with a molecular weight cut-off of 8 – 10 kD for 400 – 500 μL volumes. The protein was dialyzed according to the product instructions, inside a cold room (temperature 4°C); three buffer changes were made. Samples for TCSPC measurements were 0.5 μM DNA and 1 μM hRPA.

APPENDIX II

POLYMERASE REACTION ON DNA AND BINDING OF KLENOW FRAGMENT

The polymerase reaction was performed on the DNA samples used for experiments in Chapter 4 to ensure proper function of the KF, i.e. to make sure there is no interference from the fluorescent label.

For each dye-DNA sample four reactions were performed: the DNA (1.1 μM) was incubated in a siliconized tube with KF (0.8 μM) and dNTPs (each dNTP was added to a concentration of 100 μM) in the Number 2 buffer provided by New England Biolabs (Ipswich, MA) for approximately 30 minutes at 37°C. (The ratio of KF to DNA was chosen based on the results of previous gel electrophoresis experiments that showed more KF did not increase the efficiency of the reaction.) The first tube received only dCTP, the second received dCTP and dATP, the third received dCTP, dATP, and dGTP, while the last tube received all four dNTPs. The pol reaction was stopped by the addition of 0.5 M EDTA. The purpose of these samples is to verify that each addition step works. Two controls were prepared: a sample of the dsDNA sample alone, and a sample of the ssDNA (the 11-base primer strand). Once the reactions were complete the samples were heat denatured (at 70°C for five minutes) with TBE-urea loading buffer (Bio-Rad Laboratories, Hercules, CA) and run on a 20% denaturing polyacrylamide gel. The gels were stained with Sybr Gold for 30 minutes and imaged on a Typhoon Trio+ Variable Mode Imager using the 633 nm laser (with the Cy5 filter) and with the 488 nm laser and corresponding filter (to verify the location of the unlabeled complementary strand).

First, the polymerase reaction was tested on an identical DNA sample as used for all experiments except that it has no fluorescent modification. Sybr Gold was used to stain the gel, and the 488 nm laser on the Typhoon imager was used to visualize the stain. The gel image is shown below (Figure AII.1); samples in the lanes are as described in the

caption. The ssDNA sample is the 11-base primer strand; it runs cleanly compared to the dsDNA sample which has several low-intensity bands in addition to the primary band for the 11-base strand. The sample with added dCTPs shows a primary band significantly higher than the 11-base primer, signifying a complete reaction to the 12-base strand. The

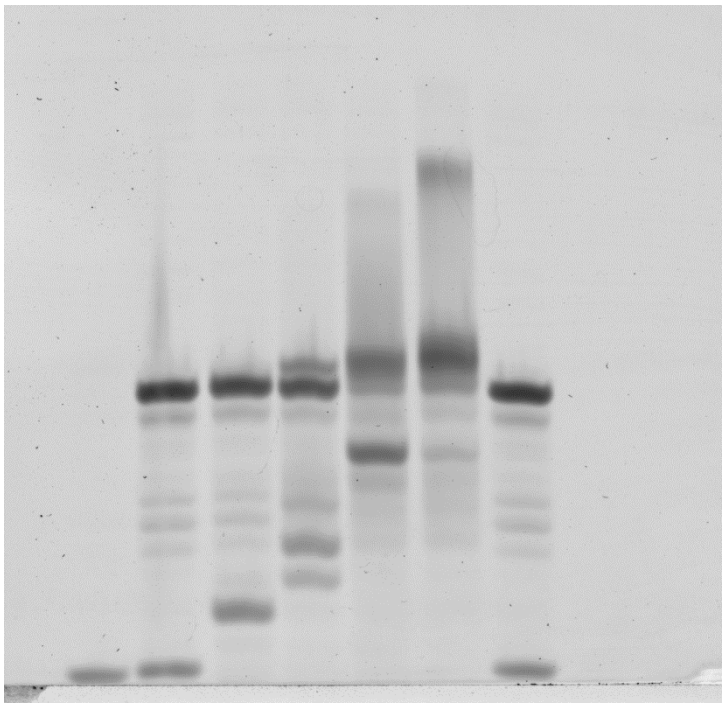


Figure AII.1: Results of polymerase reaction on unlabeled DNA primer/template sample (DNA sample as shown in Figure 4.2, Chapter 4). Samples loaded into the gel lanes from left are: ssDNA, dsDNA only, dsDNA + KF + dCTP, dsDNA + KF + dCTP + dATP, dsDNA + KF + dCTP + dATP + dGTP, dsDNA + KF + all dNTPs, dsDNA only again.

next sample shows two equal intensity bands signifying the 13- and 14-base strands that form upon addition of dATP. The primary band of the sample with three nucleotides added is much higher in the gel than the 11- through 14-base strand bands; it is assigned to the 17-base strand which forms when all C-G pairs are made. The final sample is difficult to understand due to the lack of any high intensity bands. A weak band is seen at the 17-base strand location, but the remaining intensity is concentrated towards the top of the gel; this is likely the mark of the 18-, 19-, and 20-base strands that form when

dTTPs are added. This gel demonstrates that there is no impediment to KF performing the polymerase reaction on this DNA sequence.

Below, (Figure AII.2) is the image of the gel for the polymerase reaction on Cy5-dsDNA (this sample had the same DNA sequence as Dy630/Dy632/Dy635-dsDNA samples used in this study). There were seven samples run in this gel as described in the

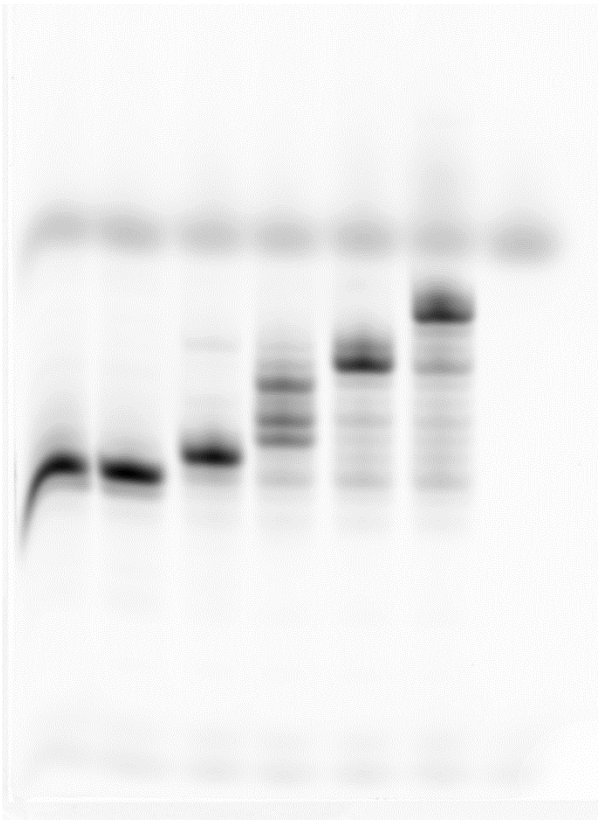


Figure AII.2: Results of polymerase reaction on Cy5-dsDNA. Samples in the lanes are, from left, Cy5-ssDNA only, Cy5-dsDNA only, Cy5-dsDNA + KF + dCTP, Cy5-dsDNA + KF + dCTP + dATP, Cy5-dsDNA + KF + dCTP + dATP + dGTP, Cy5-dsDNA + KF + all dNTPs. The right-most lane contains a sample of the unlabeled complementary strand.

caption. The complementary strand shows up in all the lanes (as the light smudge at the top); it is the longest strand in the samples at 20 bases and runs the slowest down the gel. The Cy5-ssDNA and Cy5-dsDNA lanes have a strong band at the very bottom, this

represents the labeled primer strand (11 bases) which is the shortest. The dCTP sample (third lane from left) has a strong band just above where the Cy5-ssDNA strand shows up; this is the 12-base strand formed once KF adds the dCTP to the DNA. The next lane has three bands of similar intensity, all higher in the gel than the 12-base strand formed in the previous sample. In this sample two dNTPs were added corresponding to the first three partner-less bases in the complementary strand. These three bands are likely the result of adding the dCTP and dATPs to form 12-, 13-, and 14-base strands. It is unclear why the 12-base strand in this sample did not run the same distance down the gel as the previous sample. The next sample (which included dCTP, dATP, and dGTP) shows one prominent band indicating the reaction proceeded almost to completion creating a 17-base strand. Several bands of low intensity can be seen in this lane, most likely representing the other intermediate length strands. The last lane, for the sample which received all dNTPs, has one prominent band that ran slower than the other samples; thus the strand created here was at least an 18-base strand (the band does not run with the 20-base complementary strand meaning the reaction did not go to completion). As for the previous sample, there are many low-intensity bands indicating the intermediate products.

This gel demonstrates that the commercial version of the KF used for the studies in Chapter 4 is indeed active at the *pol* site regardless of the additional Cy5 label. The same test was performed for all Dy-dye labeled samples to ensure that these dyes also do not interfere with the functioning of the protein. Figure AII.3 shows the gel image of the polymerase reaction for Dy632-dsDNA (left lanes) and Dy635-dsDNA (right lanes), and Figure AII.4 shows the polymerase reaction for Dy630-dsDNA.

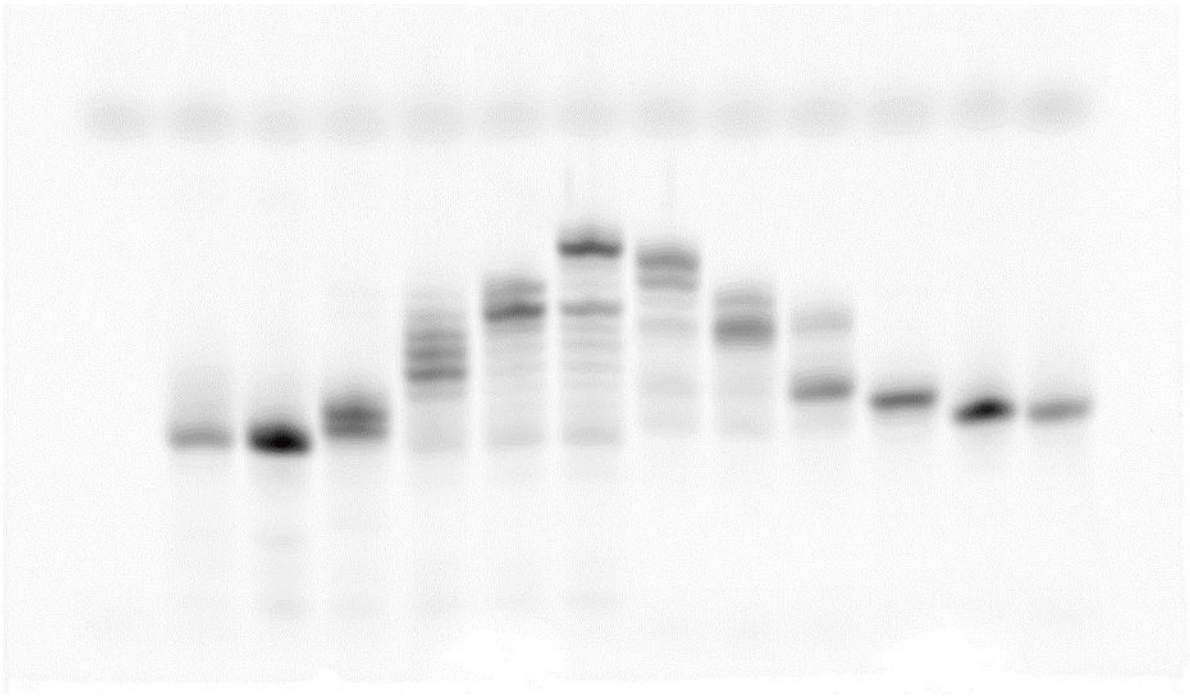


Figure AII.3: Polymerase reaction on Dy632-dsDNA (left lanes) and Dy635-dsDNA (right lanes). Samples in the lanes are as follows: from left, template (complementary) strand only, Dy632-ssDNA, Dy632-dsDNA only, Dy632-dsDNA + KF + dCTP, Dy632-dsDNA + KF + dCTP + dATP, Dy632-dsDNA + KF + dCTP + dATP + dGTP, Dy632-dsDNA + KF + all dNTPs, Dy635-dsDNA + KF + all dNTPs, Dy635-dsDNA + KF + dCTP + dATP + dGTP, Dy635-dsDNA + KF + dCTP + dATP, Dy635-dsDNA + KF + dCTP, Dy635-dsDNA only, and Dy635-ssDNA.

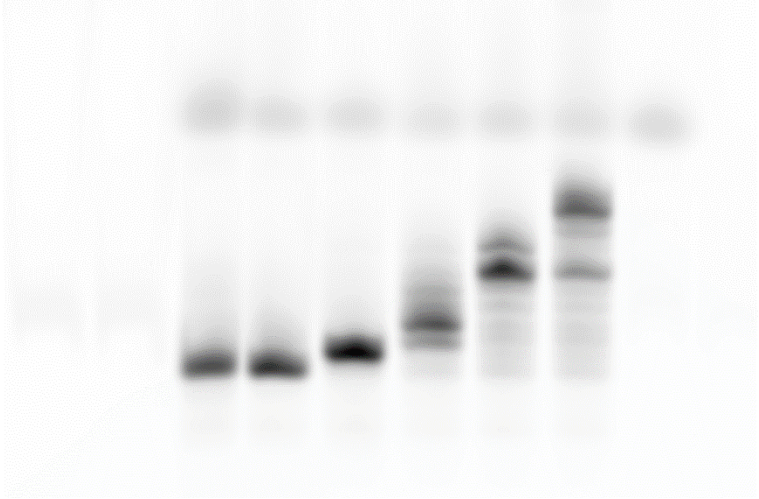


Figure AII.4: Polymerase reaction on Dy630-dsDNA. Samples in the lanes are, from left, Dy630-ssDNA only, Dy630-dsDNA only, Dy630-dsDNA + KF + dCTP, Dy630-dsDNA + KF + dCTP + dATP, Dy630-dsDNA + KF + dCTP + dATP + dGTP, Dy630-dsDNA + KF + all dNTPs.

KF titrations were performed in the cuvette to measure the increase in fluorescence intensity and anisotropy experienced by the dye in the presence of the protein environment. This measurement allows the determination of the dissociation constant, K_D, of the protein. These measurements were begun by Gabe Salmon, and continued by the author and George Brockett. These experiments were performed using the commercial version of KF.

The DNA concentration was kept low at approximately 60 nM (at a volume of 2 – 2.5 mL); the KF stock used was highly concentrated (77.4 μM) and either diluted down 10-fold (to make a 7.74 μM stock) or used as is (when the DNA concentration was increased 10-fold, for certain experiments). KF was added to the DNA in 1 μL increments until about 20 μL had been added, then the protein was added in 2-3 μL increments. KF was added until a plateau was reached in the anisotropy. Then, dNTPs were added to observe the anisotropy decrease, which occurs because as the protein adds dNTPs it moves farther away from the labeled base in position 10 on the primer strand.

The figure below, Figure AII.5, shows the increase in fluorescence anisotropy and intensity upon addition of KF to Dy632-dsDNA. The data shown was collected by Gabe Salmon (black and red data points), while the data in orange and purple was collected by the author and in green by George Brockett. For all trials shown here [Dy632-dsDNA] = 60 nM, and a 1 in 10 dilution was made of the KF stock (direct from NEB). KF was added in 1 – 3 μL increments. The green, orange, and purple data points which are below the anisotropy and intensity plateaus are the values once dNTPs were added, although not all data points are shown here. The same experiments were performed for Dy630-dsDNA. The results are shown in Figure AII.6. Interestingly, the intensity decreases for

the Dy630-dsDNA sample; this corroborates with the lack of increase in lifetime observed in the TCSPC experiments (Figures 4.23 and 4.24, and Tables 4.14 and 4.15). The titration experiment was also performed at a higher DNA concentration of 600 nM;

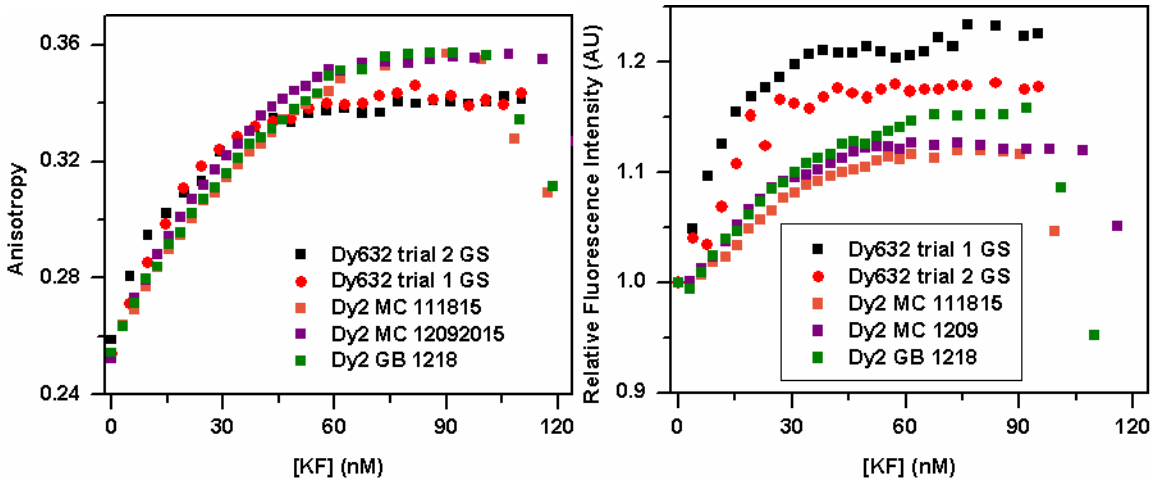


Figure AII.5: Klenow fragment titration with a solution of Dy632-dsDNA. Steady-state intensity and fluorescence anisotropy values were measured as KF was added in increments of 1 – 3 μL. It is unclear why there is such variation in intensity for data collected by Gabe Salmon ("GS"). Data collected by the author is labeled "MC", data collected by George Brockett is labeled "GB".

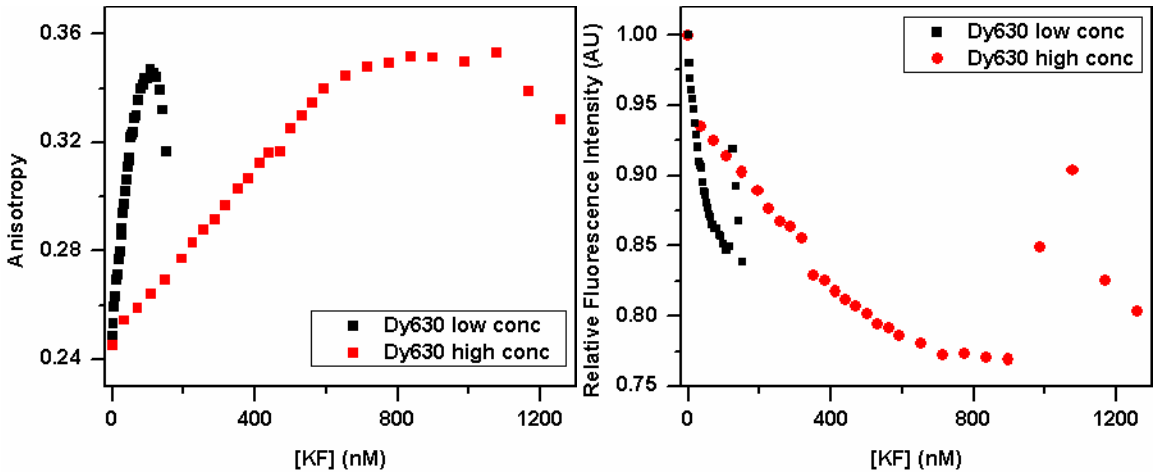


Figure AII.6: Klenow fragment titration with a solution of Dy632-dsDNA. The "low concentration" measurement was carried out at 60 nM concentration of Dy630-dsDNA; the high concentration measurement was carried out at 600 nM concentration of Dy630-dsDNA. It is unclear why there is a large disparity in the first and remaining intensity measurements for the high concentration sample.

the purpose of this was to verify whether concentration affects the results (it does not), and to measure the absorption spectra of Dy630-dsDNA before and after the addition of KF and dNTPs. These spectra are shown in Figure AII.7.

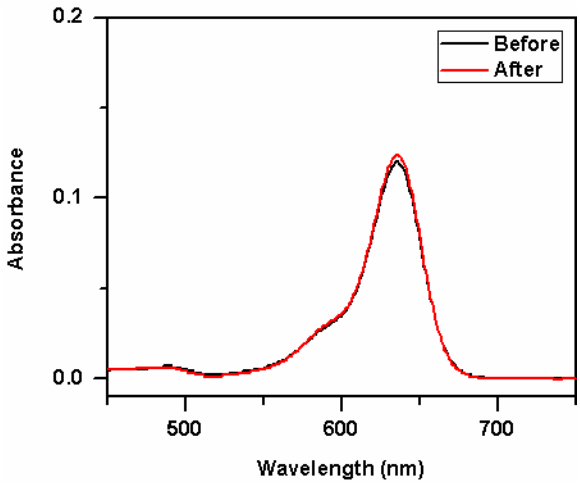


Figure AII.7: Absorption spectra of Dy630-dsDNA before the KF titration, and after the edition of over an equivalent of KF. No shift is observed.

The anisotropy data was fit to a model in order to extract out a K_D for KF binding to this particular DNA sequence. In this system there are three species, DNA, KF, and the DNA-KF complex. The dissociation reaction is shown in Equation II.1, and the relations which hold true for the system are shown in Equation II.2, below.

$$DNA - KF \rightarrow DNA + KF \tag{II.1}$$

$$K_d = \frac{[KF][DNA]}{[KF{-}DNA]} = \frac{[KF][DNA]}{[C]}$$

$$[DNA]_0 = [C] + [DNA] \tag{II.2}$$

$$[KF]_0 = [C] + [KF]$$

Here, $[C]$ represents the concentration of the complex (KF-DNA). Substituting the expressions for initial DNA and KF concentration into the expression for K_D gives

Equation II.3.

$$K_d = \frac{([KF]_0 - [C])([DNA]_0 - [C])}{[C]} \quad \text{(II.3)}$$

The DNA in the solution is either free or bound (meaning complexed to KF), hence, the fraction of DNA bound to KF, f_b, and the fraction of free DNA, f_f, must sum to one (Equation II.4). The fraction of bound DNA can be represented as Equation II.5.

$$1 = f_b + f_f \quad \text{(II.4)}$$

$$f_b = \frac{[C]}{[C]+[DNA]} = \frac{[C]}{[DNA]_0} \quad \text{(II.5)}$$

Equation II.3 can be solved for $[C]$ as a function of K_d; the resulting expression can be substituted into Equation II.5 to give Equation II.6.

$$f_b = \frac{[DNA]_0 + K_d + [KF]_0 - \sqrt{-4\,[DNA]_0\,[KF]_0 + ([DNA]_0 + K_d + [KF]_0)^2}}{2\,[DNA]_0} \quad \text{(II.6)}$$

The titration experiment measures the anisotropy of the sample, which is a sum of contributions from the bound and free DNA as shown in Equation II.7, where r is the total anisotropy, r_b is the anisotropy of the bound DNA, and r_f is that of the free DNA, and i_b and i_f represent the fractional intensity due to the bound and free DNA, respectively. The fractional intensity emitted by the bound species in the sample is due to

$$r = i_b\, r_b + i_f r_f \quad \text{(II.7)}$$

the fraction (amount) of that species present and its quantum yield, divided by the total intensity, shown in Equation II.8, where $f_i$is the fraction of species *i* present in solution and $\varphi_i$is the quantum yield of that species. Thus, the total anisotropy is Equation II.9, which is rearranged in Equation II.10.

$$i_b = \frac{f_b \varphi_b}{f_b \varphi_b + f_f \varphi_f} \quad \text{(II.8)}$$

$$r = \frac{f_b\, \varphi_b}{f_b\, \varphi_b + f_f\, \varphi_f} r_b + \left(1 - \frac{f_b\, \varphi_b}{f_b\, \varphi_b + f_f\, \varphi_f}\right) r_f \quad \text{(II.9)}$$

$$r = \frac{f_b\, \varphi_b\, r_b + f_f\, \varphi_f\, r_f}{f_b\, \varphi_b + f_f\, \varphi_f} \quad \text{(II.10)}$$

The expression can be divided by φ_f to yield Equation II.11, where *R* is a measure of the fluorescence enhancement upon KF binding to DNA. Since the total fraction of DNA species present in solution must add to 1, the equation can be rearranged once again to Equation II.12, and finally to Equation II.13. Substituting Equation II.6 (for the fraction

$$r = \frac{f_b\, R\, r_b + f_f\, r_f}{f_b\, R + f_f}, \; R = \frac{\varphi_b}{\varphi_f} \quad \text{(II.11)}$$

$$r = \frac{f_b\, R\, r_b + (1 - f_b)\, r_f}{f_b\, R + (1 - f_b)} \quad \text{(II.12)}$$

$$r = \frac{f_b\, R\, r_b + (1 - f_b)\, r_f}{1 + f_b\, (R - 1)} \quad \text{(II.13)}$$

of bound DNA) into Equation II.13 gives the final form of the anisotropy equation used to fit the raw data from the KF titrations. This final equation relates the anisotropy to the K_D of the KF. The $[DNA]_0$ and r_f (the initial anisotropy value of the titration, the anisotropy when no KF is present) are inputs to the fitting procedure, as well as $[KF]_0$ (these are the x-values of the data). The value of r_b is estimated from the last few data points of the titration (the area of the plateau). The ratio of the quantum yields, *R*, and the K_D are the fitting parameters.

The first step in the fitting procedure is to fit to the linear part of the data only. A first order Taylor series expansion of Equation II.13 is used to estimate the value of *R*. The Taylor series expansion of Equation II.13 is shown in Equation II.14. Since the K_D

$$r = r_f + \frac{R(r_b - r_f)}{[DNA]_0 + K_d}[KF]_0 \quad \text{(II.14)}$$

is expected to be on the order of about 8 nM, and when initially fitting the entire data set turned out to be lower, it can be ignored in the fit ($[DNA]_0$ is 60 nM). Hence, the first few points of the titration are fit to Equation II.15. This allows the estimation of *R*, (r_b is estimated from the last few points of the data set, before dNTPs were added). The value of *R* is then used when fitting the full set of data to Equation II.13. Below are Tables AII.1 and AII.2 with values for these parameters for the Dy632- and Dy630-dsDNA KF titration experiments.

$$r = r_f + \frac{R(r_b - r_f)}{[DNA]_0}[KF]_0 \quad \text{(II.15)}$$

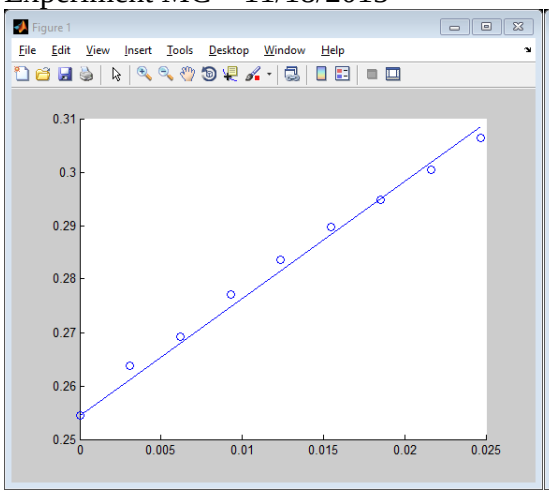
Table AII.1: Fitting Parameters for Dy632-dsDNA

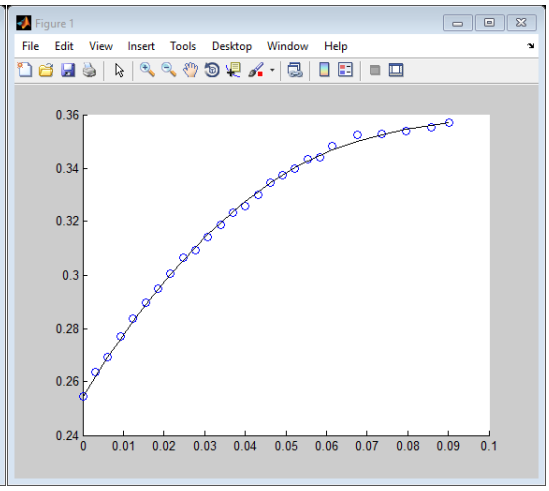
	Dy632-dsDNA		
Linear fit	**MC—11/18/15**	**MC—12/9/15**	**GB—12/18/15**
# of points	9	3	4
# of points for r_b	5	7	4
R	1.32 ± 0.02	2.00 ± 0.04	1.63 ± 0.02
sum of residuals	2.6×10^{-5}	5.5×10^{-7}	2.7×10^{-7}
Full fit	**MC—11/18/15**	**MC—12/9/15**	**GB—12/18/15**
K_D (nM)	4.6 ± 1.1	0.6 ± 0.2	5 ± 2
R	1.46 ± 0.03	2.02 ± 0.02	1.52 ± 0.04
r_b	0.366 ± 0.002	0.356 ± 0.001	0.368 ±0.004
sum of residuals	2.4×10^{-5}	1.4×10^{-5}	5.2×10^{-5}

Table AII.1: This table shows the fitting parameters from both linear and full fits of data for the Dy632-dsDNA KF titration experiments. The top of the table shows the results of the linear fits used to determine values of *R*, along with the number of initial points used for the fit, and the number of last data points used to estimate r_b. The bottom of the table shows results of the fits to the full data set to determine all three parameters.

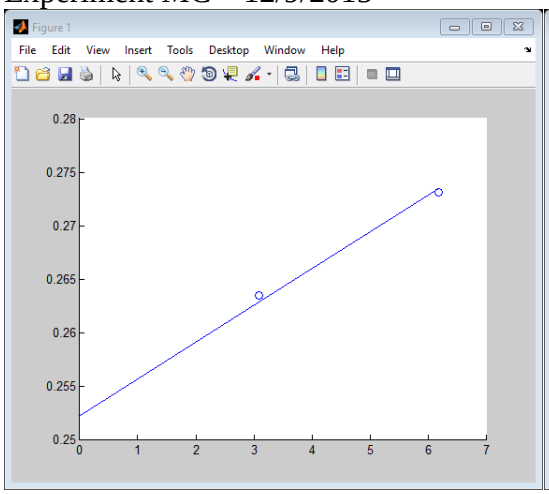
The fits were performed in MATLAB; below are screenshots of each fit (two per experiment, linear and full).

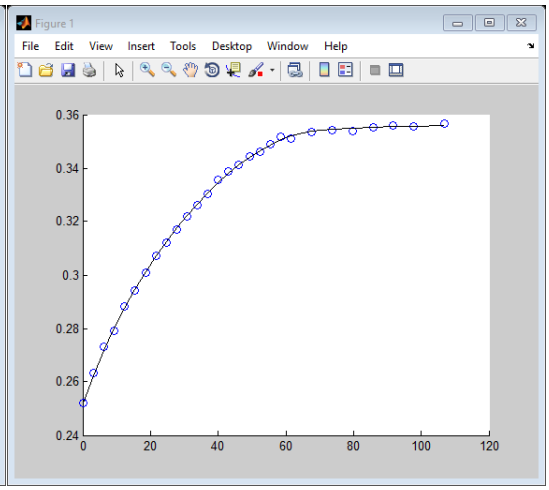
Experiment MC—11/18/2015



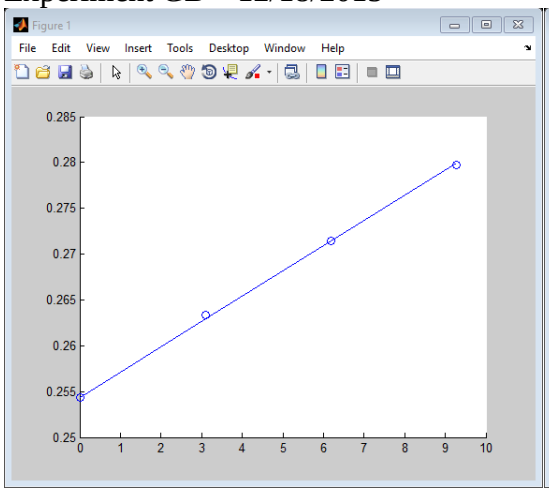


Experiment MC—12/9/2015





Experiment GB—12/18/2015



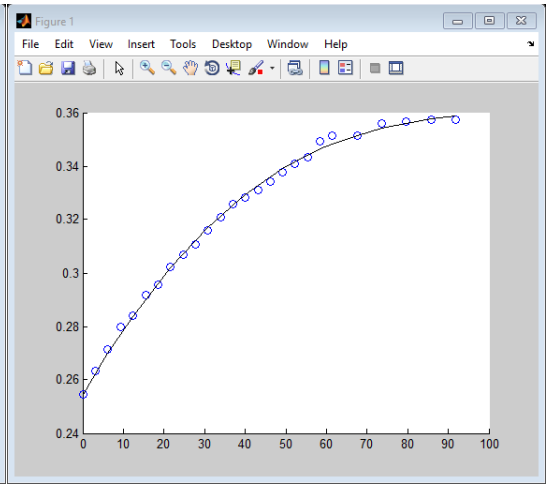


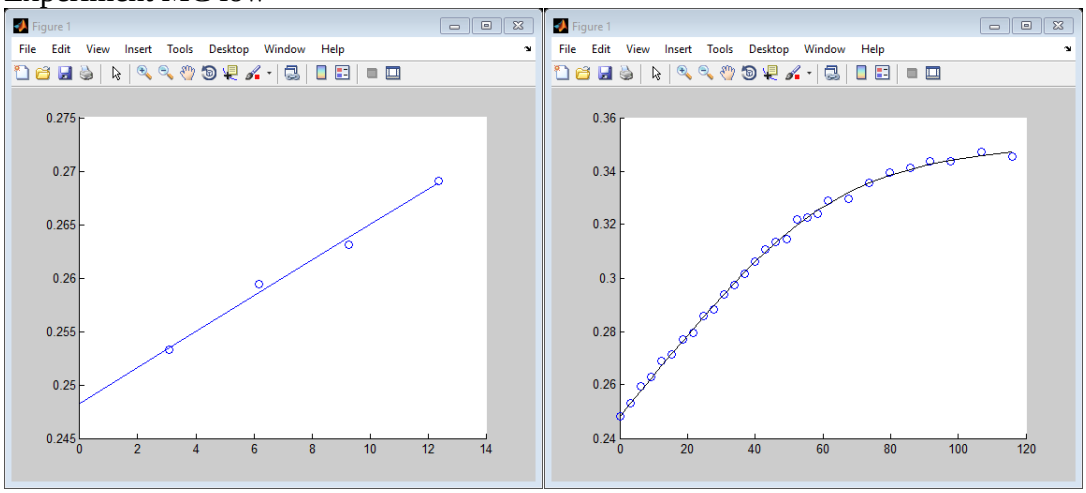
Table AII.2: Fitting Parameters for Dy630-dsDNA

	Dy630-dsDNA			
Linear fit	**MC low**	**MC low**	**MC high**	**MC high**
# of points	5		8	
# of points for r_b	3		2	
R	1.03 ± 0.02		0.94 ± 0.02	
sum of residuals	1.0×10^{-6}		1.8×10^{-5}	
Full fit	**MC low**	**MC low**	**MC high**	**MC high**
K_D (nM)	5.9 ± 0.9	4.8 ± 0.8	19 ± 6	18 ± 6
R	0.92 ± 0.02	set 0.85	0.83 ± 0.03	set 0.85
r_b	0.358 ± 0.002	0.357 ± 0.002	0.360 ± 0.004	0.359 ± 0.003
sum of residuals	4.0×10^{-5}	5.7×10^{-5}	7.2×10^{-5}	7.4×10^{-5}

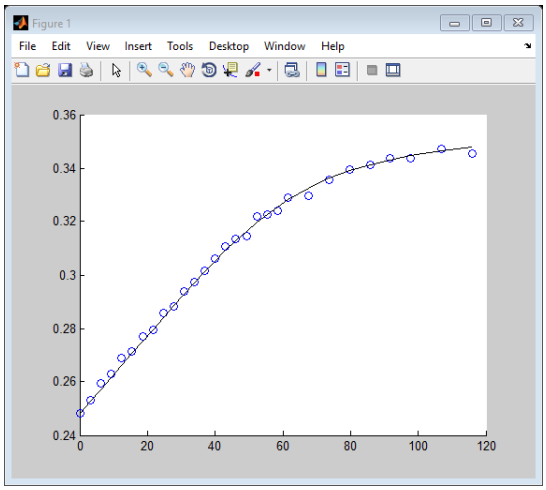
Table AII.2: This table shows the fitting parameters from both linear and full fits of data for the Dy632-dsDNA KF titration experiments. The top of the table shows the results of the linear fits used to determine values of *R*, along with the number of initial points used for the fit, and the number of last data points used to estimate r_b. The bottom of the table shows results of the fits to the full data set to determine all three parameters. The full set of data for each experiment was fit twice, once allowing all three parameters to be free, and once setting the value of *R* to 0.85, the approximated drop in intensity observed, to see the effect on the other parameters. The large drop in intensity between the first and second data points was ignored when setting the value of *R* to 0.85.

Screenshots of each fit are shown below.

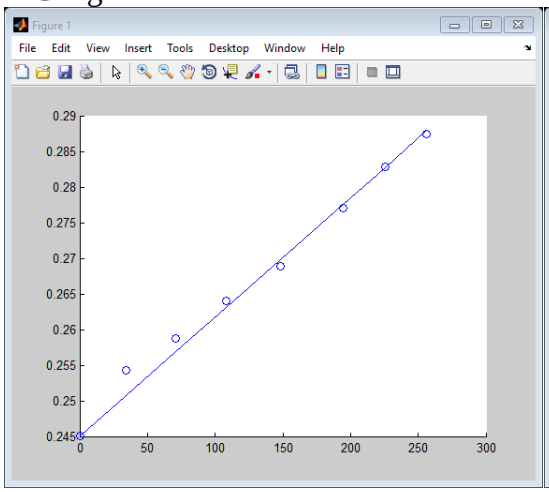
Experiment MC low

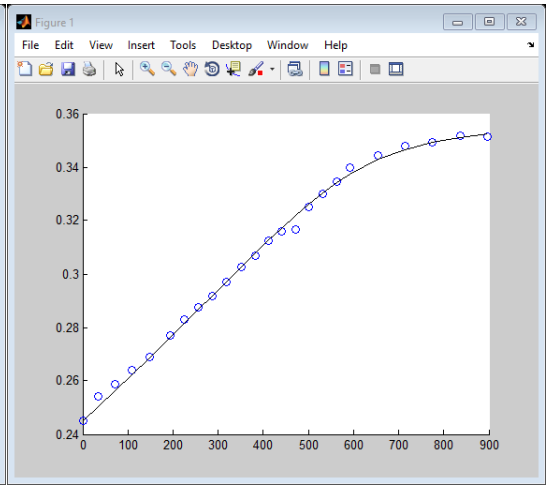


MC low set *R*

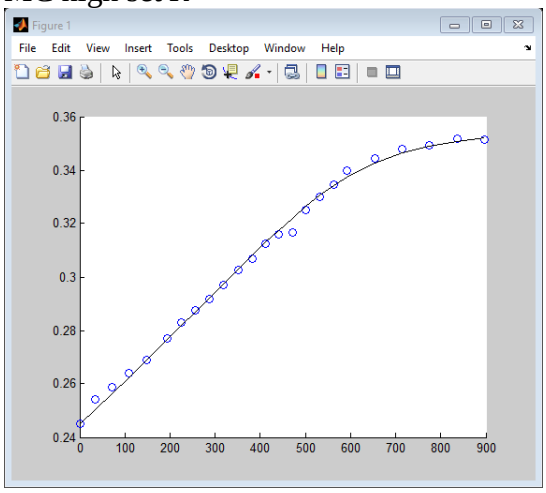


MC high





MC high set *R*



APPENDIX III

TOTAL INTERNAL REFLECTION FLUORESCENCE SPECTROSCOPY

A total internal reflection fluorescence (TIRF) instrument was custom-built by the author. This Appendix introduces the setup, describes experimental protocols, and illustrates preliminary data collected using this instrument. The design of the TIRF instrument was based on a variety of freely available sources. The parts for holding the prism were adapted from scale drawings on the website of Taekjip Ha's lab (at the Johns Hopkins School of Medicine). Several publications proved useful in the building, initial alignment, and use of the setup[186-188]. Assistance with the emission path optics was provided by Prof. Elvin A. Alemán of California State University, Stanislaus. Prof. Alemán also provided the protocols for slide cleaning, preparation, and preparation of the control "bead slides".

Below is a schematic of the prism-based TIRF instrument in the Levitus Lab (Figure III.1). The setup uses a Coherent Compass 215M-20 532 nm 20 mW laser or a Coherent CUBE 639 nm 40 mW laser depending on excitation wavelength required (purchased from Coherent Inc., Santa Clara, CA). All optics in the setup were purchased from Thorlabs Inc. (Newton, NJ). The laser beam is guided by mirrors (BB1-E02, 1" diameter, broadband 400-750 nm) to the sample stage, where it is focused by a plano convex lens (LA1509-A, 1" diameter, focal length 100.0 mm, N-BK7 A coated) onto the flat end of the Pellin Broca prism (purchased from Eksma Optics, Lithuania); the uncoated prism has dimensions 11 x 20 x 6.4 mm and is made of fused silica. The prism rests on top of the sample chamber (shown in detail in Figure III.2), which rests on top of the objective. The objective was purchased from Olympus Corp. (Japan), it is a water immersion objective with 60 x magnification and numerical aperture of 1.20 (model # UPLSAPO 60XW). In prism-based TIRF fluorescence is collected via the objective; an

appropriately chosen emission filter follows the objective. The emitted light expands at short distances out of the objective, thus a larger mirror is used immediately after the objective (BB2-E02, 2" diameter). A 2" diameter plano convex focusing lens (LA1050-A, focal length of 100.0 mm, N-BK7 A coated) focuses the emitted light onto an adjustable mechanical slit (VA100, Thorlabs). Light emerging from the slit is focused by an achromat (AC508-200-A-ML, focal length 200 mm) onto the photoactive area of the Andor iXon Ultra 897 EMCCD camera (Andor Technology, Belfast, UK). A square mirror directs the light from the achromat to the EMCCD chip (BBSQ1-E02).

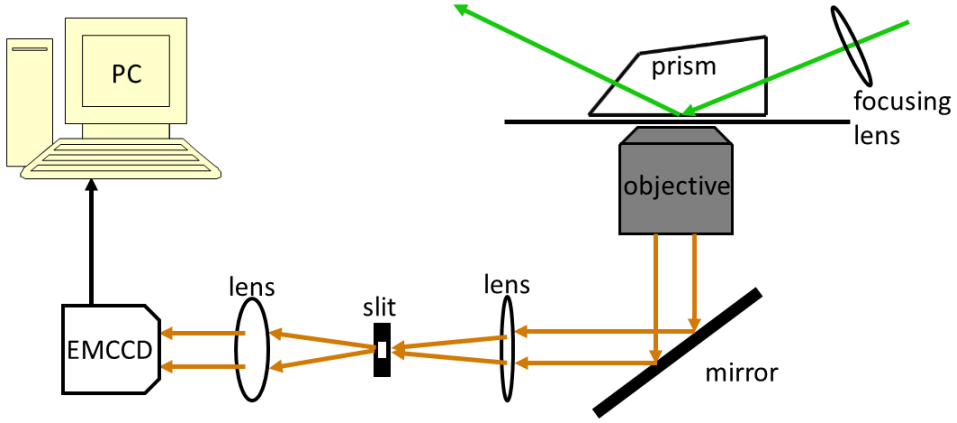


Figure AIII.1: Schematic of Levitus Lab TIRF Instrument. The instrument is a prism-based TIRF system equipped with an electron multiplying charged coupled device camera (EMCCD) as the detector.

The sample chambers are made from quartz slides (purchased from G. Finkenbeiner, Inc., Waltham, MA) and borosilicate glass coverslips (from Fisher Scientific, 24 x 50 mm, 0.16 to 0.19 mm thickness). The sample chamber is placed on top of a droplet of nanopure water atop the objective, and the prism is placed on top of the sample chamber (quartz slide is toward the prism). A layer of immersion oil (of refractive index matching the material of the prism and slide) is placed between the

sample chamber and prism. The reflected laser light is seen as three reflections due to the initial laser beam passing through the interfaces created by the imperfect match (in terms of refractive index) between the prism and quartz slide (see Figure AIII.2).

Before placing a sample chamber into the instrument the alignment must first be checked using a "bead slide". A "bead slide" consists of dye-coated polystyrene beads immobilized on the quartz surface. The polystyrene beads are commercially available in a variety of sizes; the larger the bead the more fluorescent dyes it contains and the brighter it is. The Levitus lab uses the following beads for green excitation alignment: FluoSpheres Carboxylate-Modified Microspheres orange fluorescent (540/560) from Invitrogen in 0.2 μm and 0.04 μm sizes. The crimson fluorescent (625/645) microspheres are used for red excitation alignment. At the 0.2 μm size the polystyrene beads are coated with about 10,000 dyes each, making them very bright and useful for instrument

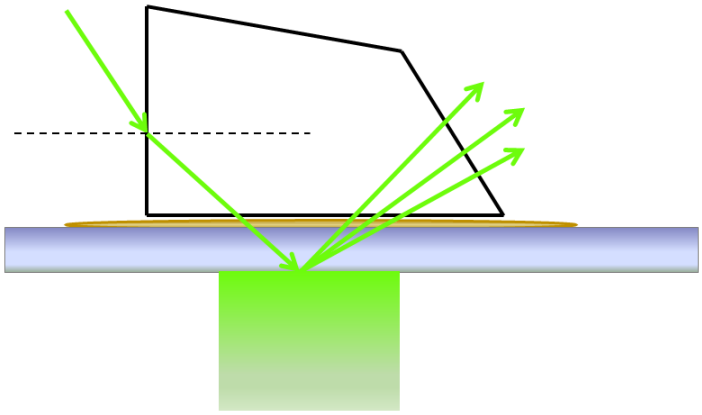


Figure AIII.2: Schematic showing the interfaces through which the exciting laser beam passes. First, the laser beam hits the flat side (left) of the prism and upon entering the quartz prism is refracted towards the normal line at the interface (dashed line). The beam then passes into the quartz slide, through a layer of oil, and is reflected off the bottom surface of the slide. The reflected beam is seen as three points of light exiting the slanted (right) side of the prism. Some intensity of the laser light refracts into the aqueous liquid inside the chamber. It is at the bottom of the quartz slide where the molecules under study are immobilized.

alignment. The bead slide is also used to find the focal plane with the objective. However, finding the focus with the large beads (0.2 μm) is not useful when the sample under study is as small as singly-labeled DNA. In this case, it is recommended to use smaller sized beads (0.04 μm or smaller, if available) in order to find the focus before switching to the sample. Although the smaller sized beads, coated with fewer dye molecules, are less bright, they are more useful for finding the focus. The preparation of a bead slide is simple. Two pieces of double-sided tape are placed along the long length of a clean quartz slide, leaving about 1 cm of uncovered space in the middle. A clean coverslip is placed over the slide such that it adheres to the tape. Excess tape is cut off with a razor blade. A bead solution is prepared from 1 – 3 μL of the commercial stock in 1 mL of water. This solution is bath sonicated for 20 minutes. This solution is then inserted into the space between the quartz slide and coverslip (requires about 30 – 50 μL). Then, a solution of 0.5 M Mg^{2+} is flowed in, 10 μL per aliquot. The Mg^{2+} aliquots should be injected on alternate sides, meaning the first aliquot should be injected from the right, the next from the left, then from the right again, etc. After injecting an aliquot, the slide must be rocked back and forth to allow the solutions to mix. Approximately ten aliquots of Mg^{2+} should be flowed in. The purpose of the Mg^{2+} is to aid in adhering the carboxylate functional groups to the quartz surface. Once the Mg^{2+} is added the edges of the coverslip are glued with epoxy to prevent evaporation of the solution.

The preparation of sample chambers is similar. The quartz slides must first be drilled to create holes for inlet and outlet tubing which will deliver and remove the sample solutions to the chamber, respectively. The drilling is done with a Dremel 200 hand tool (mounted on a stand for stability), using 1-1/4 mm size diamond drill bits for a

collet size of 1/16 of an inch (Kingsley North, Inc., 1-0502). The slides are drilled at the low setting (7000 rpm) and must be immersed in water to allow for heat dissipation. Tubing is inserted into the slide and epoxy is used to adhere it; the tubing is Silastic brand laboratory tubing, 0.020 inches inner diameter and 0.037 inches outer diameter (VWR, 62999-075). As for the bead slide, double-sided tape is used to create the chamber volume, but for the sample chambers tape is adhered to all four sides of a clean quartz slide. Once the coverslip is placed over the slide, the excess tape is removed by razor blade, and the edges of the coverslip are glued with epoxy.

The protocol for immobilizing DNA molecules at the surface of the quartz slide is as follows. A solution of biotin-BSA (bovine serum albumin) (Pierce brand, Fisher Scientific, P129130) is made in 1x T50 buffer (10 mM TRIS, 50 mM NaCl) to concentration 2 mg/mL. Small aliquots of this solution (100 μL) are stored in the freezer. Upon defrosting, the solution is diluted to 1 mg/mL with 1x T50. This solution is flowed in to the sample chamber first and is incubated for about 15 – 20 minutes. The sample chamber is then flushed with 1x T50 buffer (about 500 μL), and a solution of streptavidin is flowed in and incubated for 2 minutes; streptavidin is from Invitrogen (#434302). The streptavidin solution is used at a concentration of 0.2 mg/mL in T50 buffer. The chamber is flushed again with buffer. Then, the target molecules are flowed in. For the experiments discussed here, that is biotin labeled DNA. The sequence used is as shown in Figure 4.2; the biotin label is on the 5' end of the template strand (on the side of base 20). The DNA solution is flowed in at a concentration of 10 pM, in 1x T50 buffer. The DNA incubates for 2 minutes and is flushed with 1x T50 buffer, followed by the imaging buffer. The imaging buffer consists of a glucose/oxidase catalase oxygen scavenging

system with Trolox to prevent blinking. The imaging buffer is composed of 2-4 mM Trolox, 0.8% glucose, and 1 μL of glucose oxidase per 100 μL of solution in 1x T50. The glucose oxidase solution is made from 10 mg of glucose oxidase (Sigma-Aldrich, G2133), 60 μL of catalase (Sigma-Aldrich, C3155), and 60 μL of 1x T50. This solution is stored at 4°C and must be centrifuged at 10000 rpm for 1 minute prior to use. A 20% glucose solution was made and stored at 4°C to use for the imaging buffer (Sigma-Aldrich, G8270). The stock Trolox solution was made by dissolving 62.6 mg of Trolox in 50 mL of pure water and 25 μL of 10 M NaOH (makes 5 mM Trolox). The solution was agitated for 24 hours at room temperature while exposed to ambient light. The pH was then adjusted to 7.8, the solution was filtered twice with 0.22 μm filters, and aliquoted and stored at -20°C. For everyday use, a tube of Trolox can be stored at 4°C. Fresh imaging buffer must be flushed into the chamber every 20 – 30 minutes.

Used sample chambers are cleaned using chloroform and piranha solution. The tubing is removed and discarded, and the slides are placed in a chloroform bath for two to six hours to allow the epoxy to dissolve. The epoxy residue is removed with a Kimwipe and the coverslip gently removed from the quartz surface and discarded. Residue from the sample, the tape, and the epoxy is removed by hand with a Kimwipe, and then with hot water and a scrubbing sponge. Needles are used to ensure no epoxy residue remains inside the tubing holes. The final wash is done with Hellmanex III Liquid Cleaning Concentrate, and the slide is rinsed with pure water. The slides are then placed into an acidic piranha bath (40 mL of hydrogen peroxide and 80 mL of concentrated sulfuric acid) for at least one hour. The piranha must be prepared on an ice bath and then used in a container which sits inside an ice bath for safety. Upon removal from the piranha the

slides are rinsed with copious amounts of pure water. The clean slides are store in pure water until required again. Once removed from the water, the slides are burned in a blue flame, and the preparation process may begin again.

Below are several images and time-intensity traces illustrating the data from this instrument. Figure AIII.3 shows an image of the bead slide (with 0.2 μm beads), and an image of immobilized Dy632-dsDNA (sequence as shown in Figure 4.2). Several time-intensity traces from the DNA sample are shown in Figures AIII.4, AIII.5, and AIII.6.

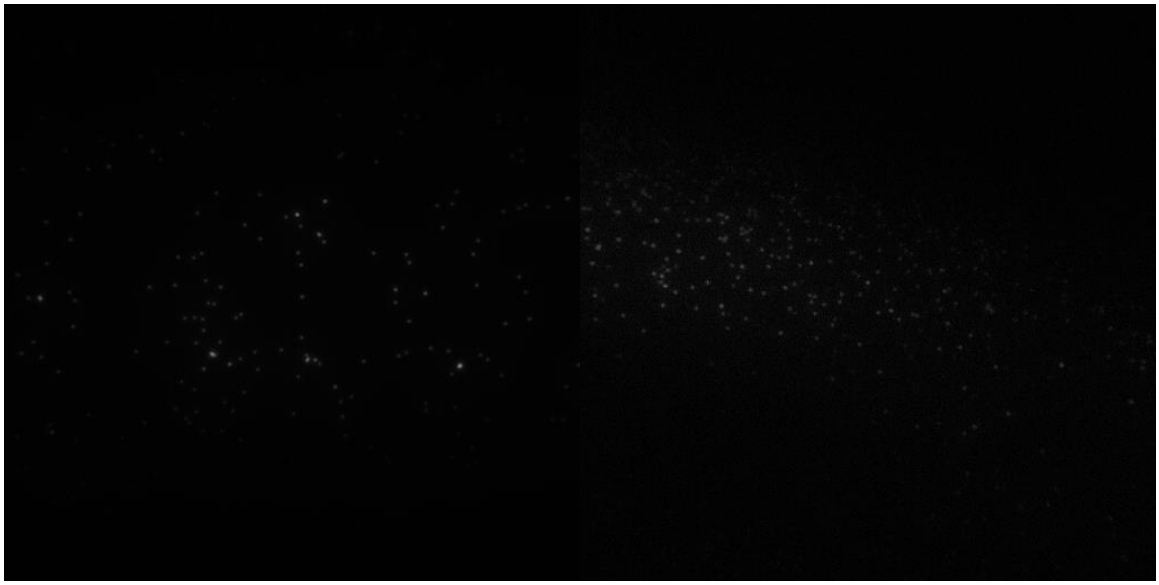


Figure AIII.3: TIRF image of 0.2 μm crimson fluorescent beads (left). The brighter spots are likely clusters of several polystyrene beads. The image on the right is of Dy632-dsDNA; this image is a still frame from a movie consisting of 1000 frames, where for each frame the EMCCD collected fluorescence for 100 ms.

This preliminary data shows what appears to be two-state behavior in the intensity (Figures AIII.4 and AIII.5). This supports the idea, presented in Chapter 4.4 section B, that the dye may be stacking with the DNA bases; in such a case the dye would have a certain fluorescence quantum yield when stacked and a different quantum yield when unstacked. This would result in two different intensity levels as are seen here. Some

intensity traces do not show the two-state behavior (Figure AIII.6, left panel). Most DNA molecules observed in this movie had a single bleaching step (Figures AIII.4, AIII.5, and AIII.6 left), however, a molecule with two bleaching steps was observed (Figure AIII.6, right panel). This indicates that two DNA molecules were immobilized in close proximity such that their point-spread functions cannot be distinguished.

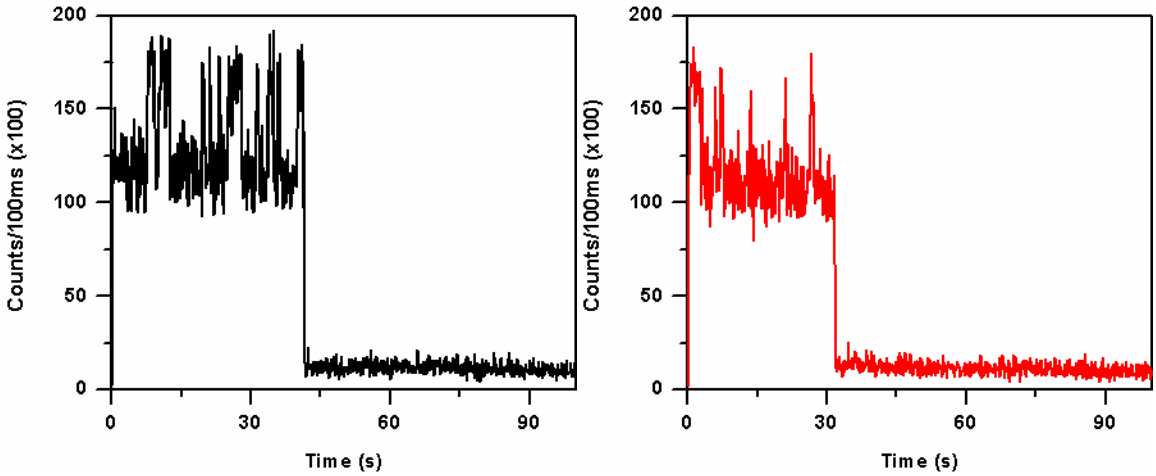


Figure AIII.4: Dy632-dsDNA time-intensity traces showing two-state intensity behavior and a single photobleaching step.

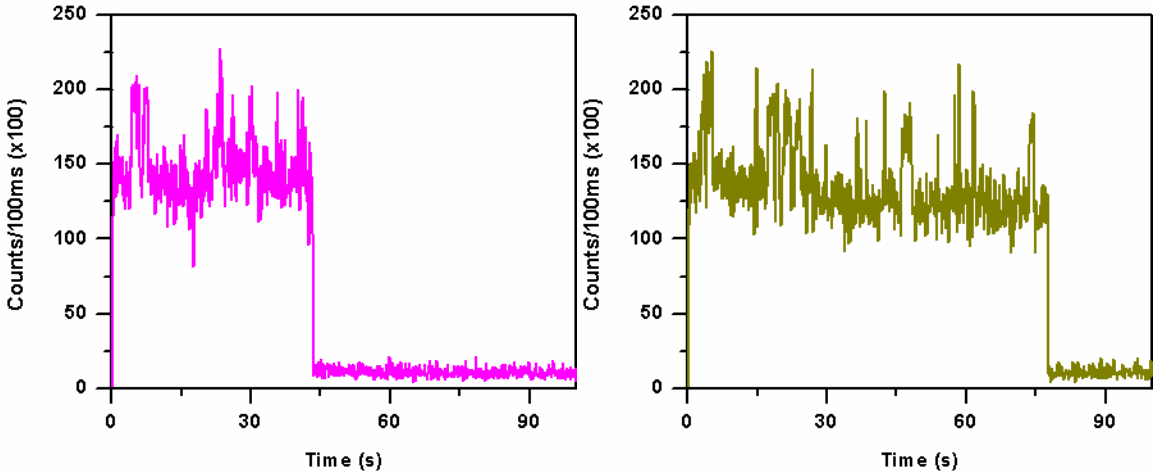


Figure AIII.5: Dy632-dsDNA time-intensity traces showing two-state intensity behavior and a single photobleaching step.

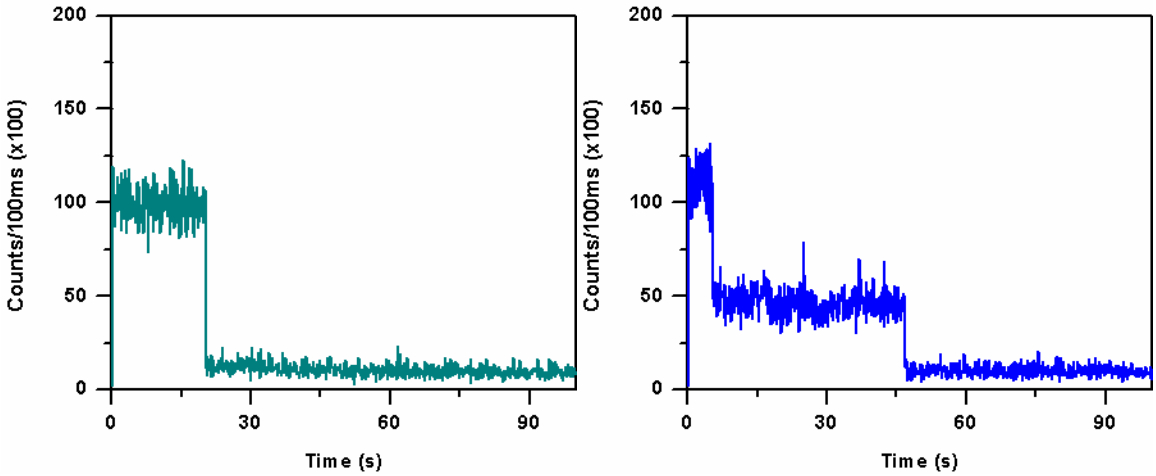


Figure AIII.6: Dy632-dsDNA time-intensity traces showing single state intensity behavior and a double photobleaching step (right).